ACTIVITY STUDIES OF PENTAMETHYLCYCLOPENTADIENYL CHROMIUM COMPLEXES IN N_2 ACTIVATION

by

Farzaneh Ahmadi Darani

A dissertation submitted to the Faculty of the University of Delaware in partial fulfillment of the requirements for the degree of Doctor of Philosophy in Chemistry and Biochemistry

Winter 2021

© 2021 Farzaneh Ahmadi Darani
All Rights Reserved

ACTIVITY STUDIES OF PENTAMETHYLCYCLOPENTADIENYL CHROMIUM COMPLEXES IN N_2 ACTIVATION

by

Farzaneh Ahmadi Darani

Approved: _____
Brian J. Bahnson, Ph.D.
Chair of the Department of Chemistry and Biochemistry

Approved: _____
John A. Pelesko, Ph.D.
Dean of the College of Arts and Sciences

Approved: _____
Louis F. Rossi, Ph.D.
Vice Provost for Graduate and Professional Education and Dean of the Graduate College

I certify that I have read this dissertation and that in my opinion it meets the academic and professional standard required by the University as a dissertation for the degree of Doctor of Philosophy.

Signed: _____

Klaus H. Theopold, Ph.D.
Professor in charge of dissertation

I certify that I have read this dissertation and that in my opinion it meets the academic and professional standard required by the University as a dissertation for the degree of Doctor of Philosophy.

Signed: _____

Joel Rosenthal, Ph.D.
Member of dissertation committee

I certify that I have read this dissertation and that in my opinion it meets the academic and professional standard required by the University as a dissertation for the degree of Doctor of Philosophy.

Signed: _____

Joseph M. Fox, Ph.D.
Member of dissertation committee

I certify that I have read this dissertation and that in my opinion it meets the academic and professional standard required by the University as a dissertation for the degree of Doctor of Philosophy.

Signed: _____

Graham E. Dobereiner, Ph.D.
Member of dissertation committee

ACKNOWLEDGMENTS

First and foremost, I would like to express my deep and sincere gratitude to my research supervisor, Dr. Klaus H. Theopold, for giving me the opportunity to do research and providing invaluable guidance and support throughout my Ph.D. study. His patience, enthusiasm, dynamism, and immense knowledge have deeply inspired me. It was a great privilege and honor to work and study under his guidance. I am extremely grateful for what he has offered me.

I would also like to express my special thanks to the rest of my dissertation committee, Dr. Joel Rosenthal, Dr. Joseph M. Fox, and Dr. Graham E. Dobereiner, for their encouragement and insightful comments.

I give special thanks to Dr. Glenn Yap for his help in X-ray crystallography during my Ph.D. research. I also thank Dr. Shi Bai for his help in NMR lab and all the facilities and staff in this department. I am especially grateful to all of those with whom I have had the pleasure to work with, and also for and all the members of our lab group, past and present, for their support and help.

I am deeply thankful to my parents, Shahla and Mohammadtaghi, my sister Shadi, and my brother Farshad whose love and guidance are with me in whatever I pursue. I would like to thank my friends, in particular Mehrnoosh, Anahita and Leila for their friendship and support throughout the years. Thanks for always being there or me. Finally, to my loving and supportive husband, Majid. Your encouragement when the times got rough are much appreciated and duly noted.

TABLE OF CONTENTS

LIST OF TABLES……...vii
LIST OF FIGURES…….……...xii
LIST OF SCHEMES……..xix
ABSTRACT…….…….....xxii

Chapter

1 INTRODUCTION…….……...1

1.1 Conclusion……11

2 SYNTHESIS AND CHARACTERIZATION OF CHROMIUM DINITROGEN AND NITRIDE COMPLEXES…….…...12

2.1 Introduction……..…12
2.2 Results and Discussion…….…....17
2.3 Conclusion……...…..113
2.4 Experimental……...…...113

2.4.1 Preparation of [Cr(μ-η^5:η^1-$C_5Me_4CH_2$)$Cr_3Cp^*_3N_3H_x$(Cl)] (1)…….....114
2.4.2 Preparation of [Cp*Cr(μ-Cl)(μ-dbabh)CrCp*] (2)…....115
2.4.3 Preparation of [Cp*Cr(N_3)$_3$Li(THF)]n (3)……....115
2.4.4 Preparation of [Cp*ClCr(μ-N_3)]$_2$ (4)……....116
2.4.5 Preparation of [Cp*ClCr]$_4$(μ-N)$_2$(μ-N_3)$_2$ (5)……....116
2.4.6 Preparation of [Cp*ClCr(N^N)] (6)…….….117
2.4.7 Preparation of [Cp*Cr(N^N)] (7)…….….117
2.4.8 Preparation of [Cp*Cr(μ-N_2)PMe_3]$_4$Na (8)…….…....118
2.4.9 Preparation of [Cp*(dmpe)CrCl] (9)…….…....118
2.4.10 Preparation of [Cp*(dmpe)Cr]$_2$(μ-N_2) (10)…….……..119
2.4.11 Preparation of [Cp*dmpeCr(μ-N)CrCp*Cl] (11)…….119
2.4.12 Preparation of [Cp*dmpeCr(μ-N)Cr(N_3)$_2$Cp*] (12)…..120
2.4.13 Preparation of [Cp*(dmpe)Cr≡N] (13)……..120
2.4.14 Preparation of [Cp*(dmpe)Cr=NMe]OTf (14)…….121
2.4.15 Preparation of [Cp*(dmpe)CrN]$_2$(μ-$MgCl_2$) (15)…....121
2.4.16 Preparation of [Cp*$(OCN)_2$Cr(μ-N)CrdmpeCp*](18)..122

3 STUDY OF THE REACTIVITY OF DINITROGEN AND NITRIDE COMPLEXES SUPPORTED BY CYCLOPENTADIENYL AND DMPE……..…....123

3.1 Introduction……..……..123
3.2 Results and Discussion……...124
3.3 Conclusion…….…….....200
3.4 Experimental…….…….....201

3.4.1 Preparation of [Cp*$_2$Cr$_2$(μ,μ-{NP(CH$_3$)$_2$}$_2$C$_2$H$_4$)] (19)202
3.4.2 Alternative preparation of [Cp*$_2$Cr$_2$(μ,μ-{NP(CH$_3$)$_2$}$_2$C$_2$H$_4$)] (19)……...……...202
3.4.3 Preparation of Na$_2$[Cp*dmpeCr(N$_2$)]$_4$ (20)…….…..202
3.4.4 Preparation of [Cp*(dmpe)Cr(μ-N$_2$)Na(TMEDA)$_2$] (21)……..……..203
3.4.5 Preparation of [Cp*(dmpe)Cr(NNSiMe$_3$)] (22)…….204
3.4.6 Preparation of [Cp*(dmpe)Cr(μ-N$_2$)Na(15-crown-5)] (23)……....204
3.4.7 Preparation of [(Cp*(dmpe)Cr)$_2$(μ-N$_2$)](FB(C$_6$F$_5$)$_3$) (24)……..205
3.4.8 Preparation of [(Cp*(dmpe)Cr)$_2$(μ-N$_2$)]BAr$^F_4$ (25)…..205
3.4.9 Preparation of [(Cp*(dmpe)Cr)$_2$(μ-N$_2$)](BAr$^F_4$)$_2$(26)...206
3.4.10 Alternative preparation of [(Cp*(dmpe)Cr)$_2$(μ-N$_2$)] (BAr$^F_4$)$_2$ (26)……...…....206
3.4.11 Preparation of [Cp*(dmpe)CrF]BAr$^F_4$ (27)…….207
3.4.12 Preparation of [Cp*(dmpe)CrCl]BAr$^F_4$ (28)……207
3.4.13 Preparation of [(Cp*(dmpe)CrN]BAr$^F_4$ (29)……...208
3.4.14 Preparation of [Cp*Cr(NPMe$_2$CH$_2$CH$_2$PMe$_2$)]BAr$^F_4$ (30)…….208
3.4.15 Preparation of [Cp*Cr(NPMe$_2$CH$_2$CH$_2$PMe$_2$)THF]BAr$^F_4$ (31)…….209

4 DFT CALCULATIONS……..…….....210

4.1 Introduction……...……...…….210
4.2 Results and Discussion……...……...210
4.3 Conclusion ……...…….....223

REFERENCES……..224

Appendix

A CRYSTALOGRAPHIC INFORMATION OF COMPLEXES……...240
B MISCELLANEOUS CRYSTAL STRUCTURES……..272

LIST OF TABLES

Table 2.1 Interatomic distances (Å) and angles (º) for [Cr(μ-η^5:η^1-$C_5Me_4CH_2$)$Cr_3Cp^*_3N_3H_x$(Cl)] (**1**).……23

Table 2.2 Interatomic distances (Å) and angles (º) for [Cp*Cr(μ-Cl)(μ-dbabh)CrCp*] (**2**).……..33

Table 2.3 Interatomic distances (Å) and angles (º) for [[Cp*Cr$(N_3)_3$]Li(THF)]$_n$ (**3**).…39

Table 2.4 Interatomic distances (Å) and angles (º) for [Cp*ClCr(μ-N_3)]$_2$ (**4**).……..43

Table 2.5 Interatomic distances (Å) and angles (º) for [Cp*ClCr]$_4$(μ-N)$_4$(μ-N_3)$_4$(**5**).…48

Table 2.6 Interatomic distances (Å) and angles (º) for [Cp*ClCr(N^N)] (**6**).……53

Table 2.7 Interatomic distances (Å) and angles (º) for [Cp*Cr(N^N)] (**7**).……57

Table 2.8 Interatomic distances (Å) and angles (º) for [Cp*Cr(μ-N_2)PMe_3]$_4$Li (**8**).…..62

Table 2.9 Interatomic distances (Å) and angles (º) for [Cp*ClCr(dmpe)] (**9**).……...67

Table 2.10 Interatomic distances (Å) and angles (º) for [Cp*(dmpe)Cr]$_2$(μ-N_2) (**10**)....71

Table 2.11 Interatomic distances (Å) and angles (º) for [Cp*dmpeCr(μ-N)CrCp*Cl] (**11**).……75

Table 2.12 Interatomic distances (Å) and angles (º) for [Cp*dmpeCr(μ-N)Cr$(N_3)_3$Cp*] (**12**).……79

Table 2.13 Interatomic distances (Å) and angles (º) for [Cp*dmpeCr≡N] (**13**).……87

Table 2.14 Interatomic distances (Å) and angles (º) for [Cp*dmpeCr=NMe]OTf (**14**)….……93

Table 2.15 Interatomic distances (Å) and angles (º) for [Cp*dmpeCrN]$_2$[μ-$MgCl_2$] (**15**)…….97

Table 2.16 Interatomic distances (Å) and angles (º) for [Cp*Cr(μ-μ-{$NPMe_2C_2H_4PMe_2$N}Cr(NCO)Cp*] (**16**).……...100

Table 2.17 Interatomic distances (Å) and angles (º) for [Cp*$(CO)_2$(OCN)Cr]$_2$(μ-dmpe) (**17**).……..104

Table 2.18 Interatomic distances (Å) and angles (º) for [Cp*$(OCN)_2$Cr(μ-N)CrdmpeCp*] (**18**).....107

Table 3.1 Interatomic distances (Å) and angles (º) for [Cp*$_2$$Cr_2$(μ,μ-{$NP(CH_3)_2$}$_2$$C_2H_4$)] (**19**).....127

Table 3.2 Interatomic distances (Å) and angles (º) for Na_2[Cp*dmpeCrN_2]$_4$ (**20**).....132

Table 3.3 Interatomic distances (Å) and angles (º) for [Cp*(dmpe)Cr(μ-N_2)Na(TMEDA)$_2$] (**21**).....138

Table 3.4 Interatomic distances (Å) and angles (º) for [Cp*(dmpe)Cr(μ-N_2)$SiMe_3$] (**22**).....144

Table 3.5 Interatomic distances (Å) and angles (º) for [Cp*(dmpe)Cr(μ-N_2)Na(15-crown-5)] (**23**).....148

Table 3.6 Interatomic distances (Å) and angles (º) for the N_2-containing cation of [(Cp*(dmpe)Cr)$_2$(μ-N_2)](FB$(C_6F_5)_3$) (**24**).....153

Table 3.7 Interatomic distances (Å) and angles (º) for the N_2-containing cation of [(Cp*(dmpe)Cr)$_2$(μ-N_2)]$BAr^F{}_4$ (**25**).....159

Table 3.8 Interatomic distances (Å) and angles (º) for the N_2-containing cation of [(Cp*(dmpe)Cr)$_2$(μ-N_2)]($BAr^F{}_4$)$_2$ (**26**).....166

Table 3.9 Interatomic distances (Å) and angles (º) for the cation of [Cp*(dmpe)CrF]$BAr^F{}_4$ (**27**).....170

Table 3.10 Interatomic distances (Å) and angles (º) for the cation of [Cp*(dmpe)CrCl]$BAr^F{}_4$ (**28**).....174

Table 3.11 Interatomic distances (Å) and angles (º) for the cation of [(Cp*(dmpe)CrN]$BAr^F{}_4$ (**29**).....178

Table 3.12 Interatomic distances (Å) and angles (º) for the cation of [Cp*Cr($NPMe_2CH_2CH_2PMe_2$)] $BAr^F{}_4$ (**30**).....186

Table 3.13 Calculated and experimental bond distances (Å) and angles (°) for [Cp*Cr($NPMe_2CH_2CH_2PMe_2$)] $BAr^F{}_4$ (**30**).....188

Table 3.14 Interatomic distances (Å) and angles (º) for the cation of [Cp*Cr($NPMe_2CH_2CH_2PMe_2$)THF] $BAr^F{}_4$ (**31**).....190

Table 3.15 Interatomic distances (Å) and angles (º) for the cation of [Cp*Cr(HNPMe$_2$CH$_2$CH$_2$PMe$_2$)F] BAr$^F{}_4$ (**32**).....195

Table 3.16 Calculated and experimental data for selected bond distances and angles of **32**.....198

Table 3.17 Selected angle and bond lengths (Å) for **30**, **31**, and **32**. 200

Table 4.1 Calculated bond distance (Å) and angle (°) for **10**, **13**, **25**, **26**, and **29** and their Cp version. E_0 (Hartree) = the total electronic energy. ^{4}**25** (4= multiplicity) did not converged with TZVP basis set. 212

Table 4.2 TS and TS′ comparison. E_0 is in Hartree. 214

Table 4.3 Selected bond distance (Å) and angles(°) for TS and TS′ (Multiplicity of 1). 215

Table 4.4 Calculated thermochemistry values from Gaussian for the reaction of two nitrides to make dinitrogen complex at 298.15 K. Al the values are in Hartree.....217

Table 4.5 Computed activation parameters and reaction thermodynamics 217

Table 4.6 NPA charges on selected atoms of Nitride, Transition state and the Dinitrogen complexes. There is an inversion center in dinitrogen and TS complexes, therefore only half of the molecule is shown in the table. 220

Table A.1 Crystal data and structure refinement for [Cp*$_4$Cr$_4$N$_3$Cl] (**1**)…….…….....240

Table A.2 Crystal data and structure refinement for [Cp*Cr(μ-Cl)(μ-dbabh)CrCp*] (**2**)…….……...241

Table A.3 Crystal data and structure refinement for [Cp*Cr(N$_3$)$_3$Li(THF)]$_n$ (**3**)…....242

Table A.4 Crystal data and structure refinement for [Cp*ClCr(μ-N$_3$)]$_2$ (**4**)……243

Table A.5 Crystal data and structure refinement for [Cp*ClCr]$_4$(μ-N)$_2$(μ-N$_3$)$_2$ (**5**)....244

Table A.6 Crystal data and structure refinement for [Cp*ClCr(N^N)] (**6**)……..245

Table A.7 Crystal data and structure refinement for [Cp*Cr(N^N)] (**7**)……..246

Table A.8 Crystal data and structure refinement for [Cp*Cr(μ-N$_2$)PMe$_3$]$_4$Na (**8**)…...247

Table A.9 Crystal data and structure refinement for [Cp*(dmpe)CrCl] (**9**)……....248

Table A.10 Crystal data and structure refinement for $[Cp^*(dmpe)Cr]_2(\mu\text{-}N_2)$ (**10**)….249

Table A.11 Crystal data and structure refinement for [Cp*dmpeCr(μ-N)CrCp*Cl] (**11**)…….....250

Table A.12 Crystal data and structure refinement for $[Cp^*dmpeCr(\mu\text{-}N)Cr(N_3)_2Cp^*]$ (**12**)…….……....251

Table A.13 Crystal data and structure refinement for [Cp*(dmpe)Cr≡N] (**13**)……....252

Table A.14 Crystal data and structure refinement for [Cp*(dmpe)Cr=NMe]OTf (**14**)……...253

Table A.15 Crystal data and structure refinement for $[Cp^*(dmpe)CrN]_2(\mu\text{-}MgCl_2)$ (**15**)……...254

Table A.16 Crystal data and structure refinement for [Cp*Cr(μ-{$NPMe_2C_2H_4PMe_2N$}Cr(NCO)Cp*] (**16**)…….…...255

Table A.17 Crystal data and structure refinement for $[Cp^*(CO)_2(OCN)Cr]_2$(μ-dmpe) (**17**)……..….256

Table A.18 Crystal data and structure refinement for $[Cp^*(OCN)_2Cr(\mu\text{-}N)CrdmpeCp^*]$ (**18**)…….…257

Table A.19 Crystal data and structure refinement for $[Cp^*_2Cr_2(\mu,\mu\text{-}\{NP(CH_3)_2\}_2C_2H_4)]$ (**19**)……..……...258

Table A.20 Crystal data and structure refinement for $Na_2[Cp^*dmpeCrN_2]_4$ (**20**)…....259

Table A.21 Crystal data and structure refinement for $[Cp^*(dmpe)Cr(\mu\text{-}N_2)Na(TMEDA)_2]$ (**21**)……...…..260

Table A.22 Crystal data and structure refinement for $[Cp^*(dmpe)Cr(\mu\text{-}N_2)SiMe_3]$ (**22**)……...261

Table A.23 Crystal data and structure refinement for $[Cp^*(dmpe)Cr(\mu\text{-}N_2)Na$(15-crown-5)] (**23**)……..262

Table A.24 Crystal data and structure refinement for $[(Cp^*(dmpe)Cr)_2(\mu\text{-}N_2)](FB(C_6F_5)_3)$ (**24**)……263

Table A.25 Crystal data and structure refinement for $[(Cp^*(dmpe)Cr)_2(\mu\text{-}N_2)]BAr^F{}_4$ (**25**)……...264

Table A.26 Crystal data and structure refinement for $[(Cp^*(dmpe)Cr)_2(\mu\text{-}N_2)](BAr^F{}_4)_2$ (**26**)……..…...…..265

Table A.27 Crystal data and structure refinement for $[Cp^*(dmpe)CrF]BAr^F{}_4$ (**27**)…...266

Table A.28 Crystal data and structure refinement for $[Cp^*(dmpe)CrCl]BAr^F{}_4$ (**28**)…..267

Table A.29 Crystal data and structure refinement for $[(Cp^*(dmpe)CrN]BAr^F{}_4$ (**29**)….268

Table A.30 Crystal data and structure refinement for $[Cp^*Cr(NPMe_2CH_2CH_2PMe_2)]BAr^F{}_4$ (**30**)……....269

Table A.31 Crystal data and structure refinement for $[Cp^*Cr(NPMe_2CH_2CH_2PMe_2)THF]BAr^F{}_4$ (**31**) …….....270

Table A.32 Crystal data and structure refinement for $[Cp^*Cr(NPMe_2CH_2CH_2PMe_2)F]BAr^F{}_4$ (**32**)……...……...271

Table B.1 Interatomic distances (Å) and angles (º) for $[Cp^*Cr(acac)THF]PF_6$ (**B.1**)....273

Table B.1.a Crystal data and structure refinement for $[Cp^*Cr(acac)THF]PF_6$ (**B.1**)….276

Table B.2 Interatomic distances (Å) and angles (º) for [Cp*Cr(N^N)OTf]OTf (**B.2**)…278

Table B.2.a Crystal data and structure refinement for [Cp*Cr(**N^N**)OTf]OTf (**B.2**)…281

Table B.3 Interatomic distances (Å) and angles (º) for [Cp*Cr(depe)N] (**B.3**)……283

Table B.3.a Crystal data and structure refinement for [Cp*Cr(depe)N] (**B.3**)……..285

Table B.4 Interatomic distances (Å) and angles (º) for $[[Cp^*(dmpe)Cr]_2(\mu\text{-}N_2)]_2$(μ-dmpe) (**B.4**)…….....287

Table B.4.a Crystal data and structure refinement for $[[Cp^*(dmpe)Cr]_2(\mu\text{-}N_2)]_2$(μ-dmpe) (**B.4**)……..290

Table B.5 Interatomic distances (Å) and angles (º) for the cation of $[[Cp^*(dmpe)Cr]_2(\mu\text{-}N_2)]_2$(μ-dmpe) (**B.5**)……..…..292

Table B.5.a Crystal data and structure refinement for $[[Cp^*(dmpe)Cr]_2(\mu\text{-}N_2)]_2$(μ-dmpe) (**B.5**)…….…297

LIST OF FIGURES

Figure 1.1 An ammonia fuel cycle involving the reduction of nitrogen coupled with water oxidation (lower left), the splitting of ammonia to nitrogen and hydrogen (top), and the oxidation of hydrogen (lower right).[8].....….2

Figure 1.2 Dissociation of dinitrogen. Haber-Bosch mechanism (left), Nitrogenase mechanisms (right). [14,22].....4

Figure 2.1 Bonding in end-on dinitrogen complexes. B is a resonance structure of σ-bonded A and can describe the back bonding between the N_2 and the metal center.[41] 13

Figure 2.2 ^{1}H-NMR spectrum of reaction of $[Cp^*Cr(\mu\text{-}Cl)]_2$ with NaN_3 in THF after 3 h, recorded in C_6D_6 at 400 MHz. 19

Figure 2.3 Molecular structure of the $[Cr(\mu\text{-}\eta^5\text{:}\eta^1\text{-}C_5Me_4CH_2)Cr_3Cp^*_3N_3H_x(Cl)]$ (**1**) represented as 50% probability thermal ellipsoids. Hydrogen atoms and a pentane molecule have been omitted for clarity. a) **1** with Cp* ligands shown in the structure, b) Three Cp* ligands are omitted for clarity. 22

Figure 2.4 LIFDI-MS of predicted isotope model for the molecular ion of $[Cr(\mu\text{-}\eta^5\text{:}\eta^1\text{-}C_5Me_4CH_2)Cr_3Cp^*_3N_3H_x(Cl)]$ (**1**) [x=3; $C_{40}H_{62}Cr_4N_3Cl$: 827.2260] (Top), and calculated pattern for $[Cr(\mu\text{-}\eta^5\text{:}\eta^1\text{-}C_5Me_4CH_2)Cr_3Cp^*_3N_3H_x(Cl)]$ (**1**) [x= 3; $C_{40}H_{62}Cr_4N_3Cl$: 827.2273] (Bottom). 29

Figure 2.5 ^{1}H-NMR spectrum of **1** recorded in C_6D_6 at 400 MHz. 30

Figure 2.6 Molecular structure of $[Cp^*Cr(\mu\text{-}Cl)(\mu\text{-dbabh})CrCp^*]$ (**2**) represented as 50% probability thermal ellipsoids. Hydrogen atoms have been omitted for clarity. 32

Figure 2.7 Molecular structure of $[[Cp^*Cr(N_3)_3Li(THF)]_n$ (**3**) represented as 50% probability thermal ellipsoids. Hydrogen atoms have been omitted for clarity. 38

Figure 2.8 Polymeric structure of $[[Cp^*Cr(N_3)_3]Li(THF)]_n$ (**3**). THF molecules on the side Cr metals have been omitted for clarity. 41

Figure 2.9 Molecular structure of [Cp*ClCr(μ-N_3)]$_2$ (**4**) represented as 50% probability thermal ellipsoids. Hydrogen atoms have been omitted for clarity. 43

Figure 2.10 Molecular structure of [Cp*ClCr]$_4$(μ-N)$_2$(μ-N_3)$_2$ (**5**) represented as 50% probability thermal ellipsoids. Hydrogen atoms have been omitted for clarity. 47

Figure 2.11 Molecular structure of [Cp*ClCr(N^N)] (**6**) represented as 50% probability thermal ellipsoids. Hydrogen atoms have been omitted for clarity. 52

Figure 2.12 The linear correlation of Cpy−Cpy (blue) and average C_{py}−N_{py} (red).[74] ...55

Figure 2.13 Molecular structure of [Cp*Cr(N^N)] (**7**) represented as 50% probability thermal ellipsoids. Hydrogen atoms have been omitted for clarity. 57

Figure 2.14 Molecular structure of [Cp*Cr(μ-N_2)PMe_3]$_4$Na (**8**) represented as 50% probability thermal ellipsoids. Hydrogen atoms and pentane solvent molecules have been omitted for clarity. 61

Figure 2.15 Molecular structure of [Cp*ClCr(dmpe)] (**9**) represented as 50% probability thermal ellipsoids. Hydrogen atoms have been omitted for clarity. 66

Figure 2.16 ^{1}H-NMR spectrum of **9** recorded in C_6D_6 at 400 MHz. 69

Figure 2.17 Molecular structure of [Cp*(dmpe)Cr]$_2$(μ-N_2) (**10**) represented as 50% probability thermal ellipsoids. Hydrogen atoms are omitted for clarity. ...70

Figure 2.18 ^{1}H- spectrum of [Cp*(dmpe)Cr]$_2$(μ-N_2) (**10**) recorded in C_6D_6 at 400 MHz. 73

Figure 2.19 Molecular structure of [Cp*dmpeCr(μ-N)CrCp*Cl] (**11**) represented as 50% probability thermal ellipsoids. Hydrogen atoms are omitted for clarity. 75

Figure 2.20 Molecular structure of [Cp*dmpeCr(μ-N)Cr(N_3)$_2$Cp*] (**12**) represented as 50% probability thermal ellipsoids. Hydrogen atoms are omitted for clarity. 79

Figure 2.21 Reaction of **9** with azide reagent in the NMR tube using THF-d_8 as the solvent. Spectra 1, 2, 3 and were taken respectively after 5 min, 15 min, 30 min and 5 days after the start of the reaction. The peaks that were recognized are marked with stars. Green: starting compound **9**, yellow: bridging nitride **11** and red: compound **12**.....84

Figure 2.22 Molecular structure of [Cp*dmpeCr≡N] (**13**) represented as 50% probability thermal ellipsoids. Hydrogen atoms have been omitted for clarity. 86

Figure 2.23 ^{1}H-NMR spectrum of [Cp*dmpeCr≡N] (**13**) recorded in C_6D_6 at 400 MHz. 89

Figure 2.24 CSD search on over 100 Cr-N bond distances in terminal chromium nitride complexes. Each number above each column shows the number of complexes in a specific bond distance range, i.e., 4 complexes with Cr-N bond distance between 1.515 to 1.525 Å. **13** is not shown in this chart. ...90

Figure 2.25 CSD search on over 100 chromium nitride complexes to show the correlation of Cr≡N bond distance and coordination number of chromium center. **13** is not shown in the graph. 91

Figure 2.26 Molecular structure of [Cp*dmpeCr=NMe]OTf (**14**) represented as 50% probability thermal ellipsoids. Hydrogen atoms have been omitted for clarity. The dmpe ligand suffer positional disorder over two sets of positions. 92

Figure 2.27 Molecular structure of [Cp*dmpeCrN]$_2$[μ-MgCl$_2$] (**15**) represented as 50% probability thermal ellipsoids. Hydrogen atoms have been omitted for clarity. 96

Figure 2.28 Molecular structure of [Cp*Cr(μ-{NPMe$_2$C$_2$H$_4$PMe$_2$N}Cr(NCO)Cp*] (**16**) represented as 50% probability thermal ellipsoids. Hydrogen atoms have been omitted for clarity. 100

Figure 2.29 Molecular structure of [Cp*(CO)$_2$(OCN)Cr]$_2$(μ-dmpe) (**17**) represented as 50% probability thermal ellipsoids. Hydrogen atoms and one THF molecule have been omitted for clarity. 104

Figure 2.30 Molecular structure of [Cp*(OCN)$_2$Cr(μ-N)CrdmpeCp*] (**18**) represented as 50% probability thermal ellipsoids. Hydrogen atoms and one THF molecule have been omitted for clarity. 107

Figure 2.31 ^{1}H-NMR spectrum of [Cp*(CO)$_2$(OCN)Cr]$_2$(μ-dmpe) (**17**) recorded in C_6D_6 at 400 MHz. 111

Figure 2.32 IR spectrum of [Cp*(CO)$_2$(OCN)Cr]$_2$(μ-dmpe) (**17**). 112

Figure 2.33 ^{1}H-NMR spectrum of [Cp*(OCN)$_2$Cr(μ-N)CrdmpeCp*] (**18**) recorded in C_6D_6 at 400 MHz. 112

Figure 2.34 IR spectrum of [Cp*$(OCN)_2$Cr(μ-N)CrdmpeCp*] (**18**). 113

Figure 3.1 Reaction of [Cp*dmpeCr≡N] (**13**) under 250 nm light in benzene-d_6 for 22 hours. Purple and green dots respectively show the proton NMR peaks of **13** and the product of reaction. During the reaction free dmpe ligand was observed (black stars). 125

Figure 3.2 Molecular structure of [$Cp^*_2Cr_2$(μ,μ-{$NP(CH_3)_2$}$_2C_2H_4$)] (**19**) represented as 50% probability thermal ellipsoids. Hydrogen atoms have been omitted for clarity. 126

Figure 3.3 Molecular structure of Na_2[Cp*dmpeCr$(N_2)]_4$ (**20**) represented as 50% probability thermal ellipsoids. Hydrogen atoms have been omitted for clarity. 131

Figure 3.4 ^{1}H-NMR spectrum of Na_2[Cp*dmpeCr$N_2]_4$ (**20**) recorded in C_6D_6 at 400 MHz. Orange stars show the peaks related to **20**, green stars show the peaks related to the dinitrogen compound **10** impurity in the sample and black stars are related to solvent impurities. 136

Figure 3.5 Molecular structure of [Cp*(dmpe)Cr(μ-N_2)Na$(TMEDA)_2$] (**21**) represented as 50% probability thermal ellipsoids. Hydrogen atoms have been omitted for clarity. 138

Figure 3.6 ^{1}H-NMR spectrum of [Cp*(dmpe)Cr(μ-N_2)Na$(TMEDA)_2$] (**21**) recorded in C_6D_6 at 400 MHz. 142

Figure 3.7 Molecular structure of [Cp*(dmpe)Cr(N_2SiMe_3)] (**22**) represented as 50% probability thermal ellipsoids. Hydrogen atoms have been omitted for clarity. 143

Figure 3.8 Molecular structure of [Cp*(dmpe)Cr(μ-N_2)Na(15-crown-5)] (**23**) represented as 50% probability thermal ellipsoids. Hydrogen atoms have been omitted for clarity. 147

Figure 3.9 Molecular structure of [$(Cp^*(dmpe)Cr)_2$(μ-N_2)]($FB(C_6F_5)_3$) (**24**) represented as 50% probability thermal ellipsoids. Hydrogen atoms have been omitted for clarity. The asymmetric unit contains two chemically equivalent molecules and one of the counterions is not shown here. 152

Figure 3.10 ^{1}H-NMR spectrum of [$(Cp^*(dmpe)Cr)_2$(μ-N_2)]($FB(C_6F_5)_3$) (**24**) recorded in THF-d_8 at 400 MHz. Peaks at 0.9 and 1.3 ppm are related to pentane solvent. 157

Figure 3.11 Molecular structure of $[(Cp^*(dmpe)Cr)_2(\mu\text{-}N_2)]BAr^F{}_4$ (**25**) represented as 50% probability thermal ellipsoids. Hydrogen atoms have been omitted for clarity. The asymmetric unit contains two molecules and one of the counterions is not shown here. 159

Figure 3.12 ^{1}H-NMR spectrum of $[(Cp^*(dmpe)Cr)_2(\mu\text{-}N_2)]BAr^F{}_4$ (**25**) recorded in THF-d_8 at 400 MHz. 163

Figure 3.13 Synthesis of $[(Cp^*(dmpe)Cr)_2(\mu\text{-}N_2)]BAr^F{}_4$ (**25**) by the reaction of **10** with 1 equivalent of Brookhart's acid. 164

Figure 3.14 Molecular structure of $[(Cp^*(dmpe)Cr)_2(\mu\text{-}N_2)](BAr^F{}_4)_2$ (**26**) represented as 50% probability thermal ellipsoids. Hydrogen atoms and one counterion have been omitted for clarity. 166

Figure 3.15 Molecular structure of $[Cp^*(dmpe)CrF]BAr^F{}_4$ (**27**) represented as 50% probability thermal ellipsoids. Hydrogen atoms have been omitted for clarity. 170

Figure 3.16 Molecular structure of $[Cp^*(dmpe)CrCl]BAr^F{}_4$ (**28**) represented as 50% probability thermal ellipsoids. Hydrogen atoms have been omitted for clarity. 173

Figure 3.17 ^{1}H-NMR spectra of the reaction of $[(Cp^*(dmpe)Cr)_2(\mu\text{-}N_2)](BAr^F{}_4)_2$ (**26**) at high temperature (70°C) in C_6D_6 for 30 days. The initial spectrum at the beginning of the experiment was not recorded due to the insolubility of the **26** in benzene. 176

Figure 3.18 Molecular structure of $[(Cp^*(dmpe)CrN]BAr^F{}_4$ (**29**) represented as 50% probability thermal ellipsoids. Hydrogen atoms and the counterion have been omitted for clarity. 178

Figure 3.19 CSD search on over 100 Cr-N bond distances in terminal chromium nitride complexes. The relation between the bond distance and the oxidation state is shown in this figure. The cationic chromium complex **29** is not shown in the graph. Each point represents a number i.e., 3 terminal nitride complexes with the Cr-N bond distance of 1.52 Å are shown in this graph. 181

Figure 3.20 ^{1}H- spectrum of $[(Cp^*(dmpe)CrN]BAr^F{}_4$ (**29**) recorded in C_6D_6 at 400 MHz. Pentanes was used to wash the crystals and peaks at 0.9 and 1.2 ppm are related to the pentanes impurities. 182

Figure 3.21 ^{1}H-NMR spectra of [(Cp*(dmpe)CrN]BAr^{F}_{4} (**29**) recorded in C_6D_6 at 400 MHz were monitored for 8 days at 70°C. The numbers on the right side of the spectra indicate the number of days from the beginning of the experiment.....183

Figure 3.22 ^{1}H-NMR spectra of [(Cp*(dmpe)CrN]BAr^{F}_{4} (**29**) recorded in THF-d_8 at 400 MHz. The first spectrum is of the starting compound and spectra 2 to 5 represents day 1 to 4 of reaction at 50°C. 184

Figure 3.23 Molecular structure of [Cp*Cr($NPMe_2CH_2CH_2PMe_2$)] BAr^{F}_{4} (**30**) represented as 50% probability thermal ellipsoids. Hydrogen atoms and the counterion have been omitted for clarity. 185

Figure 3.24 Molecular structure of [Cp*Cr($NPMe_2CH_2CH_2PMe_2$)THF] BAr^{F}_{4} (**31**) represented as 50% probability thermal ellipsoids. Hydrogen atoms and the counterion have been omitted for clarity. 189

Figure 3.25 ^{1}H- spectrum of [(Cp*(dmpe)CrN]BAr^{F}_{4} (**29**) recorded in C_6D_6 at 400 MHz was monitored for 16 days, at room temperature. The numbers on the right side of the spectra indicate the number of days from the beginning of the experiment. Black stars show the pentanes impurity peaks at 0.9 and 1.2 ppm. 193

Figure 3.26 Molecular structure of [Cp*Cr($HNPMe_2CH_2CH_2PMe_2$)F] BAr^{F}_{4} (**32**) represented as 50% probability thermal ellipsoids. Hydrogen atoms and the counterion have been omitted for clarity. 194

Figure 3.27 IR spectrum of the blue product resulted from dissolving **29** in benzene.197

Figure 3.28 LIFDI-MS spectrum of the product of the decomposition of **29** in solution (bottom), predicted isotope pattern for a complex with a formula corresponding to **32** ($C_{16}H_{32}NFP_2Cr$ top). 198

Figure 4.1 Calculated structures of TS (a) and TS′ (b). 215

Figure 4.2 Activation enthalpy profiles for the conversion of nitride complexes to the dinitrogen complex. 218

Figure 4.3 IRC path for the reaction of two **13** molecules to make **10**. 219

Figure 4.4 IRC path for the reaction of two **13′** molecules to make **10′**.....220

Figure 4.5 Qualitative frontier molecular orbitals for **13**, **TS** and **10**. 221

Figure 4.6 The energies (E_0)of the relevant frontier orbitals of **13**, **TS** and **10**. 222

Figure B.1 Molecular structure of the [Cp*Cr(acac)THF]PF_6 (**B.1**) represented as 50% probability thermal ellipsoids. Hydrogen atoms have been omitted for clarity……...273

Figure B.2 Molecular structure of the [Cp*Cr(N^N)OTf]OTf (**B.2**) represented as 50% probability thermal ellipsoids. Hydrogen atoms have been omitted for clarity……277

Figure B.3 Molecular structure of the [Cp*Cr(depe)N] (**B.3**) represented as 50% probability thermal ellipsoids. Hydrogen atoms and a pentane molecule have been omitted for clarity……282

Figure B.4 Molecular structure of the ([Cp*(dmpe)Cr](μ-N_2)[Cp*CrMe])$_2$(μ-dmpe) (**B.4**) represented as 50% probability thermal ellipsoids. Hydrogen atoms and a pentane molecule have been omitted for clarity……..286

Figure B.5 Molecular structure of the [Cp*Cr(depe)N]BAr^F_4 (**B.5**) represented as 50% probability thermal ellipsoids. Hydrogen atoms and a pentane molecule have been omitted for clarity……...291

LIST OF SCHEMES

Scheme 1.1 The interconversion between ammonia and hydrogen. [9] 2

Scheme 1.2 Cleavage of N_2 using $Mo(NRAr)_3$. 5

Scheme 1.3 The photochemical activation of the N≡N bond. 6

Scheme 1.4 The thermolysis of $([P_2N_2]Nb)_2(\mu\text{-}N_2)$. 6

Scheme 1.5 Conversion of Nitrido complex to N_2 bridging isomer. 7

Scheme 1.6 Conversion of dinitrogen complex to bis(μ-nitrido) isomer. 8

Scheme 1.7 Synthesis of dinitrogen and nitride complexes from the vanadium [(nacnac)VCl(ODiiP)] precursor. 9

Scheme 1.8 a) Photoinduced conversion of dinitrogen complex to the nitrido complex. b) Oxidation of the nitrido complex led to its dimerization to generate the dinitrogen-bridged complex. 10

Scheme 1.9 Dinitrogen splitting with molybdenum complex. 10

Scheme 2.1 Different modes of coordination of N_2 ligand in dinitrogen complexes.[41] 13

Scheme 2.2 Side-on dinitrogen chromium complex. 15

Scheme 2.3 Transformation of chromium azido complex to the dinitrogen isomer. ...15

Scheme 2.4 Synthesis of dinitrogen and nitride complexes from the chromium $[Tp^{tBu,Me}CrCl]$ precursor. 16

Scheme 2.5 Synthesis of $[Cp^*Cr(\mu\text{-}Cl)]_2$. 17

Scheme 2.6 Reduction of $[Cp^*Cr(\mu\text{-}Cl)]_2$ under dinitrogen gas using different reducing reagents. 18

Scheme 2.7 Synthesis of Nitride complex using Li-dbabh ligand.[67] 31

Scheme 2.8 Synthesis of starting complex $[Cp^*ClCr(\mu\text{-}Cl)]_2$ based on literature report. 37

Scheme 2.9 Synthesis of complex **3** from starting compound $[Cp^*ClCr(\mu\text{-}Cl)]_2$.....38

Scheme 2.10 Synthesis of $[Cp^*ClCr(\mu\text{-}N_3)]_2$ (**4**). 42

Scheme 2.11 Synthesis of [Cp*ClCr(N^N)] (**6**).....52

Scheme 2.12 Synthesis of [Cp*Cr(N^N)] (**7**). 56

Scheme 2.13 Synthesis of [Cp*ClCr(dmpe)] (**9**). 65

Scheme 2.14 Synthesis of $[Cp^*(dmpe)Cr]_2(\mu\text{-}N_2)$ (**10**). 70

Scheme 2.15 Synthesis of [Cp*dmpeCr(μ-N)CrCp*Cl] (**11**). 74

Scheme 2.16 Synthesis of [Cp*dmpeCr≡N] (**13**).....85

Scheme 2.17 a: Schlenk Equation and b: The reaction of **13** with MeMgCl reagent. 96

Scheme 3.1 Synthesis of $[Cp^*_2Cr_2(\mu,\mu\text{-}\{NP(CH_3)_2\}_2C_2H_4)]$ (**19**). 126

Scheme 3.2 Synthesis of $[Cp^*(dmpe)Cr(\mu\text{-}N_2)Na(TMEDA)_2]$ (**21**).....137

Scheme 3.3 Synthesis of $[Cp^*(dmpe)Cr(\mu\text{-}N_2)SiMe_3]$ (**22**).....143

Scheme 3.4 Synthesis of compound **B** from the reaction of **A** with Me_3SiCl reagent. [78] 146

Scheme 3.5 Synthesis of $[(Cp^*(dmpe)Cr)_2(\mu\text{-}N_2)](FB(C_6F_5)_3)]$ (**24**). 152

Scheme 3.6 Synthesis of $[(Cp^*(dmpe)Cr)_2(\mu\text{-}N_2)]BAr^F{}_4$ (**25**).....158

Scheme 3.7 Synthesis of $[(Cp^*(dmpe)Cr)_2(\mu\text{-}N_2)](BAr^F{}_4)_2$ (**26**).....165

Scheme 3.8 Synthesis of $[(Cp^*(dmpe)CrN]BAr^F{}_4$ (**29**) 177

Scheme 3.9 Synthesis of $[Cp^*Cr(HNPMe_2CH_2CH_2PMe_2)F]$ $BAr^F{}_4$ (**32**).....194

Scheme 3.10 Proposed mechanism for the production of $N[PMe_2CH_2]_2$ fragment...199

Scheme 4.1 Proposed mechanism for the coupling of two nitrides to make a dinitrogen complex.....214

Scheme B.1 Synthesis of $[Cp^*Cr(acac)THF]PF_6$ (**B.1**)…….272

Scheme B.2 Synthesis of [Cp*Cr(N^N)OTf]OTf (**B.2**)…….277

Scheme B.3 Synthesis of [Cp*Cr(depe)N] (**B.3**)……...282

Scheme B. 4 Synthesis of ([Cp*(dmpe)Cr](μ-N_2)[Cp*CrMe])$_2$(μ-dmpe) (**B.4**)……286

Scheme B. 5 Synthesis of [Cp*Cr(depe)N]BAr^F_4 (**B.5**)…….291

ABSTRACT

The discovery of mild methods for metal mediated cleavage of the dinitrogen triple bond to produce metal nitride derivatives is a fundamental aspect of nitrogen fixation. An important step in this process is to understand and study the factors that affect the ligated dinitrogen triple bond distance. Designing transition metal complexes that can coordinate to the free dinitrogen ligand, elongate the dinitrogen bond length and finally cleave its triple bonds with a low barrier, is of great importance.

Our group has previously worked on this project, using chromium complexes with two different ligand platforms, i.e. 2,4-Pentane-N,N'-bis (aryl or alkyl) ketiminato and (3-R,5-R'pyrazolyl)borate. In an effort to continue that work, this dissertation will describe the synthesis and structural characterization of a new chromium dinitrogen complex, namely $[Cp^*Cr(dmpe)]_2(\mu\text{-}N)_2$ (**10**), and it's desired cleavage product, i.e. $[Cp^*(dmpe)Cr{\equiv}N]$ (**13**), which was prepared by an independent method. **10** can be reduced and oxidized and the effect of these transformations on the N_2 ligand was monitored by structural studies.

Upon reduction of compound **10**, another dinitrogen compound with the formal Cr oxidation state of 0 was produced, namely $[Cp^*(dmpe)Cr(\mu\text{-}N_2)Na(TMEDA)_2]$ (**21**). Unexpectedly, formal reduction of chromium decreased the N-N bond distance from 1.195(4) A° in **10** to 1.175(4) A° in **21**. Upon oxidation of **10**, a mixed valent (Cr^{I}/Cr^{II}) dinitrogen compound was formed, namely $[(Cp^*(dmpe)Cr)_2(\mu\text{-}N_2)]BAr^{F}{}_4$ (**25**). The N-N bond distance in compound **25** showed an increase to 1.211(4) and 1.200(4) A°. Further oxidation of **10** resulted in a dicationic dinitrogen complex, namely $[(Cp^*(dmpe)Cr)_2(\mu\text{-}N_2)](BAr^{F}{}_4)_2$ (**26**), which showed an increase in the N-N bond distance compared to the neutral dinitrogen complex **10**, similar to the monocationic complex.

The oxidation of **13,** yielded the cationic nitride complex, i.e. [Cp*(dmpe)Cr≡N]BAr^F_4 (**29**). The neutral and cationic dinitrogen and nitride complexes were studied in different experiments including reduction, oxidation, heating and reacting with LA, to see if the interconversion of dinitrogen and nitride complexes can happen. From heating the neutral, monocationic and dicationic dinitrogen complexes, the neutral or the monocationic nitride complex were not produced. Heating the neutral nitride complex, produced a dinuclear chromium complex. In this complex the nitride does an insertion into the Cr-P bond to make a phosphiniminato ligand on the chromium complex, i.e. [$Cp^*_2Cr_2$(μ,μ-{$NP(CH_3)_2$}C_2H_4] (**19**). Upon heating the neutral, monocationic and dicationic dinitrogen complexes, the neutral or the cationic nitride complex were not produced and the neutral dinitrogen complex was decomposed to an unidentified mixture at high temperatures.

Due to the lack of experimental evidence for the interconversion between the dinitrogen and nitride isomers, it was decided to do DFT calculations to find out which way the reaction should go. DFT calculations were performed on the neutral and cationic complexes of dinitrogen and nitride to find the thermodynamic product of the interconversion reaction. The same calculations were done for the Cp analog of these complexes to get more information about the effect of Cp* ligand on the interconversion process. Based on the calculations, the dinitrogen complex is the thermodynamic product of the interconversion reaction and the $\Delta G^{\ddagger}$ for the interconversion was calculated to be 56.4 and 47.0 kcal/mol for the Cp*and Cp analog, respectively. These numbers are very large, suggesting an insurmountable intrinsic activation barrier for the formation of the N_2 molecule.

Chapter 1

INTRODUCTION

Dinitrogen, the most abundant gas in the atmosphere, is an essential element for living organisms and for industrial uses.[1] Its high thermodynamic bond strength and nonpolar nature makes it unreactive for transformations to more versatile molecules, and for this reason N_2 is usually used as an inert gas. The dinitrogen triple bond strength is extremely high (944.84 kJ/mol or 225 kcal/mol)[2,3] and the cleavage of the N–N triple bond necessitates harsh conditions in most cases.

Ammonia is the product of $6e^-$ reduction of dinitrogen in the presence of protons. The process in which dinitrogen is converted to more reactive compounds is called nitrogen fixation.[4] Industrially ammonia is produced on a large scale, for a low price, and can be easily stored.[5] NH_3 has been employed in medication, fertilizer, fuel, explosives, dyes, and chemical fibres.[6] Ammonia is a prominent carbon free energy source that can be used as a carrier for H_2 in fuel cells to avoid the difficulties related to low density hydrogen gas such as its production, storage, and transportation. Unlike hydrogen, NH_3 can be liquefied easily under 10 bar of pressure. Also, hydrogen can be recovered from the decomposition of NH_3 so the hydrogen fuel cycle will be closed by reproducing the H_2 gas from NH_3 and entering it to the H_2 fuel cells. The interconversion between ammonia and hydrogen (**Scheme 1.1**) provides a medium for handling and storage of hydrogen.[7–10]

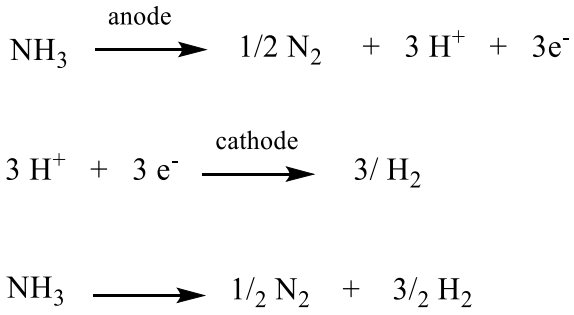

Scheme 1.1 The interconversion between ammonia and hydrogen. [9]

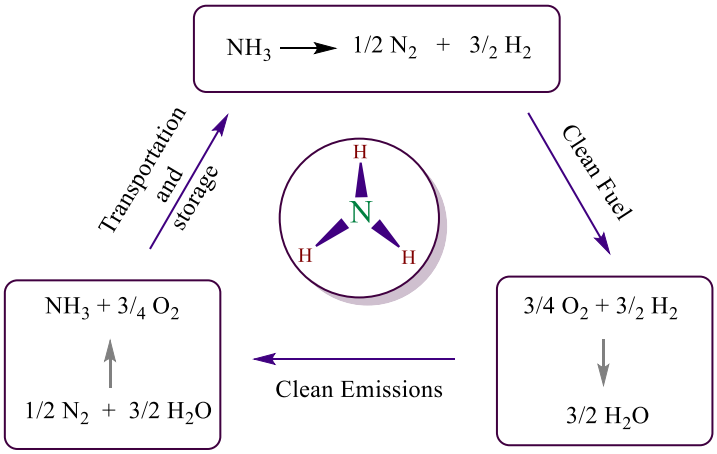

Figure 1.1 An ammonia fuel cycle involving the reduction of nitrogen coupled with water oxidation (lower left), the splitting of ammonia to nitrogen and hydrogen (top), and the oxidation of hydrogen (lower right).[8]

In industry ammonia is being produced via the energy intensive Haber-Bosch (HB) process via heterogeneous catalysis.[6,11–13] This revolutionary technique combines H_2 and N_2 gases to make ammonia at high pressures and temperatures (~500 °C, >100 atm), reflecting the challenge of cleaving the strong dinitrogen triple bond.

Various metals such as ruthenium, osmium, uranium, and, cobalt-molybdenum have been used as catalysts to reduce the activation energy of the dinitrogen reduction in

the Haber-Bosch process; however, iron is used most widely in practice due to its high abundance and low cost.[14]

The absorption and triple bond cleavage of dinitrogen, to make nitride (N^{3-}) on the iron surface sites with an average oxidation state between 0 and +1, is the rate limiting step in this process. In the next step, ammonia is produced by the combination of nitride with protons provided by dissociation of H_2 on the surface of heterogeneous iron catalyst.[12,14]

Although the Haber-Bosch process benefits from a perfect atom economy with no byproduct and a 97 % conversion of starting materials to products, an ideal feature for industrial-scale processes,[14] it has some issues like consumption of high amounts of energy as it uses H_2 (which is formed via energy intensive steam reforming of methane) as the H source and pollution the atmosphere by producing about 16.7 t of CO_2 per 1t NH_3 production. Considering about 0.4 gigatons of dinitrogen conversion to ammonia yearly, is a lot of CO_2 (3.34 gigatons) being produced by the Haber-Bosch process.[15,16] With the growth in population and increase in demand for global energy,[17–19] homogeneous nitrogen fixation at ambient condition via sustainable, environmentally benign, and carbon free[7] processes is of great importance.[4,15,16]

$$N_2\,(g) + 6\,e^- + 6\,H^+ \longrightarrow 2\,NH_3\,(aq) \qquad E^0 = 0.092\ V \quad \text{vs. NHE.}$$

There is great interest in replacing heterogeneous catalysts with homogeneous HB system as they can provide detailed information on reaction intermediates and mechanisms and do not need harsh reaction conditions.[3,12,20,21]

In nature nitrogen fixation is catalyzed by metalloenzymes called Nitrogenases under ambient temperature and pressure. However, this process requires energy and for each dinitrogen reduction, 16 ATP are consumed. Compared to Haber-Bosch, nitrogenase is more effective for ammonia production.[22] This transformation happens on the Mo-Fe cofactors of nitrogenase enzymes but their exact site of dinitrogen coordination and reduction is still in debate.[23]

Based on many studies, two possible pathways have been proposed for the dinitrogen fixation on nitrogenase enzymes, i.e. the distal (D) and alternating (A) pathway, as shown in Figure 1.2.

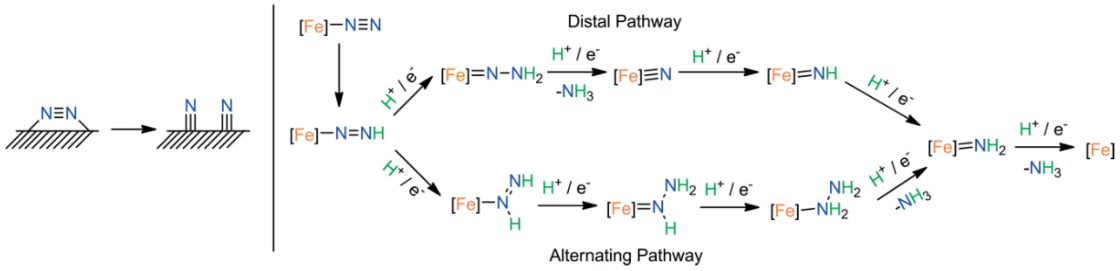

Figure 1.2 Dissociation of dinitrogen. Haber-Bosch mechanism (left), Nitrogenase mechanisms (right). [14,22]

In the distal pathway one nitrogen atom is protonated first and then released as NH_3. The remaining part, which is a nitrido species, is protonated after that and by production of the second molecule of ammonia, the cycle is complete. In the alternating pathway both nitrogen atoms get protonated and two ammonia molecules release simultaneously.[22]

Since the industrial nitrogen activation and ammonia production requires harsh reaction conditions, development of energy efficient and environmentally benign methods for reduction of dinitrogen to ammonia is highly desirable and has drawn the attention of numerous research groups world-wide.[20,21]

In this regard, the chemistry of dinitrogen adducts of transition metals can provide important insights into the structure-function relationship in nitrogenase enzyme and the HB process. Therefore extensive studies have been carried out on this subject over the past decades.[3,24–26]

For the first time in1995, Cummins et al. reported reductive cleavage of dinitrogen to two N^{3-} ligands.[27] In this process, $Mo(NRAr)_3$ [R = $C(CD_3)_2CH_3$; Ar = 3,5-$C_6H_3Me_2$] reacts with N_2 to make a binuclear μ-N_2 complex, which can thermally cleave the nitrogen-nitrogen triple bond to produce nitrido molybdenum(VI) complex $N{\equiv}Mo(NRAr)_3$, as shown in **Scheme 1.2**. In this process the Mo fragment that binds N_2 and the intermediate can be characterized spectroscopically at low temperature (-35°C). Mechanistic and theoretical studies have been done on this reaction.[28,29] Based on these computational studies, a zig-zag structure for transition state has been proposed.

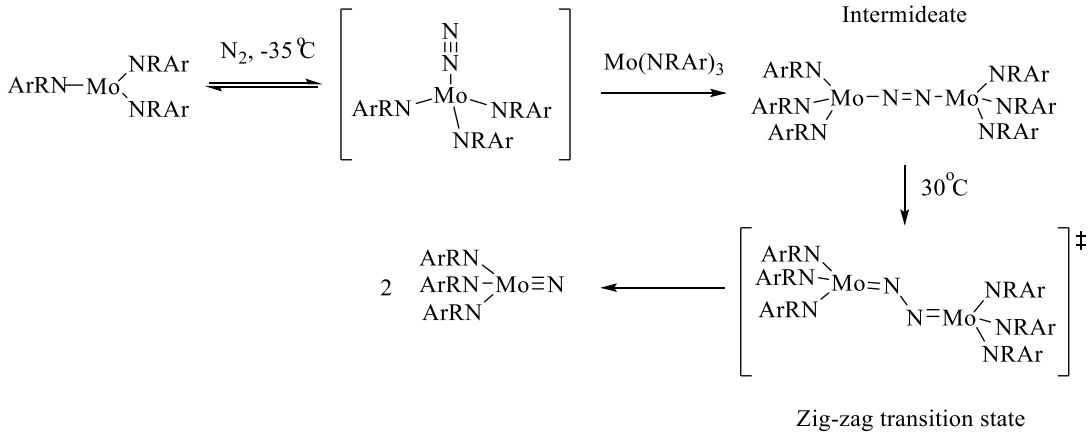

Scheme 1.2 Cleavage of N_2 using $Mo(NRAr)_3$.

In 2001, similar work was published by Floriani et. al.[30] In this study, the N≡N triple bond was cleaved using light and transition metal complexes. The $[Mo(Mes)_3]$ fragment (Mes= 2,4,6-$Me_3C_6H_2$) reacts with N_2 to produce $[(Mes)_3Mo]_2(\mu\text{-}N_2)$, which can cleave the N-N bond photolytically using UV light. Floriani et. al. suggested that the result of this reaction is presumably the monomeric nitride complex $[(Mes)_3MoN]$, which quickly reacts with $[(Mes)_3Mo]_2(\mu\text{-}N_2)$ and forms an intermediate $(\mu\text{-}N_2)[(Mes)_3MoNMo(Mes)_3]_2$. This intermediate can release N_2 to make the final complex $[(Mes)_3\,Mo]_2\,(\mu\text{-}N)$, as shown in **Scheme 1.3**. $[(Mes)_3Mo]_2(\mu\text{-}N_2)$ is thermally stable, so the cleavage of N-N bond was achieved by exposure to UV light (λ= 365 nm).

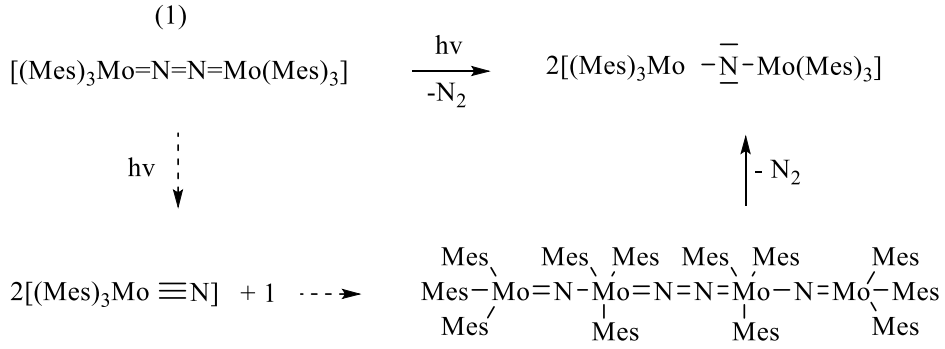

Scheme 1.3 The photochemical activation of the N≡N bond.

In 2002, Fryzuk et. al. designed a system that can activate dinitrogen and the result of N-N bond cleavage is a nitrido complex.[31] In their work, the dinuclear end-on niobium dinitrogen complex ($[P_2N_2]Nb)_2(\mu\text{-}N_2)$ ($[P_2N_2]$= $PhP(CH_2SiMe_2NSiMe_2CH_2)_2PPh$), was synthesized and characterized. This complex can undergo N-N bond cleavage thermally. The result is a bridging nitrido species and one of the activated N atoms inserts into the $[P_2N_2]$ ligand to form $[P_2N_2]Nb(\mu\text{-}N)Nb[PN_3]$ ($[PN_3]$=$PhPMe(CHSiMe_2NSiMe_2CH_2P(Ph)CH_2SiMe_2NSiMe_2N)$), as shown in **Scheme 1.4**.

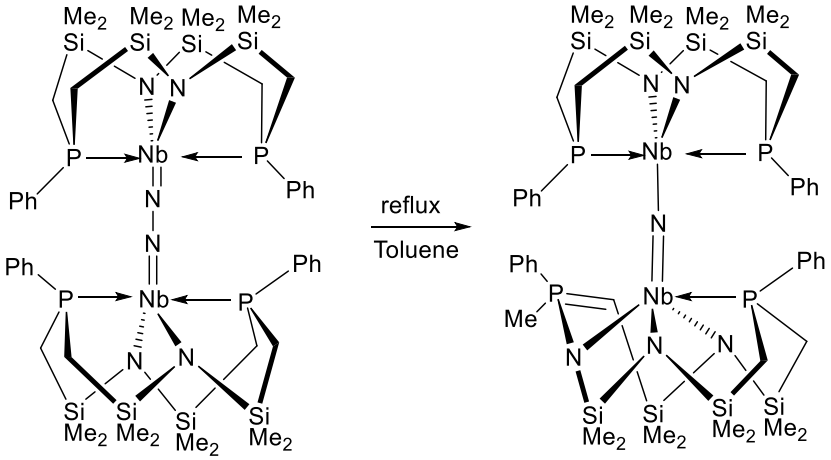

Scheme 1.4 The thermolysis of $([P_2N_2]Nb)_2(\mu\text{-}N_2)$.

In 2004, Peters et. al. reported an example of coupling of two nitrido complexes to generate a dinitrogen complex.[32] The iron nitrido complex $[PhBP^{iPr}_3]Fe{\equiv}N$ ($[PhBP^{iPr}_3]$= $[PhB(CH2P^{iPr}_2)_3]^-$) reported by this group can transform to the dinitrogen complex $([PhBP^{iPr}_3]Fe)_2(\mu\text{-}\eta^1{:}\eta^1\text{-}N_2)$. As shown in **Scheme 1.5**, from the reaction of starting iron complex with lithium amide reagent Li(dbabh) (dbabh= 2,3:5,6-dibenzo-7-azabicyclo[2.2.1]hepta-2,5-diene), amide complex $[PhBP^{iPr}_3]Fe$(dbabh) was generated as an intermediate. They monitored the existence of this intermediate using NMR spectroscopy. $[PhBP^{iPr}_3]Fe$(dbabh) is thermally unstable at room temperature. This intermediate can transform to iron nitrido complex $[PhBP^{iPr}_3]Fe{\equiv}N$, which can undergo bimolecular coupling at room temperature under argon atmosphere or vacuum to generate end-on bridged dinitrogen complex $\{[PhBP^{iPr}_3]Fe\}_2(\mu\text{-}N_2)$.

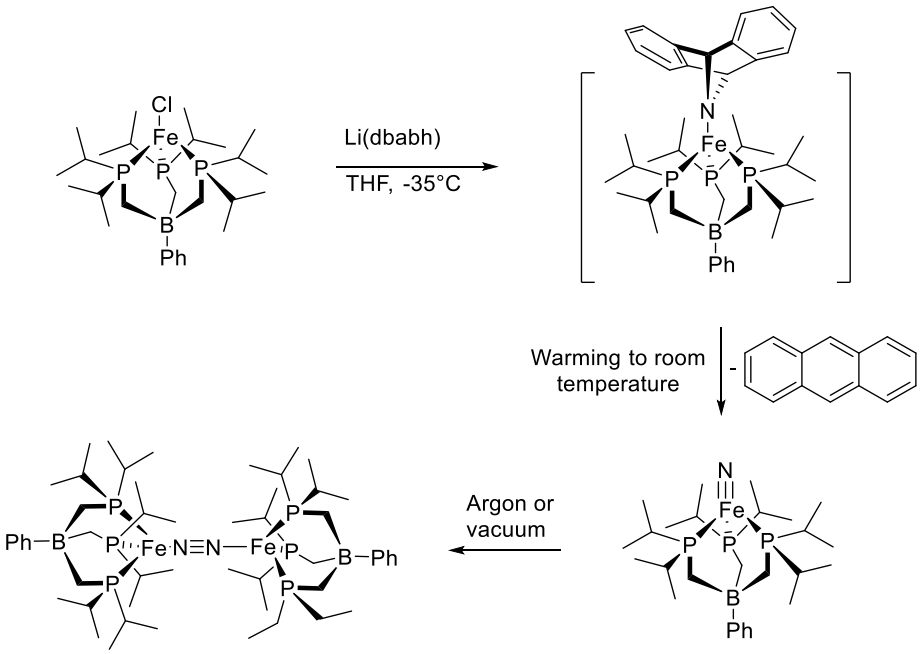

Scheme 1.5 Conversion of Nitrido complex to N_2 bridging isomer.

In 2007, Sita et. al. reported an end-on bridged $[Ta(IV)]_2(\mu\text{-}\eta^1\text{:}\eta^1\text{-}N_2)$ complex that converts to the bis(μ-nitrido) complex at temperatures above 0°C. This was the first example of conversion of a linear $[M]_2(\mu\text{-}\eta^1\text{:}\eta^1\text{-}N_2)$ structure to a $[M(\mu\text{-}N)]_2$ diamond core in which a complete N≡N bond cleavage happens.[33] The author proposed that this transformation involves an intramolecular structural isomerization ($\mu\text{-}\eta^1\text{:}\eta^1\text{-}N_2$ to $\mu\text{-}\eta^2\text{:}\eta^2\text{-}N_2$).[34,35]

Later in 2015, they reported similar reactions using $[M(IV)]_2(\mu\text{-}\eta^1\text{:}\eta^1\text{-}N_2)$ complexes (M: Nb, Mo and W). The results showed similar behavior for Nb and Ta but for Mo and W the conversion of dinitrogen complex to bis(μ-nitrido) can happen photochemically, but not thermally because too much steric hindrance around the ligand, prevents access to the required transition state geometry in these molecules.[34,36]

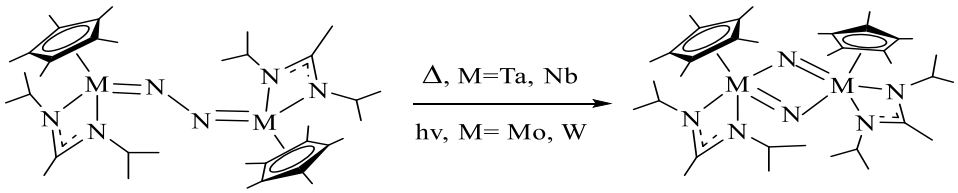

Scheme 1.6 Conversion of dinitrogen complex to bis(μ-nitrido) isomer.

In 2012, Mindiola et. al. reported the first three-coordinate vanadium(II) complex [(nacnac)V(ODiiP)] ($nacnac^-$ = $[ArNC(CH_3)]_2CH$, Ar = 2,6-$^i Pr_2C_6H_3$, ODiiP = 2,6-diisopropylphenoxide), which was synthesized from the reduction of the starting vanadium complex [(nacnac)VCl(ODiiP)] using Na/Hg under argon atmosphere as shown in **Scheme 1.7**.[37] In the presence of nitrogen gas, the three-coordinate vanadium complex [(nacnac)V(ODiiP)] can bind N_2 to form the end-on bridging dinitrogen complex $[(nacnac)(ODiiP)V]_2(\mu_2\text{-}\eta^1\text{:}\eta^1\text{-}N_2)$ with a singlet ground state. The fragmentation of this divanadium dinitrogen complex to vanadium(V) nitride molecules was not observed (calculated energy barrier for the conversion of dinitrogen complex to the nitride isomer is 83 kcal/mol), although this complex has enough electrons to populate

all the π* and σ* orbitals of N_2. The terminal nitride complex [(nacnac)V≡N(ODiiP)], can be made from the reaction of starting complex [(nacnac)VCl(ODiiP)] with NaN_3.

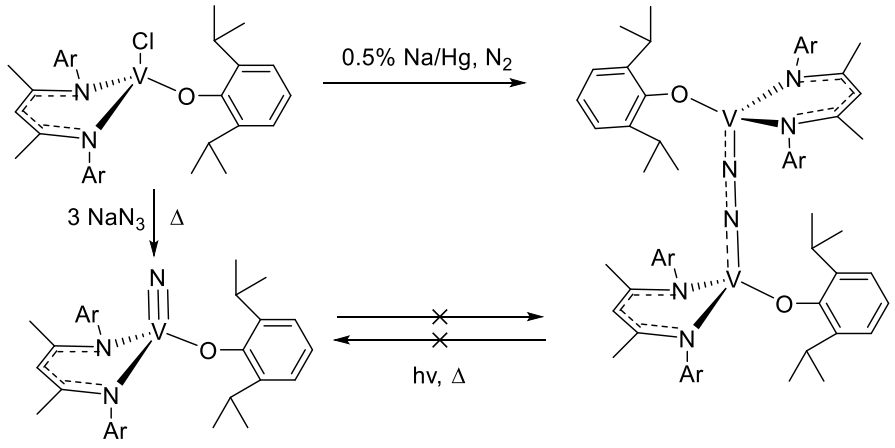

Scheme 1.7 Synthesis of dinitrogen and nitride complexes from the vanadium [(nacnac)VCl(ODiiP)] precursor.

In 2014, Nishibayashi et. al. reported a dinuclear molybdenum dinitrogen complex that undergoes N-N bond cleavage under visible light at room temperature and the result of this reaction is the corresponding molybdenum nitrido complex. As shown in **Scheme 1.8**, oxidation of this molybdenum nitrido complex at room temperature, reformed the bridging molecular dinitrogen. This is an example of cleavage and formation of molecular dinitrogen, in a single system.[38]

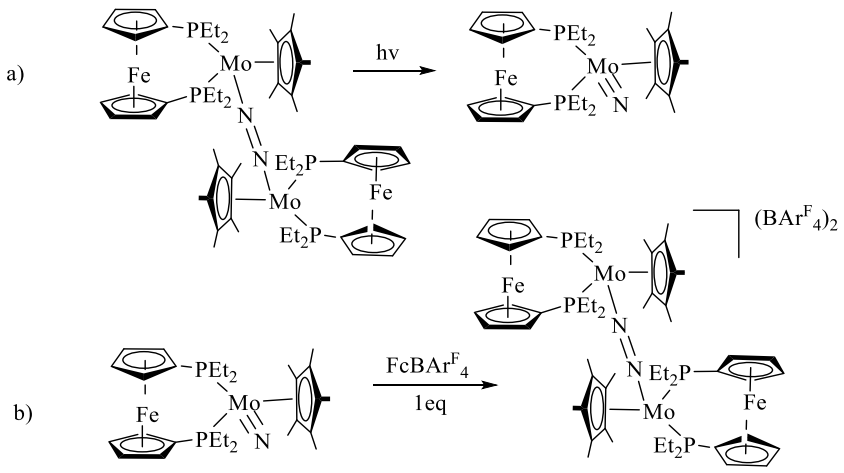

Scheme 1.8 a) Photoinduced conversion of dinitrogen complex to the nitrido complex. b) Oxidation of the nitrido complex led to its dimerization to generate the dinitrogen-bridged complex.

In 2017, Schneider et. al. reported the bridged molybdenum dinitrogen complex [{(PNP)ClMo}$_2$(N$_2$)], which was made by the reduction of starting complex [MoCl$_3$(PNP)] under nitrogen atmosphere. The dinitrogen cannot be activated thermally and even upon prolonged heating to 60°C, over several hours this complex is stable with respect to N$_2$ cleavage. The nitride complex [Mo(N)Cl(HPNP)]X (X=OTf, BAr$^F_4$) was made upon protonation of the dinitrogen complex with 1–2 equiv HOTf or [H(OEt$_2$)$_2$]BAr$^F_4$ (BAr$^F_4^-$ = B(C$_6$H$_3$-3,5-(CF$_3$)$_2$)$_4^-$) at room temperature as shown in **Scheme 1.9**.[39]

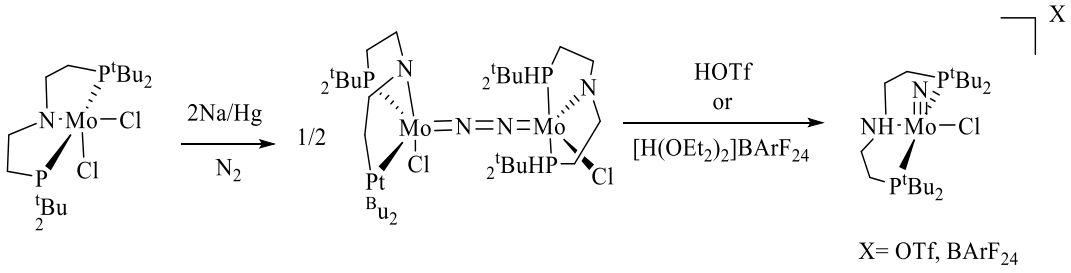

Scheme 1.9 Dinitrogen splitting with molybdenum complex.

1.1 Conclusion

Due to the high thermodynamic bond strength and nonpolar nature of dinitrogen gas, it is usually used as an inert gas. The 944.84 kJ/mol bond strength is not easy to overcome at normal conditions, therefore in Haber-Bosch process high temperatures and pressures are required to transform N_2 gas to ammonia. In nature nitrogen fixation is catalyzed by metalloenzymes called Nitrogenase under ambient conditions, on the Mo-Fe cofactors of nitrogenase enzyme. Since the industrial nitrogen activation and ammonia production requires harsh reaction conditions, development of energy efficient methods for reduction of dinitrogen to ammonia is highly desirable. Several examples of dinitrogen and nitride complexes, that are able to interconvert between the two isomers, were shown in this chapter. These interconversions can happen in different conditions such as thermally or photochemically.

Chapter 2

SYNTHESIS AND CHARACTERIZATION OF CHROMIUM DINITROGEN AND NITRIDE COMPLEXES

2.1 Introduction

In all reported nitrogen functionalization processes the cleavage of dinitrogen triple bond is the most important step, therefore controllable splitting of N_2 to produce metal nitrides is a fundamental process in nitrogen activation reaction.

The coordination of the inert dinitrogen to metal centers provides a pathway to overcome its low reactivity and makes it possible for it to be used to synthesize nitrogen containing compounds. Dinitrogen as a ligand has different modes of coordination to the metal center, which is highly dependent to the nature of metal, the oxidation state of metal, and the ligand platform around the metal center. On the other hand, the mode of coordination of dinitrogen to the metal center provides an important role in its activation. The most common modes of N_2 coordination are terminal End-on, bridging End-on, bridging Side-on and bridging Side-on End-on coordination mode, as shown in **Scheme 2.1**.[40]

In end-on dinitrogen complexes the bonding between the dinitrogen ligand and the transition metal center comprises sigma donation from N_2 to metal and back donation from metal to π^*-orbitals of dinitrogen, as shown in **Figure 2.1**.

The amount of back bonding from the transition metal center to antibonding orbitals of dinitrogen can affect the dinitrogen activation or reduction via metal. Since electrons transfer to the π^*-orbitals of N_2 during the back bonding, the bond length of N≡N increases based on the amount of back bonding (The bond length in free N_2 is 1.0975

Å).[42,43] Metals with low or negative formal oxidation states can have sufficient electron density for the back bonding and their extended valence orbitals enable a better overlap with the ligand π*- orbitals.[41,44]

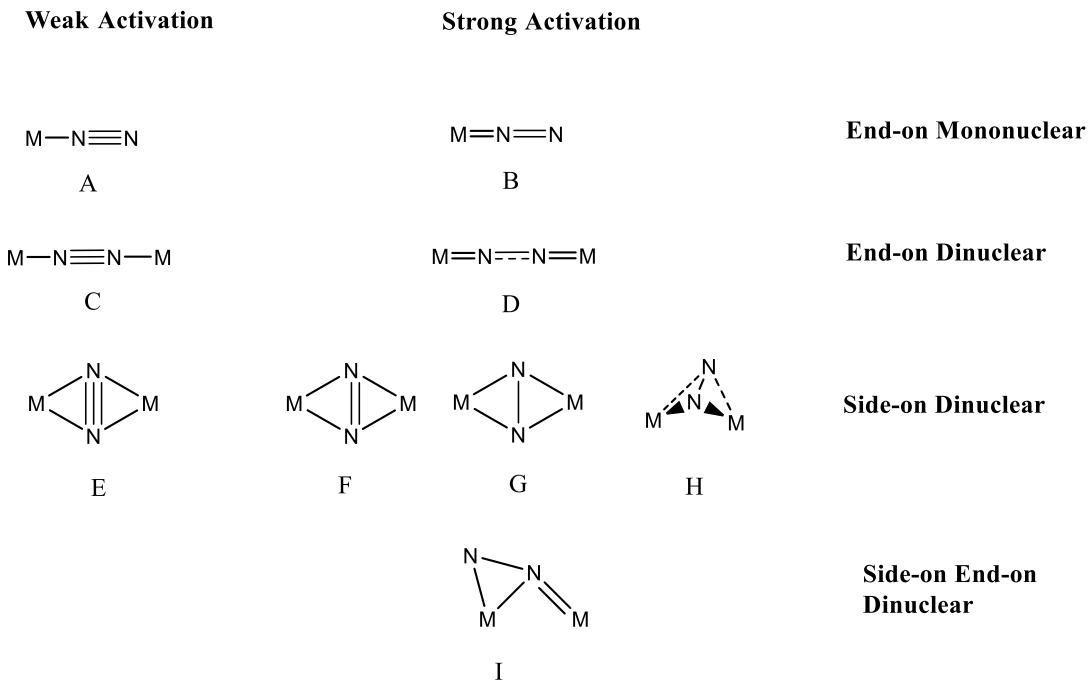

Scheme 2.1 Different modes of coordination of N_2 ligand in dinitrogen complexes.[41]

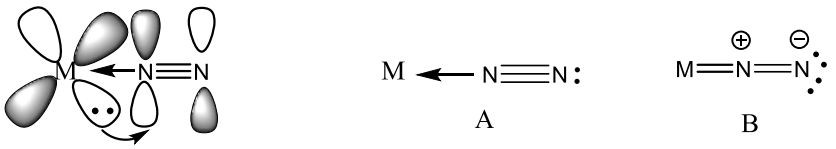

Figure 2.1 Bonding in end-on dinitrogen complexes. B is a resonance structure of σ-bonded A and can describe the back bonding between the N_2 and the metal center.[41]

Aside from the nature of the transition metal, the rational design of ligands is a crucial step to design a transition metal complex that can activate and functionalize dinitrogen. Since N_2 is a poor ligand, it can readily dissociate from the metal center and create a free coordination site that enhances the reactivity of metal center by coordinating to other ligands. Electron rich ancillary ligands can improve the π backdonation to the antibonding orbitals of dinitrogen, increase the interaction between metal center and dinitrogen and decrease the tendency of dinitrogen dissociation.

Although N_2 is a neutral and weak π-acceptor ligand, dinitrogen complexes of almost all transition metals in the periodic table are known.[4,7,21,45–51] The activity of Mo and W from group VI in the periodic table toward nitrogen activation have been vastly investigated. Many examples of Mo and W systems that can activate dinitrogen to produce the related nitride derivative have been explored.[52–59]

In the interconversion process of dinitrogen and nitride complexes, one of the isomers is the kinetic product and the other one is the thermodynamic product. Although the interconversion between the isomers is thermodynamically downhill, the process is very slow in some cases. The problem we aim to address is to develop a chromium-based system with an appropriate ligand platform that can be used to synthesize dinitrogen and nitride complexes. After the synthesis of the dinitrogen or nitride complex of that system, the propensity of the two derivatives to interconvert can be studied. Also, more information can be gained about the factors that affect the interconversion process between a nitride and its dinitrogen isomer.

Our group has worked on this project with two different ligand platforms which will be discussed here.

In 2007, Monillas et. al. reported the chromium dinitrogen complex [(i-Pr_2Ph)$_2$nacnacCr]$_2$(μ-N_2)], which was synthesized by reduction of starting complex [(i-Pr_2Ph)$_2$nacnacCr(μ-I)]$_2$ under nitrogen atmosphere.[60] Although this compound did not show isomerization, it was the first example of chromium complex with the side-on bonding of dinitrogen in the μ_2-η^2:η^2 coordination mode. They also reported the bridging

azido complex $[(i\text{-}Pr_2Ph)_2nacnacCr]_2(\mu\text{-}N_3)_2]$, which was synthesized from the reaction of $[(i\text{-}Pr_2Ph)_2nacnacCr(\mu\text{-}I)]_2$ with NaN_3.

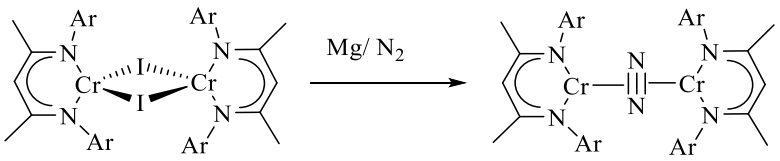

Ar= 2,6-diisopropylphenyl

Scheme 2.2 Side-on dinitrogen chromium complex.

In 2017, Hung from our research group studied the transformation of this azido complex to the side-on dinitrogen complex as shown in **Scheme 2.3**. A bis(μ-nitrido) complex $[(i\text{-}Pr_2Ph)_2nacnacCr]_2$ $(\mu\text{-}N)_2$ was reported as an intermediate in this transformation.[61] The thermal conversion of bis(nitride) complex to the dinitrogen complex was not observed in this system.

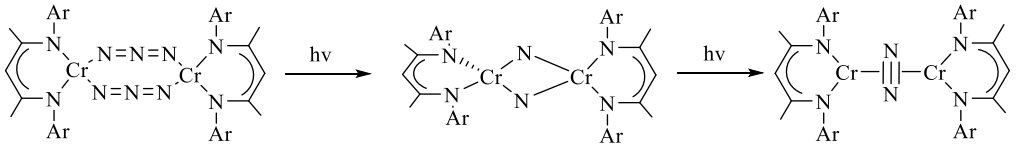

Ar= 2,6-diisopropylphenyl

Scheme 2.3 Transformation of chromium azido complex to the dinitrogen isomer.

In a separate work in 2017, Cummins from our research group synthesized the chromium nitride complex $[Tp^{tBu,Me}Cr{\equiv}N]$ from the reaction of H-dbabh with $[Tp^{tBu,Me}CrEt]$. In contrast to the work that was done by Peters et. al.,[32] attempts to convert

this complex to the dinitrogen form were unsuccessful and [Tp^{tBu,Me}Cr≡N] even at high temperatures does not convert to the known chromium dinitrogen complex [Tp^{tBu,Me}Cr]$_2$(μ-η^1:η^1-N$_2$).[62]

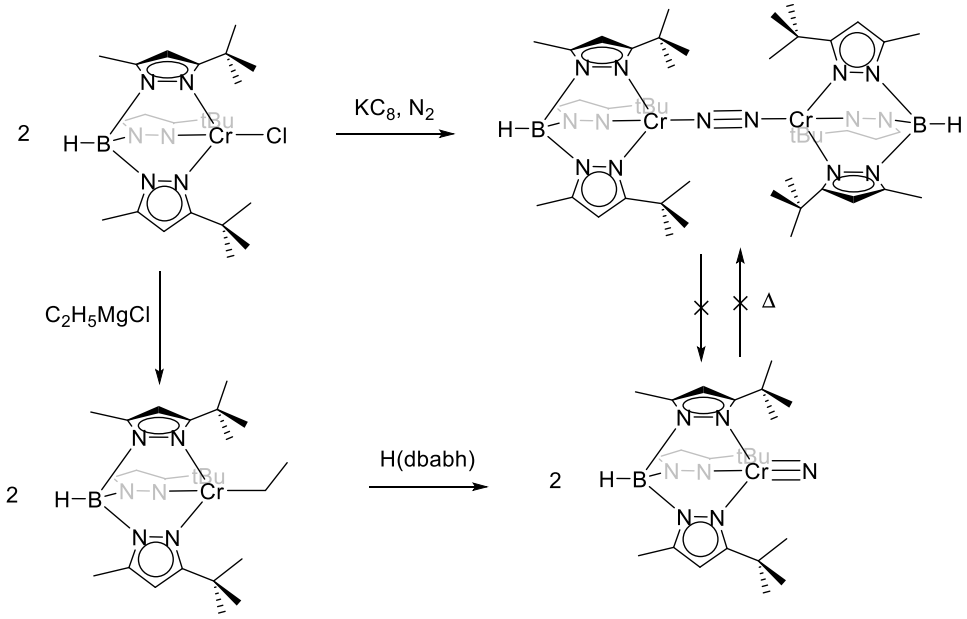

Scheme 2.4 Synthesis of dinitrogen and nitride complexes from the chromium [Tp^{tBu,Me}CrCl] precursor.

After getting the results from these two nitrogen donor ligands (nacnac and Tp′) our group decided to try a different carbon based ligand platform. Pentamethylcyclopentadienyl (Cp*) was chosen for this project. Cp* is a strong donor ligand, easy to synthesize and provides a good environment for low oxidation state chromium complexes. Also, Nishibayashi showed that this ligand with Mo metal (Cp*ML$_2$) can cleave the nitrogen triple bond to make the terminal nitride isomer.[63] The starting complex that we used, i.e., [Cp*Cr(μ-Cl)]$_2$ is a dinuclear complex, which was synthesized from the reaction of Cr(II)Cl$_2$ with Cp*Li in THF, as shown in **Scheme 2.5**.[64]

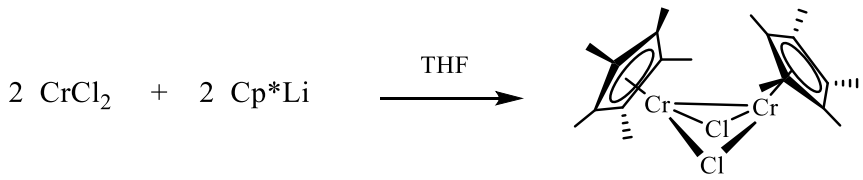

Scheme 2.5 Synthesis of $[Cp^*Cr(\mu\text{-}Cl)]_2$.

The formal oxidation state of each chromium in this complex is II. This dinuclear complex in the presence of coordinating ligands can split in half and open a coordination site for that ligand. Therefore, in theory this complex can provide enough space for the coordination of dinitrogen ligand and the metal center can provide enough electron density needed for the reduction of the N_2 triple bond to make two N^{3-} derivatives.

2.2 Results and Discussion

The reduction of $[Cp^*Cr(\mu\text{-}Cl)]_2$ was carried out under nitrogen gas in a glove box using different reducing agents such as Li, Na, K, KC_8, Mg, Al, Zn, and Mn with a variety of solvents such as THF, diethyl ether, toluene, and pentanes, with the aim of synthesizing a dinitrogen complex or nitride version of this chromium complex. Unfortunately, $[Cp^*Cr(\mu\text{-}Cl)]_2$ did not react with reducing agents like Mg, Al, Mn and Zn even after a couple of days and the result of reduction of this chromium (II) complex with stronger reducing reagents like Na, K and, KC_8 was decamethyl-chromocene and a black precipitate which can be the metallic chromium, as shown in **Scheme 2.6**. The decamethyl-Chromocene was identified using ^{1}H-NMR spectroscopy. A peak at 6.2 ppm was observed in the proton NMR of the product in C_6D_6, which was assigned to the decamethyl-Chromocene.[65]

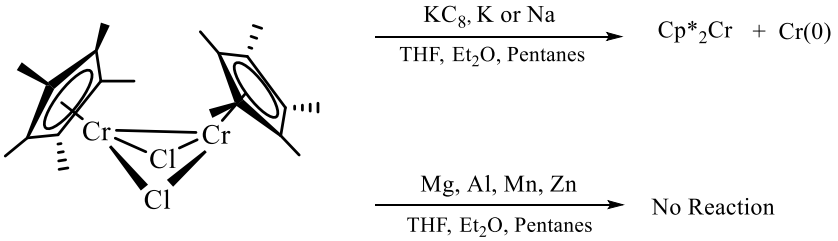

Scheme 2.6 Reduction of $[Cp^*Cr(\mu\text{-}Cl)]_2$ under dinitrogen gas using different reducing reagents.

A common method to synthesize nitride complexes is using azido reagents. The reaction of $[Cp^*Cr(\mu\text{-}Cl)]_2$ with NaN_3 or KN_3 was done in different solvents such as pentanes, toluene, diethyl ether, and THF to see if it can produce a nitride complex.

After addition of NaN_3 to the solution of $[Cp^*Cr(\mu\text{-}Cl)]_2$, bubbles started to evolve from the solution, presumably N_2 gas, and the color of solution changed from brown to red brown after a couple of minutes and then another color change to green after about 30 minutes of stirring, was observed. If the reaction continues to stir overnight the color of solution can change from green to brown again. Based on these color changes it can be concluded that several compounds are being produced during this reaction. In the NMR of the product there are many broad and shifted peaks which suggest the formation of a mixture of paramagnetic compounds as shown in **Figure 2.2**.

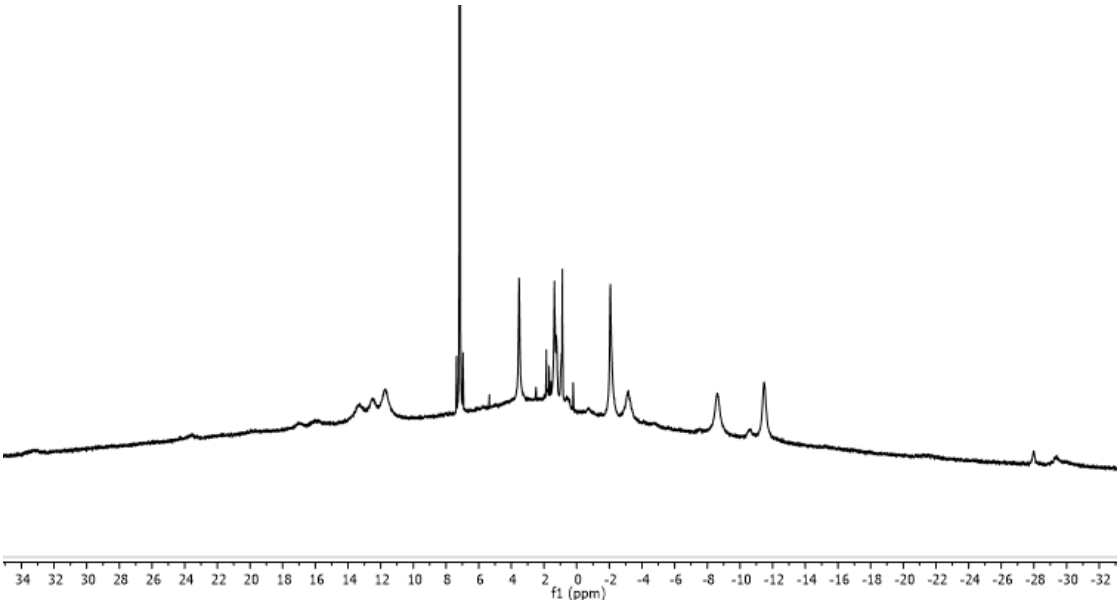

Figure 2.2 ^{1}H-NMR spectrum of reaction of $[Cp^*Cr(\mu\text{-}Cl)]_2$ with NaN_3 in THF after 3 h, recorded in C_6D_6 at 400 MHz.

This reaction was so complicated and after many trials with different conditions (time, temperature, solvent, and slow inverse addition of Cr to an excess of azide) and using different azido reagents like NaN_3, KN_3 and $TMSN_3$ finally one compound was extracted from this mixture which will be discussed here. After addition of 2 equivalents of NaN_3 to the THF solution of $[Cp^*Cr(\mu\text{-}Cl)]_2$, the bubbles started to appear, and the color of solution changed to green after about 15 minutes. After stirring the solution for 4 hours, the color changed to brown. Then the solution was filtered, and the solvent was evaporated under vacuum. The remaining brown powder was dissolved in pentanes which made a green-brown solution. The solution was filtered again, and some part of the solvent was removed under vacuum to make a concentrated solution. The solution was kept at -30 C for overnight and some green-brown crystals precipitated out of the solution during this time, but the quality of these crystals were not good enough for X-ray crystallography. The solution above the crystals was transferred to another vial (no lid) and was kept at room temperature for a couple of minutes and some brown crystals started

to come out of solution as the solution became more concentrated by the evaporation of solvent. Determination of the structure by X-ray crystallography revealed it to be a tetranuclear chromium nitride complex, i.e. $[Cr(\mu\text{-}\eta^5\text{:}\eta^1\text{-}C_5Me_4CH_2)Cr_3Cp^*_3N_3H_x(Cl)]$ (**1**). Based on the crystal structure we can see electron density of one H on the N2 ligand, but in the IR spectrum of the compound the peak related to the NH group was not observed. On the other hand, the mass spectrum of **1**, collected using LIFDI-MS, displayed the molecular ion peak that is consistent with the presence of three NH groups in the molecule, shown in **Figure 2.4**. The bond distances between Cr centers and nitride ligands (1.783(7) to 2.01(1) Å) fall into the range for Cr-N single bond distances.[60,66]

The molecular structure of **1** is depicted in **Figure 2.3** while the corresponding interatomic distances and angles are listed in **Table 2.1**.

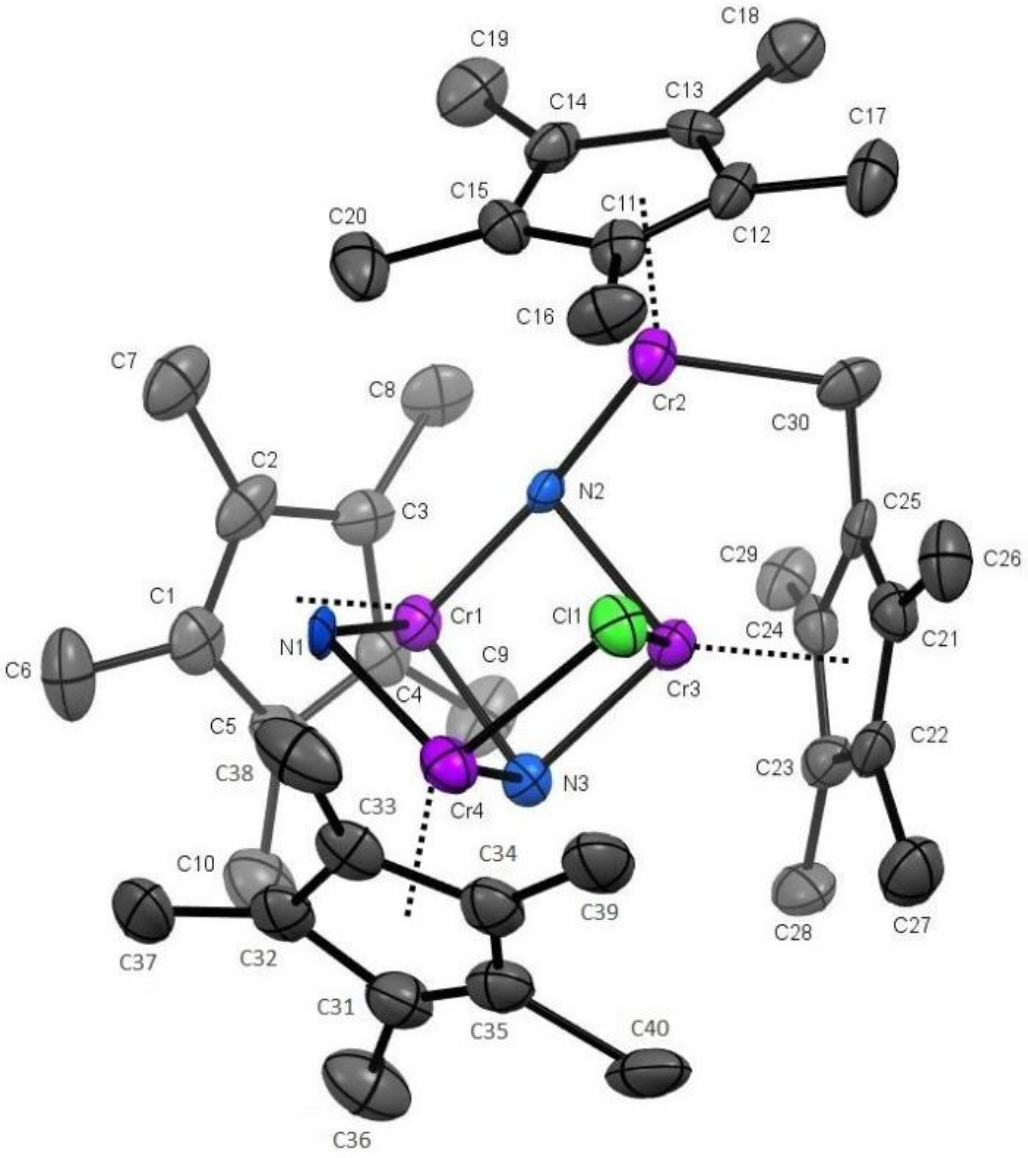
C18
C19
C14
C13
C17
C15
C11
C20
C12
C16
C7
C8
Cr2
C30
C2
N2
C25
C3
C29
C26
C1
Cr1
Cl1
C24
C21
N1
C9
C6
C4
Cr3
C5
C22
C38
C23
N3
C33
Cr4
C10
C34
C39
C28
C27
C37
C32
C31
C35
C40
C36

a

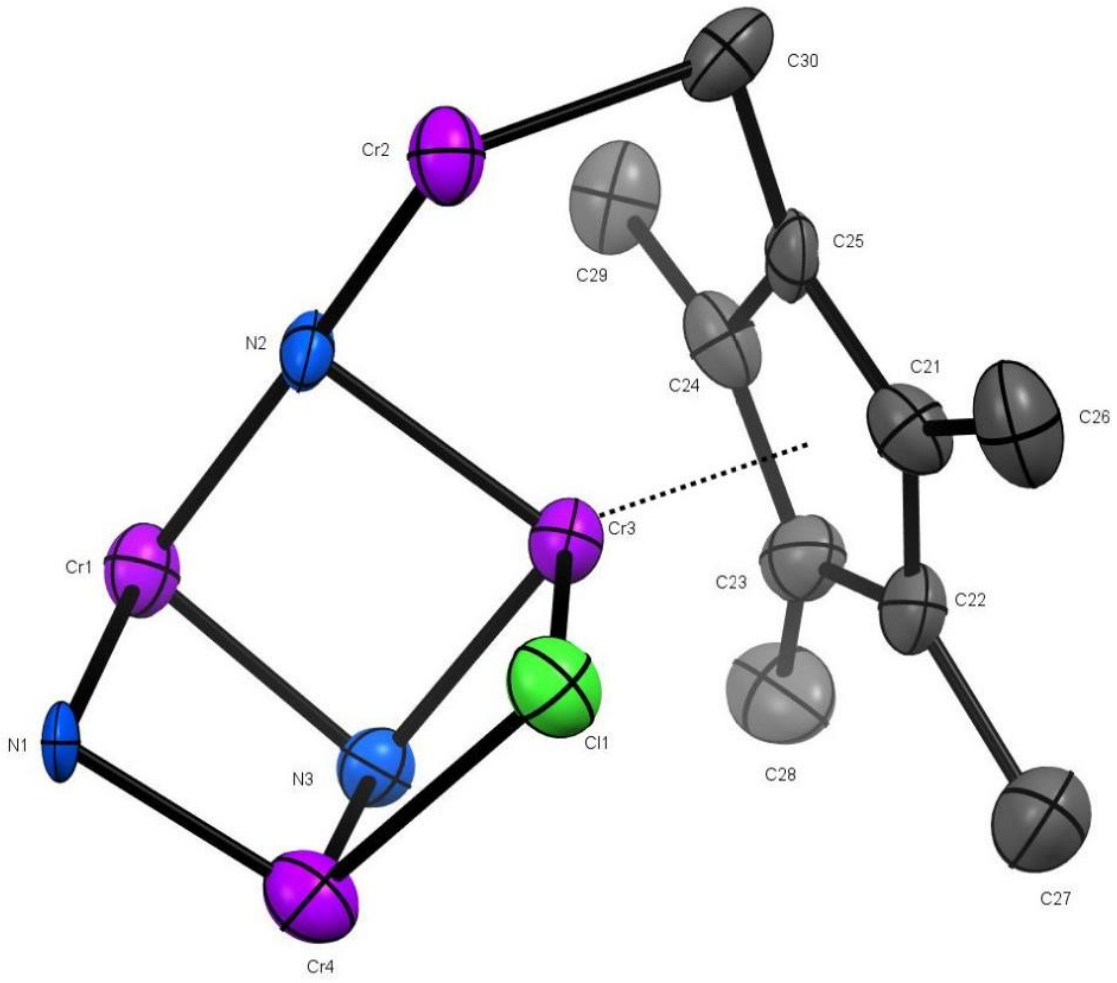

b

Figure 2.3 Molecular structure of the $[Cr(\mu\text{-}\eta^5{:}\eta^1\text{-}C_5Me_4CH_2)Cr_3Cp^*_3N_3H_x(Cl)]$ (**1**) represented as 50% probability thermal ellipsoids. Hydrogen atoms and a pentane molecule have been omitted for clarity. a) **1** with Cp* ligands shown in the structure, b) Three Cp* ligands are omitted for clarity.

Table 2.1 Interatomic distances (Å) and angles (º) for [Cr(μ-η^5:η^1-$C_5Me_4CH_2$)$Cr_3Cp^*_3N_3H_x$(Cl)] (**1**).

Distances (Å)

Cr1-Cr3	2.627(3)	C2-C3	1.43(2)
Cr1-Cr4	2.599(3)	C2-C7	1.49(2)
Cr1-N1	2.008(10)	C3-C4	1.385(19)
Cr1-N2	1.837(9)	C3-C8	1.52(2)
Cr1-N3	1.913(10)	C4-C5	1.42(2)
Cr1-C1	2.329(14)	C4-C9	1.52(2)
Cr1-C2	2.286(13)	C5-C10	1.50(2)
Cr1-C3	2.262(14)	C11-C12	1.370(18)
Cr1-C4	2.285(13)	C11-C15	1.407(18)
Cr1-C5	2.321(14)	C11-C16	1.519(19)
Cr2-Cr3	2.826(3)	C12-C13	1.416(17)
Cr2-N2	1.785(9)	C12-C17	1.504(18)
Cr2-C11	2.313(12)	C13-C14	1.415(18)
Cr2-C12	2.318(13)	C13-C18	1.487(18)
Cr2-C13	2.272(12)	C14-C15	1.443(18)
Cr2-C14	2.263(13)	C14-C19	1.486(18)
Cr2-C15	2.259(13)	C15-C20	1.495(18)
Cr2-C30	2.100(14)	C21-C22	1.392(19)
Cr3-Cr4	2.829(3)	C21-C25	1.428(18)
Cr3-Cl1	2.333(4)	C21-C26	1.526(19)
Cr3-N2	1.996(9)	C22-C23	1.421(19)
Cr3-N3	1.977(10)	C22-C27	1.524(19)
Cr3-C21	2.241(13)	C23-C24	1.432(18)
Cr3-C22	2.217(13)	C23-C28	1.506(19)
Cr3-C23	2.244(13)	C24-C25	1.469(18)
Cr3-C24	2.207(13)	C24-C29	1.488(18)

Cr3-C25	2.241(13)	C25-C30	1.426(18)
Cr4-Cl1	2.319(4)	C31-C32	1.50(10)
Cr4-N1	1.829(9)	C31-C35	1.29(10)
Cr4-N3	1.938(10)	C31-C36	1.57(9)
Cr4-C31	2.35(8)	C32-C33	1.57(12)
Cr4-C32	2.26(7)	C32-C37	1.39(9)
Cr4-C33	2.30(9)	C33-C34	1.50(17)
Cr4-C35	2.42(10)	C33-C38	1.47(11)
C1-C2	1.40(2)	C34-C35	1.27(14)
C1-C5	1.42(2)	C34-C39	1.41(14)
C1-C6	1.50(2)	C35-C40	1.72(12)

Angles (º)

Cr4-Cr1-Cr3	65.54(8)	N3-Cr4-C33	154(2)
N1-Cr1-Cr3	99.1(3)	N3-Cr4-C35	102(3)
N1-Cr1-Cr4	44.5(3)	C31-Cr4-C35	31(2)
N1-Cr1-C1	84.6(5)	C32-Cr4-Cl1	141(2)
N1-Cr1-C2	96.4(5)	C32-Cr4-C31	38(2)
N1-Cr1-C3	132.6(5)	C32-Cr4-C33	40(3)
N1-Cr1-C4	142.8(5)	C32-Cr4-C35	58(3)
N1-Cr1-C5	108.6(6)	C33-Cr4-Cl1	101(2)
N2-Cr1-Cr3	49.3(3)	C33-Cr4-C31	60(3)
N2-Cr1-Cr4	97.8(3)	C33-Cr4-C35	55(4)
N2-Cr1-N1	100.5(4)	Cr4-Cl1-Cr3	74.92(12)
N2-Cr1-N3	97.9(4)	Cr4-N1-Cr1	85.1(4)
N2-Cr1-C1	139.1(6)	Cr1-N2-Cr3	86.4(4)
N2-Cr1-C2	104.1(6)	Cr2-N2-Cr1	169.2(6)
N2-Cr1-C3	89.9(5)	Cr2-N2-Cr3	96.6(4)
N2-Cr1-C4	112.2(5)	Cr1-N3-Cr3	84.9(4)
N2-Cr1-C5	147.6(5)	Cr1-N3-Cr4	84.9(4)
N3-Cr1-Cr3	48.6(3)	Cr4-N3-Cr3	92.5(4)

N3-Cr1-Cr4	48.0(3)	C2-C1-Cr1	70.6(8)
N3-Cr1-N1	92.0(4)	C2-C1-C5	108.4(14)
N3-Cr1-C1	122.6(6)	C2-C1-C6	124.7(18)
N3-Cr1-C2	154.6(5)	C5-C1-Cr1	71.9(8)
N3-Cr1-C3	132.6(5)	C5-C1-C6	126.8(18)
N3-Cr1-C4	100.4(5)	C6-C1-Cr1	126.9(10)
N3-Cr1-C5	95.1(5)	C1-C2-Cr1	74.1(8)
C1-Cr1-Cr3	170.2(5)	C1-C2-C3	108.0(14)
C1-Cr1-Cr4	112.7(4)	C1-C2-C7	123.1(17)
C2-Cr1-Cr3	151.3(5)	C3-C2-Cr1	70.8(8)
C2-Cr1-Cr4	138.4(5)	C3-C2-C7	128.8(18)
C2-Cr1-C1	35.3(5)	C7-C2-Cr1	124.6(9)
C2-Cr1-C5	59.5(5)	C2-C3-Cr1	72.6(8)
C3-Cr1-Cr3	121.4(4)	C2-C3-C8	124.4(15)
C3-Cr1-Cr4	172.2(4)	C4-C3-Cr1	73.2(8)
C3-Cr1-C1	59.8(5)	C4-C3-C2	107.4(14)
C3-Cr1-C2	36.6(5)	C4-C3-C8	127.7(16)
C3-Cr1-C4	35.5(5)	C8-C3-Cr1	125.9(9)
C3-Cr1-C5	59.9(5)	C3-C4-Cr1	71.3(8)
C4-Cr1-Cr3	115.4(4)	C3-C4-C5	109.4(14)
C4-Cr1-Cr4	140.1(4)	C3-C4-C9	127.8(16)
C4-Cr1-C1	59.1(5)	C5-C4-Cr1	73.4(8)
C4-Cr1-C2	59.5(5)	C5-C4-C9	122.4(16)
C4-Cr1-C5	35.9(5)	C9-C4-Cr1	127.3(9)
C5-Cr1-Cr3	135.3(5)	C1-C5-Cr1	72.6(8)
C5-Cr1-Cr4	112.9(4)	C1-C5-C4	106.8(13)
C5-Cr1-C1	35.5(5)	C1-C5-C10	126.9(17)
N2-Cr2-Cr3	44.6(3)	C4-C5-Cr1	70.7(7)
N2-Cr2-C11	123.5(5)	C4-C5-C10	125.9(17)
N2-Cr2-C12	157.9(5)	C10-C5-Cr1	127.5(11)
N2-Cr2-C13	149.6(5)	C12-C11-Cr2	73.0(7)
N2-Cr2-C14	115.0(5)	C12-C11-C15	109.8(12)
N2-Cr2-C15	102.6(5)	C12-C11-C16	127.1(14)

N2-Cr2-C30	107.9(5)	C15-C11-Cr2	70.0(7)
C11-Cr2-Cr3	120.7(4)	C15-C11-C16	123.0(14)
C11-Cr2-C12	34.4(4)	C16-C11-Cr2	127.1(10)
C12-Cr2-Cr3	134.8(4)	C11-C12-Cr2	72.6(8)
C13-Cr2-Cr3	165.3(4)	C11-C12-C13	108.6(12)
C13-Cr2-C11	59.2(5)	C11-C12-C17	127.2(14)
C13-Cr2-C12	35.9(4)	C13-C12-Cr2	70.3(7)
C14-Cr2-Cr3	158.2(4)	C13-C12-C17	123.8(15)
C14-Cr2-C11	59.9(5)	C17-C12-Cr2	128.7(9)
C14-Cr2-C12	59.9(5)	C12-C13-Cr2	73.8(7)
C14-Cr2-C13	36.4(5)	C12-C13-C18	124.3(14)
C15-Cr2-Cr3	128.8(4)	C14-C13-Cr2	71.5(7)
C15-Cr2-C11	35.8(5)	C14-C13-C12	107.7(12)
C15-Cr2-C12	59.5(5)	C14-C13-C18	127.8(13)
C15-Cr2-C13	61.0(5)	C18-C13-Cr2	124.1(9)
C15-Cr2-C14	37.2(5)	C13-C14-Cr2	72.2(7)
C30-Cr2-Cr3	78.2(4)	C13-C14-C15	107.2(11)
C30-Cr2-C11	122.1(5)	C13-C14-C19	124.6(14)
C30-Cr2-C12	91.5(5)	C15-C14-Cr2	71.2(8)
C30-Cr2-C13	89.7(5)	C15-C14-C19	128.2(14)
C30-Cr2-C14	121.2(6)	C19-C14-Cr2	122.4(9)
C30-Cr2-C15	149.2(5)	C11-C15-Cr2	74.2(8)
Cr1-Cr3-Cr2	82.72(8)	C11-C15-C14	106.6(11)
Cr1-Cr3-Cr4	56.75(8)	C11-C15-C20	126.4(14)
Cr2-Cr3-Cr4	109.76(10)	C14-C15-Cr2	71.5(7)
Cl1-Cr3-Cr1	94.54(12)	C14-C15-C20	126.8(14)
Cl1-Cr3-Cr2	81.86(12)	C20-C15-Cr2	124.1(9)
Cl1-Cr3-Cr4	52.32(10)	C22-C21-Cr3	70.9(8)
N2-Cr3-Cr1	44.3(3)	C22-C21-C25	109.0(13)
N2-Cr3-Cr2	38.9(3)	C22-C21-C26	124.6(15)
N2-Cr3-Cr4	87.2(3)	C25-C21-Cr3	71.4(7)
N2-Cr3-Cl1	91.7(3)	C25-C21-C26	126.5(15)
N2-Cr3-C21	122.5(5)	C26-C21-Cr3	124.1(9)

N2-Cr3-C22	155.1(5)	C21-C22-Cr3	72.8(8)
N2-Cr3-C23	132.7(5)	C21-C22-C23	110.7(13)
N2-Cr3-C24	98.5(5)	C21-C22-C27	126.0(15)
N2-Cr3-C25	93.2(4)	C23-C22-Cr3	72.5(8)
N3-Cr3-Cr1	46.5(3)	C23-C22-C27	122.8(15)
N3-Cr3-Cr2	128.9(3)	C27-C22-Cr3	128.2(10)
N3-Cr3-Cr4	43.2(3)	C22-C23-Cr3	70.4(8)
N3-Cr3-Cl1	95.2(3)	C22-C23-C24	106.0(12)
N3-Cr3-N2	90.8(4)	C22-C23-C28	129.6(15)
N3-Cr3-C21	146.2(5)	C24-C23-Cr3	69.8(8)
N3-Cr3-C22	110.0(5)	C24-C23-C28	124.3(14)
N3-Cr3-C23	92.1(5)	C28-C23-Cr3	127.0(10)
N3-Cr3-C24	110.9(5)	C23-C24-Cr3	72.7(8)
N3-Cr3-C25	149.4(5)	C23-C24-C25	108.7(12)
C21-Cr3-Cr1	166.1(4)	C23-C24-C29	128.9(13)
C21-Cr3-Cr2	84.8(4)	C25-C24-Cr3	72.0(7)
C21-Cr3-Cr4	134.3(4)	C25-C24-C29	121.8(13)
C21-Cr3-Cl1	89.8(4)	C29-C24-Cr3	128.1(9)
C21-Cr3-C23	62.1(5)	C21-C25-Cr3	71.4(8)
C21-Cr3-C25	37.1(5)	C21-C25-C24	105.6(12)
C22-Cr3-Cr1	154.0(5)	C24-C25-Cr3	69.4(7)
C22-Cr3-Cr2	120.8(4)	C30-C25-Cr3	117.0(9)
C22-Cr3-Cr4	117.3(4)	C30-C25-C21	126.8(13)
C22-Cr3-Cl1	99.6(4)	C30-C25-C24	127.0(12)
C22-Cr3-C21	36.4(5)	C25-C30-Cr2	100.3(9)
C22-Cr3-C23	37.1(5)	C32-C31-Cr4	68(4)
C22-Cr3-C25	62.0(5)	C32-C31-C36	114(9)
C23-Cr3-Cr1	121.4(4)	C35-C31-Cr4	77(5)
C23-Cr3-Cr2	125.4(4)	C35-C31-C32	109(7)
C23-Cr3-Cr4	124.6(4)	C35-C31-C36	137(10)
C23-Cr3-Cl1	134.9(4)	C36-C31-Cr4	120(5)
C24-Cr3-Cr1	111.2(4)	C31-C32-Cr4	74(4)
C24-Cr3-Cr2	89.7(4)	C31-C32-C33	99(6)

C24-Cr3-Cr4	153.8(4)	C33-C32-Cr4	71(4)
C24-Cr3-Cl1	151.7(4)	C37-C32-Cr4	129(5)
C24-Cr3-C21	62.5(5)	C37-C32-C31	133(9)
C24-Cr3-C22	62.0(5)	C37-C32-C33	125(9)
C24-Cr3-C23	37.5(5)	C32-C33-Cr4	69(4)
C24-Cr3-C25	38.6(5)	C34-C33-Cr4	77(5)
C25-Cr3-Cr1	130.1(3)	C34-C33-C32	106(8)
C25-Cr3-Cr2	64.3(4)	C38-C33-Cr4	119(6)
C25-Cr3-Cr4	167.3(4)	C38-C33-C32	132(8)
C25-Cr3-Cl1	115.0(4)	C38-C33-C34	122(8)
C25-Cr3-C23	63.4(5)	C33-C34-Cr4	66(6)
Cl1-Cr4-C31	134(2)	C35-C34-Cr4	74(6)
Cl1-Cr4-C35	102.7(19)	C35-C34-C33	104(10)
N1-Cr4-Cl1	98.8(3)	C35-C34-C39	130(10)
N1-Cr4-N3	96.9(4)	C39-C34-Cr4	117(7)
N1-Cr4-C31	124(3)	C39-C34-C33	126(9)
N1-Cr4-C32	92(2)	C31-C35-Cr4	72(5)
N1-Cr4-C33	99(2)	C31-C35-C40	117(9)
N1-Cr4-C35	149(2)	C34-C35-Cr4	76(7)
N3-Cr4-Cl1	96.7(3)	C34-C35-C31	121(10)
N3-Cr4-C31	94(2)	C34-C35-C40	121(9)
N3-Cr4-C32	119(3)	C40-C35-Cr4	123(5)

This compound contains four chromium centers, with 3 bridging nitrogens and one chloride ligand. One interesting part of structure is that a C-H activation has happened between a methyl group of one of the Cp* ligands and Cr2, as shown in **Figure 2.3** b. The Cp* ligand coordinated to Cr4 suffer positional disorder in two sets of positions which were successfully modeled.

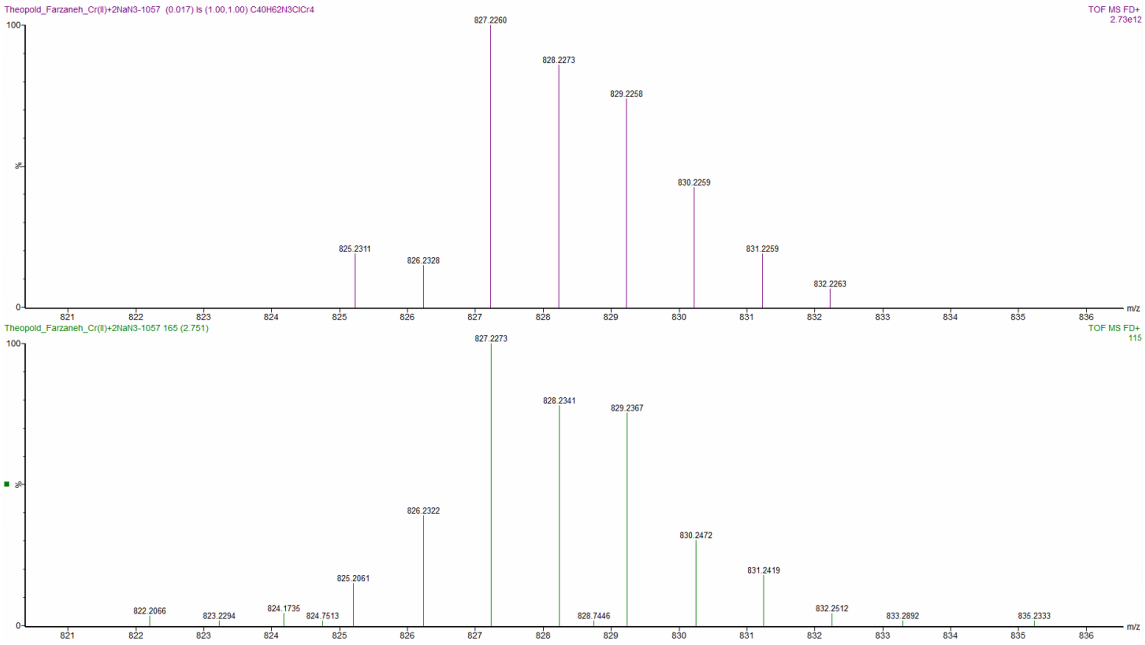

Figure 2.4 LIFDI-MS of predicted isotope model for the molecular ion of [Cr(μ-η^5:η^1-$C_5Me_4CH_2$)$Cr_3Cp^*_3N_3H_x$(Cl)] (**1**) [x=3; $C_{40}H_{62}Cr_4N_3Cl$: 827.2260] (Top), and calculated pattern for [Cr(μ-η^5:η^1-$C_5Me_4CH_2$)$Cr_3Cp^*_3N_3H_x$(Cl)] (**1**) [x= 3; $C_{40}H_{62}Cr_4N_3Cl$: 827.2273] (Bottom).

The proton NMR spectrum of **1**, as depicted in **Figure 2.5**, shows a broad range of peaks from +33.1 to -64.0 ppm, which is consistent with the presence of a paramagnetic compound. Due to the complexity of the proton NMR spectrum, the assignment of peaks was not possible, but based on the structure we can expect to see 3 peaks with the integration of 15 for three Cp* on Cr1, Cr2 and Cr4. Also, for the Cp* ligand coordinated to Cr3, we expect to see one peak with the integration of 2 for the CH_2 and four peaks with the integration of 3 for CH_3 groups. If there is a NH group in the molecule, then it is possible to see a small peak with the integration of 1 in the proton NMR of **1**. The presence of multiple peaks in the proton NMR of **1** can be the result of the C-H activation that happens on one of the Cp* ligands, that makes all the methyl groups different

chemically and magnetically. Also, it is possible that some of these peaks in the spectrum are related to the impurities in the sample.

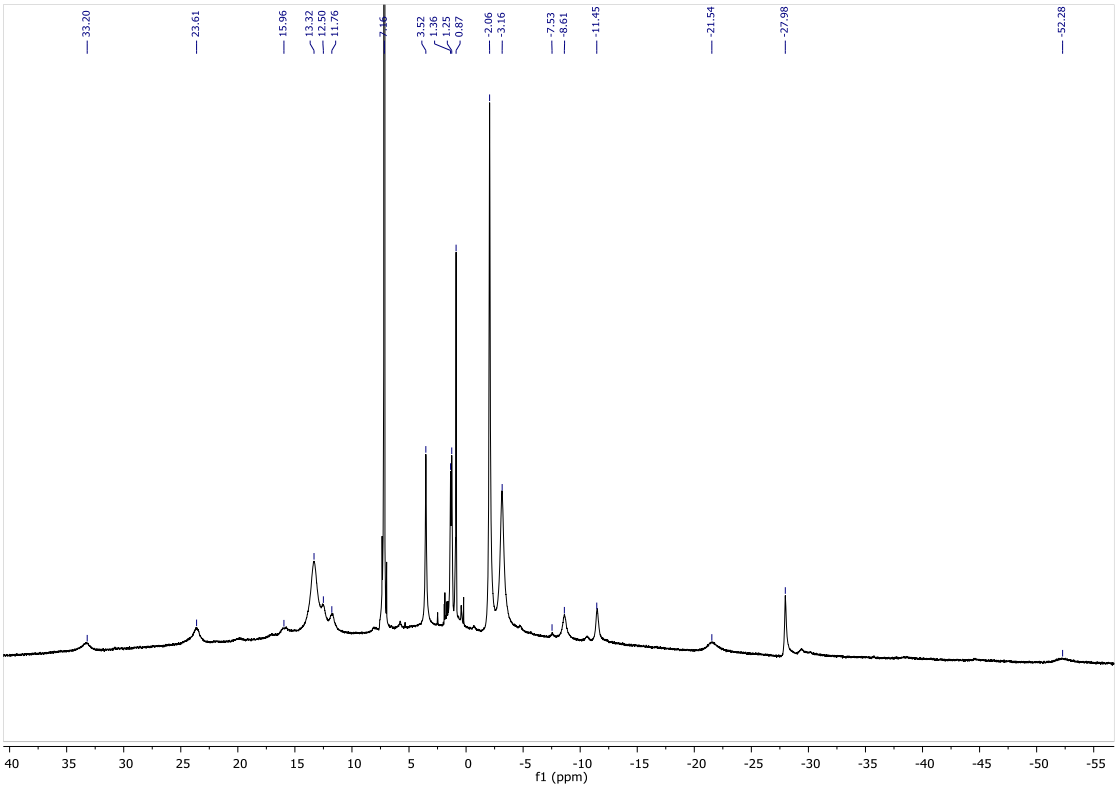

Figure 2.5 ^{1}H-NMR spectrum of **1** recorded in C_6D_6 at 400 MHz.

Although using an azide reagent is the classic way to synthesize nitride functionalities, there are limitations in using this reagent such as explosive nature, low solubility, and lack of steric protection which can lead to unselective substitution.[67]

Another method to nitride production is to use nitrogen transfer reagents such as Li-dbabh (dbabh= 2,3: 5,6-dibenzo-7-aza bicyclo[2.2.1]hepta-2,5-diene). In 1998, Mindiola et al. treated Li-dbabh with $[Cr(I)_2(NRAr_f)_2]$ in ether to get the diamagnetic $[Cr(I)\text{-}N(NRAr_f)_2]$ along with anthracene.[67]

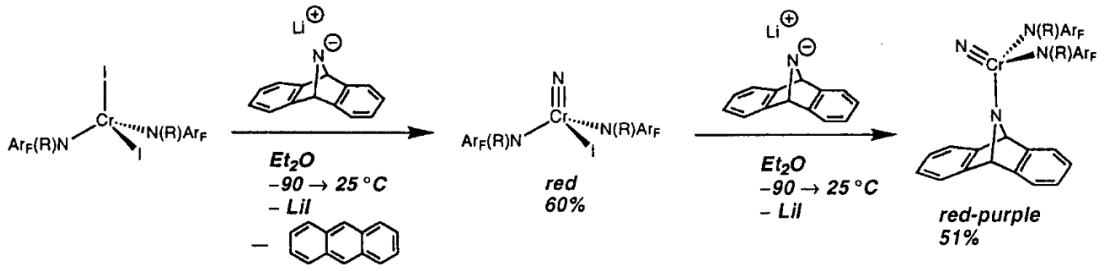

R= $C(CD_3)_2CH_3$, Ar_F =2,5-C_6H_3FMe.

Scheme 2.7 Synthesis of Nitride complex using Li-dbabh ligand.[67]

As mentioned before, this technique had been used in our group to successfully synthesize a chromium nitride complex. Therefore, the reaction of $[Cp^*Cr(\mu\text{-}Cl)]_2$ with the nitrogen transfer reagent Li-dbabh was done to see if the nitride version of this complex can be made. H-dbabh was prepared according to the literature method and was reacted with *n*-butyllithium to make Li-dbabh.[67,68]

To a THF solution of $[Cp^*Cr(\mu\text{-}Cl)]_2$ were added 2 equivalents of Li-dbabh. The color of the solution changed from brown to dark purple after the addition. The solution was stirred at room temperature for 2 hours following the addition and was then filtered. The solvent was removed under vacuum and the remaining powder was dissolved in pentanes. The solution was filtered and upon cooling to -30 °C, dark purple crystals of product were obtained. The structure of this product was determined by X-ray crystallography technique and found to be a dinuclear chromium complex, i.e. $[Cp^*Cr(\mu\text{-}Cl)(\mu\text{-}dbabh)CrCp^*]$ (**2**) as shown in **Figure 2.6**. The corresponding interatomic distances and angles are listed in **Table 2.2**.

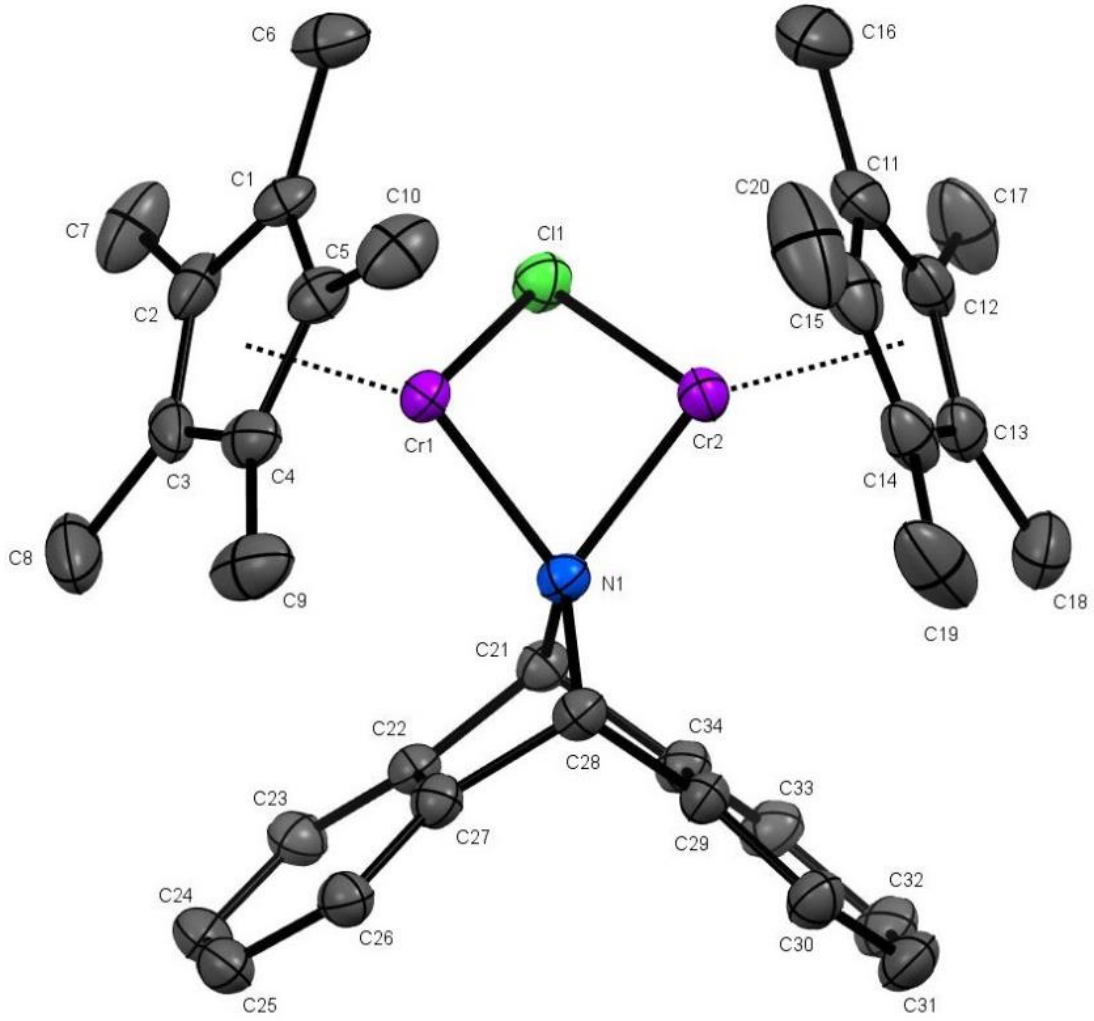

Figure 2.6 Molecular structure of [Cp*Cr(μ-Cl)(μ-dbabh)CrCp*] (**2**) represented as 50% probability thermal ellipsoids. Hydrogen atoms have been omitted for clarity.

Table 2.2 Interatomic distances (Å) and angles (º) for [Cp*Cr(μ-Cl)(μ-dbabh)CrCp*] (**2**).

Distances (Å)

Cr1-Cr2	2.4821(8)	C11-C12	1.427(7)
Cr1-N1	2.049(3)	C11-C15	1.407(7)
Cr1-Cl1	2.345(11)	C11-C16	1.502(7)
Cr1-C1	2.260(4)	C12-C13	1.391(6)
Cr1-C2	2.274(4)	C12-C17	1.503(7)
Cr1-C3	2.307(4)	C13-C14	1.421(6)
Cr1-C4	2.259(4)	C13-C18	1.499(7)
Cr1-C5	2.262(4)	C14-C15	1.416(8)
Cr2-N1	2.046(3)	C14-C19	1.496(6)
Cr2-Cl1	2.346(11)	C15-C20	1.512(8)
Cr2-C11	2.275(4)	C21-C22	1.517(5)
Cr2-C12	2.285(4)	C21-C34	1.530(5)
Cr2-C13	2.314(4)	C22-C23	1.386(5)
Cr2-C14	2.264(4)	C22-C27	1.407(5)
Cr2-C15	2.284(4)	C23-C24	1.390(6)
N1-C21	1.500(4)	C24-C25	1.376(6)
N1-C28	1.493(4)	C25-C26	1.400(6)
C1-C2	1.430(6)	C26-C27	1.365(5)
C1-C5	1.415(6)	C27-C28	1.533(5)
C1-C6	1.489(6)	C28-C29	1.529(5)
C2-C3	1.403(7)	C29-C30	1.386(5)
C2-C7	1.504(6)	C29-C34	1.389(5)
C3-C4	1.419(7)	C30-C31	1.402(6)
C3-C8	1.511(7)	C31-C32	1.378(7)
C4-C5	1.428(6)	C32-C33	1.398(6)
C4-C9	1.500(6)	C33-C34	1.380(5)
C5-C10	1.496(6)		

Angles (º)

N1-Cr1-Cr2	52.64(9)	C2-C3-Cr1	70.90(2)
N1-Cr1-Cl1	87.78(9)	C2-C3-C4	108.3(4)
N1-Cr1-C1	168.9(14)	C2-C3-C8	126.4(5)
N1-Cr1-C2	150.1(15)	C4-C3-Cr1	70.10(2)
N1-Cr1-C3	120.5(14)	C4-C3-C8	125.3(5)
N1-Cr1-C4	112.2(14)	C8-C3-Cr1	126.0(3)
N1-Cr1-C5	132.9(13)	C3-C4-Cr1	73.70(2)
Cl1-Cr1-Cr2	58.09(3)	C3-C4-C5	107.7(4)
C1-Cr1-Cr2	125.4(11)	C3-C4-C9	127.5(5)
C1-Cr1-Cl1	99.98(11)	C5-C4-Cr1	71.70(2)
C1-Cr1-C2	36.75(15)	C5-C4-C9	124.4(5)
C1-Cr1-C3	60.39(15)	C9-C4-Cr1	126.1(3)
C1-Cr1-C5	36.48(14)	C1-C5-Cr1	71.70(2)
C2-Cr1-Cr2	152.2(13)	C1-C5-C4	108.0(4)
C2-Cr1-Cl1	99.02(13)	C1-C5-C10	127.2(4)
C2-Cr1-C3	35.65(17)	C4-C5-Cr1	71.50(2)
C3-Cr1-Cr2	172.2(13)	C4-C5-C10	124.5(4)
C3-Cr1-Cl1	128.2(13)	C10-C5-Cr1	126.6(3)
C4-Cr1-Cr2	139.3(13)	C12-C11-Cr2	72.20(2)
C4-Cr1-Cl1	159.1(12)	C12-C11-C16	124.7(5)
C4-Cr1-C1	61.21(15)	C15-C11-Cr2	72.40(3)
C4-Cr1-C2	60.60(17)	C15-C11-C12	107.2(4)
C4-Cr1-C3	36.18(17)	C15-C11-C16	128.0(6)
C4-Cr1-C5	36.83(15)	C16-C11-Cr2	123.1(3)
C5-Cr1-Cr2	120.9(11)	C11-C12-Cr2	71.40(2)
C5-Cr1-Cl1	131.1(11)	C11-C12-C17	124.4(5)
C5-Cr1-C2	60.76(15)	C13-C12-Cr2	73.60(2)
C5-Cr1-C3	60.38(15)	C13-C12-C11	109.0(4)
N1-Cr2-Cr1	52.75(8)	C13-C12-C17	126.5(5)
N1-Cr2-Cl1	87.80(9)	C17-C12-Cr2	123.1(3)
N1-Cr2-C11	167.9(17)	C12-C13-Cr2	71.30(2)

N1-Cr2-C12	149.7(15)	C12-C13-C14	107.6(4)
N1-Cr2-C13	119.7(14)	C12-C13-C18	125.3(4)
N1-Cr2-C14	111.4(14)	C14-C13-Cr2	70.00(2)
N1-Cr2-C15	132.2(17)	C14-C13-C18	127.1(5)
Cl1-Cr2-Cr1	58.03(3)	C18-C13-Cr2	125.2(3)
C11-Cr2-Cr1	126.1(13)	C13-C14-Cr2	73.90(2)
C11-Cr2-Cl1	101.3(13)	C13-C14-C19	125.9(5)
C11-Cr2-C12	36.46(18)	C15-C14-Cr2	72.60(3)
C11-Cr2-C13	59.97(17)	C15-C14-C13	108.0(4)
C11-Cr2-C15	35.95(19)	C15-C14-C19	125.4(5)
C12-Cr2-Cr1	153.8(12)	C19-C14-Cr2	127.2(3)
C12-Cr2-Cl1	101.1(11)	C11-C15-Cr2	71.70(3)
C12-Cr2-C13	35.19(15)	C11-C15-C14	108.1(4)
C13-Cr2-Cr1	170.9(11)	C11-C15-C20	126.5(6)
C13-Cr2-Cl1	129.8(11)	C14-C15-Cr2	71.10(2)
C14-Cr2-Cr1	137.9(12)	C14-C15-C20	125.1(6)
C14-Cr2-Cl1	160.1(12)	C20-C15-Cr2	128.0(4)
C14-Cr2-C11	60.45(17)	N1-C21-C22	100.4(3)
C14-Cr2-C12	59.82(15)	N1-C21-C34	100.3(3)
C14-Cr2-C13	36.15(16)	C22-C21-C34	104.5(3)
C14-Cr2-C15	36.29(19)	C23-C22-C21	134.6(4)
C15-Cr2-Cr1	119.9(13)	C23-C22-C27	119.5(4)
C15-Cr2-Cl1	131.6(16)	C27-C22-C21	105.7(3)
C15-Cr2-C12	59.89(17)	C22-C23-C24	118.7(4)
C15-Cr2-C13	59.91(17)	C25-C24-C23	121.2(4)
Cr2-N1-Cr1	74.60(10)	C24-C25-C26	120.4(4)
C21-N1-Cr1	117.1(2)	C27-C26-C25	118.5(4)
C21-N1-Cr2	119.6(2)	C22-C27-C28	104.7(3)
C28-N1-Cr1	127.7(2)	C26-C27-C22	121.6(4)
C28-N1-Cr2	125.3(2)	C26-C27-C28	133.6(4)
C28-N1-C21	94.90(3)	N1-C28-C27	100.5(3)
Cr1-Cl1-Cr2	63.88(3)	N1-C28-C29	100.3(3)
C2-C1-Cr1	72.20(2)	C29-C28-C27	103.7(3)

C2-C1-C6	125.9(4)	C30-C29-C28	133.8(4)
C5-C1-Cr1	71.80(2)	C30-C29-C34	120.1(4)
C5-C1-C2	107.5(4)	C34-C29-C28	105.9(3)
C5-C1-C6	126.6(4)	C29-C30-C31	118.2(4)
C6-C1-Cr1	122.9(3)	C32-C31-C30	120.7(4)
C1-C2-Cr1	71.10(2)	C31-C32-C33	121.5(4)
C1-C2-C7	124.7(5)	C34-C33-C32	117.0(4)
C3-C2-Cr1	73.50(2)	C29-C34-C21	105.1(3)
C3-C2-C1	108.4(4)	C33-C34-C21	132.3(4)
C3-C2-C7	126.9(5)	C33-C34-C29	122.5(4)
C7-C2-Cr1	122.7(3)		

2 crystalizes in the monoclinic space group C2/c. It is a dinuclear complex with bridging chloride and dbabh ligands. It has a Cr1-Cr2 distance of 2.4821(8) Å which is shorter than 2.642(2) Å in the starting complex $[Cp^*Cr(\mu\text{-}Cl)]_2$. The core of the structure adopts a butterfly geometry, and the geometry is closely related to the structure of the starting compound. The effective magnetic moment of **2** at room temperature was measured to be 1.7 (1) μ_B. The expected magnetic moment for a system of two non-interacting intermediate spin d^4 (S=1) Cr(II) centers, is 4.0 μ_B (S=1, $(4S(S+1)*2)^{1/2}$).[69] Antiferromagnetic coupling of the Cr(II) ions mediated by the bridging ligands, metal-metal bonding, or both can cause this reduction in the effective magnetic moment. The Cr1-Cr2 bond distance is 2.4821(8) Å is inside the range of Cr-Cr bonds.[64,66,70]

The NMR of **2** shows a broad peak at -4.6 ppm which shows the paramagnetic properties of the product. Although in this reaction two equivalents of Li-dbabh was used, only one of the bridging chlorides was replaced with the new ligand. To check the possibility of replacing the second Cl, the reaction was repeated with an excess amount of Li-dbabh, but **2** was once again obtained as the product of reaction. Heating of **2** was examined to see if the anthracene can be removed from the complex, but after heating the compound to 55°C the decomposition of **2** to an unidentified mixture was observed, using

^{1}H-NMR spectroscopy. Only small amounts of free anthracene were observed after heating of **2**.

After getting these results from Cr(II) staring compound, it was decided to use a chromium complex with oxidation state of (III) to see if the change in the oxidation state can make a difference in the reactivity of chromium complex in synthesizing the dinitrogen or nitride complexes.

The synthesis of dinitrogen or nitride complexes of chromium (II) complex was not successful, so we decided to study the reactivity of a chromium complex with the oxidation state of (III), to see if the change in the oxidation state can make a difference in the reactivity of chromium complexes in synthesizing dinitrogen or nitride complexes.

The starting complex $[Cp^*ClCr(\mu\text{-}Cl)]_2$ was synthesized based on the literature procedure.[71]

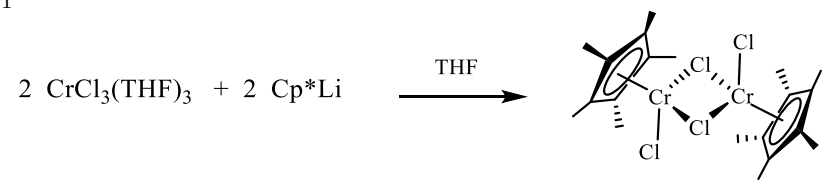

Scheme 2.8 Synthesis of starting complex $[Cp^*ClCr(\mu\text{-}Cl)]_2$ based on literature report.

The reactivity of $[Cp^*ClCr(\mu\text{-}Cl)]_2$ with azide reagents was studied in search for a nitride compound. Blue crystals of $[Cp^*ClCr(\mu\text{-}Cl)]_2$ were dissolved in THF and treated with an excess of NaN_3 powder. The color of the solution did not show any changes after the addition of azide reagent. The mixture was stirred overnight and then it was filtered to remove the excess NaN_3 and any NaCl byproduct from the solution. The solvent then was removed under vacuum and a blue powder was obtained. The remaining blue powder was washed with 10 ml of pentanes and 10 ml of diethyl ether. The blue powder was redissolved in THF and was cooled to -30°C to yield blue crystals of the product. Determination of the structure by X-ray crystallography revealed it to be a chromium

azide polymer, i.e. $[Cp^*Cr(N_3)_3Li(THF)]_n$ (**3**). The molecular structure of the repeating fragment of **3** is depicted in **Figure 2.7**, While the corresponding interatomic distances and angles are listed in **Table 2.3**.

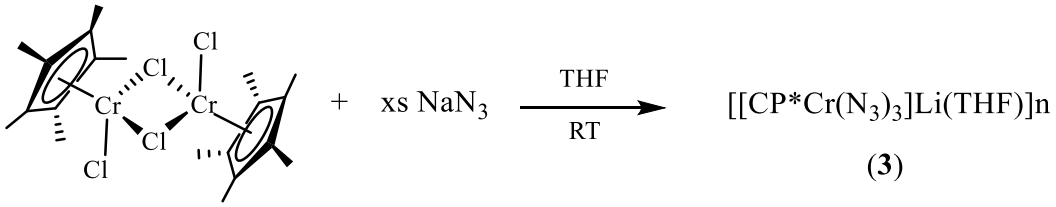

Scheme 2.9 Synthesis of complex **3** from starting compound $[Cp^*ClCr(\mu\text{-}Cl)]_2$.

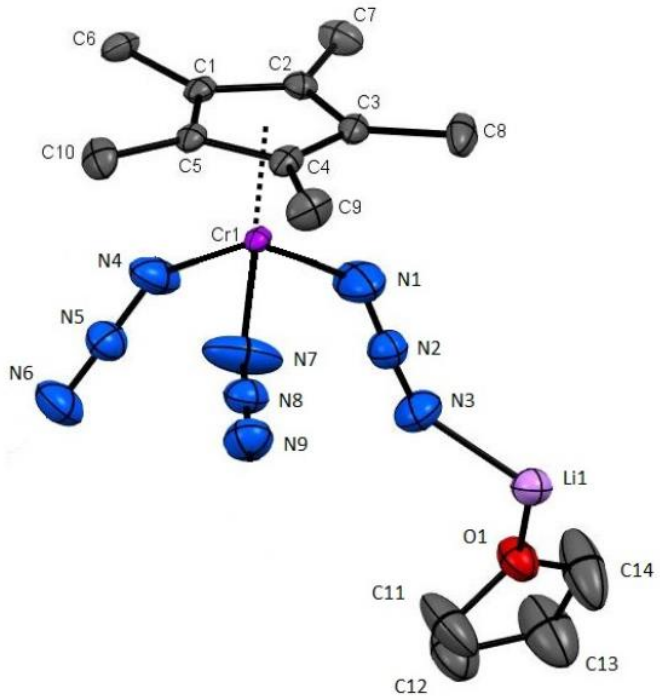

Figure 2.7 Molecular structure of $[[Cp^*Cr(N_3)_3Li(THF)]_n$ (**3**) represented as 50% probability thermal ellipsoids. Hydrogen atoms have been omitted for clarity.

Table 2.3 Interatomic distances (Å) and angles (º) for $[[Cp^*Cr(N_3)_3]Li(THF)]_n$ (**3**).

Distances (Å)

Cr1-N7	1.972(3)	Cr1-N1	2.016(3)
Cr1-N4	2.024(2)	Cr1-C5	2.219(2)
Cr1-C3	2.226(2)	Cr1-C4	2.241(2)
Cr1-C1	2.244(2)	Cr1-C2	2.250(2)
O1-C14	1.390(4)	O1-C11	1.415(3)
O1-Li1	1.941(4)	N1-N2	1.174(3)
N2-N3	1.135(3)	N3-Li1	2.041(5)
N4-N5	1.194(3)	N5-N6	1.147(3)
N6-Li1	2.027(5)	N7-N8	1.172(3)
N8-N9	1.143(3)	N9-Li1	2.010(5)
C1-C2	1.417(3)	C1-C5	1.429(4)
C1-C6	1.501(4)	C2-C3	1.426(3)
C2-C7	1.500(3)	C3-C4	1.416(3)
C3-C8	1.504(4)	C4-C5	1.423(4)
C4-C9	1.501(4)	C5-C10	1.502(4)
C11-C12	1.489(5)	C13-C14	1.478(5)
C12-C13	1.465(5)		

Angles (°)

N7-Cr1-N1	95.96(14)	N9-Li1-N6	118.3(2)
N1-Cr1-N4	96.11(12)	N9-Li1-N3	106.5(2)
N1-Cr1-C5	149.54(11)	N7-Cr1-N4	91.51(12)
N7-Cr1-C3	109.92(11)	N7-Cr1-C5	111.02(13)
N4-Cr1-C3	153.97(10)	N4-Cr1-C5	97.02(10)
N7-Cr1-C4	92.73(10)	N1-Cr1-C3	96.14(11)
N4-Cr1-C4	131.24(10)	C5-Cr1-C3	62.13(9)

C3-Cr1-C4	36.95(9)	N1-Cr1-C4	131.56(11)
N1-Cr1-C1	114.91(10)	C5-Cr1-C4	37.22(10)
C5-Cr1-C1	37.36(9)	N7-Cr1-C1	148.35(13)
C4-Cr1-C1	62.05(9)	N4-Cr1-C1	91.94(9)
N1-Cr1-C2	87.87(10)	C3-Cr1-C1	62.05(9)
C5-Cr1-C2	61.83(9)	N7-Cr1-C2	146.99(11)
C4-Cr1-C2	61.67(9)	N4-Cr1-C2	120.75(9)
C14-O1-C11	107.8(2)	C3-Cr1-C2	37.16(9)
C11-O1-Li1	125.2(2)	C1-Cr1-C2	36.77(9)
N3-N2-N1	175.5(3)	C14-O1-Li1	125.6(2)
N5-N4-Cr1	128.3(2)	N2-N1-Cr1	139.4(2)
N5-N6-Li1	163.8(3)	N2-N3-Li1	147.7(3)
N9-N8-N7	176.8(3)	N6-N5-N4	176.4(3)
C2-C1-C5	107.5(2)	N8-N7-Cr1	150.3(2)
C5-C1-C6	126.4(2)	N8-N9-Li1	171.3(2)
C5-C1-Cr1	70.37(13)	C2-C1-C6	126.0(2)
C1-C2-C3	108.2(2)	C2-C1-Cr1	71.85(13)
C3-C2-C7	124.1(2)	C6-C1-Cr1	124.32(17)
C3-C2-Cr1	70.51(13)	C1-C2-C7	127.7(2)
C4-C3-C2	108.2(2)	C1-C2-Cr1	71.38(13)
C2-C3-C8	124.4(2)	C7-C2-Cr1	124.94(16)
C2-C3-Cr1	72.33(13)	C4-C3-C8	127.4(2)
C3-C4-C5	107.8(2)	C4-C3-Cr1	72.10(13)
C5-C4-C9	126.7(2)	C8-C3-Cr1	123.42(17)
C5-C4-Cr1	70.54(13)	C3-C4-C9	125.5(3)
C4-C5-C1	108.3(2)	C3-C4-Cr1	70.95(13)
C1-C5-C10	125.1(3)	C9-C4-Cr1	125.80(17)
C1-C5-Cr1	72.28(13)	C4-C5-C10	126.6(3)
O1-C11-C12	107.1(3)	C4-C5-Cr1	72.24(14)
C13-C12-C11	104.5(3)	C10-C5-Cr1	122.03(18)
C12-C13-C14	105.4(3)	O1-Li1-N6	107.6(2)
O1-C14-C13	109.5(3)	O1-Li1-N3	112.2(2)
O1-Li1-N9	104.8(2)	N6-Li1-N3	107.5(2)

3 crystalizes in the triclinic space group $P\bar{1}$. Li(THF) fragments in the structure can make a bridge between azide groups from 3 different molecules, therefore a polymeric structure is created, as shown in **Figure 2.8**. The Li in the structure is probably coming from the LiCl impurities in the starting complex since it was recrystallized from THF. The elemental analyses result of this product shows that there is a mixture of Li and Na in the structure in the ratio of 2:8. Therefore, based on this crystal structure it cannot be concluded that all the molecules are coordinated to Li. The oxidation state of the chromium center is +III and the effective magnetic moment was measured to be 2.4 (1) μ_B at room temperature which is lower than the expected value for a Cr(III) complex. Antiferromagnetic coupling mediated by bridging azide ligands can cause this decrease in the magnetic moment.

The presence of Li and Na in the structure of this molecule can cause the coordination of polar solvents to the molecule, therefore this compound is soluble in THF. The Proton NMR of **3** in THF-d_8 shows a broad and shifted peak at -22.7 ppm which is consistent with the paramagnetic properties of **3**. In the IR spectrum of this complex there is a broad strong peak related to the azide ligands at 2080 cm^{-1}.

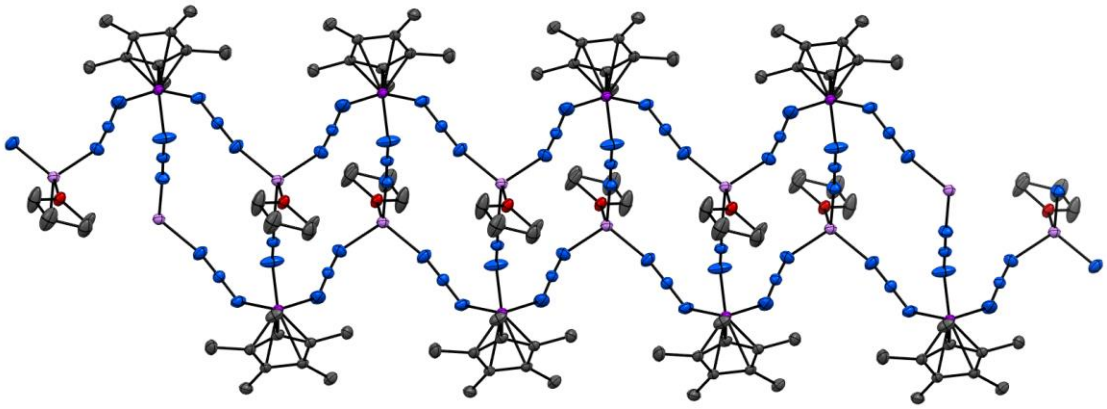

Figure 2.8 Polymeric structure of $[[Cp^*Cr(N_3)_3]Li(THF)]_n$ (**3**). THF molecules on the side Cr metals have been omitted for clarity.

The reaction of $[Cp^*ClCr(\mu\text{-}Cl)]_2$ was repeated in THF, but now with 2 equivalents of NaN_3, at room temperature. After the addition of azide reagent the blue color of solution did not change. The mixture was stirred overnight and then the solution was filtered to remove the NaCl salt from the solution. The solvent was then removed under vacuum and the remaining blue powder was washed with 10 ml of pentanes. Then the powder was redissolved in toluene and then filtered through celite. The toluene solution was then concentrated under vacuum and was cooled to -30 °C overnight to yield blue crystals. The quality of these crystals was not good enough for X-ray, therefore the crystals were redissolved in the minimum amount of THF and this solution was layered with pentanes to recrystallize the compound. Determination of the structure by X-ray crystallography revealed it to be a binuclear chromium complex with bridging azide ligands, i.e. $[Cp^*ClCr(\mu\text{-}N_3)]_2$ (**4**). The molecular structure of **4** is depicted in **Figure 2.9**, while the corresponding interatomic distances and angles are listed in **Table 2.4**.

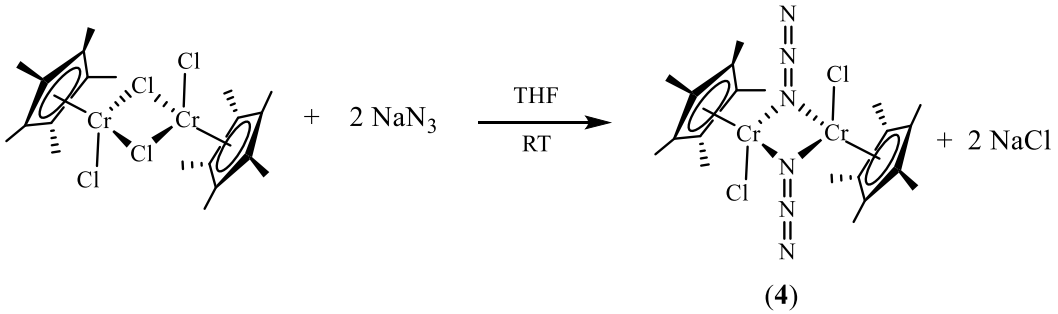

(**4**)

Scheme 2.10 Synthesis of $[Cp^*ClCr(\mu\text{-}N_3)]_2$ (**4**).

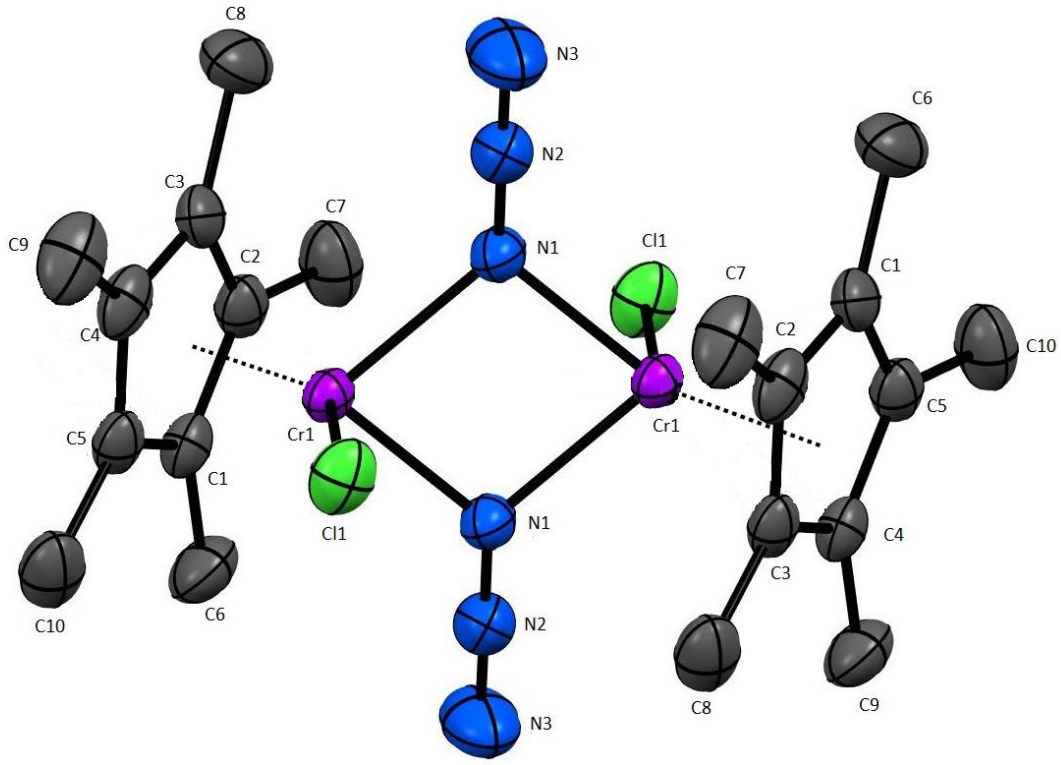

Figure 2.9 Molecular structure of $[Cp^*ClCr(\mu\text{-}N_3)]_2$ (**4**) represented as 50% probability thermal ellipsoids. Hydrogen atoms have been omitted for clarity.

Table 2.4 Interatomic distances (Å) and angles (º) for $[Cp^*ClCr(\mu\text{-}N_3)]_2$ (**4**).

Distances (Å)			
Cr1-N1	2.054(4)	Cr1-N1	2.074(4)
Cr1-C4	2.217(5)	Cr1-C3	2.218(5)
Cr1-C1	2.219(5)	Cr1-C2	2.232(5)
Cr1-C5	2.246(5)	Cr1-Cl1	2.292(16)

Cr2-C14	2.210(6)	Cr2-C13	2.210(6)
Cr2-C15	2.221(6)	Cr2-C11	2.211(5)
Cr2-Cl2	2.292(18)	Cr2-C12	2.238(5)
N2-N3	1.154(7)	N1-N2	1.195(6)
C1-C2	1.441(8)	C1-C5	1.428(8)
C2-C3	1.411(8)	C1-C6	1.492(8)
C3-C4	1.419(7)	C2-C7	1.483(8)
C4-C5	1.426(8)	C3-C8	1.506(8)
C5-C10	1.499(8)	C4-C9	1.484(8)
C11-C12	1.389(8)	C11-C15	1.430(8)
C11-C16	1.502(8)	C12-C13	1.426(8)
C12-C17	1.485(8)	C13-C14	1.424(9)
C13-C18	1.456(9)	C14-C15	1.391(9)
C14-C19	1.527(8)	C15-C20	1.484(9)

Angles (°)

N1-Cr1-N1	81.20(18)	N1-Cr1-C4	155.0(19)
N1-Cr1-C4	101.7(19)	N1-Cr1-C3	118.3(19)
N1-Cr1-C3	92.62(19)	C4-Cr1-C3	37.32(19)
N1-Cr1-C1	104.4(19)	N1-Cr1-C1	154.0(2)
C4-Cr1-C1	62.60(2)	C3-Cr1-C1	62.20(2)
N1-Cr1-C2	93.81(19)	N1-Cr1-C2	117.6(2)
C4-Cr1-C2	62.63(19)	C3-Cr1-C2	37.00(2)
C1-Cr1-C2	37.80(2)	N1-Cr1-C5	140.1(19)
N1-Cr1-C5	137.2(19)	C4-Cr1-C5	37.26(19)
C3-Cr1-C5	61.90(19)	C1-Cr1-C5	37.30(2)
C2-Cr1-C5	62.50(2)	N1-Cr1-Cl1	96.78(14)
N1-Cr1-Cl1	94.49(13)	C4-Cr1-Cl1	107.5(14)
C3-Cr1-Cl1	144.8(15)	C1-Cr1-Cl1	109.6(16)
C2-Cr1-Cl1	147.4(18)	C5-Cr1-Cl1	90.58(14)
C13-Cr2-C14	37.60(2)	C14-Cr2-C11	61.80(2)

C13-Cr2-C11	62.40(2)	C13-Cr2-C15	62.50(2)
C14-Cr2-C15	36.60(2)	C11-Cr2-C15	37.70(2)
C14-Cr2-C12	61.60(2)	C13-Cr2-C12	37.40(2)
C15-Cr2-C12	61.60(2)	C11-Cr2-C12	36.40(2)
C13-Cr2-Cl2	110.2(18)	C14-Cr2-Cl2	147.8(18)
C11-Cr2-Cl2	107.7(17)	C15-Cr2-Cl2	145.3(17)
C12-Cr2-Cl2	91.57(15)	N2-N1-Cr1	131.6(4)
N2-N1-Cr1	125.9(4)	Cr1-N1-Cr1	98.80(18)
N3-N2-N1	179.6(7)	C5-C1-C6	125.4(6)
C5-C1-C2	108.2(5)	C5-C1-Cr1	72.30(3)
C2-C1-C6	126.4(6)	C6-C1-Cr1	123.9(4)
C2-C1-Cr1	71.60(3)	C3-C2-C7	125.5(6)
C3-C2-C1	106.9(5)	C3-C2-Cr1	71.00(3)
C1-C2-C7	127.5(6)	C7-C2-Cr1	126.4(4)
C1-C2-Cr1	70.60(3)	C2-C3-C8	125.4(5)
C2-C3-C4	109.6(5)	C2-C3-Cr1	72.10(3)
C4-C3-C8	125.0(5)	C8-C3-Cr1	124.5(4)
C4-C3-Cr1	71.30(3)	C3-C4-C9	127.9(5)
C3-C4-C5	107.6(5)	C3-C4-Cr1	71.40(3)
C5-C4-C9	124.5(5)	C9-C4-Cr1	122.5(4)
C5-C4-Cr1	72.50(3)	C4-C5-C10	125.9(5)
C4-C5-C1	107.7(5)	C4-C5-Cr1	70.30(3)
C1-C5-C10	126.4(5)	C10-C5-Cr1	126.6(4)
C1-C5-Cr1	70.30(3)	C12-C11-C16	125.2(6)
C12-C11-C15	108.2(5)	C12-C11-Cr2	72.90(3)
C15-C11-C16	126.5(6)	C16-C11-Cr2	123.6(4)
C15-C11-Cr2	71.50(3)	C11-C12-C17	125.4(6)
C11-C12-C13	108.9(5)	C11-C12-Cr2	70.70(3)
C13-C12-C17	125.7(6)	C17-C12-Cr2	126.7(4)
C13-C12-Cr2	70.20(3)	C14-C13-C18	128.5(6)
C14-C13-C12	106.1(5)	C14-C13-Cr2	71.20(3)
C12-C13-C18	125.4(7)	C18-C13-Cr2	122.9(5)
C12-C13-Cr2	72.40(3)	C15-C14-C19	128.1(7)

C15-C14-C13	109.5(5)	C15-C14-Cr2	72.10(3)
C13-C14-C19	122.4(7)	C19-C14-Cr2	123.9(4)
C13-C14-Cr2	71.20(3)	C14-C15-C20	125.5(6)
C14-C15-C11	107.3(5)	C14-C15-Cr2	71.30(3)
C11-C15-C20	127.2(7)	C20-C15-Cr2	124.1(4)
C11-C15-Cr2	70.80(3)		

4 crystalizes in the triclinic space group $P\bar{1}$ and there is an inversion center in the middle of the structure. The Cr-Cr distance is 3.134 Å and there is no bond between them and the geometry around the Cr centers is octahedral. The effective magnetic moment of **4** was found to be 2.9 (1) μ_B at room temperature. For a system of two non-interacting chromium(III) high spin d^3 ions (S= 3/2), the expected magnetic moment is 5.5 μ_B. A possible interpretation of the lower moment of **4** is that the bridging azide ligands mediate antiferromagnetic coupling between the chromiums. The Proton NMR of this complex in benzene-d_6 shows a single broad peak at -32.2 ppm, indicative of paramagnetic properties of **4**. In the IR spectrum of **4** there are two intense peaks at 2062 and 2090 cm^{-1} which can be assigned to the bridging azide ligands.

The potential reactivity of this azide compound to produce nitride compounds was studied. Reduction of one equivalent of **4** with 2 equivalents of Na was done in THF. The color of the solution stared to change to green blue after 30 minutes following the addition of Na regent. The solution was stirred overnight, and the color of solution changed to brown during this time. The proton NMR of the products shows a mixture which was not identified even after several trials and extraction with various solvents such as pentanes, toluene, diethyl ether and THF. Heating of **4** did not change the complex and the THF solution of **4** was stable at high temperatures, even up to 100 °C. **4** was dissolved in toluene and was transferred to a quartz ampule under nitrogen atmosphere and the gas above the solution was removed under vacuum. The solution was exposed to UV light for 2 days. During this time, the color of solution changed from blue to green. After filtration, the solvent was removed, and a green-brown powder was collected. The

product was redissolved in toluene and was filtered to remove any insoluble impurities. The compound was recrystallized in toluene several times. Crystals generated this way were of sufficient quality to determine the structure of the product by X-ray diffraction analysis. The structure was revealed to be a tetranuclear chromium complex with azide and nitride bridging ligands, i.e. $[Cp^*ClCr]_4(\mu\text{-}N)_2(\mu\text{-}N_3)_2$ (**5**). The molecular structure of **5** is depicted in **Figure 2.10**, while the corresponding interatomic distances and angles are listed in **Table 2.5**.

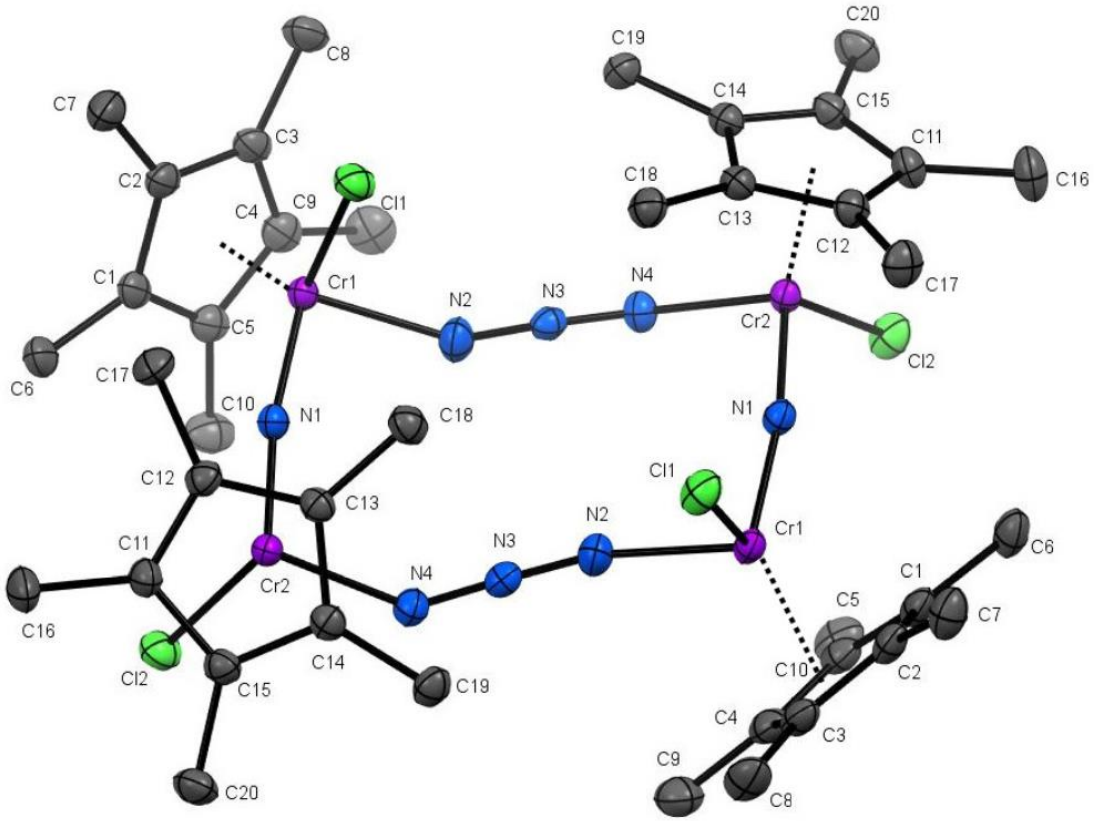

Figure 2.10 Molecular structure of $[Cp^*ClCr]_4(\mu\text{-}N)_2(\mu\text{-}N_3)_2$ (**5**) represented as 50% probability thermal ellipsoids. Hydrogen atoms have been omitted for clarity.

Table 2.5 Interatomic distances (Å) and angles (º) for $[Cp^*ClCr]_4(\mu\text{-}N)_4(\mu\text{-}N_3)_4$ (**5**).

Distances (Å)			
Cr1-Cl1	2.2830(8)	C1-C6	1.497(3)
Cr1-N1	1.7995(16)	C2-C3	1.419(3)
Cr1-N2	2.0128(19)	C2-C7	1.503(3)
Cr1-C1	2.2177(19)	C3-C4	1.413(3)
Cr1-C2	2.2383(19)	C3-C8	1.499(3)
Cr1-C3	2.288(2)	C4-C5	1.437(3)
Cr1-C4	2.280(2)	C4-C9	1.495(3)
Cr1-C5	2.2064(19)	C5-C10	1.495(3)
Cr2-Cl2	2.2866(7)	C11-C12	1.415(3)
Cr2-N1	1.7128(16)	C11-C15	1.432(3)
Cr2-C11	2.2603(18)	C11-C16	1.502(3)
Cr2-C12	2.2299(18)	C12-C13	1.425(3)
Cr2-C13	2.2066(18)	C12-C17	1.497(3)
Cr2-C14	2.2932(18)	C13-C14	1.432(2)
Cr2-C15	2.3191(19)	C13-C18	1.497(2)
N2-N3	1.159(2)	C14-C15	1.407(3)
N3-N4	1.168(2)	C14-C19	1.493(3)
C1-C2	1.429(3)	C15-C20	1.496(3)
C1-C5	1.420(3)		

Angles (°)			
Cl1-Cr1-C3	91.77(5)	C2-C1-Cr1	72.08(10)
N1-Cr1-Cl1	102.7(5)	C2-C1-C6	126.4(2)
N1-Cr1-N2	93.75(7)	C5-C1-Cr1	70.84(11)
N1-Cr1-C1	90.38(7)	C5-C1-C2	107.8(17)
N1-Cr1-C2	118.3(7)	C5-C1-C6	125.9(18)
N1-Cr1-C3	151.7(7)	C6-C1-Cr1	123.6(14)

N1-Cr1-C4	133.5(7)	C1-C2-Cr1	70.51(10)
N1-Cr1-C5	98.00(7)	C1-C2-C7	126.9(19)
N2-Cr1-Cl1	96.48(6)	C3-C2-Cr1	73.66(11)
N2-Cr1-C1	139.4(8)	C3-C2-C1	107.9(18)
N2-Cr1-C2	145.1(8)	C3-C2-C7	125.2(18)
N2-Cr1-C3	108.8(8)	C7-C2-Cr1	123.4(14)
N2-Cr1-C4	87.14(7)	C2-C3-Cr1	69.83(11)
N2-Cr1-C5	102.0(8)	C2-C3-C8	126.0(2)
C1-Cr1-Cl1	121.9(6)	C4-C3-Cr1	71.67(11)
C1-Cr1-C2	37.41(7)	C4-C3-C2	108.8(17)
C1-Cr1-C3	61.42(7)	C4-C3-C8	125.2(2)
C1-Cr1-C4	61.87(8)	C8-C3-Cr1	125.5(14)
C2-Cr1-Cl1	89.97(5)	C3-C4-Cr1	72.30(11)
C2-Cr1-C3	36.51(8)	C3-C4-C5	107.5(19)
C2-Cr1-C4	61.27(8)	C3-C4-C9	126.4(19)
C4-Cr1-Cl1	123.5(6)	C5-C4-Cr1	68.55(11)
C4-Cr1-C3	36.03(7)	C5-C4-C9	126.1(2)
C5-Cr1-Cl1	151.2(5)	C9-C4-Cr1	124.8(14)
C5-Cr1-C1	37.45(8)	C1-C5-Cr1	71.71(11)
C5-Cr1-C2	62.38(7)	C1-C5-C4	108.1(17)
C5-Cr1-C3	61.47(7)	C1-C5-C10	125.8(19)
C5-Cr1-C4	37.33(7)	C4-C5-Cr1	74.12(11)
Cl2-Cr2-C14	121.38(5)	C4-C5-C10	126.1(2)
Cl2-Cr2-C15	90.85(5)	C10-C5-Cr1	122.4(14)
N1-Cr2-Cl2	104.3(5)	C12-C11-Cr2	70.48(10)
N1-Cr2-N41	96.98(7)	C12-C11-C15	108.1(16)
N1-Cr2-C11	118.4(7)	C12-C11-C16	126.4(17)
N1-Cr2-C12	91.15(7)	C15-C11-Cr2	74.03(10)
N1-Cr2-C13	98.74(7)	C15-C11-C16	125.4(17)
N1-Cr2-C14	134.1(7)	C16-C11-Cr2	124.7(15)
N1-Cr2-C15	151.9(7)	C11-C12-Cr2	72.81(10)
N41-Cr2-Cl2	94.49(5)	C11-C12-C13	107.9(16)
N41-Cr2-C11	141.6(7)	C11-C12-C17	125.9(18)

N41-Cr2-C12	138.0(7)	C13-C12-Cr2	70.39(10)
N41-Cr2-C13	100.6(7)	C13-C12-C17	126.1(17)
N41-Cr2-C14	84.53(6)	C17-C12-Cr2	124.9(13)
N41-Cr2-C15	105.4(6)	C12-C13-Cr2	72.16(10)
C11-Cr2-Cl2	90.94(5)	C12-C13-C14	107.8(15)
C11-Cr2-C14	60.63(7)	C12-C13-C18	125.9(16)
C11-Cr2-C15	36.41(6)	C14-C13-Cr2	74.76(10)
C12-Cr2-Cl2	123.2(6)	C14-C13-C18	126.1(16)
C12-Cr2-C11	36.72(7)	C18-C13-Cr2	123.4(12)
C12-Cr2-C14	61.35(7)	C13-C14-Cr2	68.19(10)
C12-Cr2-C15	60.82(6)	C13-C14-C19	126.1(16)
C13-Cr2-Cl2	150.6(5)	C15-C14-Cr2	73.24(10)
C13-Cr2-C11	61.83(7)	C15-C14-C13	108.0(15)
C13-Cr2-C12	37.45(7)	C15-C14-C19	125.9(16)
C13-Cr2-C14	37.05(6)	C19-C14-Cr2	124.8(12)
C13-Cr2-C15	60.96(6)	C11-C15-Cr2	69.56(10)
C14-Cr2-C15	35.53(6)	C11-C15-C20	126.1(18)
Cr2-N1-Cr1	170.5(10)	C14-C15-Cr2	71.23(10)
N3-N2-Cr1	153.8(16)	C14-C15-C11	108.1(15)
N2-N3-N4	175.2(19)	C14-C15-C20	125.8(18)
N3-N4-Cr21	135.4(13)	C20-C15-Cr2	125.8(13)

5 crystallizes in the orthorhombic space group Pbcn. The bond angle for Cr1-N1-Cr2 is 170.36° and the Cr1-N1 and Cr2-N1 bond lengths are respectively 1.7995(16) Å and 1.7128(16) Å. These distances fall in to the range between single and double bond distances.[60,66] it can be concluded that the bridging nitride is slightly out of plane of four chromium centers.

The proton NMR spectrum of **5** shows a broad peak at -30.4 ppm, which is consistent with the presence of a paramagnetic chromium complex. **5** displayed an effective magnetic moment of 2.1 (1) μ_B at room temperature. For a system of four non-interacting chromium(IV) high spin d^2 ions the expected magnetic moment is 5.6 μ_B.

The low effective magnetic moment of **5** indicates antiferromagnetic coupling between chromium ions caused by the bridging azide and nitride ligands. In the IR spectrum of **5** there are two intense peaks at 2140 and 2056 cm^{-1} which are presumably due to the bridging azide ligands.

After getting these results from chromium complexes with oxidation state (II) and (III) with Cp* ligand, we realized that the reactivity of chromium (II) with azide reagents is higher compared to chromium (III). The azide decomposes to nitrides in reaction with the Cr(II) complex. Therefore, we decided to use chromium in oxidation state of (II) but make some modifications in the ligands present on the metal center to see if we can stabilize any dinitrogen or nitride complexes.

In this context, different ligands such as Tetramethylethylenediamine (TMEDA), Dimethoxyethane (DME), 4,4'-dimethyl-2.2'-dipyridyl (N^N), 1,3-Bis(diphenylphosphino)propane (dppp), 1,2-Bis(diphenylphosphino)ethane (dppe), 1,2-Bis(dimethylphosphino)ethane (dmpe), and PMe_3 were added to the starting chromium compound $[Cp^*Cr(\mu\text{-}Cl)]_2$. The resulting new compounds were examined to synthesize dinitrogen and nitride complexes based on previous methods, i.e., reduction under dinitrogen atmosphere and reaction with azide reagents, but the products were only identified for the reaction with 4'-dimethyl-2.2'-dipyridyl and PMe_3 ligands. Due to complexity of reactions and existence of several products, separation of those mixtures was not achieved in most cases.

The reduction of these new chromium complexes under dinitrogen atmosphere and their reaction with azide reagents were studied with the goal of synthesizing new dinitrogen or nitride complexes.

To a THF solution of $[Cp^*Cr(\mu\text{-}Cl)]_2$ was added two equivalents of 4'-dimethyl-2.2'-dipyridyl (N^N). After the addition, the color of solution changed to maroon. The mixture was stirred for about two hours. After filtration and removal of solvent under vacuum, the remaining maroon powder was washed with 10 ml of pentanes. The powder was dissolved in a minimum amount of THF and at -30°C maroon crystals of the product

was collected. Determination of the structure by X-ray crystallography revealed it to be a mononuclear chromium complex, i.e. [Cp*ClCr(N^N)] (**6**). The molecular structure of **6** is depicted in **Figure 2.11** while the corresponding interatomic distances and angles are listed in

Table 2.6.

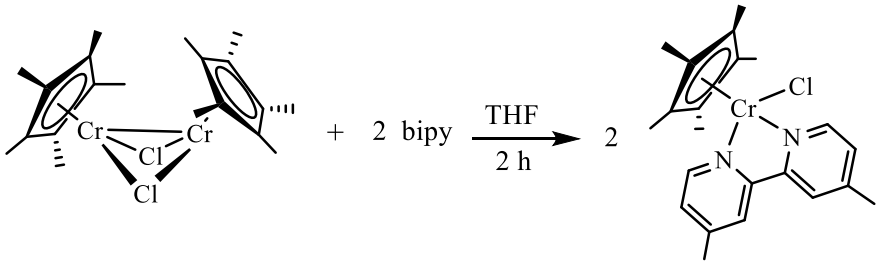

(**6**)

Scheme 2.11 Synthesis of [Cp*ClCr(N^N)] (**6**).

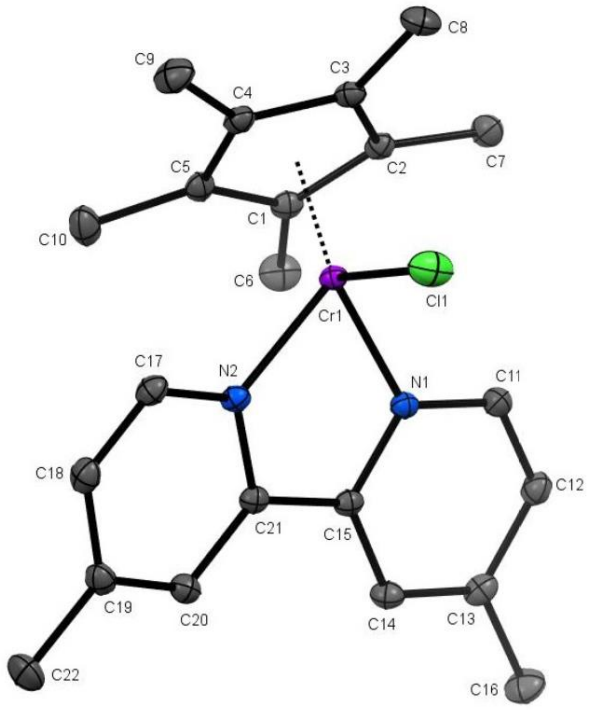

Figure 2.11 Molecular structure of [Cp*ClCr(N^N)] (**6**) represented as 50% probability thermal ellipsoids. Hydrogen atoms have been omitted for clarity.

Table 2.6 Interatomic distances (Å) and angles (º) for [Cp*ClCr(N^N)] (**6**).

Distances (Å)

Cr1-Cl1	2.3123(5)	C3-C4	1.423(2)
Cr1-N1	1.9927(14)	C3-C8	1.498(2)
Cr1-N2	1.9950(14)	C4-C5	1.422(2)
Cr1-C1	2.2193(16)	C4-C9	1.498(2)
Cr1-C2	2.2627(16)	C5-C10	1.500(2)
Cr1-C3	2.2748(16)	C11-C12	1.363(2)
Cr1-C4	2.2588(16)	C12-C13	1.416(2)
Cr1-C5	2.2418(16)	C13-C14	1.373(2)
N1-C11	1.363(2)	C13-C16	1.503(2)
N1-C15	1.381(2)	C14-C15	1.414(2)
N2-C17	1.364(2)	C15-C21	1.427(2)
N2-C21	1.382(2)	C17-C18	1.365(3)
C1-C2	1.431(2)	C18-C19	1.418(3)
C1-C5	1.426(2)	C19-C20	1.371(2)
C1-C6	1.501(2)	C19-C22	1.507(2)
C2-C3	1.416(2)	C20-C21	1.414(2)
C2-C7	1.503(2)		

Angles (°)

N1-Cr1-Cl1	100.7(4)	C1-C2-C7	127.6(15)
N1-Cr1-N2	78.70(6)	C3-C2-Cr1	72.28(9)
N1-Cr1-C1	92.58(6)	C3-C2-C1	107.6(14)
N1-Cr1-C2	99.60(6)	C3-C2-C7	124.6(15)
N1-Cr1-C3	133.5(6)	C7-C2-Cr1	127.7(11)
N1-Cr1-C4	154.5(6)	C2-C3-Cr1	71.35(9)
N1-Cr1-C5	120.7(6)	C2-C3-C4	108.6(14)
N2-Cr1-Cl1	95.86(4)	C2-C3-C8	126.1(16)
N2-Cr1-C1	113.3(6)	C4-C3-Cr1	71.09(9)

N2-Cr1-C2	150.5(6)	C4-C3-C8	125.2(16)
N2-Cr1-C3	145.4(6)	C8-C3-Cr1	125.7(12)
N2-Cr1-C4	109.1(6)	C3-C4-Cr1	72.32(9)
N2-Cr1-C5	93.47(6)	C3-C4-C9	125.8(17)
C1-Cr1-Cl1	149.9(5)	C5-C4-Cr1	70.93(9)
C1-Cr1-C2	37.22(6)	C5-C4-C3	107.8(14)
C1-Cr1-C3	61.48(6)	C5-C4-C9	126.3(17)
C1-Cr1-C4	61.91(6)	C9-C4-Cr1	126.2(12)
C1-Cr1-C5	37.27(6)	C1-C5-Cr1	70.51(9)
C2-Cr1-Cl1	113.3(4)	C1-C5-C10	126.1(17)
C2-Cr1-C3	36.37(6)	C4-C5-Cr1	72.23(9)
C3-Cr1-Cl1	90.37(4)	C4-C5-C1	108.0(14)
C4-Cr1-Cl1	102.5(5)	C4-C5-C10	125.8(17)
C4-Cr1-C2	61.33(6)	C10-C5-Cr1	125.5(12)
C4-Cr1-C3	36.59(6)	N1-C11-C12	123.5(16)
C5-Cr1-Cl1	138.6(5)	C11-C12-C13	120.0(16)
C5-Cr1-C2	61.70(6)	C12-C13-C16	120.1(16)
C5-Cr1-C3	61.19(6)	C14-C13-C12	117.3(15)
C5-Cr1-C4	36.84(6)	C14-C13-C16	122.5(17)
C11-N1-Cr1	125.5(11)	C13-C14-C15	121.1(16)
C11-N1-C15	117.5(14)	N1-C15-C14	120.6(15)
C15-N1-Cr1	116.8(11)	N1-C15-C21	113.6(14)
C17-N2-Cr1	126.0(11)	C14-C15-C21	125.9(15)
C17-N2-C21	117.2(14)	N2-C17-C18	123.6(16)
C21-N2-Cr1	116.8(11)	C17-C18-C19	120.1(16)
C2-C1-Cr1	73.04(9)	C18-C19-C22	120.5(17)
C2-C1-C6	126.8(16)	C20-C19-C18	117.0(16)
C5-C1-Cr1	72.23(9)	C20-C19-C22	122.4(17)
C5-C1-C2	107.9(14)	C19-C20-C21	121.4(16)
C5-C1-C6	125.3(16)	N2-C21-C15	113.4(14)
C6-C1-Cr1	121.7(12)	N2-C21-C20	120.6(15)
C1-C2-Cr1	69.74(9)	C20-C21-C15	126.0(15)

6 crystallizes in the monoclinic space group $P2_1/c$ and the geometry around the chromium center is pseudo-octahedral. Cp* can be considered as a tridentate L_2X ligand covering three coordination sites of a trigonal face of an octahedron. The ^{1}H-NMR spectrum of **6** shows a broad range of peaks from +82.9 to −82.5 ppm, which is consistent with the presence of a paramagnetic chromium complex. The effective magnetic moment was found to be 2.8 (1) μ_B when measured at room temperature, consistent with the assignment of the metal center as an intermediate spin d^4 (S=1) Cr(II) ion.

Examples of structures with mono and dianion bipyridine ligands are known.[72] Based on the C_{py}−C_{py} and C_{py}−N_{py} bond distances in the bpy ligand, it is possible to measure the charge of the ligand. Several reported structures for neutral bpy (bpy^0), the paramagnetic π-radical monoanion $(bpy•)^{-1}$, and the diamagnetic dianion form $(bpy^{-2})^{-2}$, with accurate measurements of C_{py}−C_{py} and C_{py}−N_{py} bond distances are known.[73] There is a linear relation between the C_{py}−C_{py} and C_{py}−N_{py} bond distances. As the negative charge increases in bpy ligand, the C_{py}−C_{py} bond length decreases but the C_{py}−N_{py} shows an increase in the length.[73] This effect is due to population of the π* LUMO of (bpy^0) upon one and two electron reduction, resulting in a decrease in C_{py}−C_{py} and an increase in neighbor C_{py}−N_{py} bond distance.[74]

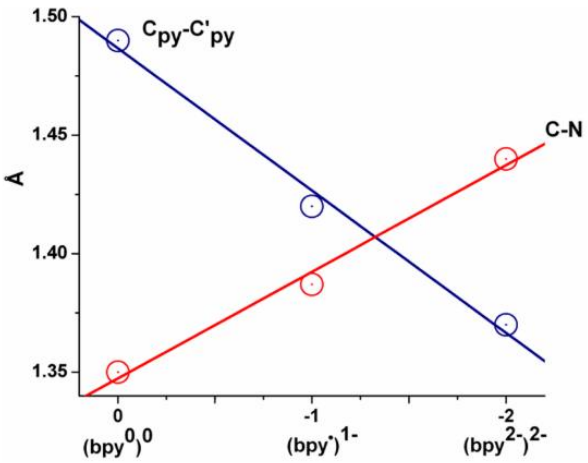

Figure 2.12 The linear correlation of Cpy−Cpy (blue) and average C_{py}−N_{py} (red).[74]

It has been shown that the difference between the $C_{py}-C'_{py}$ and the average $C_{py}-N_{py}$ bond length (Δ (Å)) decreases linearly with increasing charge on bpy ligand. The Δ-value is a measure to find out about the oxidation level of bpy, for $(bpy)^0$, $(bpy\bullet)^{1-}$ and $(bpy^{2-})^{2-}$ the Δ (Å) is 0.10 ± 0.02, 0.05 ± 0.02, and −0.07 ± 0.02 respectively. Most importantly, the Δ-value is independent of the d^n electron configuration of the central first-row metal ion.[73] The Δ-value for N^N ligand in **6** was calculated to be 0.05 Å, which is in the range for the $(bpy\bullet)^{1-}$ ligand.

The reduction of **6** under nitrogen atmosphere was studied. To a THF solution of **6** was added one equivalent of metallic sodium. The solution was stirred for one day and during this time the color of solution changed to brown. After filtration and removal of solvent a brown powder was produced. The brown solution from pentanes washing was concentrated and after 2 days at -30 °C, brown crystals of the product, i.e. [Cp*Cr(N^N)] (**7**) were formed. The molecular structure of **7** is depicted in **Figure 2.13** while the corresponding interatomic distances and angles are listed in **Table 2.7**.

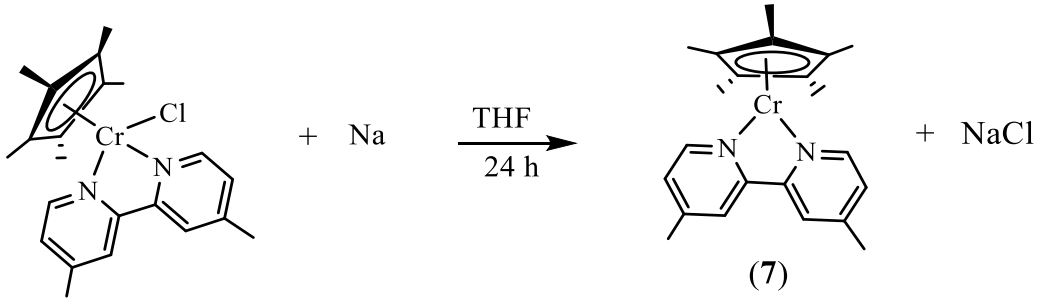

Scheme 2.12 Synthesis of [Cp*Cr(N^N)] (**7**).

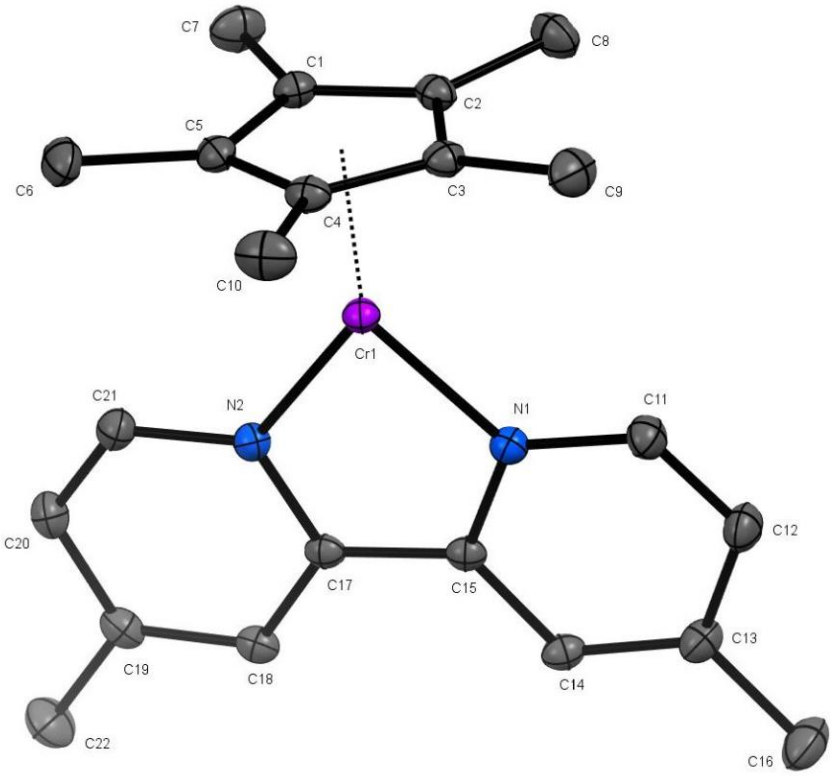

Figure 2.13 Molecular structure of [Cp*Cr(N^N)] (**7**) represented as 50% probability thermal ellipsoids. Hydrogen atoms have been omitted for clarity.

Table 2.7 Interatomic distances (Å) and angles (º) for [Cp*Cr(N^N)] (**7**).

Distances (Å)			
Cr1-N1	1.9908(12)	C14-C15	1.4187(19)
Cr1-N2	1.9882(12)	C14-C13	1.368(2)
Cr1-C3	2.2820(14)	C1-C2	1.420(2)
Cr1-C1	2.2849(14)	C1-C5	1.4300(19)

Cr1-C4	2.3006(14)	C1-C7	1.502(2)
Cr1-C2	2.2838(13)	C4-C5	1.422(2)
Cr1-C5	2.2779(14)	C4-C10	1.501(2)
N1-C15	1.3940(17)	C2-C8	1.506(2)
N1-C11	1.3683(18)	C5-C6	1.503(2)
N2-C17	1.3937(17)	C18-C19	1.367(2)
N2-C21	1.3698(18)	C19-C20	1.423(2)
C17-C15	1.4101(18)	C19-C22	1.503(2)
C17-C18	1.4192(19)	C21-C20	1.359(2)
C3-C4	1.422(2)	C11-C12	1.358(2)
C3-C2	1.432(2)	C13-C12	1.424(2)
C3-C9	1.505(2)	C13-C16	1.504(2)

Angles (°)

N1-Cr1-C3	110.8(5)	N1-C15-C14	120.2(12)
N1-Cr1-C1	142.0(5)	C17-C15-C14	125.2(12)
N1-Cr1-C4	136.1(5)	C2-C1-Cr1	71.85(8)
N1-Cr1-C2	113.4(5)	C2-C1-C5	107.8(12)
N1-Cr1-C5	171.3(5)	C2-C1-C7	126.5(14)
N2-Cr1-N1	80.04(5)	C5-C1-Cr1	71.47(8)
N2-Cr1-C3	168.4(5)	C5-C1-C7	125.8(14)
N2-Cr1-C1	113.5(5)	C7-C1-Cr1	122.5(10)
N2-Cr1-C4	132.7(5)	C3-C4-Cr1	71.21(8)
N2-Cr1-C2	143.8(5)	C3-C4-C5	107.8(12)
N2-Cr1-C5	108.5(5)	C3-C4-C10	127.0(14)
C3-Cr1-C1	60.66(5)	C5-C4-Cr1	71.04(8)
C3-Cr1-C4	36.15(5)	C5-C4-C10	125.2(14)
C3-Cr1-C2	36.55(5)	C10-C4-Cr1	126.0(10)
C1-Cr1-C4	60.55(5)	C3-C2-Cr1	71.66(8)
C2-Cr1-C1	36.22(5)	C3-C2-C8	126.1(14)
C2-Cr1-C4	60.54(5)	C1-C2-Cr1	71.94(8)

C5-Cr1-C3	60.52(5)	C1-C2-C3	107.9(12)
C5-Cr1-C1	36.53(5)	C1-C2-C8	125.9(14)
C5-Cr1-C4	36.19(5)	C8-C2-Cr1	122.7(10)
C5-Cr1-C2	60.64(5)	C1-C5-Cr1	72.00(8)
C15-N1-Cr1	115.5(9)	C1-C5-C6	126.1(14)
C11-N1-Cr1	127.5(10)	C4-C5-Cr1	72.77(8)
C11-N1-C15	116.9(12)	C4-C5-C1	108.3(12)
C17-N2-Cr1	115.8(9)	C4-C5-C6	125.2(14)
C21-N2-Cr1	127.2(10)	C6-C5-Cr1	126.8(10)
C21-N2-C17	116.9(12)	C19-C18-C17	121.5(13)
N2-C17-C15	114.2(11)	C18-C19-C20	117.4(13)
N2-C17-C18	120.3(12)	C18-C19-C22	122.5(15)
C15-C17-C18	125.5(12)	C20-C19-C22	120.1(14)
C4-C3-Cr1	72.64(8)	C20-C21-N2	124.0(14)
C4-C3-C2	108.2(12)	C12-C11-N1	124.1(14)
C4-C3-C9	125.6(14)	C14-C13-C12	117.3(13)
C2-C3-Cr1	71.79(8)	C14-C13-C16	122.3(14)
C2-C3-C9	125.9(14)	C12-C13-C16	120.4(14)
C9-C3-Cr1	126.9(10)	C21-C20-C19	119.9(14)
C13-C14-C15	121.6(13)	C11-C12-C13	119.9(14)
N1-C15-C17	114.5(11)		

7 crystalizes in the triclinic space group $P\bar{1}$ and has a very interesting structure. There is no dinitrogen ligand coordinated to the metal center and compared to the starting compound **6**, there is a free coordination site on the chromium center. The complex displayed an effective magnetic moment, of 2.7 (1) μ_B at 295 K. Oxidation state of chromium is dependent to the charge of ^{Me}bpy ligand. This ligand can be found as a neutral ligand or with one or two negative charges on that. For **7**, the Δ was calculated to be 0.01 Å, which is closest to, but below the number expected for $(bpy\bullet)^{1-}$. Therefore, in

7 the Δ value categorizes the bpy ligand as a radical anion coordinated ligand and the oxidation state of chromium center can be counted as II.

The next ligand was PMe_3. Four equivalents of PMe_3 were added to a THF solution of $[Cp^*CrCl]_2$. The solution was stirred for about 1h and the color of solution changed to blue-purple which can be the result of the coordination of PMe_3 to the chromium complex. After that 2 equivalents of sodium metal were added to the solution. The solution was stirred overnight and during this time the color of solution changed to green-brown. The solution was filtered, and the solvent was evaporated under vacuum. The remaining brown powder was extracted with pentanes and a green solution was collected. The solution was concentrated and at -30°C purple crystals of the product were collected in 10 % yield. Determination of the structure by X-ray crystallography revealed it to be a tetranuclear chromium dinitrogen complex, i.e. $[Cp^*Cr(\mu\text{-}N_2)PMe_3]_4Na$ (**8**). The molecular structure of **8** is depicted in **Figure 2.14** while the corresponding interatomic distances and angles are listed in **Table 2.8**.

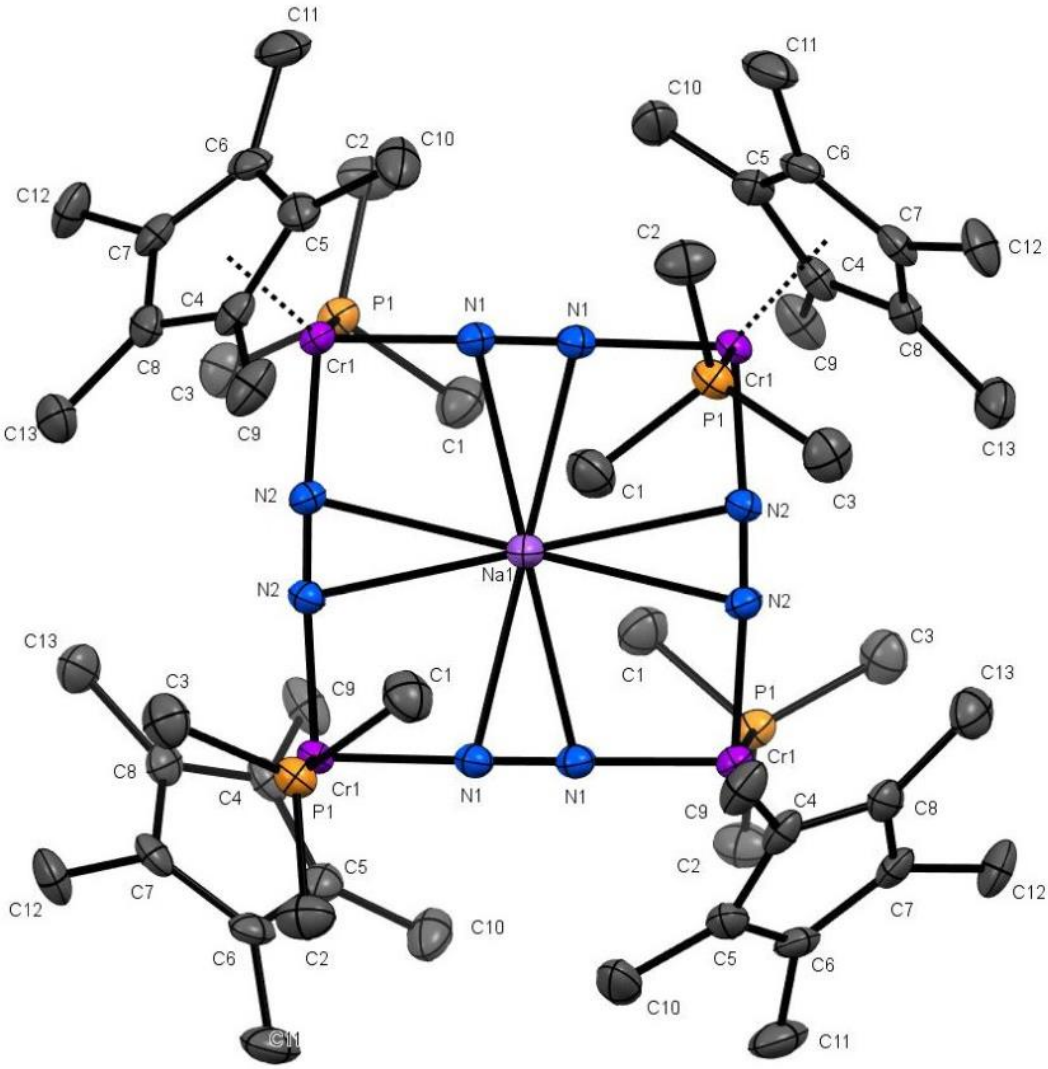

Figure 2.14 Molecular structure of $[Cp^*Cr(\mu\text{-}N_2)PMe_3]_4Na$ (**8**) represented as 50% probability thermal ellipsoids. Hydrogen atoms and pentane solvent molecules have been omitted for clarity.

Table 2.8 Interatomic distances (Å) and angles (º) for $[Cp^*Cr(\mu\text{-}N_2)PMe_3]_4Li$ (**8**).

Distances (Å)

Cr1-P1	2.3303(15)	N1-Na1	2.531(4)
Cr1-N1	1.846(4)	N2-N2	1.155(7)
Cr1-N2	1.867(4)	N2-Na1	2.608(4)
Cr1-C4	2.221(6)	C4-C5	1.433(8)
Cr1-C5	2.217(5)	C4-C8	1.426(8)
Cr1-C6	2.223(5)	C4-C9	1.492(9)
Cr1-C7	2.239(5)	C5-C6	1.415(9)
Cr1-C8	2.230(5)	C5-C10	1.483(9)
Cr1-Na1	3.4483(8)	C6-C7	1.433(8)
P1-C1	1.820(6)	C6-C1	1.512(9)
P1-C2	1.838(6)	C7-C8	1.395(8)
P1-C3	1.820(7)	C7-C12	1.514(9)
N1-N1	1.183(8)	C8-C13	1.499(8)

Angles (°)

P1-Cr1-Na1	90.04(4)	N1-N1-Cr1	177.2(5)
N1-Cr1-P1	91.15(14)	N1-N1-Na1	76.48(9)
N1-Cr1-N2	93.95(16)	Cr1-N2-Na1	99.46(15)
N1-Cr1-C4	108.8(2)	N2-N2-Cr1	176.3(3)
N1-Cr1-C5	90.58(19)	N2-N2-Na1	77.21(8)
N1-Cr1-C6	109.23(19)	C5-C4-Cr1	71.0(3)
N1-Cr1-C7	146.70(18)	C5-C4-C9	126.4(6)
N1-Cr1-C8	146.1(2)	C8-C4-Cr1	71.7(3)
N1-Cr1-Na1	45.70(11)	C8-C4-C5	107.4(5)
N2-Cr1-P1	89.74(13)	C8-C4-C9	126.1(5)
N2-Cr1-C4	101.7(2)	C9-C4-Cr1	126.4(4)
N2-Cr1-C5	137.2(2)	C4-C5-Cr1	71.3(3)

N2-Cr1-C6	154.9(2)	C4-C5-C10	126.6(6)
N2-Cr1-C7	118.88(19)	C6-C5-Cr1	71.7(3)
N2-Cr1-C8	93.38(19)	C6-C5-C4	107.9(5)
N2-Cr1-Na1	48.26(11)	C6-C5-C10	125.5(6)
C4-Cr1-P1	156.05(15)	C10-C5-Cr1	123.7(4)
C4-Cr1-C6	62.4(2)	C5-C6-Cr1	71.2(3)
C4-Cr1-C7	61.8(2)	C5-C6-C7	107.7(5)
C4-Cr1-C8	37.4(2)	C5-C6-C11	125.2(6)
C4-Cr1-Na1	113.30(14)	C7-C6-Cr1	71.9(3)
C5-Cr1-P1	132.76(16)	C7-C6-C11	126.6(6)
C5-Cr1-C4	37.7(2)	C11-C6-Cr1	129.1(4)
C5-Cr1-C6	37.2(2)	C6-C7-Cr1	70.7(3)
C5-Cr1-C7	62.1(2)	C6-C7-C12	125.9(6)
C5-Cr1-C8	62.4(2)	C8-C7-Cr1	71.4(3)
C5-Cr1-Na1	122.76(16)	C8-C7-C6	108.4(5)
C6-Cr1-P1	99.03(17)	C8-C7-C12	125.5(6)
C6-Cr1-C7	37.5(2)	C12-C7-Cr1	127.6(4)
C6-Cr1-C8	62.0(2)	C4-C8-Cr1	71.0(3)
C6-Cr1-Na1	153.85(15)	C4-C8-C13	125.7(6)
C7-Cr1-P1	94.22(17)	C7-C8-Cr1	72.2(3)
C7-Cr1-Na1	166.52(15)	C7-C8-C4	108.7(5)
C8-Cr1-P1	121.94(16)	C7-C8-C13	125.6(6)
C8-Cr1-C7	36.4(2)	C13-C8-Cr1	124.6(4)
C8-Cr1-Na1	131.99(15)	N1-Na1-N1	178.16(19)
C1-P1-Cr1	110.0(3)	N1-Na1-N1	27.03(18)
C1-P1-C2	101.1(4)	N1-Na1-N1	153.03(18)
C1-P1-C3	101.2(3)	N1-Na1-N2	63.74(12)
C2-P1-Cr1	122.7(2)	N1-Na1-N2	90.72(12)
C3-P1-Cr1	118.9(2)	N1-Na1-N2	116.24(12)
C3-P1-C2	99.7(4)	N1-Na1-N2	89.30(12)
Cr1-N1-Na1	102.84(16)		

Although two equivalents of the PMe_3 ligand was added to the reaction mixture, in the product only one of them is coordinated to the chromium center. It is possible that the PMe_3 ligand had been removed under vacuum during the workup of the product, that is why there is only one PMe_3 ligand coordinated to each chromium center.

8 crystalizes in the monoclinic space group C2. The geometry around each chromium center is pseudo-octahedral. Four chromium metals make a square with almost right angles (93.95(16)°) in each corner. There is an atom in the middle of the structure that can be refined as Li, but in the synthesis of **8** sodium metal was used and it is unlikely to have Li in the final product. On the other hand, the bond distances between that atom with N1 and N2 are respectively 2.531(4) and 2.608(4) Å, which are in the range of previously reported N-Na bond distances.[75,76] Therefore the structure was refined as partially occupied with 21% site occupancy of Na atom, in other words this is a cocrystal structure of two compounds with 21% being Na atom. The formal oxidation state of three chromiums ions is +I and there is one chromium with the formal oxidation state of 0. The Cr-N distances are 1.846(4) and 1.867(4) Å. The N-N distances are 1.183(8) and 1.155(7) Å for the bridging dinitrogen ligands, which are in the range of N-N triple bond distances.

In 2019, Hung et.al., reported a similar tetranuclear chromium complex $[(2,6\text{-}Me_2Ph)_2nacnacCr(\mu\text{-}N_2)]_4$ with bridging dinitrogen ligand [77]. In this complex there is a two-fold axis and the geometry around each chromium center is approximately square planar and the four Cr atoms form a tetrahedron structure. In this molecule the average Cr-N (2.062(3)–2.092(3) Å) and N-N (1.171(4) and 1.176 (4) Å) distances are slightly larger compared to **8**.

The ^{1}H-NMR spectrum of **8** shows a broad range of peaks from +30.7 to −13.0 ppm, which is consistent with the paramagnetic property of this chromium complex. Due to the low yield of this reaction magnetic moment measurement was not performed.

Using a phosphorus-based ligand such as PMe_3 showed promising results for the synthesis of dinitrogen complexes. Also, examples of chromium dinitrogen complexes with phosphorous donor ligands are known.[78] Therefore, it was decided to use a ligand in

this process that can coordinate to the chromium center stronger. The bidentate ligand, 1,2-Bis(dimethylphosphino)ethane (dmpe) was the next ligand that was used to modify the starting complex $[Cp^*CrCl]_2$.

Reaction of 2 equivalents of dmpe with a THF solution of $[Cp^*CrCl]_2$, resulted in a color change from green-brown to light brown. The solution was stirred for 2 hours and then it was filtered. The solvent was removed in vacuo and a brown powder was collected which was washed with cold pentanes. The brown powder was collected and was dissolved in a minimum amount of THF and after staying at -30°C for overnight, brown crystals of the product were collected. The structure of the compound was determined using X-ray crystallography; it is a mononuclear chromium complex, i.e. [Cp*ClCr(dmpe)] (**9**). The molecular structure of **9** is depicted in **Figure 2.15**, while the corresponding interatomic distances and angles are listed in **Table 2.9**.

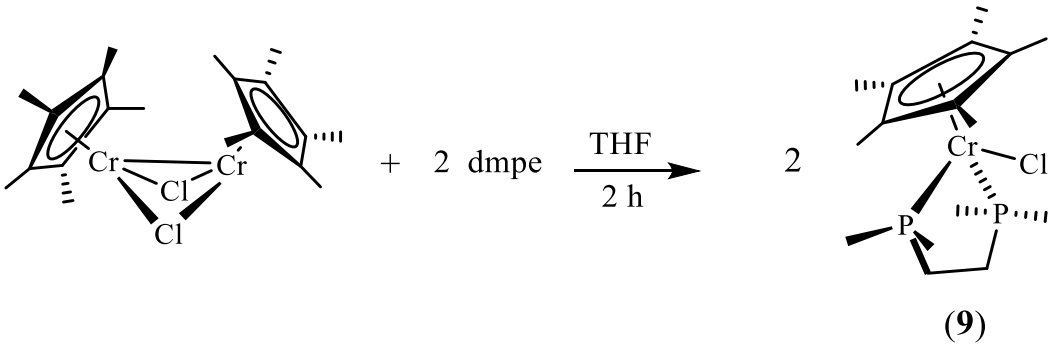

(**9**)

Scheme 2.13 Synthesis of [Cp*ClCr(dmpe)] (**9**).

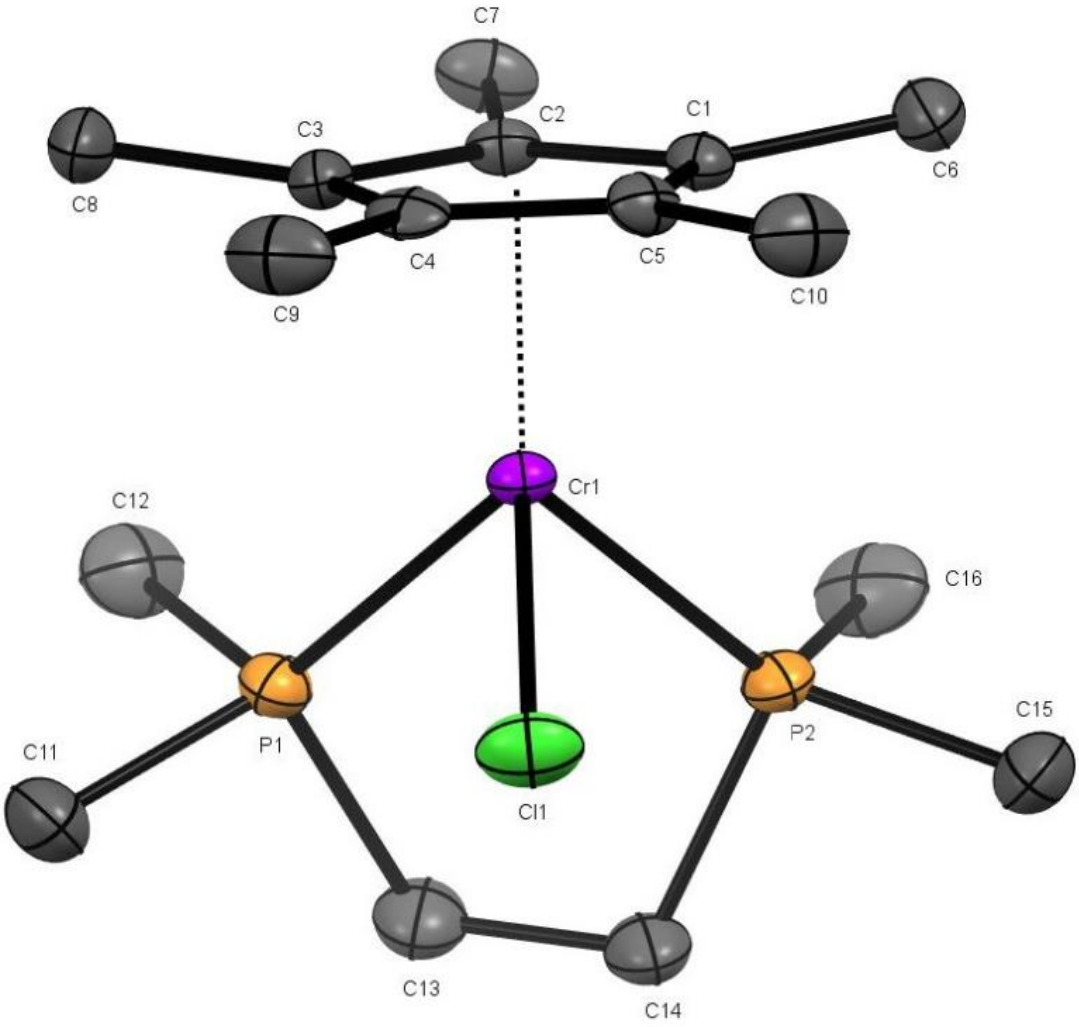

Figure 2.15 Molecular structure of [Cp*ClCr(dmpe)] (**9**) represented as 50% probability thermal ellipsoids. Hydrogen atoms have been omitted for clarity.

Table 2.9 Interatomic distances (Å) and angles (º) for [Cp*ClCr(dmpe)] (**9**).

Distances (Å)

Cr1-Cl1	2.3165(13)	P2-C16	1.817(5)
Cr1-P1	2.3308(14)	C1-C2	1.421(5)
Cr1-P2	2.3234(14)	C1-C5	1.404(6)
Cr1-C1	2.208(4)	C1-C6	1.501(6)
Cr1-C2	2.173(4)	C2-C3	1.435(5)
Cr1-C3	2.186(4)	C2-C7	1.498(6)
Cr1-C4	2.217(4)	C3-C4	1.405(6)
Cr1-C5	2.224(4)	C3-C8	1.494(6)
P1-C11	1.827(5)	C4-C5	1.427(6)
P1-C12	1.823(5)	C4-C9	1.494(6)
P1-C13	1.854(5)	C5-C10	1.494(6)
P2-C14	1.843(5)	C13-C14	1.481(8)
P2-C15	1.823(5)		

Angles (°)

Cl1-Cr1-P1	90.78(5)	C15-P2-C14	100.4(2)
Cl1-Cr1-P2	88.60(5)	C16-P2-Cr1	121.3(2)
P2-Cr1-P1	81.87(5)	C16-P2-C14	103.0(3)
C1-Cr1-Cl1	128.7(11)	C16-P2-C15	101.8(3)
C1-Cr1-P1	140.5(11)	C2-C1-Cr1	69.70(2)
C1-Cr1-P2	96.97(11)	C2-C1-C6	126.0(4)
C1-Cr1-C4	62.31(15)	C5-C1-Cr1	72.20(2)
C1-Cr1-C5	36.93(14)	C5-C1-C2	108.3(3)
C2-Cr1-Cl1	157.3(12)	C5-C1-C6	125.4(4)
C2-Cr1-P1	105.2(11)	C6-C1-Cr1	128.8(3)
C2-Cr1-P2	109.2(11)	C1-C2-Cr1	72.40(2)

C2-Cr1-C1	37.85(14)	C1-C2-C3	107.7(3)
C2-Cr1-C3	38.45(14)	C1-C2-C7	126.0(4)
C2-Cr1-C4	62.87(15)	C3-C2-Cr1	71.30(2)
C2-Cr1-C5	62.77(15)	C3-C2-C7	125.7(4)
C3-Cr1-Cl1	125.2(12)	C7-C2-Cr1	129.0(3)
C3-Cr1-P1	96.33(11)	C2-C3-Cr1	70.30(2)
C3-Cr1-P2	146.2(12)	C2-C3-C8	127.1(4)
C3-Cr1-C1	63.34(15)	C4-C3-Cr1	72.60(2)
C3-Cr1-C4	37.22(15)	C4-C3-C2	107.4(4)
C3-Cr1-C5	62.87(15)	C4-C3-C8	124.7(4)
C4-Cr1-Cl1	95.13(11)	C8-C3-Cr1	130.4(3)
C4-Cr1-P1	121.9(13)	C3-C4-Cr1	70.20(2)
C4-Cr1-P2	155.8(13)	C3-C4-C5	108.6(4)
C4-Cr1-C5	37.49(17)	C3-C4-C9	126.6(4)
C5-Cr1-Cl1	96.80(11)	C5-C4-Cr1	71.50(2)
C5-Cr1-P1	158.4(11)	C5-C4-C9	124.8(4)
C5-Cr1-P2	118.4(12)	C9-C4-Cr1	123.7(3)
C11-P1-Cr1	117.8(2)	C1-C5-Cr1	70.90(2)
C11-P1-C13	103.2(3)	C1-C5-C4	107.9(3)
C12-P1-Cr1	122.2(19)	C1-C5-C10	126.3(4)
C12-P1-C11	100.6(3)	C4-C5-Cr1	71.00(2)
C12-P1-C13	99.90(3)	C4-C5-C10	125.8(4)
C13-P1-Cr1	110.3(18)	C10-C5-Cr1	123.8(3)
C14-P2-Cr1	106.4(17)	C14-C13-P1	112.6(3)
C15-P2-Cr1	120.8(19)	C13-C14-P2	111.0(3)

9 crystalizes in the orthorhombic space group Pbca. The chromium center has pseudo-octahedral coordination geometry. The effective magnetic moment of **9** was found to be 2.6 (1) μ_B at room temperature, consistent with the assignment of the metal center as an intermediate spin (S=1) d^4 Cr(II) complex. ^{1}H-NMR spectra recorded in deuterated benzene-d_6 solution of **9** displayed 3 well defined resonances at -20.5, -7.8 and

1.9 ppm, which were assigned to the protons of the dmpe and Cp* ligands, as shown in **Figure 2.16**. In 1991, a chromium complex with dmpe ligand was synthesized in our group, i.e. [Cp*Cr(dmpe)Me], which only showed two peaks in the proton NMR at 5.84 and -15.88 ppm, with the integrations of 12 and 15.[79]

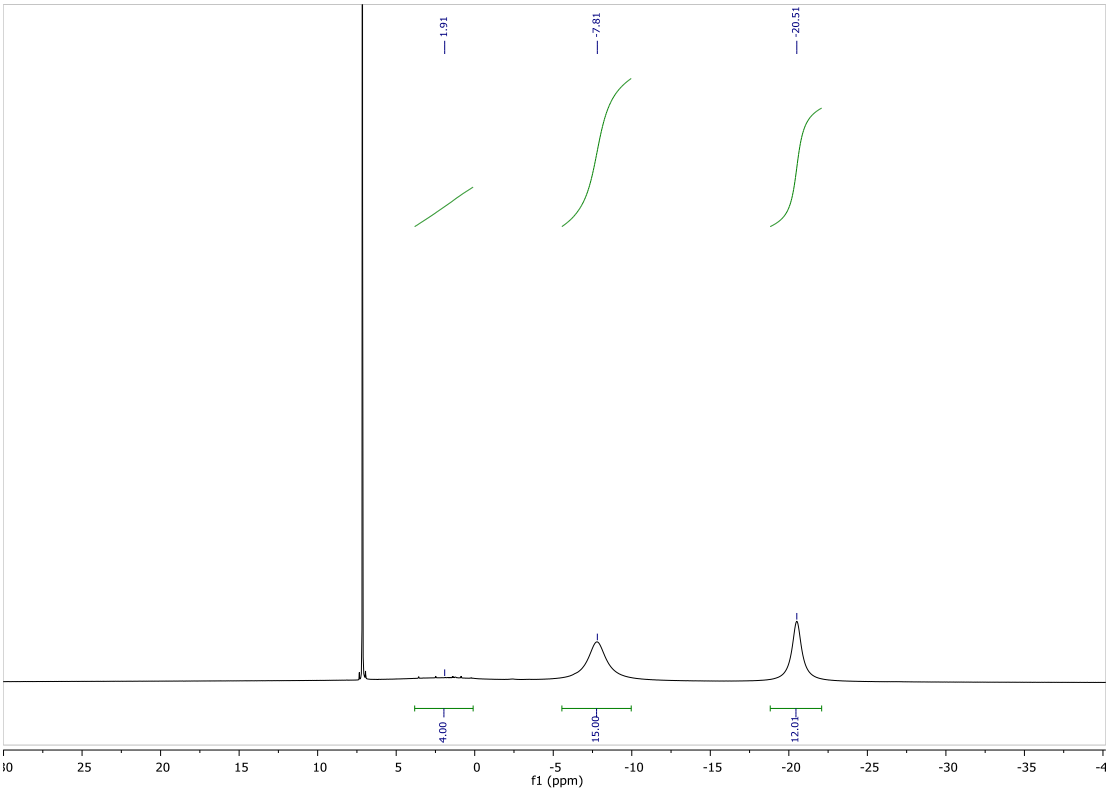

Figure 2.16 ^{1}H-NMR spectrum of **9** recorded in C_6D_6 at 400 MHz.

The ligated chromium halide complex **9** can provide a new pathway into the synthesis of various classes of inorganic and organometallic compounds. The reduction of **9** under nitrogen atmosphere was examined next.

Reaction of **9** with 1.0 equivalent of sodium metal, while stirring overnight at room temperature under nitrogen atmosphere, resulted in a color change from brown to green-brown in THF. The THF was removed and the residue was washed with 10 ml of

cold pentanes and diethyl ether. The remaining brown powder was redissolved in THF and was cooled to -30°C for overnight to yield green-brown crystals. Determination of the structure by X-ray crystallography revealed it to be a dinuclear dinitrogen chromium complex, i.e. $[Cp^*(dmpe)Cr]_2(\mu\text{-}N_2)$ (**10**). The molecular structure of **10** is depicted in **Figure 2.17**, while the corresponding bond distances and angles are listed in **Table 2.1**.

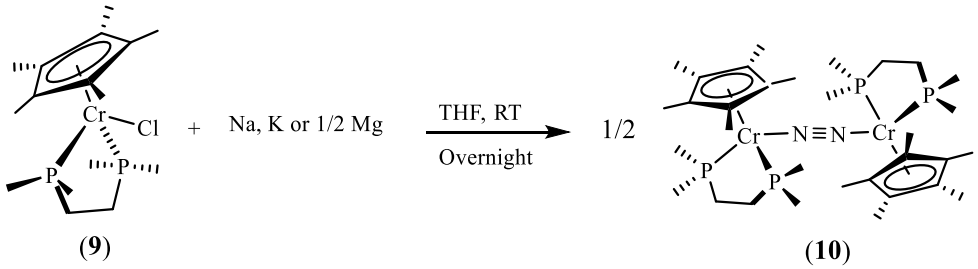

(**9**) (**10**)

Scheme 2.14 Synthesis of $[Cp^*(dmpe)Cr]_2(\mu\text{-}N_2)$ (**10**).

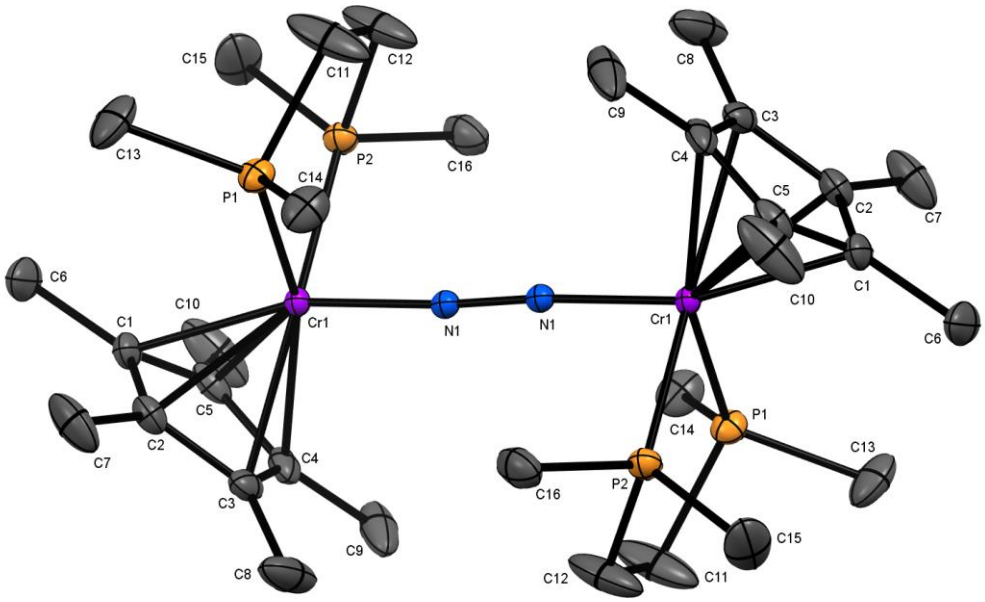

Figure 2.17 Molecular structure of $[Cp^*(dmpe)Cr]_2(\mu\text{-}N_2)$ (**10**) represented as 50% probability thermal ellipsoids. Hydrogen atoms are omitted for clarity.

Table 2.10 Interatomic distances (Å) and angles (º) for $[Cp^*(dmpe)Cr]_2(\mu\text{-}N_2)$ (**10**).

Distances (Å)

Cr1-P1	2.2661(8)	P2-C16	1.830(4)
Cr1-P2	2.2712(8)	N1-N1	1.195(4)
Cr1-N1	1.838(2)	C1-C2	1.430(4)
Cr1-C1	2.213(3)	C1-C5	1.428(4)
Cr1-C2	2.218(3)	C1-C6	1.499(4)
Cr1-C3	2.236(3)	C2-C3	1.414(4)
Cr1-C4	2.229(3)	C2-C7	1.504(4)
Cr1-C5	2.211(3)	C3-C4	1.402(5)
P1-C11	1.842(4)	C3-C8	1.510(5)
P1-C13	1.831(4)	C4-C5	1.418(5)
P1-C14	1.827(3)	C4-C9	1.504(5)
P2-C12	1.847(4)	C5-C10	1.499(5)
P2-C15	1.827(4)	C11-C12	1.373(6)

Angles (°)

P1-Cr1-P2	81.69(3)	C15-P2-C16	100.6(2)
N1-Cr1-P1	87.90(7)	C16-P2-Cr1	119.5(13)
N1-Cr1-P2	88.31(7)	C16-P2-C12	100.4(2)
N1-Cr1-C1	164.0(10)	N11-N1-Cr1	175.5(3)
N1-Cr1-C2	131.4(10)	C2-C1-Cr1	71.36(15)
N1-Cr1-C3	102.3(10)	C2-C1-C6	125.9(3)
N1-Cr1-C4	102.9(10)	C5-C1-Cr1	71.07(15)
N1-Cr1-C5	133.1(11)	C5-C1-C2	107.0(3)
C1-Cr1-P1	103.4(8)	C5-C1-C6	126.4(3)
C1-Cr1-P2	104.3(8)	C6-C1-Cr1	130.2(2)
C1-Cr1-C2	37.66(11)	C1-C2-Cr1	70.98(15)

C1-Cr1-C3	62.32(10)	C1-C2-C7	126.5(3)
C1-Cr1-C4	62.49(11)	C3-C2-Cr1	72.17(16)
C2-Cr1-P1	94.89(8)	C3-C2-C1	108.1(3)
C2-Cr1-P2	140.2(8)	C3-C2-C7	124.6(3)
C2-Cr1-C3	37.02(11)	C7-C2-Cr1	130.7(2)
C2-Cr1-C4	61.87(11)	C2-C3-Cr1	70.82(16)
C3-Cr1-P1	120.6(9)	C2-C3-C8	123.5(4)
C3-Cr1-P2	155.2(9)	C4-C3-Cr1	71.42(16)
C4-Cr1-P1	156.0(9)	C4-C3-C2	108.6(3)
C4-Cr1-P2	119.5(10)	C4-C3-C8	127.5(4)
C4-Cr1-C3	36.61(12)	C8-C3-Cr1	129.1(2)
C5-Cr1-P1	138.8(9)	C3-C4-Cr1	71.98(16)
C5-Cr1-P2	94.51(8)	C3-C4-C5	108.3(3)
C5-Cr1-C1	37.67(11)	C3-C4-C9	126.0(4)
C5-Cr1-C2	62.50(11)	C5-C4-Cr1	70.68(17)
C5-Cr1-C3	61.88(11)	C5-C4-C9	125.4(4)
C5-Cr1-C4	37.26(13)	C9-C4-Cr1	127.3(2)
C11-P1-Cr1	110.4(16)	C1-C5-Cr1	71.26(16)
C13-P1-Cr1	124.2(14)	C1-C5-C10	127.0(4)
C13-P1-C11	99.10(3)	C4-C5-Cr1	72.06(16)
C14-P1-Cr1	117.7(12)	C4-C5-C1	108.1(3)
C14-P1-C11	101.6(2)	C4-C5-C10	124.1(4)
C14-P1-C13	100.3(19)	C10-C5-Cr1	130.5(2)
C12-P2-Cr1	108.9(15)	C12-C11-P1	115.7(3)
C15-P2-Cr1	123.8(15)	C11-C12-P2	114.8(3)
C15-P2-C12	99.90(3)		

10 crystalizes in the monoclinic space group $P2_1/c$ and has an inversion center about the midpoint of the N-N bond. The geometry around each chromium center is pseudo-octahedral with the Cp* ligand occupying three adjacent coordination sites. The Cr-N bond distance is 1.838(2) Å. The N-N bond distance is 1.195(3) Å, which is larger

than the bond distance in free nitrogen (1.0975 Å),[80] suggesting a mild degree of reduction of coordinated N_2 in **10**.

The formal oxidation state of chromium in **10** is +I and the complex has a 17-electron configuration. The effective magnetic moment of **10** was measured to be 2.0 (1) μ_B at room temperature. For a system of two non-interacting low spin d^5 chromium (I) ions (assuming the N_2 ligand is not reduced), the expected magnetic moment is 2.4 μ_B. A possible interpretation of the lower moment of **10** is that the bridging N_2 ligand mediates antiferromagnetic coupling between the chromium centers. The IR spectrum in the solid state did not show the stretching frequency of N_2 ligand due to the inversion symmetry of **10**. The proton NMR of **10** shows broad, shifted peaks, consistent with the paramagnetic behavior of **10**, as shown in **Figure 2.18**.

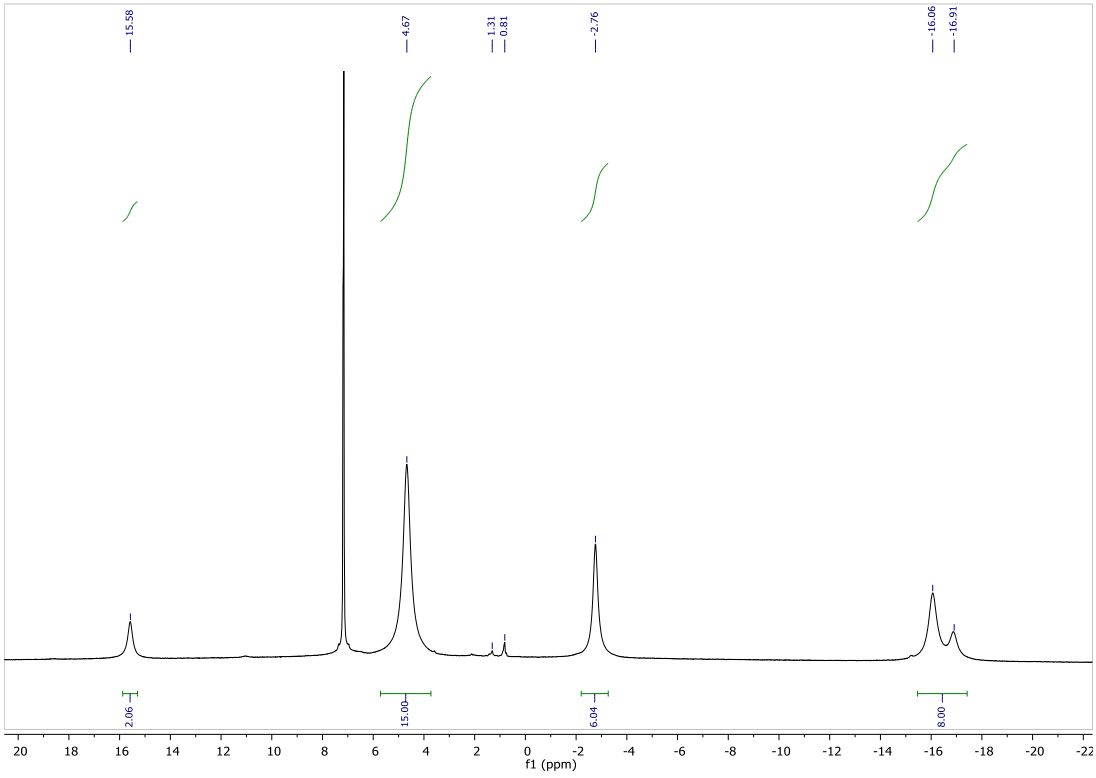

Figure 2.18 ^{1}H- spectrum of $[Cp^*(dmpe)Cr]_2(\mu\text{-}N_2)$ (**10**) recorded in C_6D_6 at 400 MHz.

With the dinitrogen complex **10** in hand, it was decided to attempt the synthesis of the corresponding chromium nitride complex, thus motivating the reaction of **9** with azide reagents.

Reaction of **9** with 1.0 equivalent of NaN_3 in THF resulted in a color change from brown to blue after 3 h of stirring. The solvent was then removed under vacuum and the residue was washed with 10 ml of cold pentanes and 15 ml of cold diethyl ether. The remaining blue powder was dissolved in THF, and the solution was cooled to low temperature (-30°C) overnight to yield blue-purple crystals. Determination of the structure by X-ray crystallography revealed it to be a dinuclear chromium complex with a bridging nitride, i.e. [Cp*dmpeCr(μ-N)CrCp*Cl] (**11**). The molecular structure of **11** is depicted in **Figure 2.19** while the corresponding interatomic distances and angles are listed in **Table 2.11**.

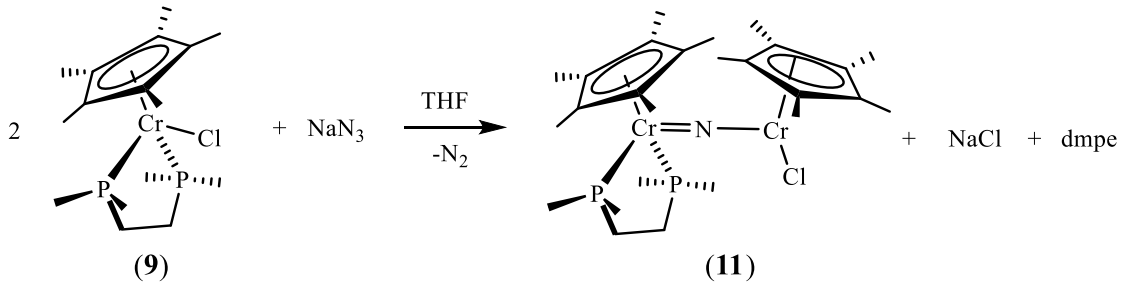

(**9**) (**11**)

Scheme 2.15 Synthesis of [Cp*dmpeCr(μ-N)CrCp*Cl] (**11**).

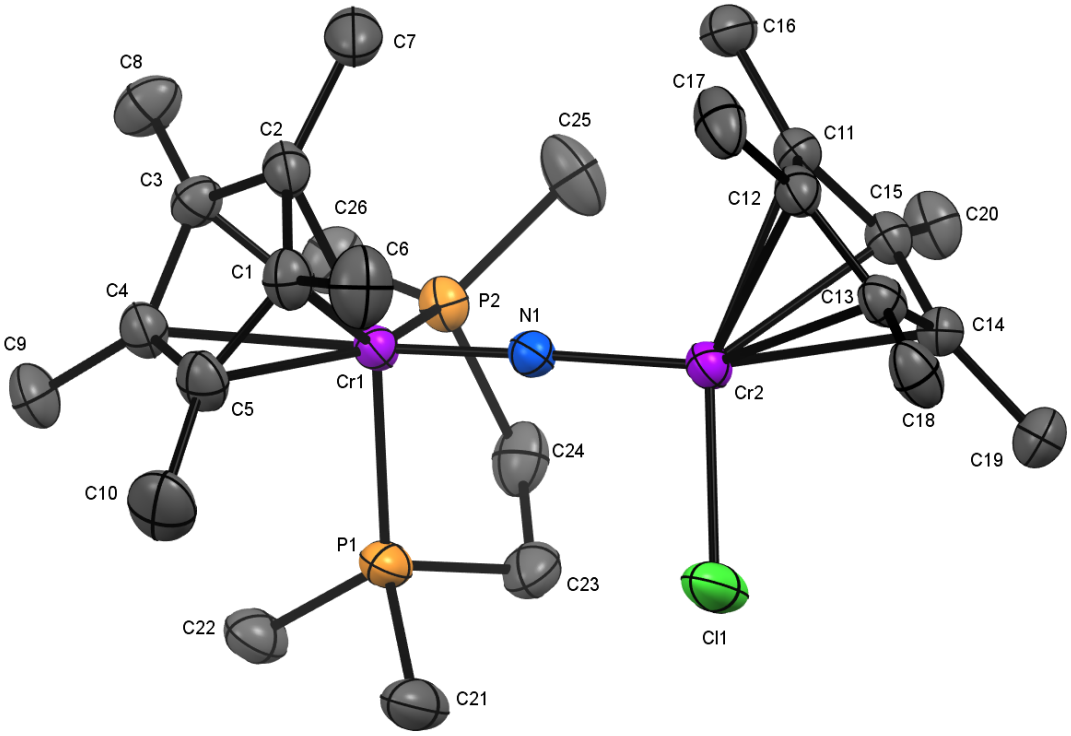

Figure 2.19 Molecular structure of [Cp*dmpeCr(μ-N)CrCp*Cl] (**11**) represented as 50% probability thermal ellipsoids. Hydrogen atoms are omitted for clarity.

Table 2.11 Interatomic distances (Å) and angles (º) for [Cp*dmpeCr(μ-N)CrCp*Cl] (**11**).

Distances (Å)

Cr1-P1	2.293(2)	C1-C2	1.403(11)
Cr1-P2	2.307(2)	C1-C5	1.424(11)
Cr1-N1	1.644(6)	C1-C6	1.503(11)
Cr1-C1	2.174(8)	C2-C3	1.431(10)
Cr1-C2	2.221(8)	C2-C7	1.495(11)

Cr1-C3	2.310(7)	C3-C4	1.402(10)
Cr1-C4	2.325(8)	C3-C8	1.506(9)
Cr1-C5	2.225(8)	C4-C5	1.445(10)
Cr2-Cl1	2.299(2)	C4-C9	1.503(10)
Cr2-N1	1.942(6)	C5-C10	1.492(11)
Cr2-C11	2.303(7)	C11-C12	1.442(10)
Cr2-C12	2.333(7)	C11-C15	1.424(11)
Cr2-C13	2.329(6)	C11-C16	1.512(10)
Cr2-C14	2.335(7)	C12-C13	1.391(10)
Cr2-C15	2.338(7)	C12-C17	1.491(11)
P1-C21	1.822(9)	C13-C14	1.428(11)
P1-C22	1.835(8)	C13-C18	1.505(9)
P1-C23	1.804(10)	C14-C15	1.425(10)
P2-C24	1.867(10)	C14-C19	1.480(10)
P2-C25	1.833(10)	C15-C20	1.485(10)
P2-C26	1.817(8)	C23-C24	1.530(14)

Angles (°)

P1-Cr1-P2	81.70(8)	C2-C1-Cr1	73.20(5)
P1-Cr1-C3	128.1(2)	C2-C1-C5	108.9(7)
P1-Cr1-C4	97.70(2)	C2-C1-C6	126.6(8)
P2-Cr1-C3	94.35(18)	C5-C1-Cr1	73.10(5)
P2-Cr1-C4	109.6(2)	C5-C1-C6	124.4(8)
N1-Cr1-P1	91.70(2)	C6-C1-Cr1	122.8(6)
N1-Cr1-P2	91.70(2)	C1-C2-Cr1	69.60(5)
N1-Cr1-C1	96.70(3)	C1-C2-C3	107.6(6)
N1-Cr1-C2	105.5(3)	C1-C2-C7	127.8(8)
N1-Cr1-C3	140.2(3)	C3-C2-Cr1	75.00(4)
N1-Cr1-C4	157.7(3)	C3-C2-C7	124.3(8)
N1-Cr1-C5	122.3(3)	C7-C2-Cr1	125.5(5)
C1-Cr1-P1	126.8(2)	C2-C3-Cr1	68.20(4)

C1-Cr1-P2	149.7(2)	C2-C3-C8	125.8(7)
C1-Cr1-C2	37.20(3)	C4-C3-Cr1	73.00(4)
C1-Cr1-C3	61.30(3)	C4-C3-C2	108.7(6)
C1-Cr1-C4	61.60(3)	C4-C3-C8	124.8(7)
C1-Cr1-C5	37.70(3)	C8-C3-Cr1	132.5(6)
C2-Cr1-P1	156.8(2)	C3-C4-Cr1	71.80(4)
C2-Cr1-P2	112.5(2)	C3-C4-C5	107.7(7)
C2-Cr1-C3	36.80(3)	C3-C4-C9	125.8(7)
C2-Cr1-C4	60.80(3)	C5-C4-Cr1	67.80(4)
C2-Cr1-C5	62.30(3)	C5-C4-C9	126.1(7)
C3-Cr1-C4	35.20(3)	C9-C4-Cr1	131.1(7)
C5-Cr1-P1	95.50(2)	C1-C5-Cr1	69.20(4)
C5-Cr1-P2	146.0(2)	C1-C5-C4	107.1(7)
C5-Cr1-C3	60.80(3)	C1-C5-C10	125.9(8)
C5-Cr1-C4	36.90(3)	C4-C5-Cr1	75.30(5)
Cl1-Cr2-C11	153.1(19)	C4-C5-C10	126.2(8)
Cl1-Cr2-C12	124.2(2)	C10-C5-Cr1	129.1(8)
Cl1-Cr2-C13	94.88(18)	C12-C11-Cr2	73.00(4)
Cl1-Cr2-C14	95.63(18)	C12-C11-C16	125.5(7)
Cl1-Cr2-C15	126.6(2)	C15-C11-Cr2	73.50(4)
N1-Cr2-Cl1	100.8(17)	C15-C11-C12	107.9(6)
N1-Cr2-C11	106.1(2)	C15-C11-C16	126.0(7)
N1-Cr2-C12	121.8(3)	C16-C11-Cr2	125.8(5)
N1-Cr2-C13	155.6(3)	C11-C12-Cr2	70.70(4)
N1-Cr2-C14	156.4(2)	C11-C12-C17	124.8(8)
N1-Cr2-C15	121.8(2)	C13-C12-Cr2	72.50(4)
C11-Cr2-C12	36.30(3)	C13-C12-C11	107.8(6)
C11-Cr2-C13	59.30(2)	C13-C12-C17	127.4(8)
C11-Cr2-C14	59.40(2)	C17-C12-Cr2	122.7(5)
C11-Cr2-C15	35.70(3)	C12-C13-Cr2	72.80(4)
C12-Cr2-C14	58.90(2)	C12-C13-C14	108.9(6)
C12-Cr2-C15	59.50(2)	C12-C13-C18	126.9(8)
C13-Cr2-C12	34.70(3)	C14-C13-Cr2	72.40(4)

C13-Cr2-C14	35.70(3)	C14-C13-C18	124.2(7)
C13-Cr2-C15	59.30(2)	C18-C13-Cr2	123.4(5)
C14-Cr2-C15	35.50(2)	C13-C14-Cr2	72.00(4)
C21-P1-Cr1	121.6(4)	C13-C14-C19	126.7(7)
C21-P1-C22	100.4(4)	C15-C14-Cr2	72.40(4)
C22-P1-Cr1	122.1(3)	C15-C14-C13	107.9(6)
C23-P1-Cr1	105.1(3)	C15-C14-C19	125.3(7)
C23-P1-C21	102.3(5)	C19-C14-Cr2	123.1(5)
C23-P1-C22	102.2(5)	C11-C15-Cr2	70.80(4)
C24-P2-Cr1	108.6(3)	C11-C15-C14	107.4(6)
C25-P2-Cr1	116.3(3)	C11-C15-C20	126.9(7)
C25-P2-C24	104.6(6)	C14-C15-Cr2	72.10(4)
C26-P2-Cr1	124.6(3)	C14-C15-C20	125.5(7)
C26-P2-C24	99.60(5)	C20-C15-Cr2	126.8(5)
C26-P2-C25	100.4(5)	C24-C23-P1	108.7(6)
Cr1-N1-Cr2	174.4(4)	C23-C24-P2	111.8(7)

Displacement of the dmpe ligand in **9** with the nitride ligand of a second molecule results in a dinuclear molecule (**11**) which crystalizes in the orthorhombic space group $P2_12_12_1$. The geometry around Cr1 is pseudo-octahedral and the Cr1-N1 bond distance is 1.644(6) Å, which is in the range of Cr-N double bond distances. [66,81] The Cr2 center is five coordinate and the bond distance between Cr2 and the bridging nitride is 1.942(6) Å, which is in the range of Cr-N single bond distances.[66] The Cr_1-N-Cr_2 bond angle about the bridging nitride is 174.6(4)°. The effective magnetic moment of **11** could not be measured due to the lack of enough pure material.

The presence of one remaining chloride ligand on Cr2 suggests that the reaction with azide is not complete. To test if this reaction can be moved forward, the reaction was repeated, but for a longer duration. This time, after the addition of 1 equivalent azide, the mixture was allowed to stir for 24 h. The color of solution changed from brown to blue during this time. After filtration, the solvent was removed under vacuum and the

remaining powder was washed with cold pentanes and diethyl ether. The remaining residue was dissolved in THF and was cooled at -30°C for overnight to yield blue crystals of the product. Using X-ray crystallography, the structure of the product was identified as a dinuclear chromium complex with bridging nitride and two terminal azides on one of the chromium centers, i.e. [Cp*dmpeCr(μ-N)Cr(N_3)$_2$Cp*] (**12**), as shown in **Figure 2.20**. The corresponding interatomic distances and angles are listed in **Table 2.12**.

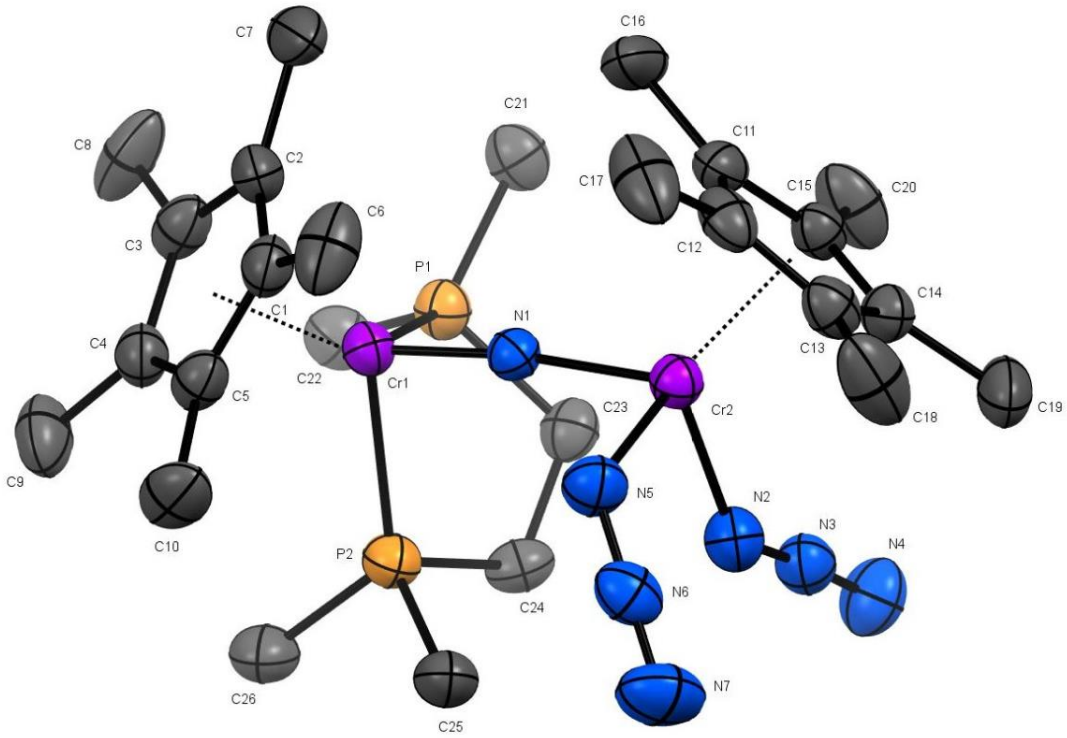

Figure 2.20 Molecular structure of [Cp*dmpeCr(μ-N)Cr(N_3)$_2$Cp*] (**12**) represented as 50% probability thermal ellipsoids. Hydrogen atoms are omitted for clarity.

Table 2.12 Interatomic distances (Å) and angles (º) for [Cp*dmpeCr(μ-N)Cr(N_3)$_3$Cp*] (**12**).

Distances (Å)

Cr1-P1	2.314(2)	N5-N6	1.216(11)
Cr1-P2	2.315(2)	N6-N7	1.155(11)
Cr1-N1	1.637(6)	C1-C2	1.392(12)
Cr1-C1	2.164(8)	C1-C5	1.425(12)
Cr1-C2	2.244(9)	C1-C6	1.517(12)
Cr1-C3	2.324(9)	C2-C3	1.397(12)
Cr1-C4	2.338(8)	C2-C7	1.482(12)
Cr1-C5	2.191(8)	C3-C4	1.427(12)
Cr2-N1	1.972(6)	C3-C8	1.522(12)
Cr2-N2	1.973(8)	C4-C5	1.446(12)
Cr2-N5	1.998(8)	C4-C9	1.474(12)
Cr2-C11	2.259(8)	C5-C10	1.492(11)
Cr2-C12	2.234(8)	C11-C12	1.416(12)
Cr2-C13	2.270(8)	C11-C15	1.431(11)
Cr2-C14	2.290(8)	C11-C16	1.487(12)
Cr2-C15	2.249(8)	C12-C13	1.404(12)
P1-C21	1.817(9)	C12-C17	1.509(12)
P1-C22	1.804(9)	C13-C14	1.394(11)
P1-C23	1.819(8)	C13-C18	1.492(12)
P2-C24	1.854(9)	C14-C15	1.395(11)
P2-C25	1.829(9)	C14-C19	1.495(11)
P2-C26	1.811(9)	C15-C20	1.515(12)
N2-N3	1.216(10)	C23-C24	1.535(12)
N3-N4	1.165(10)		

Angles (°)

P1-Cr1-P2	81.03(9)	Cr1-N1-Cr2	170.3(4)
P1-Cr1-C3	92.70(2)	N3-N2-Cr2	136.4(7)

P1-Cr1-C4	109.7(2)	N4-N3-N2	175.4(10)
P2-Cr1-C3	123.6(3)	N6-N5-Cr2	126.0(7)
P2-Cr1-C4	94.40(2)	N7-N6-N5	179.0(11)
N1-Cr1-P1	94.10(2)	C2-C1-Cr1	74.70(5)
N1-Cr1-P2	89.70(2)	C2-C1-C5	109.1(7)
N1-Cr1-C1	98.30(3)	C2-C1-C6	127.1(9)
N1-Cr1-C2	111.9(3)	C5-C1-Cr1	71.90(5)
N1-Cr1-C3	146.7(3)	C5-C1-C6	123.6(9)
N1-Cr1-C4	156.2(3)	C6-C1-Cr1	123.7(6)
N1-Cr1-C5	119.2(3)	C1-C2-Cr1	68.50(5)
C1-Cr1-P1	144.7(3)	C1-C2-C3	107.4(7)
C1-Cr1-P2	131.7(3)	C1-C2-C7	128.3(9)
C1-Cr1-C2	36.80(3)	C3-C2-Cr1	75.30(5)
C1-Cr1-C3	60.00(3)	C3-C2-C7	123.4(10)
C1-Cr1-C4	61.90(3)	C7-C2-Cr1	130.0(6)
C1-Cr1-C5	38.20(3)	C2-C3-Cr1	69.10(5)
C2-Cr1-P1	108.0(3)	C2-C3-C4	110.8(8)
C2-Cr1-P2	155.3(2)	C2-C3-C8	125.9(10)
C2-Cr1-C3	35.60(3)	C4-C3-Cr1	72.70(5)
C2-Cr1-C4	61.00(3)	C4-C3-C8	122.7(10)
C3-Cr1-C4	35.70(3)	C8-C3-Cr1	132.2(6)
C5-Cr1-P1	146.7(2)	C3-C4-Cr1	71.60(5)
C5-Cr1-P2	97.20(2)	C3-C4-C5	104.8(8)
C5-Cr1-C2	62.30(3)	C3-C4-C9	127.6(9)
C5-Cr1-C3	60.50(3)	C5-C4-Cr1	65.90(4)
C5-Cr1-C4	37.10(3)	C5-C4-C9	126.8(9)
N1-Cr2-N2	97.60(3)	C9-C4-Cr1	134.2(6)
N1-Cr2-N5	95.20(3)	C1-C5-Cr1	69.90(5)
N1-Cr2-C11	92.80(3)	C1-C5-C4	107.9(8)
N1-Cr2-C12	114.1(3)	C1-C5-C10	125.0(8)
N1-Cr2-C13	150.2(3)	C4-C5-Cr1	77.00(5)
N1-Cr2-C14	142.8(3)	C4-C5-C10	126.4(8)
N1-Cr2-C15	107.4(3)	C10-C5-Cr1	126.4(6)

N2-Cr2-N5	91.70(3)	C12-C11-Cr2	70.70(5)
N2-Cr2-C11	139.5(3)	C12-C11-C15	106.6(7)
N2-Cr2-C12	147.3(3)	C12-C11-C16	128.4(9)
N2-Cr2-C13	111.3(3)	C15-C11-Cr2	71.10(4)
N2-Cr2-C14	89.80(3)	C15-C11-C16	124.9(9)
N2-Cr2-C15	102.9(3)	C16-C11-Cr2	125.3(6)
N5-Cr2-C11	126.3(3)	C11-C12-Cr2	72.60(4)
N5-Cr2-C12	93.20(3)	C11-C12-C17	125.9(10)
N5-Cr2-C13	91.20(3)	C13-C12-Cr2	73.30(5)
N5-Cr2-C14	121.0(3)	C13-C12-C11	108.2(7)
N5-Cr2-C15	150.9(3)	C13-C12-C17	125.8(10)
C11-Cr2-C13	60.60(3)	C17-C12-Cr2	123.2(6)
C11-Cr2-C14	60.30(3)	C12-C13-Cr2	70.40(4)
C12-Cr2-C11	36.70(3)	C12-C13-C18	124.7(9)
C12-Cr2-C13	36.30(3)	C14-C13-Cr2	73.00(5)
C12-Cr2-C14	60.20(3)	C14-C13-C12	108.4(8)
C12-Cr2-C15	61.30(3)	C14-C13-C18	126.9(9)
C13-Cr2-C14	35.60(3)	C18-C13-Cr2	123.5(6)
C15-Cr2-C11	37.00(3)	C13-C14-Cr2	71.40(4)
C15-Cr2-C13	60.20(3)	C13-C14-C15	108.6(7)
C15-Cr2-C14	35.80(3)	C13-C14-C19	124.8(9)
C21-P1-Cr1	122.6(3)	C15-C14-Cr2	70.50(4)
C21-P1-C23	104.6(4)	C15-C14-C19	126.5(8)
C22-P1-Cr1	120.3(3)	C19-C14-Cr2	126.0(6)
C22-P1-C21	100.5(4)	C11-C15-Cr2	71.90(4)
C22-P1-C23	102.8(4)	C11-C15-C20	126.5(8)
C23-P1-Cr1	103.5(3)	C14-C15-Cr2	73.70(4)
C24-P2-Cr1	108.5(3)	C14-C15-C11	108.0(7)
C25-P2-Cr1	116.9(3)	C14-C15-C20	125.3(8)
C25-P2-C24	103.9(4)	C20-C15-Cr2	124.2(6)
C26-P2-Cr1	124.2(3)	C24-C23-P1	110.7(6)
C26-P2-C24	101.1(4)	C23-C24-P2	112.1(5)
C26-P2-C25	99.60(5)		

12 crystalizes in the orthorhombic space group Pbca. The geometry around Cr1 is similar to that of **11** but Cr2 is six-coordinated, including two azide ligands. The Cr1-N1 bond distance is 1.637(6) Å which is in the range of Cr-N double bond distances. [66,81] Cr2-N1 distance is 1.972(6) Å and matches with a single Cr-N bond distance. [66] Based on these bond distances, each chromium center should have a different formal oxidation state, i.e., Cr1(III) and Cr2(IV). The effective magnetic moment of **12** was measured to be 1.9 (1) μ_B at room temperature. For a system of two non-interacting chromium ions of oxidation state III (S = 3/2) and IV (S = 1), the expected magnetic moment is 4.8 μ_B. A possible interpretation of the lower moment of **12** is that the bridging nitride ligand mediates strong antiferromagnetic coupling between the chromium centers, resulting in a predominant population of the S = ½ ground state of the molecule.

The reaction of **9** with azide reagents was carried out in an NMR tube, to follow the reaction more precisely. **9** was transferred to a J-Young tube in a glove box under nitrogen atmosphere, and to that was added an excess of potassium azide. THF-d_8 was vacuum transferred to the NMR tube, and the reaction was monitored for five days using proton NMR. After addition of the azide reagent the starting compound reacts with the azide and peaks of the products appear in the proton NMR spectrum. Based on the results from this experiment, other compounds beside **11** and **12** are formed after the addition of azide but only **11** and **12** were separated and characterized from this reaction.

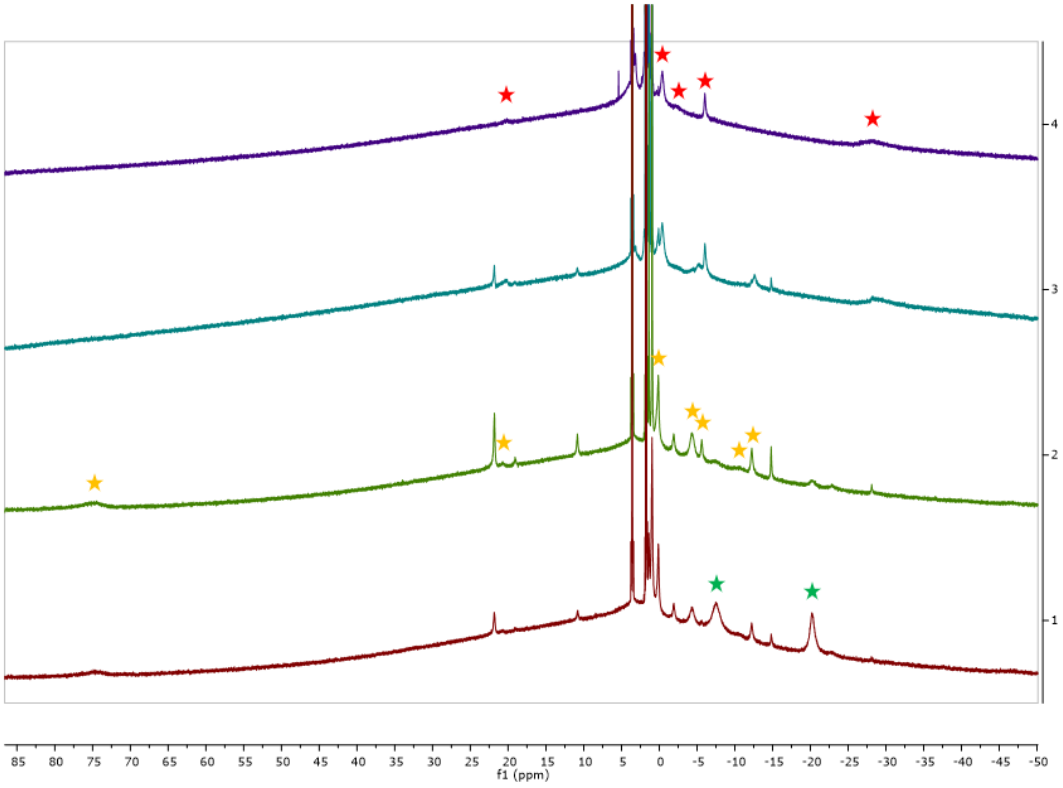

Figure 2.21 Reaction of **9** with azide reagent in the NMR tube using THF-d_8 as the solvent. Spectra 1, 2, 3 and were taken respectively after 5 min, 15 min, 30 min and 5 days after the start of the reaction. The peaks that were recognized are marked with stars. Green: starting compound **9**, yellow: bridging nitride **11** and red: compound **12**.

The reaction of **9** with azide reagent in the NMR tube was followed for 20 days. During this time some diamagnetic peaks started to appear in the proton NMR spectrum. To identify this product, the reaction was repeated on a larger scale, to facilitate isolation of this diamagnetic compound from the reaction mixture.

Accordingly, one equivalent of NaN_3 was added to the THF solution of 100 mg of **9**. The mixture was allowed to stir for 2 weeks, during which time the color of solution changed from brown to blue after a couple of hours and finally changed to purple after 2 weeks. The solvent was then removed under vacuum and the remaining purple powder was dissolved in pentanes. After filtration, the solution was concentrated and then cooled to low temperature (-30°C) overnight to yield purple crystals (74%). Determination of the structure of this compound by X-ray crystallography revealed it to be a mononuclear chromium nitride complex, i.e. [Cp*dmpeCr≡N] (**13**). The molecular structure of **13** is depicted in **Figure 2.22** while the corresponding interatomic distances and angles are listed in **Table 2.13**.

13 is an 18-electron complex, also the ^1H NMR spectrum of **13** shows the same sharp peaks in the diamagnetic range that were observed in the NMR experiment (**Figure 2.21**), indicating **13** is a diamagnetic compound, as shown in **Figure 2.23**.

The rate of reaction can be improved to reach completion after about 2 days, by using excess azide reagent (The yield of reaction is not changing).

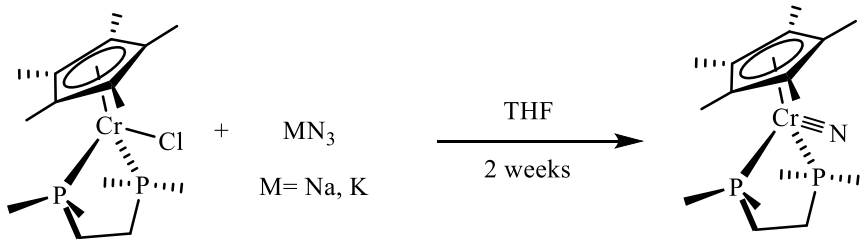

(**9**) (**13**)

Scheme 2.16 Synthesis of [Cp*dmpeCr≡N] (**13**).

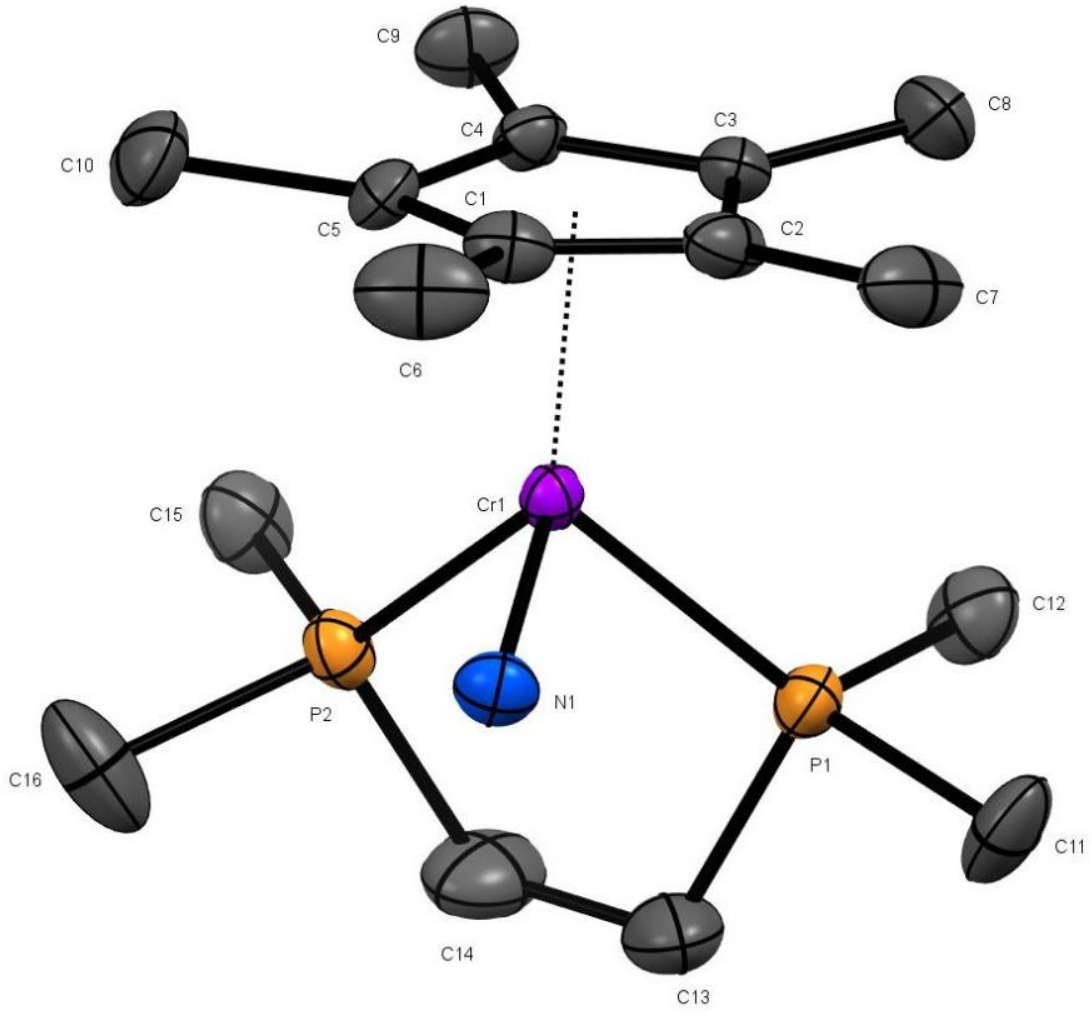

Figure 2.22 Molecular structure of [Cp*dmpeCr≡N] (**13**) represented as 50% probability thermal ellipsoids. Hydrogen atoms have been omitted for clarity.

Table 2.13 Interatomic distances (Å) and angles (º) for [Cp*dmpeCr≡N] (**13**).

Distances (Å)

Cr1-P1	2.2858(11)	P2-C16	1.814(5)
Cr1-P2	2.2877(11)	C1-C2	1.414(6)
Cr1-N1	1.588(3)	C1-C5	1.432(5)
Cr1-C1	2.171(4)	C1-C6	1.496(5)
Cr1-C2	2.210(4)	C2-C3	1.427(5)
Cr1-C3	2.381(3)	C2-C7	1.512(5)
Cr1-C4	2.380(3)	C3-C4	1.392(5)
Cr1-C5	2.207(3)	C3-C8	1.503(5)
P1-C11	1.841(4)	C4-C5	1.428(5)
P1-C12	1.823(4)	C4-C9	1.511(5)
P1-C13	1.833(5)	C5-C10	1.499(5)
P2-C14	1.857(5)	C13-C14	1.433(7)
P2-C15	1.819(4)		

Angles (°)

P1-Cr1-P2	83.28(4)	C15-P2-C14	98.30(3)
P1-Cr1-C3	95.61(9)	C16-P2-Cr1	115.4(17)
P1-Cr1-C4	116.7(9)	C16-P2-C14	104.4(3)
P2-Cr1-C3	124.9(10)	C16-P2-C15	101.1(2)
P2-Cr1-C4	98.91(9)	C2-C1-Cr1	72.70(2)
N1-Cr1-P1	89.17(12)	C2-C1-C5	107.9(3)
N1-Cr1-P2	88.43(12)	C2-C1-C6	127.2(4)
N1-Cr1-C1	96.61(15)	C5-C1-Cr1	72.30(2)
N1-Cr1-C2	111.0(15)	C5-C1-C6	124.8(4)
N1-Cr1-C3	146.6(15)	C6-C1-Cr1	121.5(3)
N1-Cr1-C4	153.6(15)	C1-C2-Cr1	69.70(2)

N1-Cr1-C5	117.8(15)	C1-C2-C3	107.7(3)
C1-Cr1-P1	141.8(11)	C1-C2-C7	125.3(4)
C1-Cr1-P2	134.5(11)	C3-C2-Cr1	78.50(2)
C1-Cr1-C2	37.64(15)	C3-C2-C7	126.4(4)
C1-Cr1-C3	60.33(13)	C7-C2-Cr1	123.7(3)
C1-Cr1-C4	60.38(12)	C2-C3-Cr1	65.50(2)
C1-Cr1-C5	38.17(13)	C2-C3-C8	125.6(4)
C2-Cr1-P1	105.3(12)	C4-C3-Cr1	73.00(2)
C2-Cr1-P2	158.5(9)	C4-C3-C2	108.3(3)
C2-Cr1-C3	35.98(13)	C4-C3-C8	126.0(4)
C2-Cr1-C4	59.55(12)	C8-C3-Cr1	130.8(3)
C4-Cr1-C3	34.00(12)	C3-C4-Cr1	73.05(19)
C5-Cr1-P1	152.7(10)	C3-C4-C5	108.9(3)
C5-Cr1-P2	100.6(10)	C3-C4-C9	126.1(3)
C5-Cr1-C2	62.79(15)	C5-C4-Cr1	65.38(18)
C5-Cr1-C3	59.86(13)	C5-C4-C9	124.8(3)
C5-Cr1-C4	36.02(12)	C9-C4-Cr1	130.4(3)
C11-P1-Cr1	118.6(17)	C1-C5-Cr1	69.50(2)
C12-P1-Cr1	124.2(15)	C1-C5-C10	125.7(3)
C12-P1-C11	101.1(2)	C4-C5-Cr1	78.60(2)
C12-P1-C13	102.6(2)	C4-C5-C1	106.8(3)
C13-P1-Cr1	106.3(18)	C4-C5-C10	126.2(3)
C13-P1-C11	100.9(3)	C10-C5-Cr1	127.1(3)
C14-P2-Cr1	108.9(17)	C14-C13-P1	111.3(4)
C15-P2-Cr1	125.7(16)	C13-C14-P2	113.7(4)

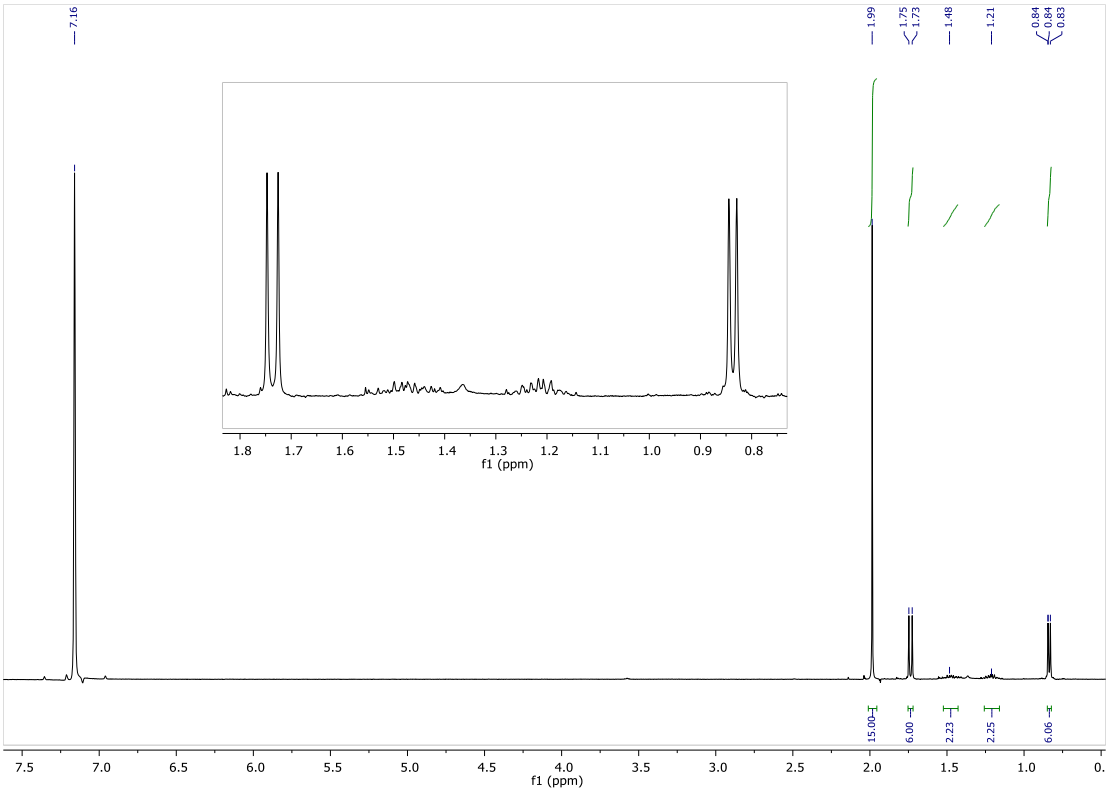

Figure 2.23 ^{1}H-NMR spectrum of [Cp*dmpeCr≡N] (**13**) recorded in C_6D_6 at 400 MHz.

13 crystalizes in the monoclinic space group $P2_1/n$. The geometry around Cr1 is pseudo-octahedral and the Cr≡N bond distance is 1.584(3) Å. Based on a CSD search on over 100 terminal chromium nitride complexes this bond distance is in the expected range, but on the long side, of bond distances for terminal chromium nitride compounds, as shown in **Figure 2.24**. Another CSD search showed that the Cr≡N bond distance is dependent on the coordination number of chromium center. The higher the coordination number, the larger the Cr≡N bond distance, shown in **Figure 2.25**.

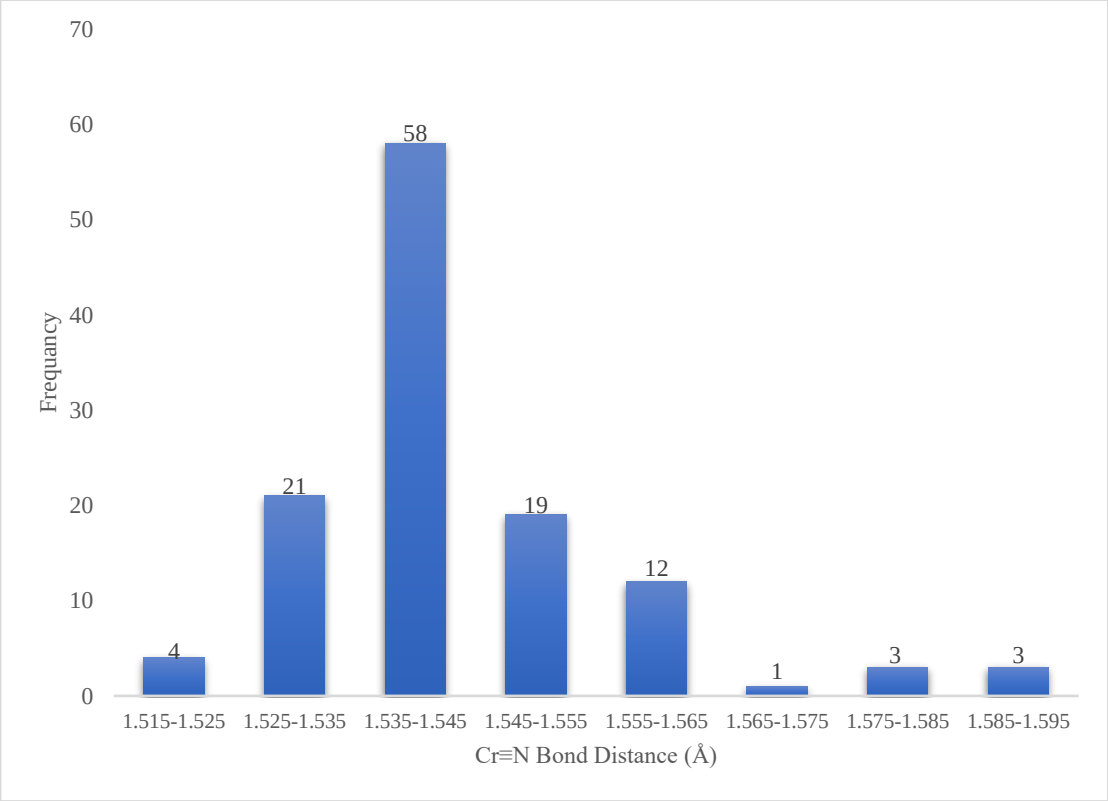

Figure 2.24 CSD search on over 100 Cr-N bond distances in terminal chromium nitride complexes. Each number above each column shows the number of complexes in a specific bond distance range, i.e., 4 complexes with Cr-N bond distance between 1.515 to 1.525 Å. **13** is not shown in this chart.

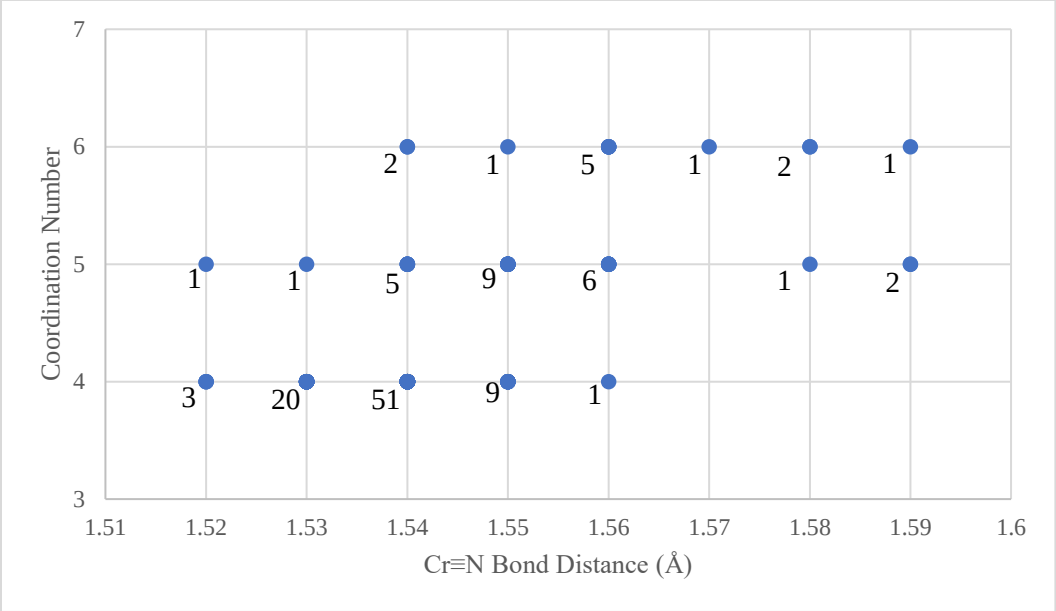

Figure 2.25 CSD search on over 100 chromium nitride complexes to show the correlation of Cr≡N bond distance and coordination number of chromium center. **13** is not shown in the graph.

Terminal metal nitrides can react as nucleophiles or as electrophiles.[82,83] To examine if the nitride complex behaves as a nucleophile or electrophile, the reactivity of this complex was studied toward methyl trifluoromethanesulfonate (MeOTf), methylmagnesium chloride (MeMgCl), and CO gas.

1 equivalent of MeOTf was added to a THF solution of **13** at room temperature. The color of the solution changed from purple to pale green immediately after the addition. The solution was stirred for 1 h and then was filtered. The solvent was removed under vacuum and the remaining powder was washed with pentanes and diethyl ether. The green residue was redissolved in minimal amount of THF and cooled to low temperature (-30°C) overnight to yield green crystals. Determination of the structure by X-ray crystallography revealed it to be a mononuclear chromium complex, i. e., [Cp*dmpeCr=NMe]OTf (**14**). The molecular structure of **14** is depicted in **Figure 2.26** while the corresponding interatomic distances and angles are listed in **Table 2.14**.

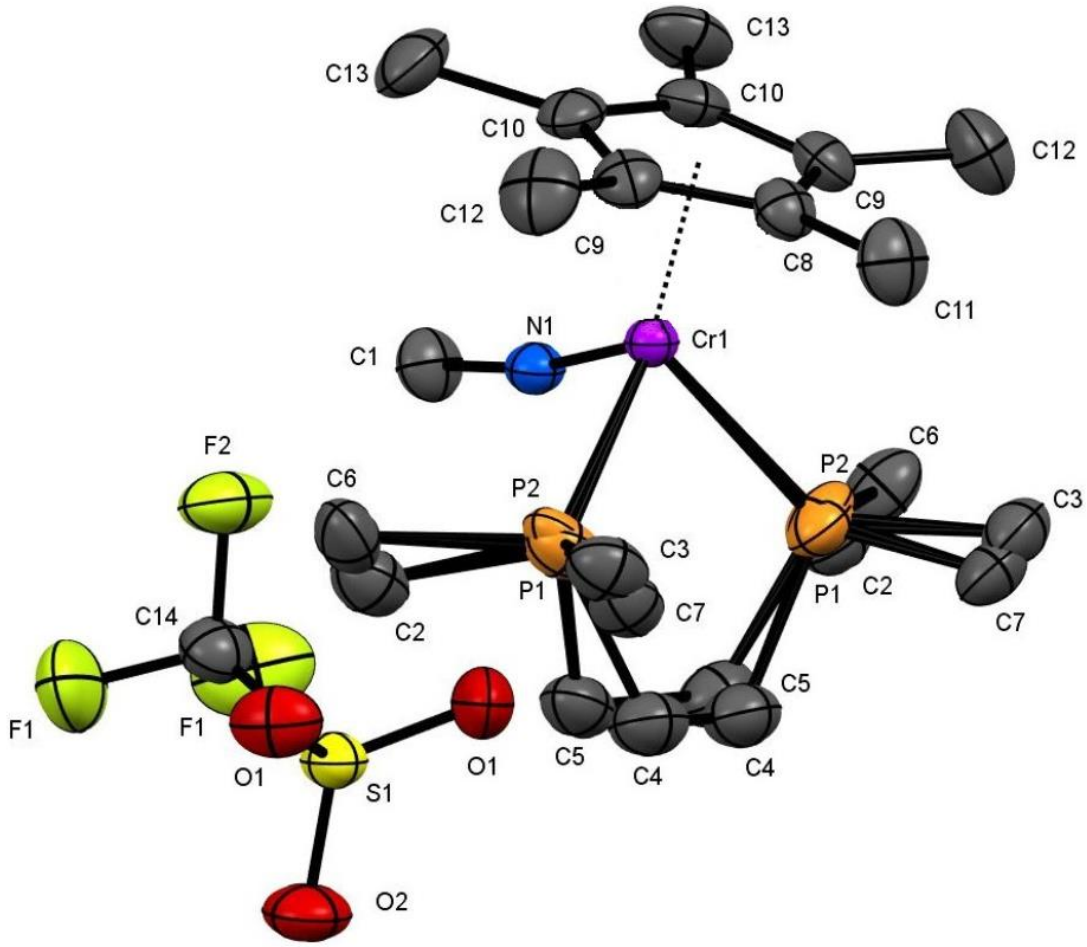

Figure 2.26 Molecular structure of [Cp*dmpeCr=NMe]OTf (**14**) represented as 50% probability thermal ellipsoids. Hydrogen atoms have been omitted for clarity. The dmpe ligand suffer positional disorder over two sets of positions.

Table 2.14 Interatomic distances (Å) and angles (º) for [Cp*dmpeCr=NMe]OTf (**14**).

Distances (Å)

Cr1-N1	1.626(3)	C10-C13	1.505(4)
Cr1-C8	2.234(3)	P1-C2	1.739(14)
Cr1-C9	2.219(2)	P1-C3	1.855(18)
Cr1-C9	2.219(2)	P1-C4	1.887(14)
Cr1-C10	2.198(2)	P2-C5	1.826(14)
Cr1-C10	2.198(2)	P2-C6	1.886(13)
Cr1-P1	2.339(13)	P2-C7	1.789(17)
Cr1-P2	2.286(12)	C4-C5	1.512(8)
N1-C1	1.430(4)	S1-O1	1.4387(19)
C8-C9	1.430(3)	S1-O1	1.4387(19)
C8-C9	1.430(3)	S1-O2	1.436(3)
C8-C11	1.505(5)	S1-C14	1.819(4)
C9-C10	1.415(3)	F1-C14	1.324(3)
C9-C12	1.499(4)	F2-C14	1.331(4)
C10-C10	1.420(5)		

Angles (°)

N1-Cr1-C8	156.62(13)	C10-C9-Cr1	70.51(13)
N1-Cr1-C9	127.11(9)	C10-C9-C8	108.0(2)
N1-Cr1-C9	127.11(9)	C10-C9-C12	124.6(2)
N1-Cr1-C10	95.44(10)	C12-C9-Cr1	130.38(19)
N1-Cr1-C10	95.44(10)	C9-C10-Cr1	72.11(13)
N1-Cr1-P1	93.5(3)	C9-C10-C10	108.25(15)
N1-Cr1-P2	93.0(3)	C9-C10-C13	125.1(2)
C8-Cr1-P1	104.3(3)	C10-C10-Cr1	71.16(7)
C8-Cr1-P2	104.2(3)	C10-C10-C13	126.66(17)
C9-Cr1-C8	37.45(8)	C13-C10-Cr1	123.01(17)

C9-Cr1-C8	37.45(8)	C2-P1-Cr1	114.7(7)
C9-Cr1-C9	62.62(13)	C2-P1-C3	105.9(8)
C9-Cr1-P1	95.1(3)	C2-P1-C4	103.3(7)
C9-Cr1-P1	139.4(3)	C3-P1-Cr1	120.4(7)
C9-Cr1-P2	139.8(3)	C3-P1-C4	102.9(7)
C9-Cr1-P2	93.8(3)	C4-P1-Cr1	107.6(6)
C10-Cr1-C8	62.56(10)	C5-P2-Cr1	106.4(6)
C10-Cr1-C8	62.56(10)	C5-P2-C6	101.6(6)
C10-Cr1-C9	37.38(9)	C6-P2-Cr1	115.6(6)
C10-Cr1-C9	37.38(9)	C7-P2-Cr1	126.3(7)
C10-Cr1-C9	62.68(9)	C7-P2-C5	102.1(7)
C10-Cr1-C9	62.68(9)	C7-P2-C6	101.6(7)
C10-Cr1-C10	37.68(14)	C5-C4-P1	112.1(5)
C10-Cr1-P1	156.9(3)	C4-C5-P2	107.1(5)
C10-Cr1-P1	120.2(3)	O1-S1-O1	114.35(18)
C10-Cr1-P2	118.3(3)	O1-S1-C14	102.82(11)
C10-Cr1-P2	155.2(3)	O1-S1-C14	102.82(11)
P2-Cr1-P1	82.38(6)	O2-S1-O1	115.49(10)
C1-N1-Cr1	170.4(2)	O2-S1-O1	115.49(10)
C9-C8-Cr1	70.70(15)	O2-S1-C14	103.26(18)
C9-C8-Cr1	70.70(15)	F1-C14-S1	112.0(2)
C9-C8-C9	107.5(3)	F1-C14-S1	112.0(2)
C9-C8-C11	125.99(15)	F1-C14-F1	107.0(3)
C9-C8-C11	125.99(15)	F1-C14-F2	106.6(2)
C11-C8-Cr1	130.2(3)	F1-C14-F2	106.6(2)
C8-C9-Cr1	71.85(15)	F2-C14-S1	112.3(2)
C8-C9-C12	126.7(2)		

The result of this reaction indicates nucleophilic behavior of **13** toward electrophiles. **14** crystalizes in the orthorhombic space group Pnma. Atoms in the dmpe ligand suffer positional disorder over two sets of positions which were successfully

modeled. The Cr1-N1 bond length is 1.626(3) Å which is in the range of Cr-N double bond distances.[66,81] The formal oxidation states of Cr in **14** is IV i.e. the same as in the starting nitride complex. **14** is 16 electron complex and its proton NMR shows sharp peaks in the range characteristic of diamagnetic compounds, which suggests that **14** is a low spin d^2 Cr complex.

It was shown that this chromium nitride complex behaves as a nucleophile, therefore it was not expected that **13** would interact with nucleophiles. The reaction of **13** with methylmagnesium chloride was done to test this hypothesis.

1 equivalent of MeMgCl was added to an Et_2O solution of **13**. A blue product precipitated out of solution after the addition. After removal of the solvent under vacuum, the blue powder was dissolved in THF and the solution was filtered. The blue-purple solution was stored at -30°C overnight to yield blue crystals. Using X-ray crystallography, the structure of the product was determined to be a dinuclear chromium complex, i.e. $[Cp^*dmpeCrN]_2[\mu\text{-}MgCl_2]$ (**15**). The nitride complex behaves as a nucleophile and coordinates to the $MgCl_2$ in this reaction. Base on the Schlenk equilibrium for MeMgCl , on one side of the reaction there are two equivalents of methyl magnesium chloride and on the other side one equivalent of dimethyl magnesium and magnesium halide salt should exist.[84–86] The molecular structure of **15** is depicted in **Figure 2.27** while the corresponding interatomic distances and angles are listed in **Table 2.15**.

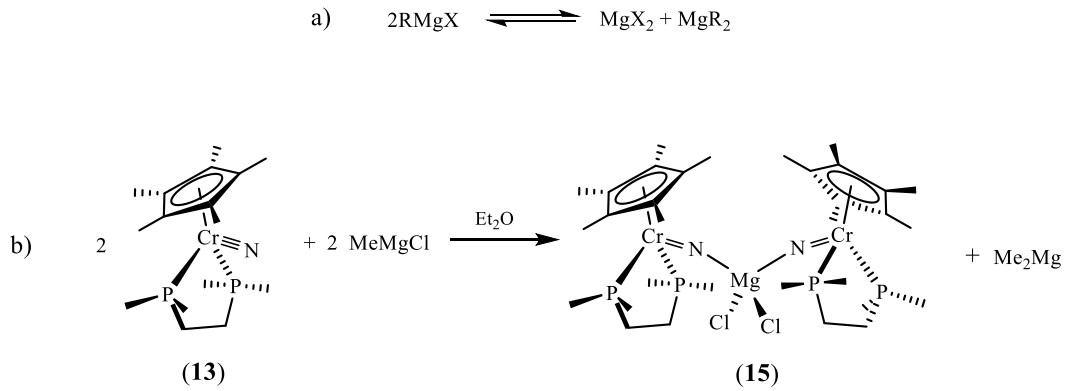

Scheme 2.17 a: Schlenk Equation and b: The reaction of **13** with MeMgCl reagent.

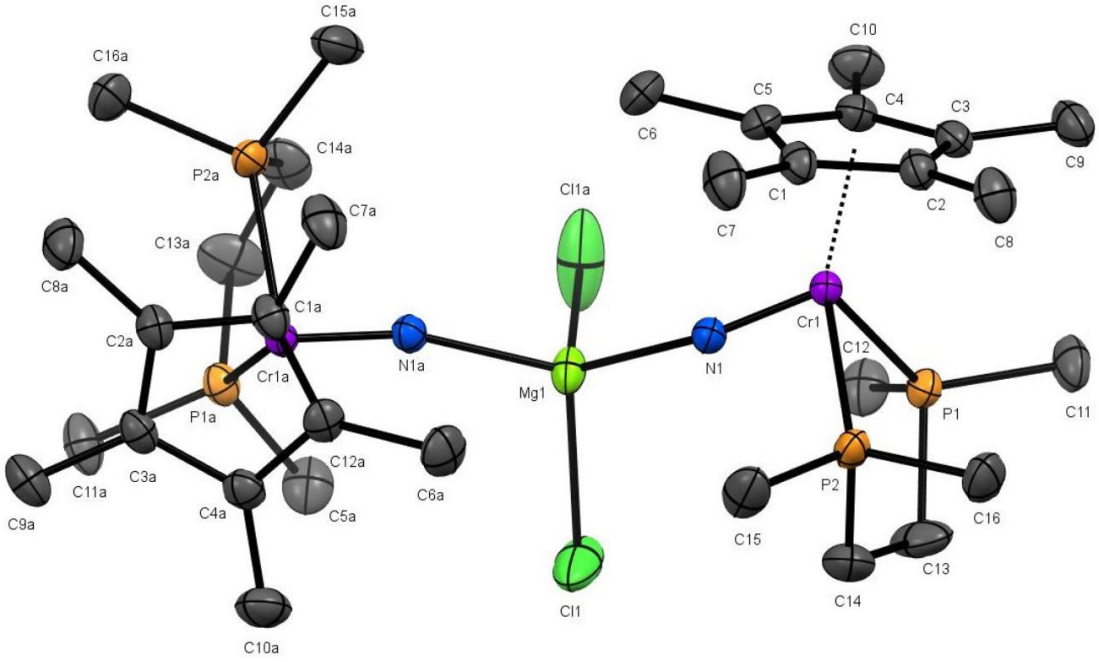

Figure 2.27 Molecular structure of $[Cp^*dmpeCrN]_2[\mu\text{-}MgCl_2]$ (**15**) represented as 50% probability thermal ellipsoids. Hydrogen atoms have been omitted for clarity.

Table 2.15 Interatomic distances (Å) and angles (º) for $[Cp^*dmpeCrN]_2[\mu\text{-}MgCl_2]$ (**15**).

Distances (Å)

Cr1-N1	1.608(3)	C2-C8	1.507(5)
Cr1-C1	2.200(3)	C3-C4	1.434(5)
Cr1-C2	2.359(3)	C3-C9	1.502(5)
Cr1-C3	2.358(3)	C4-C5	1.426(5)
Cr1-C4	2.194(3)	C4-C10	1.498(5)
Cr1-C5	2.150(3)	C5-C6	1.505(5)
Cr1-P1	2.309(4)	P1-C11	1.843(6)
Cr1-P2	2.304(4)	P1-C12	1.819(7)
Cl1-Mg1	2.3170(18)	P1-C13	1.847(6)
Mg1-N1	2.072(3)	P2-C14	1.842(7)
C1-C2	1.436(4)	P2-C15	1.812(6)
C1-C5	1.424(5)	P2-C16	1.828(6)
C1-C7	1.508(5)	C13-C14	1.478(10)
C2-C3	1.398(5)		

Angles (°)

N1-Cr1-C1	111.2(12)	C5-C1-C2	107.2(3)
N1-Cr1-C2	147.7(12)	C5-C1-C7	125.5(3)
N1-Cr1-C3	149.5(13)	C7-C1-Cr1	124.5(3)
N1-Cr1-C4	113.0(13)	C1-C2-Cr1	65.70(17)
N1-Cr1-C5	93.65(13)	C1-C2-C8	126.2(3)
N1-Cr1-P1	90.76(15)	C3-C2-Cr1	72.74(19)
N1-Cr1-P2	91.01(16)	C3-C2-C1	108.6(3)
C1-Cr1-C2	36.50(11)	C3-C2-C8	125.0(3)
C1-Cr1-C3	60.53(11)	C8-C2-Cr1	131.1(3)
C1-Cr1-P1	157.4(14)	C2-C3-Cr1	72.78(18)
C1-Cr1-P2	101.5(14)	C2-C3-C4	108.5(3)
C3-Cr1-C2	34.48(12)	C2-C3-C9	126.0(3)

C4-Cr1-C1	63.45(13)	C4-C3-Cr1	65.50(17)
C4-Cr1-C2	60.50(13)	C4-C3-C9	125.2(3)
C4-Cr1-C3	36.50(12)	C9-C3-Cr1	132.3(2)
C4-Cr1-P1	103.8(13)	C3-C4-Cr1	78.00(19)
C4-Cr1-P2	154.7(16)	C3-C4-C10	126.3(3)
C5-Cr1-C1	38.20(13)	C5-C4-Cr1	69.17(18)
C5-Cr1-C2	61.16(12)	C5-C4-C3	107.2(3)
C5-Cr1-C3	61.23(12)	C5-C4-C10	125.8(3)
C5-Cr1-C4	38.32(12)	C10-C4-Cr1	125.1(3)
C5-Cr1-P1	139.3(13)	C1-C5-Cr1	72.79(18)
C5-Cr1-P2	137.4(14)	C1-C5-C4	108.3(3)
P1-Cr1-C2	121.5(14)	C4-C5-C6	126.4(3)
P1-Cr1-C3	97.83(14)	C6-C5-Cr1	121.2(2)
P2-Cr1-C2	95.00(15)	C11-P1-Cr1	125.2(5)
P2-Cr1-C3	119.0(15)	C11-P1-C13	103.5(5)
P2-Cr1-P1	82.82(10)	C12-P1-Cr1	115.6(4)
Cl1a-Mg1-Cl1	119.5(14)	C12-P1-C11	97.90(4)
N1-Mg1-Cl1	106.7(9)	C12-P1-C13	102.3(4)
N1-Mg1-Cl1a	102.2(9)	C13-P1-Cr1	109.5(3)
N1-Mg1-N1	120.6(16)	C14-P2-Cr1	104.2(3)
Cr1-N1-Mg1	165.4(16)	C15-P2-Cr1	120.0(3)
C2-C1-Cr1	77.79(18)	C15-P2-C14	102.7(4)
C2-C1-C7	126.9(3)	C15-P2-C16	103.2(4)
C5-C1-Cr1	69.02(18)	C16-P2-Cr1	121.9(3)
C1-C5-C6	125.3(3)	C16-P2-C14	101.7(4)
C4-C5-Cr1	72.50(18)	C14-C13-P1	112.3(5)
		C13-C14-P2	112.3(5)

15 crystalizes in the monoclinic space group C2/c and features a two-fold axis in the middle of the molecule. The Cr1-N1 bond distance is 1.608(3) Å in **15**. The geometry

around the Mg is roughly tetrahedral having a geometry index τ_4 = 0.85.[87] The sharp peaks in the diamagnetic region indicates that **15** is a low spin d^2 chromium (IV) complex. Nitride complexes are usually reactive toward small molecules, electrophilic substrates, and hydrogen atom donor reagents.[88–90]

The reactivity of **13** toward CO gas, 1,4-cyclohexadiene, 9,10-dihydroanthracene was investigated. Also, the polymerization of 3,3-dimethyl-1-butene (Neohexene) upon reaction with 13 was examined. The reactions with 1,4-cyclohexadiene, 9,10-dihydroanthracene, and neohexene resulted in no reaction, even in the presence of excess amount of these reagents or elevated temperatures.

The next reagent to try was carbon monoxide gas. Although there are many examples of imide-CO coupling, the coupling between nitride and CO is not very common.[91–93] In the case of **13**, the reaction between the CO gas and nitride complex was observed. **13** reacts with carbon monoxide at room temperature and produces multiple products. 1 atm. of CO gas was introduced to a pentanes solution of **13** and the color of solution changed from purple to brown-purple after about 30 minutes. The solution was allowed to stir overnight during which time the color of solution turned brown completely. After removal of CO gas and the solvent a dark powder was produced. Pentanes, toluene, diethyl ether, and THF extractions were undertaken of the powder. Unfortunately, due to the existence of multiple products separation and characterization of all was not possible. Only from the pentanes and THF extraction small quantities of the product were collected. X-ray crystallography was used to determine the structure of these compounds as dinuclear chromium complexes which are shown in **Figure 2.28** and **Figure 2.29**.

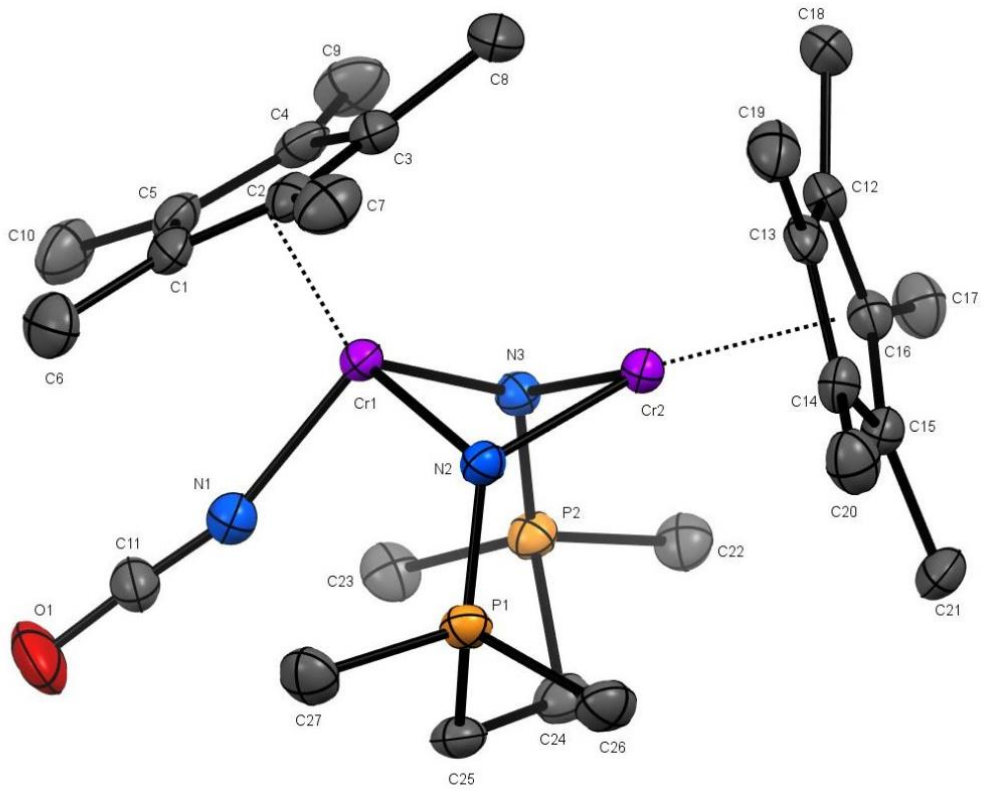

Figure 2.28 Molecular structure of [Cp*Cr(μ-{NPMe$_2$C$_2$H$_4$PMe$_2$N}Cr(NCO)Cp*] (**16**) represented as 50% probability thermal ellipsoids. Hydrogen atoms have been omitted for clarity.

Table 2.16 Interatomic distances (Å) and angles (º) for [Cp*Cr(μ-μ-{NPMe$_2$C$_2$H$_4$PMe$_2$N}Cr(NCO)Cp*] (**16**).

Distances (Å)

Cr1-C1	2.281(4)	Cr2-C15	2.364(4)
Cr1-N1	2.018(4)	C2-C3	1.419(6)
Cr1-Cr2	2.7028(9)	C2-C7	1.498(7)

Cr1-C2	2.259(4)	P2-N3	1.570(3)
Cr1-N2	2.005(3)	P2-C24	1.845(5)
Cr1-N3	2.020(3)	P2-C23	1.806(5)
Cr1-C3	2.232(4)	P2-C22	1.803(5)
Cr1-C5	2.290(4)	C3-C8	1.493(7)
Cr1-C4	2.263(4)	C3-C4	1.434(7)
O1-C11	1.203(6)	C16-C12	1.428(6)
C1-C2	1.396(6)	C16-C15	1.418(6)
C1-C6	1.505(7)	C16-C17	1.493(7)
C1-C5	1.435(7)	C5-C4	1.401(7)
P1-N2	1.575(3)	C5-C10	1.506(7)
P1-C25	1.837(5)	C4-C9	1.499(7)
P1-C27	1.804(5)	C14-C13	1.428(6)
P1-C26	1.798(5)	C14-C15	1.424(6)
N1-C11	1.161(6)	C14-C20	1.494(7)
Cr2-N2	2.020(4)	C13-C12	1.402(7)
Cr2-N3	2.035(4)	C13-C19	1.509(6)
Cr2-C16	2.366(4)	C12-C18	1.501(7)
Cr2-C14	2.349(4)	C15-C21	1.510(6)
Cr2-C13	2.387(4)	C25-C24	1.532(7)
Cr2-C12	2.405(4)		

Angles (°)

C1-Cr1-Cr2	140.05(12)	C15-Cr2-Cr1	167.50(11)
C1-Cr1-C5	36.59(18)	C15-Cr2-C16	34.90(15)
N1-Cr1-C1	87.04(16)	C15-Cr2-C13	57.99(15)
N1-Cr1-Cr2	127.58(11)	C15-Cr2-C12	57.74(15)
N1-Cr1-C2	119.70(16)	C1-C2-Cr1	73.0(2)
N1-Cr1-N3	99.88(15)	C1-C2-C3	108.0(4)
N1-Cr1-C3	144.75(16)	C1-C2-C7	127.2(5)
N1-Cr1-C5	85.22(16)	C3-C2-Cr1	70.5(2)

N1-Cr1-C4	116.22(17)	C3-C2-C7	124.8(5)
C2-Cr1-C1	35.83(16)	C7-C2-Cr1	122.7(3)
C2-Cr1-Cr2	104.3(12)	N3-P2-C24	118.8(2)
C2-Cr1-C5	60.58(17)	N3-P2-C23	114.6(2)
C2-Cr1-C4	61.46(18)	N3-P2-C22	113.5(2)
N2-Cr1-C1	115.9(17)	C23-P2-C24	106.2(2)
N2-Cr1-N1	98.53(15)	C22-P2-C24	99.00(2)
N2-Cr1-Cr2	48.05(10)	C22-P2-C23	102.4(2)
N2-Cr1-C2	94.66(16)	Cr1-N2-Cr2	84.36(13)
N2-Cr1-N3	85.41(15)	P1-N2-Cr1	119.6(19)
N2-Cr1-C3	107.8(16)	P1-N2-Cr2	124.1(2)
N2-Cr1-C5	152.4(17)	Cr1-N3-Cr2	83.58(13)
N2-Cr1-C4	144.2(17)	P2-N3-Cr1	121.9(2)
N3-Cr1-C1	156.6(17)	P2-N3-Cr2	116.3(19)
N3-Cr1-Cr2	48.45(10)	C2-C3-Cr1	72.60(2)
N3-Cr1-C2	139.8(16)	C2-C3-C8	126.1(5)
N3-Cr1-C3	105.2(16)	C2-C3-C4	108.1(4)
N3-Cr1-C5	121.1(17)	C8-C3-Cr1	131.6(3)
N3-Cr1-C4	96.40(16)	C4-C3-Cr1	72.60(3)
C3-Cr1-C1	60.63(16)	C4-C3-C8	124.2(5)
C3-Cr1-Cr2	87.67(12)	C12-C16-Cr2	74.10(2)
C3-Cr1-C2	36.85(17)	C12-C16-C17	123.0(4)
C3-Cr1-C5	60.68(17)	C15-C16-Cr2	72.50(2)
C3-Cr1-C4	37.20(17)	C15-C16-C12	108.0(4)
C5-Cr1-Cr2	144.5(13)	C15-C16-C17	128.0(4)
C4-Cr1-C1	60.76(17)	C17-C16-Cr2	127.9(3)
C4-Cr1-Cr2	108.9(13)	C1-C5-Cr1	71.40(2)
C4-Cr1-C5	35.84(17)	C1-C5-C10	125.4(5)
C2-C1-Cr1	71.2(2)	C4-C5-Cr1	71.10(2)
C2-C1-C6	126.4(5)	C4-C5-C1	108.2(4)
C2-C1-C5	108.2(4)	C4-C5-C10	126.4(5)
C6-C1-Cr1	124.1(3)	C10-C5-Cr1	124.4(3)
C5-C1-Cr1	72.0(2)	C3-C4-Cr1	70.20(2)

C5-C1-C6	125.3(5)	C3-C4-C9	125.5(5)
N2-P1-C25	119.2(2)	C5-C4-Cr1	73.10(3)
N2-P1-C27	113.2(2)	C5-C4-C3	107.4(4)
N2-P1-C26	113.1(2)	C5-C4-C9	127.1(5)
C27-P1-C25	103.1(2)	C9-C4-Cr1	123.2(3)
C26-P1-C25	102.4(2)	C13-C14-Cr2	73.90(2)
C26-P1-C27	104.1(3)	C13-C14-C20	123.5(4)
C11-N1-Cr1	164.2(4)	C15-C14-Cr2	73.00(2)
N2-Cr2-Cr1	47.59(10)	C15-C14-C13	107.7(4)
N2-Cr2-N3	84.64(14)	C15-C14-C20	127.7(4)
N2-Cr2-C16	161.9(15)	C20-C14-Cr2	128.0(3)
N2-Cr2-C14	106.6(15)	C14-C13-Cr2	71.00(2)
N2-Cr2-C13	116.9(16)	C14-C13-C19	122.4(5)
N2-Cr2-C12	148.5(16)	C12-C13-Cr2	73.70(2)
N2-Cr2-C15	126.9(15)	C12-C13-C14	108.3(4)
N3-Cr2-Cr1	47.97(10)	C12-C13-C19	128.8(4)
N3-Cr2-C16	107.2(15)	C19-C13-Cr2	127.0(3)
N3-Cr2-C14	160.3(15)	C16-C12-Cr2	71.10(2)
N3-Cr2-C13	151.4(16)	C16-C12-C18	122.7(5)
N3-Cr2-C12	119.3(16)	C13-C12-Cr2	72.30(2)
N3-Cr2-C15	125.3(15)	C13-C12-C16	108.2(4)
C16-Cr2-Cr1	149.8(12)	C13-C12-C18	128.2(4)
C16-Cr2-C13	57.66(16)	C18-C12-Cr2	130.6(3)
C16-Cr2-C12	34.83(15)	C16-C15-Cr2	72.60(2)
C14-Cr2-Cr1	150.0(12)	C16-C15-C14	107.8(4)
C14-Cr2-C16	58.29(16)	C16-C15-C21	126.0(4)
C14-Cr2-C13	35.10(16)	C14-C15-Cr2	71.80(2)
C14-Cr2-C12	57.73(16)	C14-C15-C21	126.1(4)
C14-Cr2-C15	35.17(15)	C21-C15-Cr2	124.4(3)
C13-Cr2-Cr1	133.7(11)	C24-C25-P1	115.6(3)
C13-Cr2-C12	34.03(17)	C25-C24-P2	118.7(3)
C12-Cr2-Cr1	133.7(11)	N1-C11-O1	176.8(6)

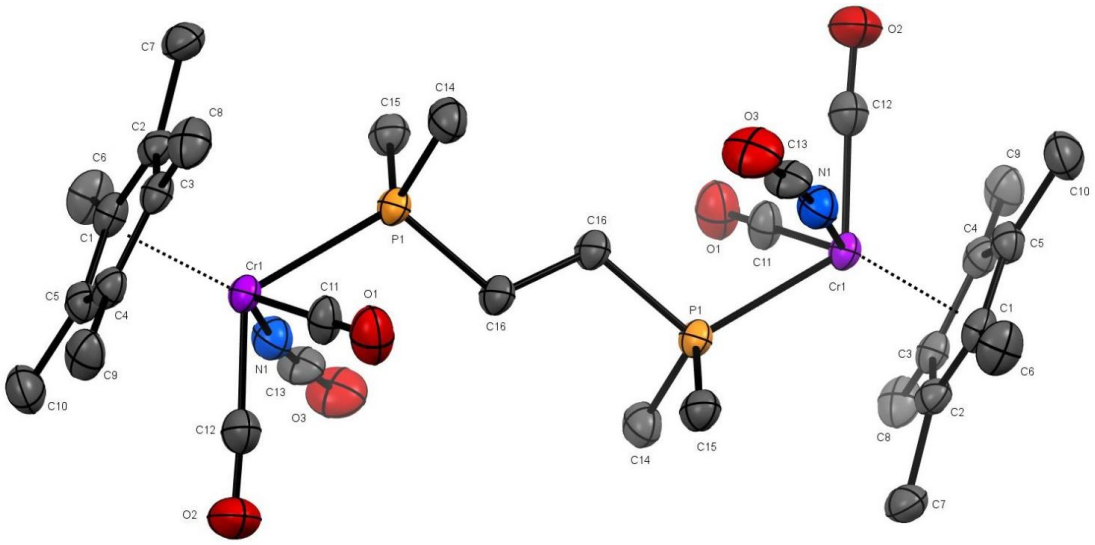

Figure 2.29 Molecular structure of $[Cp^*(CO)_2(OCN)Cr]_2(\mu\text{-dmpe})$ (**17**) represented as 50% probability thermal ellipsoids. Hydrogen atoms and one THF molecule have been omitted for clarity.

Table 2.17 Interatomic distances (Å) and angles (º) for $[Cp^*(CO)_2(OCN)Cr]_2(\mu\text{-dmpe})$ (**17**).

Distances (Å)			
Cr1-P1	2.3895(12)	C1-C2	1.396(6)
Cr1-N1	2.034(4)	C1-C5	1.429(6)
Cr1-C1	2.267(4)	C1-C6	1.492(6)
Cr1-C2	2.278(4)	C2-C3	1.428(6)
Cr1-C3	2.211(4)	C2-C7	1.505(6)
Cr1-C4	2.174(4)	C3-C4	1.427(6)
Cr1-C5	2.191(4)	C3-C8	1.493(6)
Cr1-C11	1.830(5)	C4-C5	1.427(6)

Cr1-C12	1.851(6)	C4-C9	1.482(6)
P1-C14	1.806(5)	C5-C10	1.505(7)
P1-C15	1.810(5)	C16-C16a	1.533(8)
P1-C16	1.841(4)	O4-C17	1.394(8)
O1-C11	1.184(6)	O4-C20	1.374(7)
O2-C12	1.172(6)	C17-C18	1.522(11)
O3-C13	1.202(5)	C18-C19	1.412(10)
N1-C13	1.143(5)	C19-C20	1.495(10)

Angles (°)

N1-Cr1-P1	76.30(12)	C16-P1-Cr1	110.4(15)
N1-Cr1-C1	84.76(16)	C13-N1-Cr1	169.9(4)
N1-Cr1-C2	109.8(16)	C2-C1-Cr1	72.50(2)
N1-Cr1-C3	145.4(17)	C2-C1-C5	108.6(4)
N1-Cr1-C4	132.7(17)	C2-C1-C6	126.5(4)
N1-Cr1-C5	95.24(16)	C5-C1-Cr1	68.40(2)
C1-Cr1-P1	109.9(12)	C5-C1-C6	124.8(4)
C1-Cr1-C2	35.77(16)	C6-C1-Cr1	127.0(3)
C2-Cr1-P1	90.95(11)	C1-C2-Cr1	71.70(2)
C3-Cr1-P1	106.8(12)	C1-C2-C3	108.3(4)
C3-Cr1-C1	61.48(16)	C1-C2-C7	125.9(4)
C3-Cr1-C2	37.07(15)	C3-C2-Cr1	68.90(2)
C4-Cr1-P1	144.5(13)	C3-C2-C7	124.9(4)
C4-Cr1-C1	62.50(16)	C7-C2-Cr1	133.5(3)
C4-Cr1-C2	62.39(16)	C2-C3-Cr1	74.00(2)
C4-Cr1-C3	37.96(16)	C2-C3-C8	125.7(4)
C4-Cr1-C5	38.17(16)	C4-C3-Cr1	69.60(2)
C5-Cr1-P1	147.2(13)	C4-C3-C2	107.9(4)
C5-Cr1-C1	37.35(16)	C4-C3-C8	126.0(4)
C5-Cr1-C2	61.76(16)	C8-C3-Cr1	127.6(3)
C5-Cr1-C3	63.06(16)	C3-C4-Cr1	72.40(2)

C11-Cr1-P1	78.12(15)	C3-C4-C5	107.5(4)
C11-Cr1-N1	125.5(18)	C3-C4-C9	125.6(4)
C11-Cr1-C1	149.6(18)	C5-C4-Cr1	71.60(2)
C11-Cr1-C2	118.0(2)	C5-C4-C9	126.7(4)
C11-Cr1-C3	88.12(18)	C9-C4-Cr1	125.7(3)
C11-Cr1-C4	93.54(18)	C1-C5-Cr1	74.20(2)
C11-Cr1-C5	129.3(18)	C1-C5-C10	125.1(4)
C11-Cr1-C12	75.50(2)	C4-C5-Cr1	70.30(2)
C12-Cr1-P1	122.2(16)	C4-C5-C1	107.6(4)
C12-Cr1-N1	78.80(2)	C4-C5-C10	127.1(4)
C12-Cr1-C1	118.8(2)	C10-C5-Cr1	124.7(3)
C12-Cr1-C2	146.8(19)	O1-C11-Cr1	176.2(4)
C12-Cr1-C3	122.6(2)	O2-C12-Cr1	176.7(5)
C12-Cr1-C4	87.80(2)	N1-C13-O3	176.7(6)
C12-Cr1-C5	86.00(2)	C161-C16-P1	115.4(4)
C14-P1-Cr1	119.0(16)	C20-O4-C17	110.0(5)
C14-P1-C15	103.4(2)	O4-C17-C18	107.5(6)
C14-P1-C16	102.3(2)	C19-C18-C17	104.6(7)
C15-P1-Cr1	115.9(16)	C18-C19-C20	107.9(6)
C15-P1-C16	104.0(2)	O4-C20-C19	107.9(6)

The reaction of **13** with 1 equivalent of carbon monoxide was done to see if the reaction can be controlled. To a toluene solution of **13** was added 1 equivalent of CO gas. After one day of stirring the color of the solution had changed to red brown and some precipitation was observed in the flask. The solution was degassed, and the solvent was removed under vacuum. The concentrated THF extraction was stored at -30°C for overnight to yield blue crystals, affording a 30% isolated yield. Determination of the structure by X-ray crystallography revealed it to be a dinuclear chromium complex with a bridging nitride ligand, i.e. [Cp*$(OCN)_2$Cr(μ-N)CrdmpeCp*] (**18**). The molecular structure of **18** is depicted in **Figure 2.30** while the corresponding interatomic distances and angles are listed in **Table 2.18**.

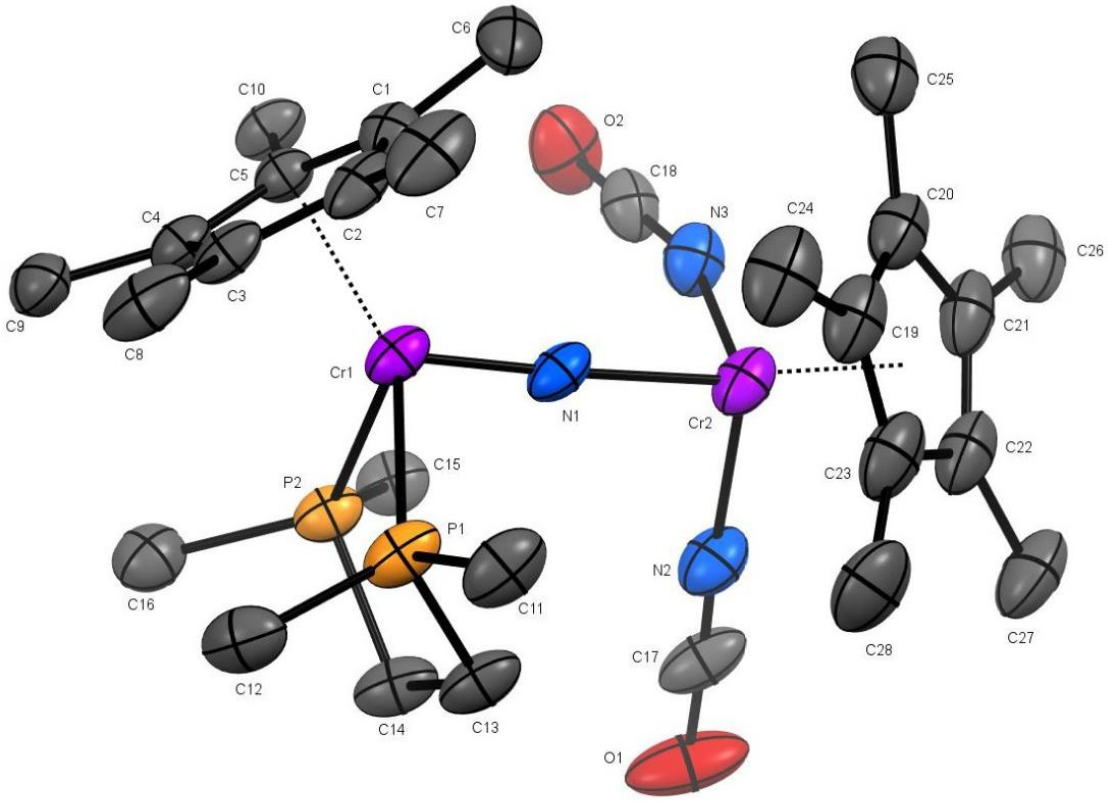

Figure 2.30 Molecular structure of [Cp*(OCN)$_2$Cr(μ-N)CrdmpeCp*] (**18**) represented as 50% probability thermal ellipsoids. Hydrogen atoms and one THF molecule have been omitted for clarity.

Table 2.18 Interatomic distances (Å) and angles (º) for [Cp*(OCN)$_2$Cr(μ-N)CrdmpeCp*] (**18**).

Distances (Å)

Cr1-P1	2.3087(15)	N2-C17	1.156(7)
Cr1-P2	2.3252(14)	N3-C18	1.172(6)
Cr1-N1	1.633(4)	C1-C2	1.433(7)

Cr1-C1	2.155(5)	C1-C5	1.414(6)
Cr1-C2	2.215(4)	C1-C6	1.494(7)
Cr1-C3	2.343(4)	C2-C3	1.418(7)
Cr1-C4	2.351(4)	C2-C7	1.514(7)
Cr1-C5	2.185(4)	C3-C4	1.399(6)
Cr2-N1	1.970(4)	C3-C8	1.497(7)
Cr2-N2	1.984(5)	C4-C5	1.427(6)
Cr2-N3	1.974(5)	C4-C9	1.488(7)
Cr2-C19	2.253(5)	C5-C10	1.495(6)
Cr2-C20	2.248(6)	C13-C14	1.526(7)
Cr2-C21	2.256(6)	C19-C20	1.401(9)
Cr2-C22	2.274(5)	C19-C23	1.414(8)
Cr2-C23	2.228(5)	C19-C24	1.500(8)
P1-C11	1.820(5)	C20-C21	1.425(8)
P1-C12	1.812(6)	C20-C25	1.502(8)
P1-C13	1.835(5)	C21-C22	1.408(9)
P2-C14	1.856(5)	C21-C26	1.510(9)
P2-C15	1.809(5)	C22-C23	1.427(9)
P2-C16	1.822(6)	C22-C27	1.509(8)
O1-C17	1.197(7)	C23-C28	1.515(9)
O2-C18	1.194(6)		

Angles (°)

P1-Cr1-P2	81.41(5)	Cr1-N1-Cr2	171.1(2)
P1-Cr1-C3	92.62(13)	C17-N2-Cr2	173.5(5)
P1-Cr1-C4	112.9(13)	C18-N3-Cr2	161.3(4)
P2-Cr1-C3	118.6(15)	C2-C1-Cr1	73.20(3)
P2-Cr1-C4	92.87(12)	C2-C1-C6	126.0(5)
N1-Cr1-P1	93.29(14)	C5-C1-Cr1	72.20(2)
N1-Cr1-P2	90.84(13)	C5-C1-C2	108.0(4)

N1-Cr1-C1	98.43(18)	C5-C1-C6	125.9(5)
N1-Cr1-C2	114.7(2)	C6-C1-Cr1	123.5(3)
N1-Cr1-C3	150.5(19)	C1-C2-Cr1	68.60(2)
N1-Cr1-C4	153.8(18)	C1-C2-C7	128.0(6)
N1-Cr1-C5	117.3(18)	C3-C2-Cr1	76.80(3)
C1-Cr1-P1	142.6(14)	C3-C2-C1	107.1(4)
C1-Cr1-P2	133.5(13)	C3-C2-C7	123.8(5)
C1-Cr1-C2	38.26(19)	C7-C2-Cr1	129.2(3)
C1-Cr1-C3	61.14(19)	C2-C3-Cr1	67.10(3)
C1-Cr1-C4	60.98(17)	C2-C3-C8	124.0(5)
C1-Cr1-C5	38.01(17)	C4-C3-Cr1	73.00(2)
C2-Cr1-P1	104.9(15)	C4-C3-C2	108.9(4)
C2-Cr1-P2	152.8(15)	C4-C3-C8	126.5(5)
C2-Cr1-C3	36.10(19)	C8-C3-Cr1	132.9(3)
C2-Cr1-C4	60.17(18)	C3-C4-Cr1	72.30(3)
C3-Cr1-C4	34.69(16)	C3-C4-C5	108.2(4)
C5-Cr1-P1	149.4(13)	C3-C4-C9	125.5(5)
C5-Cr1-P2	97.88(12)	C5-C4-Cr1	65.50(2)
C5-Cr1-C2	63.13(17)	C5-C4-C9	125.9(4)
C5-Cr1-C3	60.61(16)	C9-C4-Cr1	133.4(3)
C5-Cr1-C4	36.44(16)	C1-C5-Cr1	69.80(2)
N1-Cr2-N2	95.84(17)	C1-C5-C4	107.6(4)
N1-Cr2-N3	94.24(16)	C1-C5-C10	124.8(4)
N1-Cr2-C19	93.80(19)	C4-C5-Cr1	78.10(2)
N1-Cr2-C20	114.3(19)	C4-C5-C10	126.4(4)
N1-Cr2-C21	151.1(18)	C10-C5-Cr1	127.3(3)
N1-Cr2-C22	144.2(2)	C14-C13-P1	109.0(3)
N1-Cr2-C23	107.8(2)	C13-C14-P2	112.4(3)
N2-Cr2-C19	133.9(2)	N2-C17-O1	178.0(7)
N2-Cr2-C20	146.9(19)	N3-C18-O2	179.2(6)
N2-Cr2-C21	111.6(2)	C20-C19-Cr2	71.70(3)
N2-Cr2-C22	86.60(2)	C20-C19-C23	108.2(6)
N2-Cr2-C23	97.70(2)	C20-C19-C24	126.3(6)

N3-Cr2-N2	97.20(18)	C23-C19-Cr2	70.60(3)
N3-Cr2-C19	126.9(2)	C23-C19-C24	125.5(7)
N3-Cr2-C20	94.00(2)	C24-C19-Cr2	123.6(4)
N3-Cr2-C21	91.10(2)	C19-C20-Cr2	72.00(3)
N3-Cr2-C22	121.0(2)	C19-C20-C21	107.9(6)
N3-Cr2-C23	151.9(2)	C19-C20-C25	127.5(6)
C19-Cr2-C21	60.90(2)	C21-C20-Cr2	71.90(3)
C19-Cr2-C22	61.10(2)	C21-C20-C25	124.5(6)
C20-Cr2-C19	36.30(2)	C25-C20-Cr2	124.5(4)
C20-Cr2-C21	36.90(2)	C20-C21-Cr2	71.20(3)
C20-Cr2-C22	61.10(2)	C20-C21-C26	125.0(6)
C21-Cr2-C22	36.20(2)	C22-C21-Cr2	72.60(3)
C23-Cr2-C19	36.80(2)	C22-C21-C20	108.5(6)
C23-Cr2-C20	61.30(2)	C22-C21-C26	126.5(6)
C23-Cr2-C21	61.20(3)	C26-C21-Cr2	123.6(4)
C23-Cr2-C22	36.90(2)	C21-C22-Cr2	71.20(3)
C11-P1-Cr1	122.6(2)	C21-C22-C23	107.2(5)
C11-P1-C13	104.3(2)	C21-C22-C27	125.9(6)
C12-P1-Cr1	121.7(2)	C23-C22-Cr2	69.80(3)
C12-P1-C11	100.0(3)	C23-C22-C27	126.9(7)
C12-P1-C13	102.9(3)	C27-C22-Cr2	124.2(4)
C13-P1-Cr1	102.8(17)	C19-C23-Cr2	72.60(3)
C14-P2-Cr1	107.8(17)	C19-C23-C22	108.2(6)
C15-P2-Cr1	116.0(17)	C19-C23-C28	127.2(6)
C15-P2-C14	105.5(2)	C22-C23-Cr2	73.30(3)
C15-P2-C16	99.50(3)	C22-C23-C28	124.4(6)
C16-P2-Cr1	125.2(19)	C28-C23-Cr2	124.2(4)
C16-P2-C14	100.4(3)		

In **16** there is an inversion center around the bridging dmpe ligand, and the molecule crystalizes in the triclinic space group $P\bar{1}$, but **17** and **18** both crystallize in the monoclinic space group $P2_1/c$. In all these structures the isocyanate ligand is the result of

coupling of nitride ligand with the CO molecule. The magnetic moment of **18** was measured to be 1.9(1) μ_B at room temperature. The structure of **18** (including the symmetry around the chromium centers and the Cr-N bond distances) is very close to compound **12**. The proton NMR of **16** and **18** show broad shifted peaks consistent with the paramagnetism of these complexes (**Figure 2.31** and **Figure 2.33**). In contrast, the proton NMR of 17 shows sharp peaks in the diamagnetic region (**Figure 2.21**). In the IR spectrum of **17** there is a peak at 2217cm^{-1}, which is a characteristic of a terminal isocyanate group. Also peaks at 1937 and 1861 cm^{-1} indicate the presence of two terminal CO groups in the structure, as shown in **Figure 2.32**.[94–96] In the IR spectrum of **18** two peaks related to terminal isocyanate group at 2222 and 2203 cm^{-1} (**Figure 2.34**).

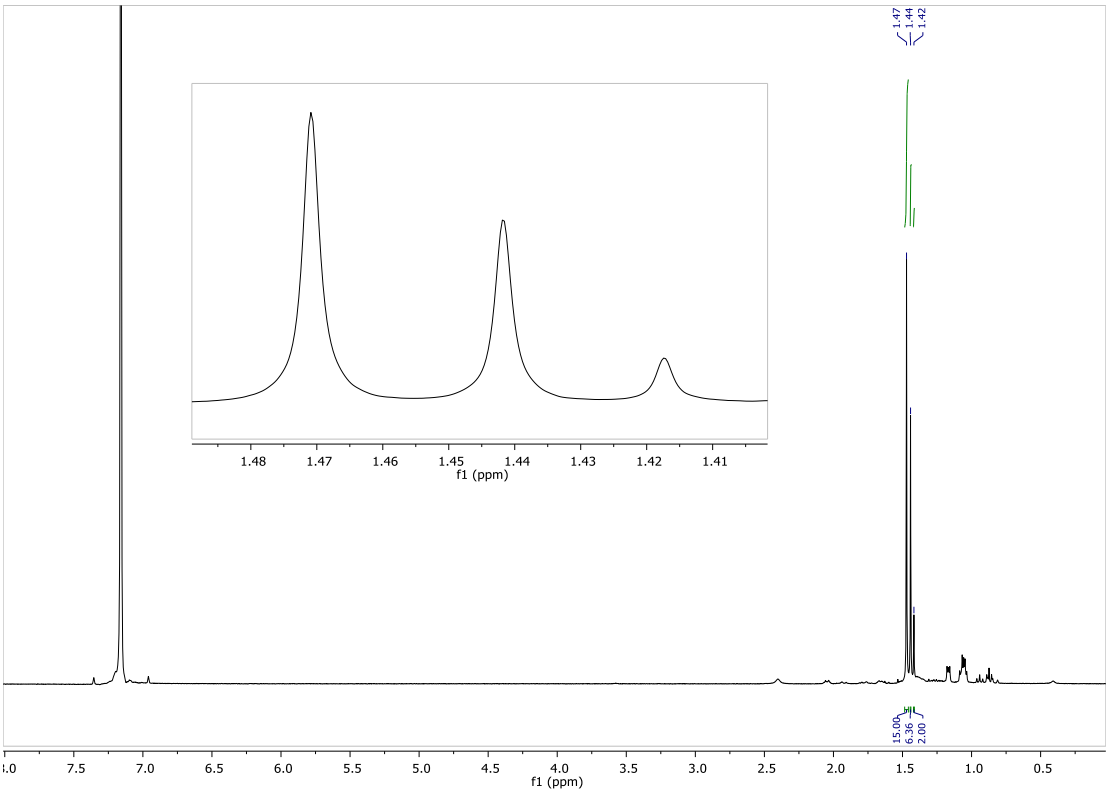

Figure 2.31 ^{1}H-NMR spectrum of [Cp*(CO)$_2$(OCN)Cr]$_2$(μ-dmpe) (**17**) recorded in C_6D_6 at 400 MHz.

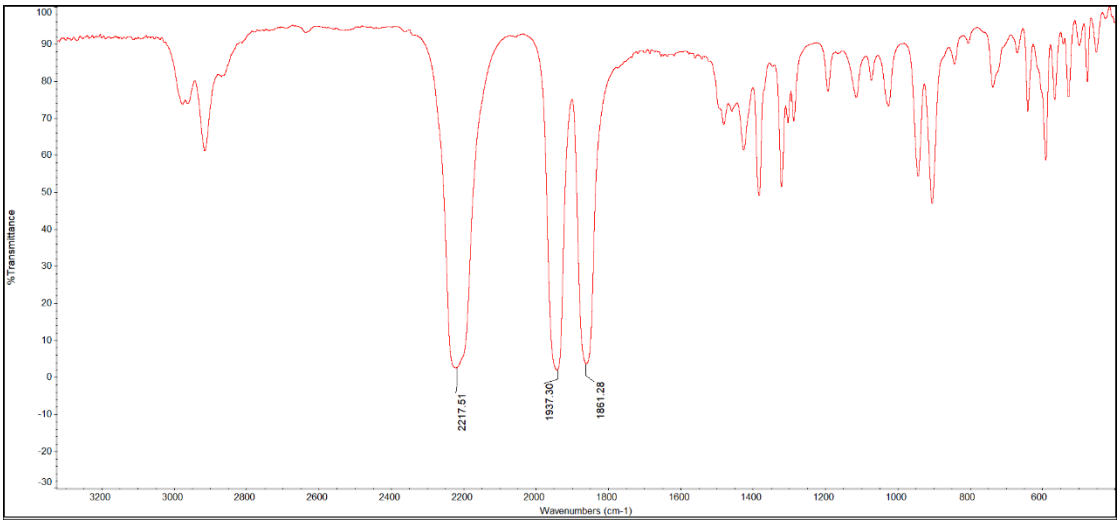

Figure 2.32 IR spectrum of $[Cp^*(CO)_2(OCN)Cr]_2(\mu\text{-dmpe})$ (**17**).

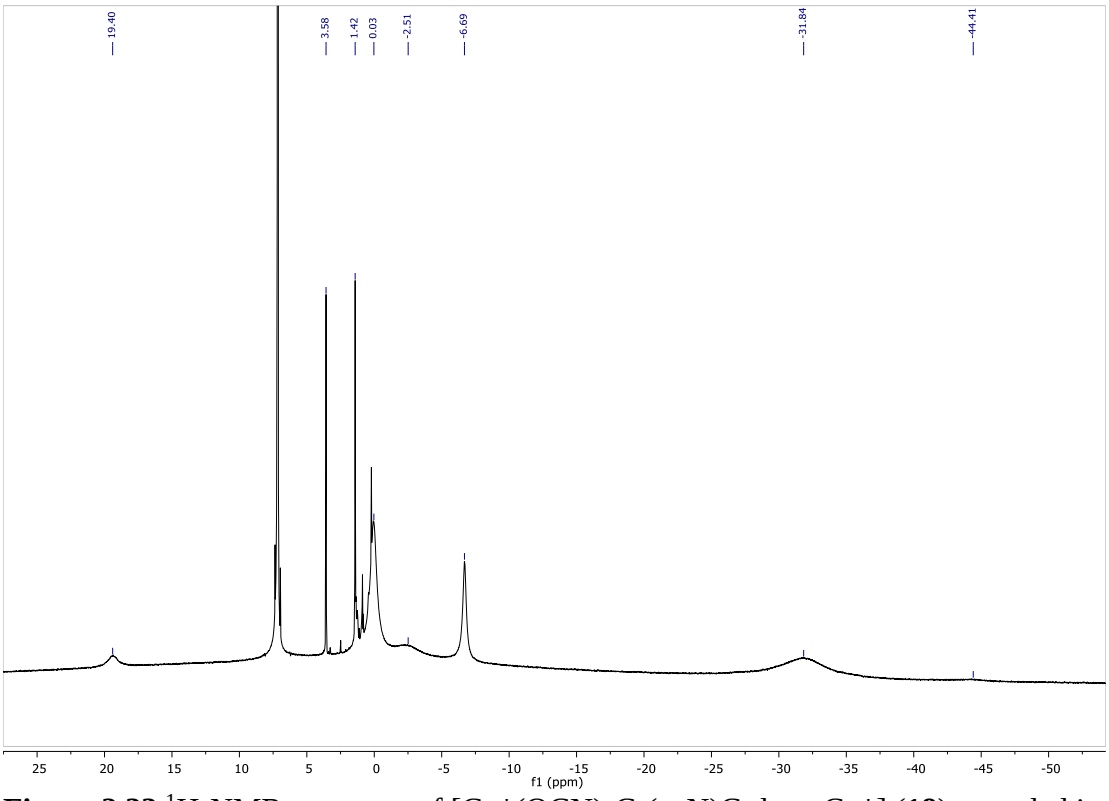

Figure 2.33 ^{1}H-NMR spectrum of $[Cp^*(OCN)_2Cr(\mu\text{-N})CrdmpeCp^*]$ (**18**) recorded in C_6D_6 at 400 MHz.

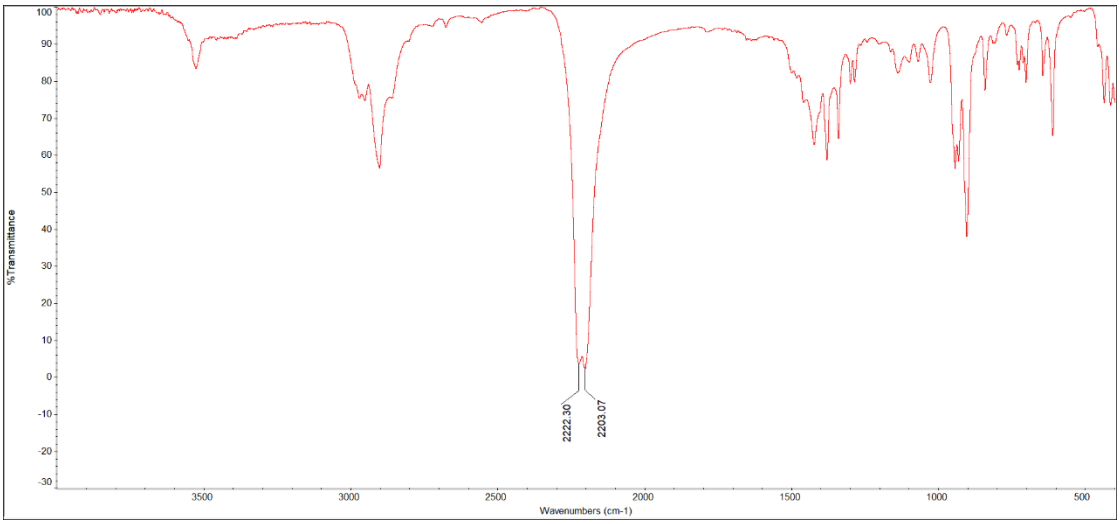

Figure 2.34 IR spectrum of [Cp*(OCN)$_2$Cr(μ-N)CrdmpeCp*] (**18**).

2.3 Conclusion

Cr(II) and Cr(III) complexes of Cp* ligand, were used to synthesize dinitrogen and nitride complexes. Cr(II) complexes showed more reactivity toward synthesizing dinitrogen and nitride complexes, compared to Cr(III) complexes; therefore, some modifications with additional ligands were done on the starting complex [Cp*ClCr(μ-Cl)]$_2$. Among the list of ligands that were used, dmpe showed promising reactivity (**9**). The dinitrogen (**10**) and the nitride (**13**) complexes of chromium metal were synthesized using dmpe ligand. With the dinitrogen and the nitride derivative of the starting chromium complex in hand, the interconversion of these compounds can be studied. The details of this study will be discussed in the next chapter.

2.4 Experimental

General considerations

All reactions were done under a nitrogen atmosphere using standard Schlenk, vacuum line, and glove box techniques. Pentane, toluene, and diethyl ether were dried by passing through activated alumina columns followed by a nitrogen purge to remove

dissolved oxygen. Tetrahydrofuran (THF) was dried under nitrogen gas by distillation over Na and benzophenone ketyl solution. C_6D_6 and THF-d_8 were dried over sodium and stored over Na/K alloy under vacuum. Organic chemicals were bought from Fischer, Aldrich, or Acros and all inorganic chemicals were purchased from Strem. Carbon monoxide gas was purchased from Matheson. $[Cp^*CrCl]_2$ was prepared by the literature procedure.[64] The starting complex $[Cp^*ClCr(\mu\text{-}Cl)]_2$ was synthesized based on the literature procedure.[71] H-dbabh was prepared according to the literature method and was reacted with *n*-butyllithium to make Li-dbabh.[67,68] NMR spectra were taken on a Bruker AVIII-400 spectrometer and were referenced to the residual protons of the solvent (C_6D_6, 7.16 ppm; THF-d_8, 3.58, 1.73 ppm). FT-IR spectra were recorded on a Nicolet Magna-IR 560 spectrometer with a resolution of 4 cm^{-1}. Magnetic susceptibilities (χ_m) were obtained in the solid state at room temperature using a Johnson Matthey magnetic susceptibility balance and corrected for diamagnetism. Mass spectra (LIFDI-MS) were obtained in the University of Delaware Mass Spectrometry Laboratory. X-ray crystallographic studies were conducted at the University of Delaware X-ray crystallographic facility. Elemental analyses were obtained from Robertson Microlit, Ledgewood, NJ 07852. The photochemical reactor was a Rayonet Model RPR100, equipped with 16 14W monochromatic 254 nm low-pressure mercury vapor lamps.

2.4.1 Preparation of $[Cr(\mu\text{-}\eta5{:}\eta1\text{-}C_5Me_4CH_2)Cr_3Cp^*_3N_3Hx(Cl)]$ (1): $[Cp^*CrCl]_2$ (0.741 g, 1.667 mmol) was dissolved in 20 ml THF and allowed to stir for 5 minutes before NaN_3 (0.216 g, 3.330 mmol) was added slowly over the course of 5 minutes. After about 15 minutes the color of solution turned from green-brown to green. The solution was allowed to stir for 4 hours and during this time the color of solution changed to brown. The solution was filtered, and the solvent was removed under vacuum to yield a brown residue. $[Cr(\mu\text{-}\eta^5{:}\eta^1\text{-}C_5Me_4CH_2)Cr_3Cp^*_3N_3H_x(Cl)]$ (**1**) was crystalized by cooling a saturated pentanes solution to -30 °C overnight to yield dark brown crystals (0.210 g, 35 % yield). ^{1}H-NMR (400 MHz, C_6D_6) -64.0 (br), -29.4 (br), -28.0 (br), -11.5 (br), -10.7 (br), -8.6 (br), -3.2 (br), -2.0 (br), 3.5 (br), 11.7 (br), 12.5 (br), 13.4 (br), 16.1 (br), 17.1

(br), 23.7 (br), 33.1 (br) ppm; IR(KBr): 2956 (m), 2903 (m), 2851 (m), 1438 (m), 1372 (s), 1163 (s), 1071 (s), 1024 (s), 936 (m), 807 (m), 752 (m), 672(m), 608 (m), 549 (m) cm^{-1}; m.p. 190-194 °C; μ_{eff} (293 K) = 2.9 (1) μ_B; LIFDI-MS Spectrum : m/z 827.2273 [[$Cr(\mu\text{-}\eta^5\text{:}\eta^1\text{-}C_5Me_4CH_2)Cr_3Cp^*_3N_3H_3(Cl)]^+$]. Calcd.: m/z 827.2260 [[$Cr(\mu\text{-}\eta^5\text{:}\eta^1\text{-}C_5Me_4CH_2)Cr_3Cp^*_3N_3H_3(Cl)]^+$].

2.4.2 Preparation of [Cp*Cr(μ-Cl)(μ-dbabh)CrCp*] (2): $[Cp^*CrCl]_2$ (0.146 g, 0.330 mmol) was dissolved in 10 ml THF and allowed to stir for 5 minutes before Li-dbabh (0.132 g, 0.660 mmol) was added slowly over the course of 5 minutes. After the addition, the color of solution turned from green-brown to purple. The solution was filtered after 2 h of stirring. The solvent was then removed under vacuum and the remaining purple powder was redissolved in minimal amounts of pentanes. [Cp*Cr(μ-Cl)(μ-dbabh)CrCp*] (**2**) was crystalized by cooling the saturated pentanes solution to -30 °C overnight to yield dark purple crystals (0.169g, 85 % yield). ^{1}H-NMR (400 MHz, C_6D_6) 3.6 (br), 4.6 (br), 4.9 (br), 6.6 (br), 6.9(br) ppm; IR(KBr): 2976 (m), 2903 (m), 2853 (m), 1454 (m), 1378 (m), 1251 (s), 1174 (m), 1145 (m), 1071 (s), 1022 (m), 965 (m), 914 (s), 891 (s), 836 (m), 809 (m), 775 (s), 746 (s), 717 (s), 695 (s), 615 (s), 596 (m), 531 (s) cm^{-1}; m.p. 162-165 °C; μ_{eff} (293 K) = 1.7 (1) μ_B; LIFDI-MS Spectrum : m/z 602.1676 [M^+]. Calcd.: m/z 602.1660 [M^+].

2.4.3 Preparation of $[Cp^*Cr(N_3)_3Li(THF)]_n$ (3): $[Cp^*ClCr(\mu\text{-}Cl)]_2$ (0.860 g, 1.667 mmol) was dissolved in 30 ml THF and allowed to stir for 5 minutes before NaN_3 (0.542 g, 8.335 mmol) was added slowly over the course of 5 minutes. The solution was allowed to stir for overnight and during this time no color change was observed. Then the solution was filtered, and the solvent was removed under vacuum to yield a blue residue. The blue powder was washed with 10 ml of pentanes and cold Et_2O, then it was redissolved in a minimal amount of THF. $[Cp^*Cr(N_3)_3Li(THF)]_n$(**3**) was crystalized by cooling the saturated THF solution to -30 °C overnight to yield blue crystals (0.589 g, 90 % yield). ^{1}H-NMR (400 MHz, C_6D_6) -22.7 (br, 15H) ppm; IR(KBr): 2962 (m), 2917 (m), 2868 (m),

2080 (w), 1889 (s), 1458 (m), 1382 (s), 1354 (s), 1333 (s), 1282 (m), 1161 (s), 1053 (m), 906 (m), 803 (m), 650 (s), 599 (s), 455 (s) cm^{-1}; m.p. 250-255 °C; μeff (293 K) = 2.4 (1) μ_B; UV-Vis (THF): λ_{max} (ε) 258 (13107), 305 (10666), 506 (216), 631 (1673) nm (cm^{-1} M^{-1}); Anal. Calcd For $C_{14}H_{23}N_9LiOCr$: C, 42.86; H, 5.91; N, 32. 13. Found C, 36.28; H, 4.45; N, 36.93. The results match with the loss of the THF molecule under high vacuum and also presence of a mixture for Li and Na in the molecule with the ratio of 2:8 = Calc for $C_{10}H_{15}N_9Na_{0.8}Li_{0.2}Cr$: C, 36.06; H, 4.54; N, 37.85.

2.4.4 Preparation of [Cp*ClCr(μ-N_3)]$_2$ (4): [Cp*ClCr(μ-Cl)]$_2$ (0.860 g, 1.667 mmol) was dissolved in 30 ml THF and allowed to stir for 5 minutes before NaN_3 (0.217 g, 3.334 mmol) was added slowly over the course of 10 minutes. The solution was allowed to stir for overnight and during this time no color change was observed. Then the solution was filtered, and the solvent was removed under vacuum to yield a blue residue. The blue powder was washed with 10 ml of pentanes and cold Et_2O, then was redissolved in a minimal amount of THF. [Cp*ClCr(μ-N_3)]$_2$ (**4**) was crystalized by cooling the saturated THF solution to -30 °C overnight to yield blue crystals (0.706 g, 80 % yield). ^{1}H-NMR (400 MHz, C_6D_6) -32.2 (br, 15H) ppm; IR(KBr): 2957 (m), 2914 (m), 2860 (m), 2090 (w), 2054 (w), 1634 (m), 1486 (s), 1447 (s), 1423 (s), 1381 (s), 1342 (m), 1291 (s), 1163 (s), 1069 (s), 1027 (s), 925 (m), 801 (m), 661 (m), 451 (s) cm^{-1}; m.p. 200-205 °C; μ_{eff} (293 K) = 2.9 (1) μ_B; LIFDI-MS Spectrum : m/z 528.0736 [M^+]. Calcd.: m/z 528.0719 [M^+]; UV-Vis (THF): λ_{max} (ε) 260 (23500), 319 (26400), 459 (1420), 616 (5000) nm (cm^{-1} M^{-1}). Anal. Calcd For $C_{20}H_{30}N_6Cl_2Cr_2$: C, 45.38; H, 5.71; N, 15.87. Found C, 45.94; H, 5.65; N, 15.62.

2.4.5 Preparation of [Cp*ClCr]$_4$(μ-N)$_2$(μ-N_3)$_2$ (5): [Cp*ClCr(μ-N_3)]$_2$ (**4**) (0.794 g, 1.500 mmol) was dissolved in 30 ml toluene and transferred to a quartz ampule. The gas above the solution was evacuated and the solution was exposed to UV light for 2 days. During this time, the color of the solution changed from blue to green. After filtration, the solvent was removed, and a green-brown powder was collected. The product was

redissolved in toluene and was filtered. $[Cp^*ClCr]_4(\mu\text{-}N)_2(\mu\text{-}N_3)_2$ (**5**) was crystalized by cooling the saturated toluene solution to -30 °C overnight to yield green crystals (0.489 g, 65 % yield). ^{1}H-NMR (400 MHz, C_6D_6) -30.4 (br, 15H) ppm; IR(KBr): 2957 (m), 2914 (m), 2860 (m), 2090 (w), 2054 (w), 1634 (m), 1486 (s), 1447 (s), 1423 (s), 1381 (s), 1342 (m), 1291 (s), 1163 (s), 1069 (s), 1027 (s), 925 (m), 801 (m), 661 (m), 451 (s)cm^{-1}; m.p. 195-200 °C; μ_{eff} (293 K) = 2.1 (1) μ_B; Anal. Calcd For $C_{40}H_{60}N_8Cl_4Cr_4$: C, 47.91; H, 6.03; N, 11.17. Found C, 47.84; H, 6.37; N, 10.10.

2.4.6 Preparation of [Cp*ClCr(N^N)] (6): $[Cp^*CrCl]_2$ (0.146 g, 0.330 mmol) was dissolved in 10 ml THF and allowed to stir for 5 minutes before 4,4'-dimethyl-2.2'-dipyridyl (i.e. **N^N,** 0.122 g, 0.660 mmol) was added slowly. After the addition, the color of the solution turned from green-brown to maroon. The solution was filtered after 2 h of stirring to remove any solid impurities. The solvent was then removed under vacuum and the remaining maroon powder was washed with 10 ml of cold pentanes and diethyl ether. [Cp*ClCr(N^N)] (**6**) was crystalized by cooling the saturated THF solution to -30 °C overnight to yield maroon crystals (0.241 g, 90 % yield). ^{1}H-NMR (400 MHz, C_6D_6) -82.5 (s, 6H), -4.7 (br, 15H), 24.7 (s, 4H), 82.9 (s, 2H) ppm; IR(KBr): 2958 (m), 2910 (m), 2854 (m), 1618 (s), 1593 (s), 1498 (s), 1463 (s), 1440 (s), 1379 (m), 1211 (m), 1105 (m), 1071 (s), 1026 (m), 977 (m), 903 (m), 821 (m), 786 (s), 561 (s), 539 (s), 523 (s), 485 (s), 435 (m) cm^{-1}; m.p. 182-185 °C; μ_{eff} (293 K) = 2.8 (1) μ_B; LIFDI-MS Spectrum : m/z 406.1367 [M^+]. Calcd.: m/z 406.1269 [M^+]; UV-Vis (Et_2O): λ_{max} (ε) 275 (29781), 356 (21826), 519 (15266), 658 (9134) nm (cm^{-1} M^{-1}). Anal. Calcd For $C_{20}H_{27}N_2ClCr$: C, 64.94; H, 6.69; N, 6.88. Found C, 63.78; H, 6.74; N, 6.68.

2.4.7 Preparation of [Cp*Cr(N^N)] (7): To a THF solution (10 mL) of [Cp*ClCr(N^N)] (**6**) (0.114 g, 0.280 mmol) was added Na chunks (0.006 g, 0.280 mmol). The solution was allowed to stir overnight and the color of the solution turned from maroon to brown during this time. After filtration, the solvent was removed under vacuum and the remaining brown powder was redissolved in pentanes. [Cp*Cr(N^N)] (**7**) was

crystalized by cooling the saturated pentanes solution to -30 °C overnight to yield brown crystals (0.046 g, 35 % yield). ^{1}H-NMR (400 MHz, C_6D_6) -71.6 (s, 6H), 62.8, 63.2 (br, 21H) ppm; IR(KBr): 2962 (m), 2905 (m), 2852 (m), 1599 (m), 1490 (m), 1443 (m), 1373 (s), 1327 (s), 1272 (m), 1217 (m), 1174 (s), 1104 (m), 1065 (s), 1023 (s), 969 (m), 902 (m), 824 (m), 543 (m) cm^{-1}; m.p. 165-169 °C; μ_{eff} (293 K) = 2.7 (1) μ_B; LIFDI-MS Spectrum : m/z 371.1562 [M^+]. Calcd.: m/z 371.1579 [M^+]; UV-Vis (Et_2O): λ_{max} (ε) (270) 27679, 314 (23518), 358 (20847), 483 (20998), 545 (8186), 723 (16869) nm (cm^{-1} M^{-1}). Anal. Calcd For $C_{22}H_{27}N_2CrO_2$: C, 65.49; H, 6.75; N, 6.94. Found C, 63.86; H, 6.51; N, 6.84.

2.4.8 Preparation of [Cp*Cr(μ-N_2)PMe_3]$_4$Na (8): [Cp*CrCl]$_2$ (0.146 g, 0.330 mmol) was dissolved in 10 ml THF and allowed to stir for 5 minutes, after which PMe_3 (0.100 g, 1.320 mmol) was added slowly. After 1 h of stirring, Na chunks (0.015 g, 0.660 mmol) were added to the solution. The solution was allowed to stir overnight, and the color of the solution turned green during this time. The solution was then filtered, and the solvent was removed under vacuum. [Cp*Cr(μ-N_2)PMe_3]$_4$Na (**8**) was crystalized by cooling the saturated pentanes solution to -30 °C overnight to yield purple crystals (0.197 g, 10 % yield). ^{1}H-NMR (400 MHz, C_6D_6) -12.9 (br), -9.8 (br), -6.9 (br), 9.9 (br), 16.0 (br), 20.6 (br), 30.2 (br) ppm; IR(KBr): 2969 (m), 2901 (m), 2852 (m), 1937 (m), 1849 (m), 1796 (m), 1757 (m), 1440 (m), 1376 (s), 1292 (s), 1274 (m), 1151 (m), 1069 (s), 1024 (s), 942 (s), 558 (s) cm^{-1}; m.p. 172-175 °C.

2.4.9 Preparation of [Cp*(dmpe)CrCl] (9): [Cp*CrCl]$_2$ (1.482 g, 3.330 mmol) was dissolved in 20 ml THF and allowed to stir for 5 minutes before dmpe (1.000 g, 6.660 mmol) was added dropwise over the course of 5 minutes. Upon addition of dmpe the solution turned from green-brown to brown. The solution was allowed to stir for an additional hour. The solution was filtered, and the solvent was removed under vacuum to yield a brown residue. The solid was washed with cold diethyl ether. [Cp*(dmpe)CrCl] (**9**) was crystalized by cooling a saturated THF solution to -30 °C overnight to yield dark

brown crystals (2.100g, 85 % yield). ^{1}H-NMR (400 MHz, C_6D_6) -20.5 (br, 12H), -7.8 (br, 15H), 2.5 (br, 4H) ppm; IR(KBr): 2959 (m), 2892 (m), 2855 (m), 1414 (s), 1377 (s), 1372 (s), 1268 (s), 1274 (s), 1234 (w), 1173 (w), 1128 (m), 1022 (s), 930 (s), 922 (s), 900 (s),889 (s), 853 (s), 827 (s), 797 (m), 767 (w), 719 (s), 691(s), 634 (s), 606 (s), 586 (s), 527 (m), 451 (s), 431 (m) cm^{-1}; m.p. 180-186 °C; μ_{eff} (293 K) = 2.6 (1) μ_B; LIFDI-MS Spectrum : m/z 372.1004 [M^+]. Calcd.: m/z 372.0995 [M^+]; UV-Vis (Et_2O): λ_{max} (ε) 249 (5369), 264 (6129), 361 (3987), 500 (300) nm (cm^{-1} M^{-1}). Anal. Calcd For $C_{16}H_{31}P_2ClCr$: C, 51.55; H, 8.38. Found C, 51.01; H, 8.82.

2.4.10 Preparation of [Cp*(dmpe)Cr]$_2$(μ-N$_2$) (10): 1 equivalent of Na metal chunks (0.031 g, 1.341 mmol) was added to the THF solution of [Cp*(dmpe)CrCl] (0.500 g, 1.341 mmol) and the mixture was allowed to stir overnight to ensure the complete reduction of [Cp*(dmpe)CrCl]. The solution turned from brown to green-brown and a white precipitate formed. The white solid was removed *via* filtration. The THF solvent was then removed under vacuum to yield a brown residue. The brown solid was recrystallized by cooling a saturated THF solution to -30 °C overnight to yield green-brown crystals (0.410 g, 87 % yield). ^{1}H-NMR (400 MHz, C_6D_6) -17.1 (br, 2H), -16.2 (br, 6H), -2.8 (br, 6H), 4.7 (br, 15H), 15.7 (br, 2H) ppm; IR(KBr): 2956 (m), 2899 (s), 2850 (s), 1894 (w), 1421 (w), 1376 (s), 1294 (s), 1266 (s), 1165 (s), 1118 (s), 1097 (s), 1073 (w), 1022 (s), 928 (s), 885 (m), 828 (s), 803 (w), 750 (w), 711 (s), 685 (s), 639 (s), 621 (s), 539 (w), 461 (m), 415 (w) cm^{-1}; m.p. 145-149 °C; μ_{eff} (293 K) = 2.0 (1) μ_B; LIFDI-MS Spectrum : m/z 702.2628 [M^+]. Calcd.: m/z 702.2674 [M^+]; UV-Vis (Et_2O): λ_{max} (ε) 275 (9445), 367 (13830), 526 (1872), 868 (5650) nm (cm^{-1} M^{-1}). Anal. Calcd For $C_{32}H_{62}P_4N_2Cr_2$: C, 54.69; H, 8.89; N, 3.99; Found C, 53.94; H, 8.98; N, 2.96.

2.4.11 Preparation of [Cp*dmpeCr(μ-N)CrCp*Cl] (11): NaN_3 (0.024 g, 0.368 mmol) was added to a stirred THF solution of [Cp*(dmpe)CrCl] (0.137 g, 0.368 mmol). The color of solution changed from brown to blue after 3h. The solution was then filtered, and the solvent was removed under vacuum to yield a blue residue. The blue solid was washed

with 10 ml of pentanes and Et_2O and was recrystallized by cooling a saturated THF solution to -30 °C overnight to yield blue crystals (0.026 g, 25 % yield). ^{1}H-NMR (400 MHz, THF-d_8) -12.2 (br), -10.7 (br), -6.0 (br), -4.3 (br), 0.3 (br), 74.15 (br) ppm; IR(KBr): 2960 (m), 2905 (m), 2854 (m), 1438 (m), 1382 (s), 1290 (m), 1174 (m), 1069 (s), 1022 (s), 940 (s), 901 (s), 721 (w), 531 (m) cm^{-1}.

2.4.12 Preparation of [Cp*dmpeCr(μ-N)Cr(N_3)$_2$Cp*] (12): NaN_3 (0.024 g, 0.368 mmol) was added to a stirred THF solution of [Cp*(dmpe)CrCl] (0.137 g, 0.368 mmol). The color of solution changed from brown to blue after 3h. The solution was allowed to stir for 24 h before filtration. The solvent was then removed under vacuum to yield a blue residue. The blue solid was washed with 10 ml of pentanes and Et_2O and was recrystallized by cooling a saturated THF solution to -30 °C overnight to yield blue crystals (0.063 g, 55 % yield). ^{1}H-NMR (400 MHz, THF-d_8) -27.9 (br), -6.0 (br), -2.3 (br), -0.3 (br), 20.3 (br) ppm; IR(KBr): 2966 (m), 2901 (m), 2852 (m), 2066 (s), 2050 (s), 1423 (m), 1378 (s), 1341 (m), 1298 (s), 1282 (s), 1071 (s), 1024 (s), 936 (m), 899 (s), 840 (S), 807 (s), 711 (m), 646 (m), 437 (s); m.p. 205-210 °C ; μ_{eff} (293 K) = 1.9 (1) μ_B; LIFDI-MS Spectrum : m/z 622.2095 [M^+]. Calcd.: m/z 622.2100 [M^+]; Anal. Calcd For $C_{26}H_{46}P_2N_7Cr_2$: C, 50.15; H, 7.45; N, 15.75; Found C, 49.21; H, 7.39; N, 15.01.

2.4.13 Preparation of [Cp*(dmpe)Cr≡N] (13): NaN_3 (0.105 g, 1.608mmol) was added to a stirred THF solution (15 mL) of [Cp*(dmpe)CrCl] (**9**) (0.200 g, 0.536 mmol). The color of the solution changed from brown to blue after 3h. The mixture was allowed to stir for an additional 48 hours, during which time the solution turned from blue to purple and a white precipitate formed. The white solid was removed *via* filtration. The THF solvent was then removed under vacuum to yield a purple residue. The purple solid was recrystallized by cooling a saturated pentanes solution to -30 °C overnight to yield purple crystals of [Cp*(dmpe)Cr≡N] (**13**) (0.139 g, 74 % yield). ^{1}H-NMR (400 MHz, C_6D_6) 0.82 (d,$^2J_{PH}$ = 8.0 Hz, 6H), 1.21 (m, 2H), 1.45 (m, 2H), 1.74 (d, $^2J_{PH}$ = 8.0 Hz, 6H), 1.98 (s, 15H) ppm; IR(KBr): 2960 (m), 2898 (m), 1421 (w), 1386 (s), 1376 (s), 1292 (s), 1274

(s), 1161 (s), 1078 (w), 1064 (w), 1026 (s), 980 (s), 936 (w), 924 (w), 908 (s), 891 (s), 860 (s), 836 (s), 805 (w), 772 (w), 727 (s), 701 (s), 643 (m), 549 (s), 455 (w), 423 (w) cm^{-1}; m.p. 120-125 °C; LIFDI-MS Spectrum : m/z 351.1327 [M^+]. Calcd.: m/z 351.1337 [M^+]; UV-Vis (Et_2O): λ_{max} (ε) 255 (6615), 308 (6068), 534 (421) nm ($cm^{-1}M^{-1}$). Anal. Calcd For $C_{16}H_{31}P_2NCr$: C, 54.69; H, 8.89; N, 3.99; Found C, 53.66; H, 8.47; N, 3.75.

2.4.14 Preparation of [Cp*(dmpe)Cr=NMe]OTf (14): [Cp*(dmpe)Cr≡N] (**13**) (0.118 g, 0.336 mmol) was dissolved in 10 ml THF and 1 equivalent of MeOTf (0.055 g, 0.336 mmol) was added to this solution. The color of solution changed from purple to pale green immediately after the addition. The solution was stirred for 1 h and was then filtered. The solvent was removed under vacuum and the remaining powder was washed with pentanes and diethyl ether. [Cp*(dmpe)Cr=NMe]OTf (**14**) was recrystallized by cooling a saturated THF solution to -30 °C (0.156 g, 90 % yield). ^{1}H-NMR (400 MHz, THF-d_8) 1.41 (d, $^2J_{PH}$ = 8.0 Hz, 6H), 1.57 (d, $^2J_{PH}$ = 12.0 Hz, 6H), 1.84 (s, 15H), 2.30 (m, 4H), 3.39 (t, 3H) ppm; IR(KBr): 2984 (s), 2858 (s), 2911 (m), 1487 (s), 1460 (s), 1423 (s), 1386 (s), 1266 (w), 1225 (s), 1151 (w), 1096 (s), 1073 (s), 1030 (s), 951 (m), 934 (m), 901 (s), 850 (s), 813 (s), 781 (s), 744 (s), 707 (s), 635 (m), 574 (s), 521 (s), 465 (s) cm^{-1}; m.p. 210-216 °C; LIFDI-MS Spectrum : m/z 366.1588 [M^+]. Calcd.: m/z 366.1572 [M^+]; UV-Vis (Et_2O): λ_{max} (ε) 255 (6615), 308 (6068), 534 (421) nm (cm^{-1} M^{-1}). Anal. Calcd For $C_{18}H_{34}P_2NF_3O_3SCr$: C, 41.94; H, 6.65; N, 2.72; Found C, 42.08; H, 6.33; N, 2.61.

2.4.15 Preparation of [Cp*(dmpe)CrN]$_2$(μ-MgCl$_2$) (15): [Cp*(dmpe)Cr≡N] (**13**) (0.118 g, 0.336 mmol) was dissolved in Et_2O and to this solution, 1 equivalent of MeMgCl (0.33μl, 0.336 mmol) was added slowly. A blue product precipitated out of solution after the addition. After removal of solvent, the blue powder was dissolved in THF and was filtered to remove the insoluble byproducts. The blue-purple solution was stored at -30°C overnight to yield blue crystals of [Cp*dmpeCrN]$_2$[μ-$MgCl_2$] (**15**) (0.113 g, 84 % yield). ^{1}H-NMR (400 MHz, THF-d_8) 1.17 (d, 6H), 1.33 (m, 2H), 1.64 (m, 2H), 1.85 (br, 6H), 1.87 (s, 15H) ppm; IR(KBr): 2968 (m), 2894 (s), 2857 (s), 1422 (s), 1380

(s), 1302 (s), 1284 (s), 1013 (s), 938 (s), 895 (m), 838 (s), 733 (s), 701 (s), 642 (m), 457 (m) cm^{-1}; m.p. 178-186 °C; LIFDI-MS Spectrum : m/z 351.1336 [(M^+- $MgCl_2$)/2]. Calcd.: m/z 351.1337 [M^+-$MgCl_2$]; UV-Vis (THF): λ_{max} (ε) 253 (9493), 312 (8526), 542 (983) nm (cm^{-1} M^{-1}). Anal. Calcd For $C_{16}H_{31}P_2NCr$: C, 54.69; H, 8.89; N, 3.99; Found C, 53.66; H, 8.47; N, 3.75.

2.4.16 Preparation of [Cp*(OCN)$_2$Cr(μ-N)CrdmpeCp*] (18): [Cp*(dmpe)Cr≡N] (**13**) (0.123 g, 0.350 mmol) was dissolved in 20 ml toluene and transferred to an ampule in the glove box. The gas above the solution was removed and then 1 equivalent of carbon monoxide was introduced to the stirred solution of **13** at room temperature. The solution was allowed to stir for 24 h. The solution was degassed, filtered and the solvent was removed under vacuum. The remaining powder was washed with 10 ml of pentanes and diethyl ether. [Cp*(OCN)$_2$Cr(μ-N)CrdmpeCp*] (**18**) was crystalized by cooling a saturated THF solution to -30°C overnight to yield blue crystals (0.033 g, 30 % yield). ^{1}H-NMR (400 MHz, C_6D_6) -44.4 (br), -31.8 (br), -6.7 (br), -2.5 (br), 0.03 (br), 19.4 (br) ppm; m.p. 209-2015 °C; μ_{eff} (293 K) = 1.9 (1) μ_B; LIFDI-MS Spectrum : m/z 622.1870 [M^+]. Calcd.: m/z 622.1875 [M^+]; UV-Vis (Et_2O): λ_{max} (ε) 291 (11411), 576 (607) nm (cm^{-1} M^{-1}). Anal. Calcd For $C_{28}H_{46}P_2N_3O_4Cr_2$ (This complex is extremely sensitive to air, the elemental analysis matches the incorporation of O_2.): C, 51.37; H, 7.08; N, 6.42; Found C, 51.66; H, 7.27; N, 6.43.

Chapter 3

STUDY OF THE REACTIVITY OF DINITROGEN AND NITRIDE COMPLEXES SUPPORTED BY CYCLOPENTADIENYL AND DMPE

3.1 Introduction

There are many examples of transition metal complexes that can coordinate free dinitrogen and split the N-N triple bond to make the nitride complex. We were able to synthesize both isomers, the chromium dinitrogen and the nitride complexes. The existence of both isomers proves the stability of these complexes. One of these compounds should be the kinetic and the other one should be the thermodynamic product. The interconversion from the kinetic to the thermodynamic isomer should be downhill, but the rate of this reaction can be slow in some cases, depending on the nature of metal, the oxidation state of metal and the ligands.

In the case of dinitrogen, there are several factors that can cause the slow rate for the splitting of triple bond in dinitrogen. The large HOMO-LUMO gap of 10.82 ev, can result in a slow reaction of N_2. Also low proton affinity, and high ionization potential of the dinitrogen, can make it difficult to activate this molecule.[97]

In this chapter the interconversion between the two isomers (**10** and **13**) will be investigated.

3.2 Results and Discussion

Dinitrogen complex **10**, was heated to high temperatures up to100 ^{o}C in a variety of solvents, including benzene and THF, but unfortunately the conversion to the nitride complex **13** was not observed, but instead the dinitrogen complex decomposed to an unidentified mixture. Also, in the case of nitride complex, the interconversion to the dinitrogen complex was not observed upon heating in the NMR tube. Using NMR spectroscopy it was shown that these two decompositions do not have any products in common.

Prolonged exposure of the dinitrogen complex in solution to UV light did not form the corresponding nitride complex. The irradiation of **13** with UV light was tracked using ^{1}H-NMR spectra. Under nitrogen atmosphere **13** was transferred to a J.Young NMR tube. C_6D_6 was vacuum transferred to the NMR tube and the tube was exposed to 250 nm light. After 3 h from the start of the reaction, a ^{1}H-NMR spectrum of the sample showed the appearance of new broad shifted peaks and decay of peaks related to the nitride complex in the diamagnetic region. The starting complex was completely transformed into a new paramagnetic compound after 22h of exposure, as shown in **Figure 3.1**. The same results were found upon heating the nitride complex to 85 °C.

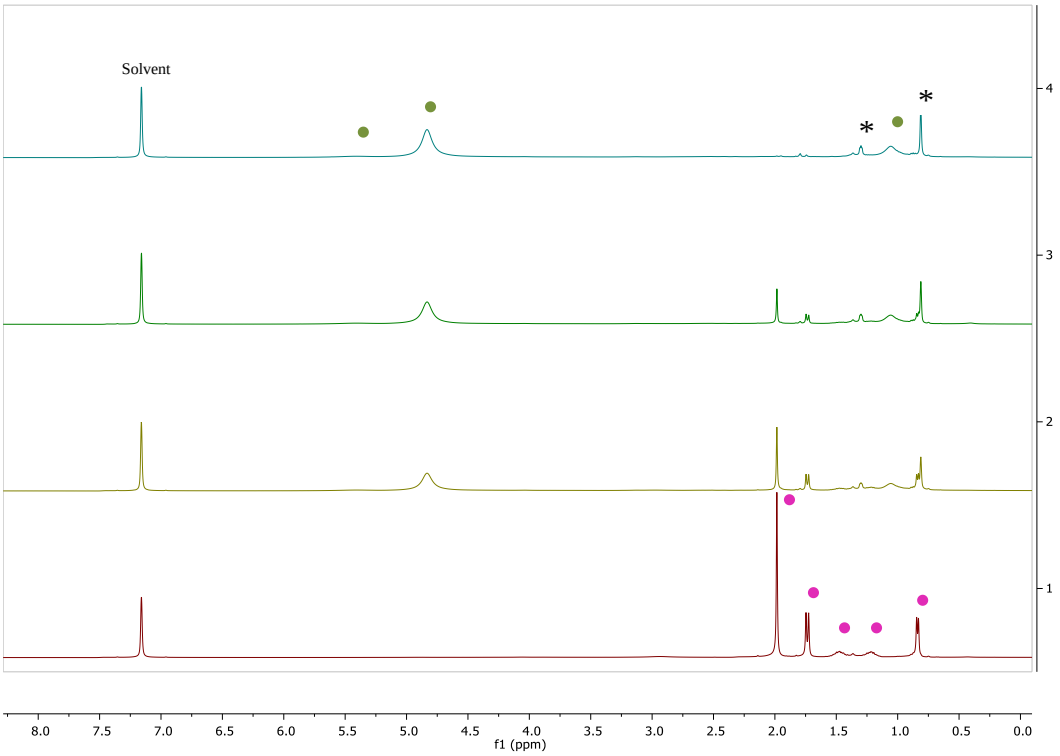

Figure 3.1 Reaction of [Cp*dmpeCr≡N] (**13**) under 250 nm light in benzene-d_6 for 22 hours. Purple and green dots respectively show the proton NMR peaks of **13** and the product of reaction. During the reaction free dmpe ligand was observed (black stars).

To be able to characterize the product, the reaction was repeated on a larger scale in a quartz ampule. In the glove box, **13** was dissolved in THF and then transferred to an ampule under nitrogen atmosphere. The gas above the solution was evacuated and the ampule was brought out of the box. After 24 h of irradiation under light the reaction appeared to be complete, and the color of solution had changed from purple to green during this time. The flask was transferred to the glove box and the solvent was removed under vacuum. The remaining green residue was washed with cold pentanes. The remaining green powder was dissolved in Et_2O and filtered through celite. The solution

was then concentrated and cooled to -30 °C overnight to yield green crystals of the product. Determination of the structure by X-ray crystallography revealed it to be a dinuclear chromium complex, i.e., [Cp*$_2$Cr$_2$(μ,μ-{NP(CH$_3$)$_2$}$_2$C$_2$H$_4$)] (**19**) The molecular structure of **19** is depicted in **Figure 3.2**, while the corresponding interatomic distances and angles are listed in **Table 3.1**.

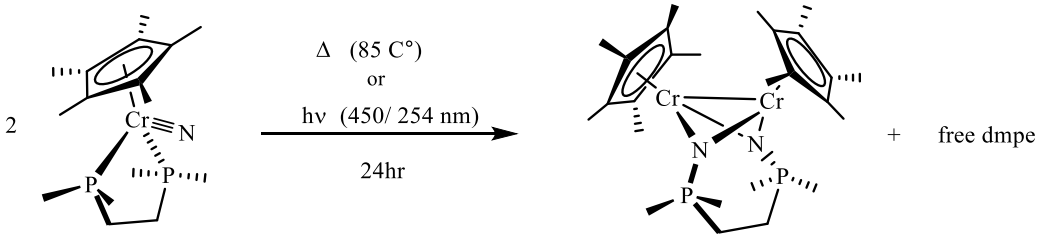

Scheme 3.1 Synthesis of [Cp*$_2$Cr$_2$(μ,μ-{NP(CH$_3$)$_2$}$_2$C$_2$H$_4$)] (**19**).

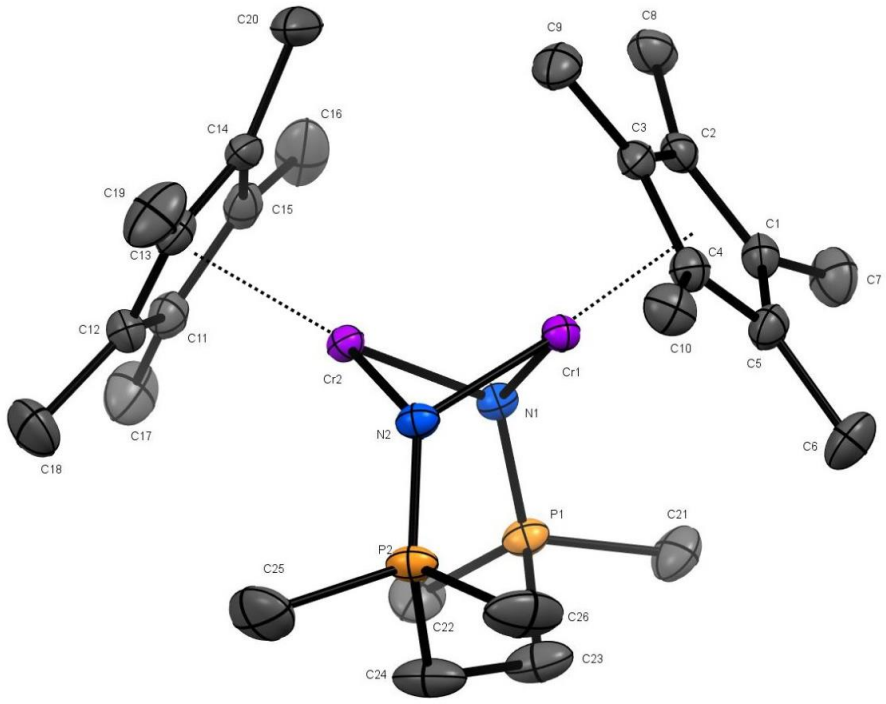

Figure 3.2 Molecular structure of [Cp*$_2$Cr$_2$(μ,μ-{NP(CH$_3$)$_2$}$_2$C$_2$H$_4$)] (**19**) represented as 50% probability thermal ellipsoids. Hydrogen atoms have been omitted for clarity.

Table 3.1 Interatomic distances (Å) and angles (º) for $[Cp^*_2Cr_2(\mu,\mu\text{-}\{NP(CH_3)_2\}_2C_2H_4)]$ (**19**).

Distances (Å)			
Cr1-Cr2	2.4120(5)	P2-C26	1.791(3)
Cr1-N1	2.0120(17)	C1-C2	1.423(3)
Cr1-N2	2.0162(18)	C1-C5	1.420(3)
Cr1-C1	2.323(2)	C1-C7	1.500(3)
Cr1-C2	2.308(2)	C2-C3	1.414(3)
Cr1-C3	2.313(2)	C2-C8	1.505(3)
Cr1-C4	2.310(2)	C3-C4	1.426(3)
Cr1-C5	2.349(2)	C3-C9	1.499(3)
Cr2-N1	2.0122(18)	C4-C5	1.414(3)
Cr2-N2	2.0068(17)	C4-C10	1.504(3)
Cr2-C11	2.339(2)	C5-C6	1.507(3)
Cr2-C12	2.345(2)	C11-C12	1.405(3)
Cr2-C13	2.300(2)	C11-C15	1.415(3)
Cr2-C14	2.310(2)	C11-C17	1.505(3)
Cr2-C15	2.294(2)	C12-C13	1.420(3)
P1-N1	1.5613(18)	C12-C18	1.509(3)
P1-C21	1.811(3)	C13-C14	1.415(4)
P1-C22	1.795(3)	C13-C19	1.506(4)
P1-C23	1.829(3)	C14-C15	1.414(4)
P2-N2	1.5604(17)	C14-C20	1.496(3)
P2-C24	1.828(3)	C15-C16	1.508(4)
P2-C25	1.814(3)	C23-C24	1.491(4)

Angles (°)

N1-Cr1-Cr2	53.18(5)	Cr1-N1-Cr2	73.65(6)
N1-Cr1-N2	88.82(7)	P1-N1-Cr1	123.1(10)
N1-Cr1-C1	105.9(8)	P1-N1-Cr2	126.9(11)
N1-Cr1-C2	114.1(7)	Cr2-N2-Cr1	73.68(6)
N1-Cr1-C3	146.3(8)	P2-N2-Cr1	125.7(10)
N1-Cr1-C4	163.1(8)	P2-N2-Cr2	124.7(10)
N1-Cr1-C5	127.8(8)	C2-C1-Cr1	71.56(12)
N2-Cr1-Cr2	52.98(5)	C2-C1-C7	124.5(2)
N2-Cr1-C1	160.6(8)	C5-C1-Cr1	73.31(13)
N2-Cr1-C2	147.2(8)	C5-C1-C2	108.1(19)
N2-Cr1-C3	114.1(8)	C5-C1-C7	127.1(2)
N2-Cr1-C4	104.1(8)	C7-C1-Cr1	125.4(17)
N2-Cr1-C5	125.2(8)	C1-C2-Cr1	72.65(12)
C1-Cr1-Cr2	146.4(6)	C1-C2-C8	123.9(2)
C1-Cr1-C5	35.40(8)	C3-C2-Cr1	72.38(12)
C2-Cr1-Cr2	122.2(5)	C3-C2-C1	108.0(19)
C2-Cr1-C1	35.79(8)	C3-C2-C8	128.0(2)
C2-Cr1-C3	35.63(8)	C8-C2-Cr1	123.2(15)
C2-Cr1-C4	59.57(8)	C2-C3-Cr1	71.99(12)
C2-Cr1-C5	59.24(8)	C2-C3-C4	107.8(19)
C3-Cr1-Cr2	121.1(5)	C2-C3-C9	127.5(2)
C3-Cr1-C1	59.35(8)	C4-C3-Cr1	71.89(12)
C3-Cr1-C5	59.17(8)	C4-C3-C9	124.6(2)
C4-Cr1-Cr2	143.7(6)	C9-C3-Cr1	125.2(15)
C4-Cr1-C1	59.22(8)	C3-C4-Cr1	72.18(12)
C4-Cr1-C3	35.93(8)	C3-C4-C10	124.6(2)
C4-Cr1-C5	35.31(8)	C5-C4-Cr1	73.86(12)
C5-Cr1-Cr2	178.2(6)	C5-C4-C3	108.3(2)
N1-Cr2-Cr1	53.17(5)	C5-C4-C10	127.0(2)
N1-Cr2-C11	113.6(8)	C10-C4-Cr1	122.9(16)
N1-Cr2-C12	144.8(8)	C1-C5-Cr1	71.29(12)

N1-Cr2-C13	164.4(8)	C1-C5-C6	126.0(2)
N1-Cr2-C14	128.9(8)	C4-C5-Cr1	70.83(12)
N1-Cr2-C15	105.9(8)	C4-C5-C1	107.7(19)
N2-Cr2-Cr1	53.34(5)	C4-C5-C6	126.2(2)
N2-Cr2-N1	89.07(7)	C6-C5-Cr1	124.9(18)
N2-Cr2-C11	146.9(8)	C12-C11-Cr2	72.75(13)
N2-Cr2-C12	114.5(8)	C12-C11-C15	107.8(2)
N2-Cr2-C13	103.8(8)	C12-C11-C17	126.3(2)
N2-Cr2-C14	125.1(9)	C15-C11-Cr2	70.47(12)
N2-Cr2-C15	160.8(8)	C15-C11-C17	125.6(2)
C11-Cr2-Cr1	159.7(6)	C17-C11-Cr2	126.6(18)
C11-Cr2-C12	34.92(8)	C11-C12-Cr2	72.33(13)
C12-Cr2-Cr1	161.9(6)	C11-C12-C13	108.5(2)
C13-Cr2-Cr1	128.8(6)	C11-C12-C18	126.8(2)
C13-Cr2-C11	59.21(8)	C13-C12-Cr2	70.50(12)
C13-Cr2-C12	35.58(8)	C13-C12-C18	124.5(2)
C13-Cr2-C14	35.75(9)	C18-C12-Cr2	127.5(18)
C14-Cr2-Cr1	114.7(6)	C12-C13-Cr2	73.92(13)
C14-Cr2-C11	59.07(8)	C12-C13-C19	125.9(3)
C14-Cr2-C12	58.85(8)	C14-C13-Cr2	72.51(13)
C15-Cr2-Cr1	127.4(6)	C14-C13-C12	107.5(2)
C15-Cr2-C11	35.55(8)	C14-C13-C19	126.6(3)
C15-Cr2-C12	58.84(8)	C19-C13-Cr2	120.4(18)
C15-Cr2-C13	59.72(9)	C13-C14-Cr2	71.74(12)
C15-Cr2-C14	35.78(9)	C13-C14-C20	126.0(3)
N1-P1-C21	113.7(12)	C15-C14-Cr2	71.48(12)
N1-P1-C22	114.5(12)	C15-C14-C13	107.9(19)
N1-P1-C23	118.2(11)	C15-C14-C20	125.8(3)
C21-P1-C23	99.70(14)	C20-C14-Cr2	127.3(17)
C22-P1-C21	103.5(14)	C11-C15-Cr2	73.98(13)
C22-P1-C23	105.2(16)	C11-C15-C16	124.8(3)
N2-P2-C24	118.6(11)	C14-C15-Cr2	72.74(12)
N2-P2-C25	113.5(14)	C14-C15-C11	108.2(2)

N2-P2-C26	114.6(13)	C14-C15-C16	126.9(3)
C25-P2-C24	99.93(17)	C16-C15-Cr2	122.8(17)
C26-P2-C24	104.3(17)	C24-C23-P1	116.2(2)
C26-P2-C25	103.9(2)	C23-C24-P2	117.3(2)

19 crystalizes in the orthorhombic space group Pbca. This molecule has been generated from the combination of two nitride molecules by losing one dmpe ligand. The insertion of nitride into the Cr-P bond makes a butterfly geometry with chromium and nitride atoms. The Cr1-N1, Cr2-N2, Cr1-N2, and Cr2-N1 bond distances are 2.0120(17), 2.0162(18), 2.0162(18), and 2.0122(18) Å respectively, which are in the range of Cr-N single bond length.[66] The mean N-P bond distance in the dianionic phosphiniminato unit is 1.56085 Å and the nitrogen atoms of this ligand act as bridging donors to the two Cr(II) centers. The complex displayed an effective magnetic moment of 2.0 (1) μ_B at room temperature, which is lower than the expected magnetic moment (4.0 μ_B) for a system with two noninteracting Cr(II) (S = 1) centers. Antiferromagnetic coupling or metal-metal interactions[64,98–100]of different magnitudes can cause this reduction in the effective magnetic moment.

Heating the dinitrogen and nitride complexes did not result in the interconversion between these two isomers. In the case of dinitrogen complex, upon heating or reacting with light, decomposition of **10** to some unidentified compounds was observed using NMR spectroscopy. The nitride complex **13** decomposes to a dinuclear complex (**19**) under light or at high temperatures.

Based on these results from heating and exposing **10** and **13** to UV light the interconversion between isomers was not observed, therefore it was decided to try other reactions on the dinitrogen and nitride complex to further study their reactivity. Reduction of the dinitrogen complex **10** was examined to see the effect of an increase in the electron density of the molecule. Reaction of 2.0 equivalents of Na with a THF solution of **10** resulted in a color change from green-brown to orange overnight. The solution was stirred

for 24h and then it was filtered. The solvent was removed in vacuo and an orange-brown powder was collected. Extraction with pentanes yielded an orange-red solution. After filtration, the solution was concentrated under vacuum. The solution was kept at -30°C overnight; after that time orange-red crystals of the product were collected. The structure of the product was determined using X-ray crystallography; it is a tetranuclear chromium complex, i.e. $Na_2[Cp^*dmpeCr(N_2)]_4$ (**20**). The molecular structure of **20** is depicted in **Figure 3.3**, while the corresponding interatomic distances and angles are listed in **Table 3.2**.

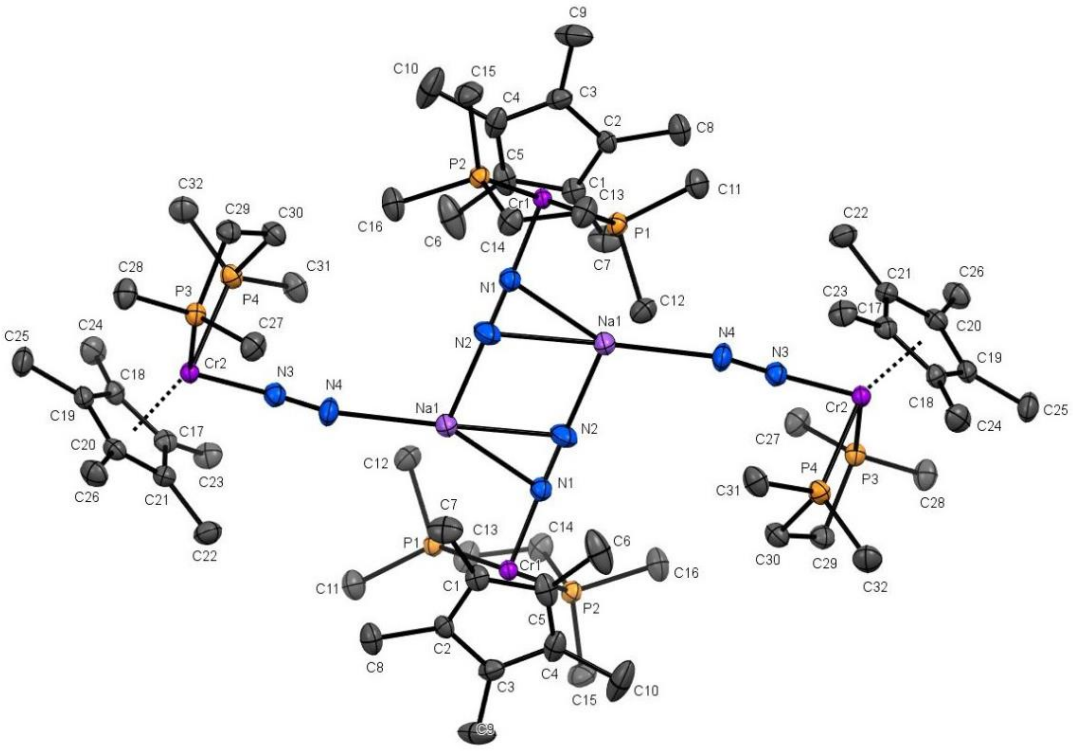

Figure 3.3 Molecular structure of $Na_2[Cp^*dmpeCr(N_2)]_4$ (**20**) represented as 50% probability thermal ellipsoids. Hydrogen atoms have been omitted for clarity.

Table 3.2 Interatomic distances (Å) and angles (º) for $Na_2[Cp^*dmpeCrN_2]_4$ (**20**).

Distances (Å)			
Cr1-P1	2.2647(12)	Na1-N1	2.569(3)
Cr1-P2	2.2537(11)	Na1-N2	2.589(4)
Cr1-Na1	3.3947(17)	Na1-N2	2.320(4)
Cr1-N1	1.777(4)	Na1-N4	2.411(4)
Cr1-C1	2.228(4)	Na1-C7	2.878(6)
Cr1-C2	2.221(4)	Na1-C12	3.068(5)
Cr1-C3	2.211(4)	N1-N2	1.185(5)
Cr1-C4	2.180(4)	N3-N4	1.153(4)
Cr1-C5	2.196(4)	C1-C2	1.419(6)
Cr2-P3	2.3211(11)	C1-C5	1.429(6)
Cr2-P4	2.3256(13)	C1-C7	1.494(6)
Cr2-N3	1.806(3)	C2-C3	1.416(5)
Cr2-C17	2.173(4)	C2-C8	1.503(6)
Cr2-C18	2.213(4)	C3-C4	1.425(7)
Cr2-C19	2.227(4)	C3-C9	1.495(7)
Cr2-C20	2.226(4)	C4-C5	1.411(7)
Cr2-C21	2.197(4)	C4-C10	1.525(6)
P1-C11	1.836(5)	C5-C6	1.484(7)
P1-C12	1.843(5)	C13-C14	1.517(6)
P1-C13	1.865(5)	C17-C18	1.425(5)
P2-C14	1.842(5)	C17-C21	1.427(6)
P2-C15	1.850(5)	C17-C23	1.488(6)
P2-C16	1.839(5)	C18-C19	1.430(6)
P3-C27	1.828(4)	C18-C24	1.488(6)
P3-C28	1.828(4)	C19-C20	1.424(6)
P3-C29	1.846(5)	C19-C25	1.504(6)
P4-C30	1.835(4)	C20-C21	1.407(6)
P4-C31	1.819(5)	C20-C26	1.503(6)
P4-C32	1.820(5)	C21-C22	1.495(6)

Na1-Na1	3.622(3)	C29-C30	1.519(6)

Angles (°)

P2-Cr1-P1	82.09(4)	N2-Na1-N4	103.7(15)
N1-Cr1-P1	92.57(12)	N2-Na1-C71	106.6(17)
N1-Cr1-P2	88.77(11)	N2-N1-Cr1	174.9(4)
N1-Cr1-C1	99.22(16)	N1-N2-Na1	157.8(4)
N1-Cr1-C2	133.9(15)	N4-N3-Cr2	176.9(4)
N1-Cr1-C3	154.5(17)	N3-N4-Na1	166.4(4)
N1-Cr1-C4	119.4(19)	C2-C1-Cr1	71.1(2)
N1-Cr1-C5	91.61(18)	C2-C1-C5	107.6(4)
C1-Cr1-P1	119.9(11)	C2-C1-C7	125.5(4)
C1-Cr1-P2	155.9(12)	C5-C1-Cr1	69.90(2)
C2-Cr1-P1	99.32(11)	C5-C1-C7	126.0(4)
C2-Cr1-P2	136.8(11)	C7-C1-Cr1	132.3(3)
C2-Cr1-C1	37.19(15)	C1-C2-Cr1	71.70(2)
C3-Cr1-P1	111.8(13)	C1-C2-C8	124.6(4)
C3-Cr1-P2	101.8(11)	C3-C2-Cr1	71.00(2)
C3-Cr1-C1	62.45(16)	C3-C2-C1	108.6(4)
C3-Cr1-C2	37.26(15)	C3-C2-C8	125.7(4)
C4-Cr1-P1	147.8(15)	C8-C2-Cr1	132.8(3)
C4-Cr1-P2	93.47(12)	C2-C3-Cr1	71.70(2)
C4-Cr1-C1	62.72(16)	C2-C3-C4	107.4(4)
C4-Cr1-C2	62.70(15)	C2-C3-C9	125.2(4)
C4-Cr1-C3	37.85(18)	C4-C3-Cr1	69.90(2)
C4-Cr1-C5	37.62(19)	C4-C3-C9	126.8(4)
C5-Cr1-P1	157.6(12)	C9-C3-Cr1	130.4(3)
C5-Cr1-P2	120.0(13)	C3-C4-Cr1	72.30(2)
C5-Cr1-C1	37.68(15)	C3-C4-C10	126.4(5)
C5-Cr1-C2	62.71(16)	C5-C4-Cr1	71.80(3)
C5-Cr1-C3	62.99(18)	C5-C4-C3	108.6(4)
P3-Cr2-P4	84.24(4)	C5-C4-C10	124.4(5)

N3-Cr2-P3	88.41(11)	C10-C4-Cr1	128.7(3)
N3-Cr2-P4	84.79(12)	C1-C5-Cr1	72.40(2)
N3-Cr2-C17	98.41(15)	C1-C5-C6	125.9(5)
N3-Cr2-C18	134.5(15)	C4-C5-Cr1	70.60(2)
N3-Cr2-C19	152.3(16)	C4-C5-C1	107.8(4)
N3-Cr2-C20	117.1(16)	C4-C5-C6	126.2(5)
N3-Cr2-C21	90.26(15)	C6-C5-Cr1	125.2(4)
C17-Cr2-P3	165.4(12)	C14-C13-P1	108.1(3)
C17-Cr2-P4	109.1(12)	C13-C14-P2	107.6(3)
C17-Cr2-C18	37.91(15)	C18-C17-Cr2	72.50(2)
C17-Cr2-C19	63.03(15)	C18-C17-C21	107.8(3)
C17-Cr2-C20	63.06(15)	C18-C17-C23	125.4(4)
C17-Cr2-C21	38.11(16)	C21-C17-Cr2	71.80(2)
C18-Cr2-P3	137.1(11)	C21-C17-C23	126.6(4)
C18-Cr2-P4	97.28(12)	C23-C17-Cr2	125.0(3)
C18-Cr2-C19	37.57(15)	C17-C18-Cr2	69.60(2)
C18-Cr2-C20	62.79(16)	C17-C18-C19	107.4(4)
C19-Cr2-P3	105.7(11)	C17-C18-C24	126.0(4)
C19-Cr2-P4	119.7(12)	C19-C18-Cr2	71.80(2)
C20-Cr2-P3	102.4(11)	C19-C18-C24	126.3(4)
C20-Cr2-P4	157.0(12)	C24-C18-Cr2	129.0(3)
C20-Cr2-C19	37.31(15)	C18-C19-Cr2	70.70(2)
C21-Cr2-P3	129.7(12)	C18-C19-C25	125.9(4)
C21-Cr2-P4	145.7(12)	C20-C19-Cr2	71.30(2)
C21-Cr2-C18	63.03(15)	C20-C19-C18	108.2(3)
C21-Cr2-C19	62.33(15)	C20-C19-C25	125.2(4)
C21-Cr2-C20	37.07(15)	C25-C19-Cr2	130.9(3)
C11-P1-Cr1	125.2(18)	C19-C20-Cr2	71.40(2)
C11-P1-C12	99.10(2)	C19-C20-C26	125.4(4)
C11-P1-C13	98.50(2)	C21-C20-Cr2	70.30(2)
C12-P1-Cr1	118.5(16)	C21-C20-C19	107.9(4)
C12-P1-C13	98.20(2)	C21-C20-C26	126.6(4)
C13-P1-Cr1	112.5(15)	C26-C20-Cr2	127.2(3)

C14-P2-Cr1	110.6(14)	C17-C21-Cr2	70.00(2)
C14-P2-C15	99.80(2)	C17-C21-C22	125.5(4)
C15-P2-Cr1	124.0(17)	C20-C21-Cr2	72.60(2)
C16-P2-Cr1	119.5(16)	C20-C21-C17	108.6(4)
C16-P2-C14	99.70(2)	C20-C21-C22	125.9(4)
C16-P2-C15	99.20(2)	C22-C21-Cr2	124.2(3)
C27-P3-Cr2	115.9(15)	C30-C29-P3	110.2(3)
C27-P3-C28	100.8(2)	C29-C30-P4	108.9(3)
C27-P3-C29	102.7(2)	C31-P4-C30	104.0(2)
C28-P3-Cr2	125.3(16)	C31-P4-C32	101.0(2)
C28-P3-C29	100.6(2)	C32-P4-Cr2	126.2(18)
C29-P3-Cr2	108.6(15)	C32-P4-C30	101.6(2)
C30-P4-Cr2	105.6(16)		
C31-P4-Cr2	115.9(18)		

20 crystalizes in the triclinic space group $P\bar{1}$ and there is an inversion center in the middle of the structure. One dinitrogen ligand is coordinated to each chromium center and all four units of the molecule are connected to each other through sodium atoms. The bond distances for N1-N2 and N3-N4 are 1.185(5)Å and 1.153(4)Å, respectively. These bond distances are shorter than the N-N bond distance in the starting complex **10** (1.195 Å).

Upon reduction of a dinitrogen complex, the strength of the π-back donation to the anti-bonding orbitals of dinitrogen can increase, so it is possible to see a decrease in Cr-N and an increase in the N-N bond distances. The former was observed in **20**, and the Cr-N bond distances decreased slightly compared to **10**, but the N-N bond distance did not follow the expected direction. **20** can be described as a mixed valent chromium complex with two Cr(0) and two Cr(I) centers. The effective magnetic moment of **20** was found to be 1.6 (1) μ_B at room temperature. For a system of two non-interacting chromium(I) low spin d^5 ions the expected magnetic moment is 2.4 μ_B. A possible interpretation of the lower moment of **20** is that the bridging N_2 ligands mediate antiferromagnetic coupling between the chromium centers. The ^{1}H-NMR spectrum of **20**

shows a broad range of peaks from +21.8 to −28.4 ppm, which is consistent with the presence of a paramagnetic complex. The proton NMR of this compound shows only one set of resonances which can be due to fluxionality of the tetranuclear compound in the solution. The fast exchange of fragments in the time scale of NMR results in the presence of only one peak for the Cp* ligands, as shown in **Figure 3.4**.

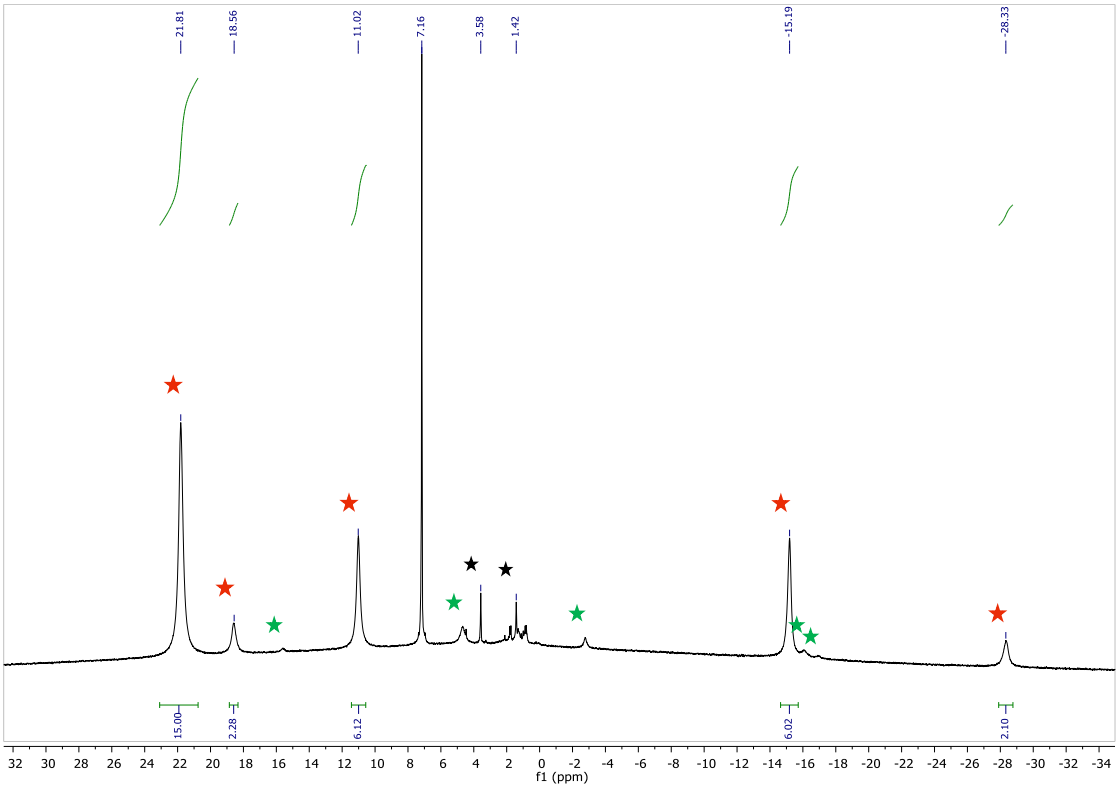

Figure 3.4 ^{1}H-NMR spectrum of $Na_2[Cp^*dmpeCrN_2]_4$ (**20**) recorded in C_6D_6 at 400 MHz. Orange stars show the peaks related to **20**, green stars show the peaks related to the dinitrogen compound **10** impurity in the sample and black stars are related to solvent impurities.

To study the changes that may happen in the bond distance of coordinated dinitrogen ligand, reduction of all the chromium centers to Cr(0) was investigated. To the THF solution of **9** was added 2 equivalents of sodium metal. This addition resulted in a color change from brown to orange after 2 h. The solution was stirred overnight and then it was filtered. To this orange-red solution, 2 equivalents of tetramethylethylenediamine (TMEDA) was added. After 1h of stirring, the solution was filtered, and the solvent was removed under vacuo. The orange-brown residue was then extracted with pentanes and filtered through celite. The solution was concentrated under vacuum and was kept at -30°C overnight, to get the orange-red crystals of the product. The structure of the product was determined using X-ray crystallography to be a mononuclear chromium complex, i.e. [Cp*(dmpe)Cr(μ-N_2)Na(TMEDA)$_2$] (**21**). The molecular structure of **21** is depicted in **Figure 3.5**, while the corresponding interatomic distances and angles are listed in **Table 3.3**.

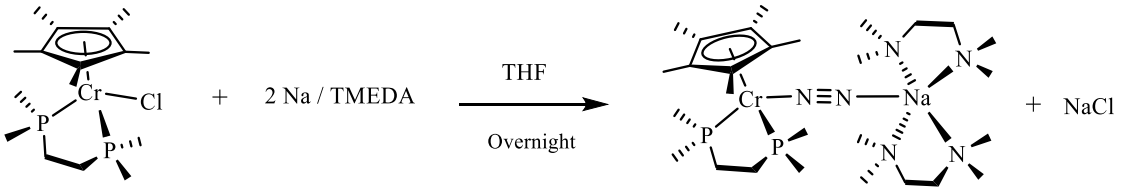

(**9**) (**21**)

Scheme 3.2 Synthesis of [Cp*(dmpe)Cr(μ-N_2)Na(TMEDA)$_2$] (**21**).

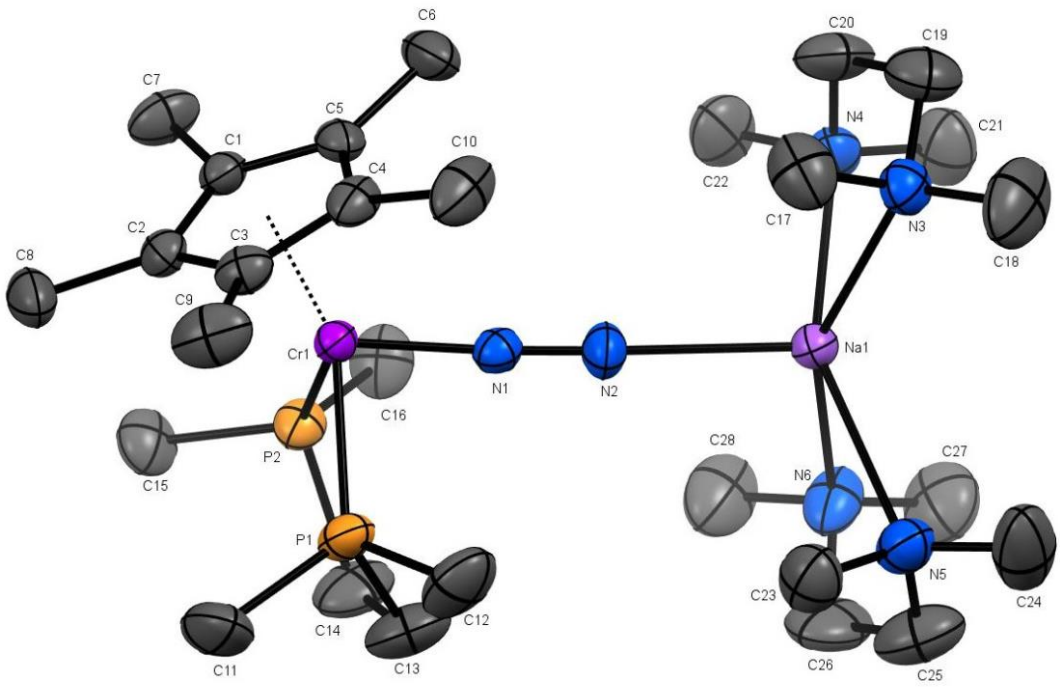

Figure 3.5 Molecular structure of [Cp*(dmpe)Cr(μ-N_2)Na(TMEDA)$_2$] (**21**) represented as 50% probability thermal ellipsoids. Hydrogen atoms have been omitted for clarity.

Table 3.3 Interatomic distances (Å) and angles (º) for [Cp*(dmpe)Cr(μ-N_2)Na(TMEDA)$_2$] (**21**).

Distances (Å)

Cr1-P1	2.2088(10)	N4-C20	1.485(6)
Cr1-P2	2.1993(9)	N4-C21	1.427(6)
Cr1-N1	1.785(3)	N4-C22	1.450(5)
Cr1-C1	2.200(3)	N5-C23	1.411(6)

Cr1-C2	2.216(3)	N5-C24	1.448(7)
Cr1-C3	2.213(3)	N5-C25	1.441(7)
Cr1-C4	2.199(3)	N6-C26	1.564(8)
Cr1-C5	2.193(3)	N6-C27	1.417(7)
P1-C11	1.823(5)	N6-C28	1.426(6)
P1-C12	1.822(5)	C1-C2	1.424(4)
P1-C13	1.854(6)	C1-C5	1.418(4)
P2-C14	1.869(5)	C1-C7	1.498(5)
P2-C15	1.839(4)	C2-C3	1.415(5)
P2-C16	1.853(5)	C2-C8	1.505(5)
Na1-N2	2.324(3)	C3-C4	1.419(5)
Na1-N3	2.573(3)	C3-C9	1.491(5)
Na1-N4	2.477(3)	C4-C5	1.425(5)
Na1-N5	2.571(3)	C4-C10	1.492(5)
Na1-N6	2.582(3)	C5-C6	1.499(5)
N1-N2	1.175(4)	C13-C14	1.458(8)
N3-C17	1.436(6)	C19-C20	1.465(7)
N3-C18	1.427(6)	C25-C26	1.441(9)
N3-C19	1.482(6)		

Angles (°)

P1-Cr1-C2	111.2(9)	C18-N3-C19	106.5(5)
P1-Cr1-C3	96.77(9)	C19-N3-Na1	103.9(2)
P2-Cr1-P1	83.19(4)	C20-N4-Na1	102.0(2)
P2-Cr1-C1	98.67(9)	C21-N4-Na1	113.9(3)
P2-Cr1-C2	108.6(9)	C21-N4-C20	110.7(4)
P2-Cr1-C3	143.2(10)	C21-N4-C22	112.8(4)
N1-Cr1-P1	87.67(9)	C22-N4-Na1	111.0(3)
N1-Cr1-P2	88.21(9)	C22-N4-C20	105.5(4)
N1-Cr1-C1	124.5(12)	C23-N5-Na1	100.3(3)

N1-Cr1-C2	155.7(12)	C23-N5-C24	109.8(4)
N1-Cr1-C3	128.6(13)	C23-N5-C25	113.2(5)
N1-Cr1-C4	95.56(13)	C24-N5-Na1	121.5(3)
N1-Cr1-C5	93.51(12)	C25-N5-Na1	108.1(3)
C1-Cr1-P1	147.8(9)	C25-N5-C24	104.2(5)
C1-Cr1-C2	37.63(12)	C26-N6-Na1	98.50(3)
C1-Cr1-C3	62.76(12)	C27-N6-Na1	120.3(4)
C3-Cr1-C2	37.27(13)	C27-N6-C26	108.2(5)
C4-Cr1-P1	116.5(11)	C27-N6-C28	114.4(5)
C4-Cr1-P2	160.0(10)	C28-N6-Na1	107.1(3)
C4-Cr1-C1	63.10(12)	C28-N6-C26	106.4(5)
C4-Cr1-C2	62.72(13)	C2-C1-Cr1	71.79(17)
C4-Cr1-C3	37.53(14)	C2-C1-C7	125.6(3)
C5-Cr1-P1	154.4(10)	C5-C1-Cr1	70.90(17)
C5-Cr1-P2	122.4(10)	C5-C1-C2	107.9(3)
C5-Cr1-C1	37.66(12)	C5-C1-C7	125.8(3)
C5-Cr1-C2	62.81(12)	C7-C1-Cr1	130.3(2)
C5-Cr1-C3	62.85(13)	C1-C2-Cr1	70.58(16)
C5-Cr1-C4	37.87(14)	C1-C2-C8	125.0(3)
C11-P1-Cr1	125.6(19)	C3-C2-Cr1	71.26(18)
C11-P1-C13	104.1(3)	C3-C2-C1	108.0(3)
C12-P1-Cr1	119.5(2)	C3-C2-C8	126.6(3)
C12-P1-C11	97.00(3)	C8-C2-Cr1	129.4(2)
C12-P1-C13	98.10(3)	C2-C3-Cr1	71.47(17)
C13-P1-Cr1	108.5(17)	C2-C3-C4	108.3(3)
C14-P2-Cr1	110.8(16)	C2-C3-C9	125.3(4)
C15-P2-Cr1	125.7(16)	C4-C3-Cr1	70.71(19)
C15-P2-C14	99.60(2)	C4-C3-C9	126.0(4)
C15-P2-C16	97.40(2)	C9-C3-Cr1	129.7(3)
C16-P2-Cr1	118.9(15)	C3-C4-Cr1	71.76(18)
C16-P2-C14	100.3(3)	C3-C4-C5	107.7(3)
N2-Na1-N3	104.6(11)	C3-C4-C10	126.0(4)
N2-Na1-N4	102.2(12)	C5-C4-Cr1	70.82(18)

N2-Na1-N5	105.9(12)	C5-C4-C10	126.3(4)
N2-Na1-N6	102.9(12)	C10-C4-Cr1	124.1(3)
N3-Na1-N6	152.5(12)	C1-C5-Cr1	71.44(17)
N4-Na1-N3	75.52(11)	C1-C5-C4	108.1(3)
N4-Na1-N5	151.8(12)	C1-C5-C6	124.8(3)
N4-Na1-N6	97.66(14)	C4-C5-Cr1	71.31(18)
N5-Na1-N3	99.70(12)	C4-C5-C6	127.1(3)
N5-Na1-N6	73.59(13)	C6-C5-Cr1	123.9(2)
N2-N1-Cr1	177.0(3)	C14-C13-P1	110.0(3)
N1-N2-Na1	178.1(3)	C13-C14-P2	113.3(3)
C17-N3-Na1	100.4(3)	C20-C19-N3	115.8(4)
C17-N3-C19	110.5(4)	C19-C20-N4	116.2(4)
C18-N3-Na1	125.2(3)	N5-C25-C26	114.7(5)
C18-N3-C17	109.8(4)	C25-C26-N6	115.5(5)

21 crystalizes in the monoclinic space group $P2_1/c$. The geometry around the Cr1 is pseudo-octahedral and the Cr-N bond distance is 1.785(3)Å, which is in the range of Cr-N double bond distances.[66] Similar to **20**, the N-N bond distance in **21** (1.175(4) Å) is shorter than in neutral dinitrogen complex **10**. The IR spectrum taken in the solid state showed a peak at 1942 cm^{-1}, which is in the range of N≡N triple bond stretching frequencies. This frequency is lower compared to free dinitrogen IR frequency of 2331 cm^{-1}.[80,101] The magnetic moment of the complex was found to be 0.8 (1) μ_B when measured at room temperature, which is not expected for a diamagnetic, 18 electron Cr(0) complex (S=0). A possible explanation for the measured magnetic moment of **21**, is the presence of solid paramagnetic impurities like **10** in the sample. As shown in **Figure 3.6**, the proton NMR of **21** shows peaks in the diamagnetic region, between 1.1 to 2.3 ppm, consistent with the diamagnetic properties of the complex.

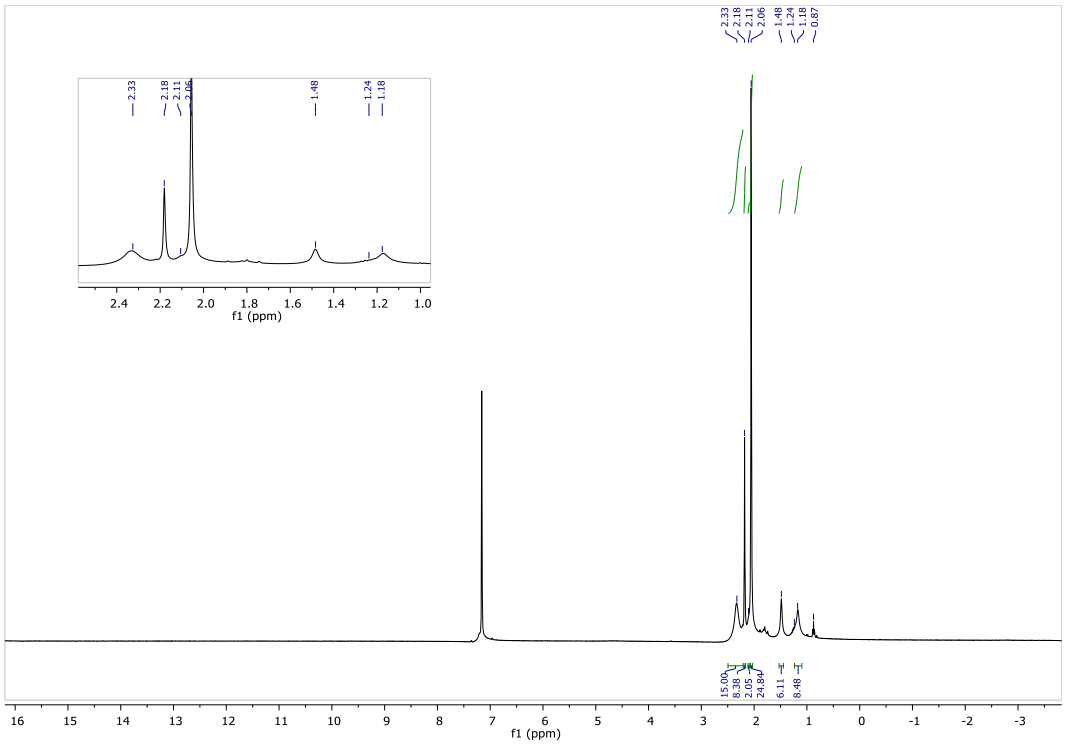

Figure 3.6 ^{1}H-NMR spectrum of [Cp*(dmpe)Cr(μ-N_2)Na(TMEDA)$_2$] (**21**) recorded in C_6D_6 at 400 MHz.

In an effort to study the possibility of functionalization of the dinitrogen ligand, the reaction of **21** with trimethylsilyl chloride (TMSCl) was explored. To a THF solution of **21**, 1 equivalent of TMSCl was added. The color of solution changed from orange to brown in 2 hours. The solution was stirred for an additional hour before filtration. After the removal of solvent, the brown solid was extracted with pentanes. The solution was stored at -30°C to yield brown crystals of the product. Determination of the structure by X-ray crystallography revealed it to be a chromium silyldiazenido complex, i.e. [Cp*(dmpe)Cr(N_2SiMe_3)] (**22**). The molecular structure of **22** is depicted in **Figure 3.7** while the corresponding interatomic distances and angles are listed in **Table 3.4**.

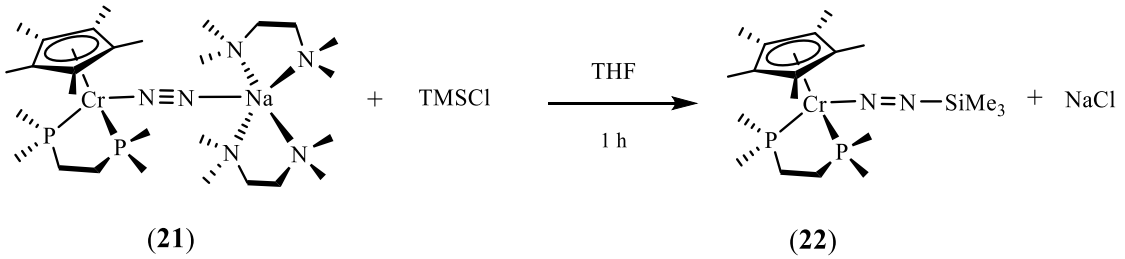

(**21**) (**22**)

Scheme 3.3 Synthesis of [Cp*(dmpe)Cr(μ-N_2)$SiMe_3$] (**22**).

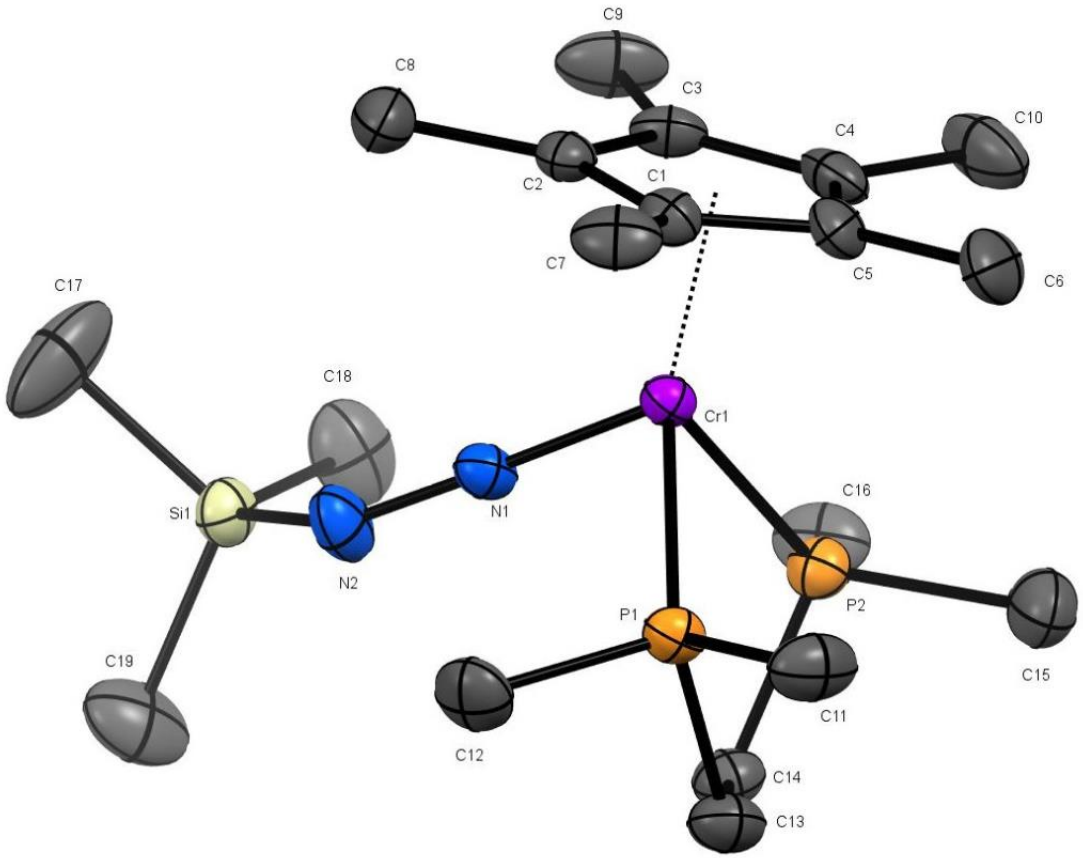

Figure 3.7 Molecular structure of [Cp*(dmpe)Cr(N_2SiMe_3)] (**22**) represented as 50% probability thermal ellipsoids. Hydrogen atoms have been omitted for clarity.

Table 3.4 Interatomic distances (Å) and angles (º) for [Cp*(dmpe)Cr(μ-N_2)$SiMe_3$] (**22**).

Distances (Å)

Cr1-P1	2.2689(14)	Si1-C17	1.824(8)
Cr1-P2	2.2667(15)	Si1-C18	1.865(8)
Cr1-N1	1.684(4)	Si1-C19	1.848(8)
Cr1-C1	2.189(5)	N1-N2	1.257(6)
Cr1-C2	2.193(5)	C1-C2	1.417(7)
Cr1-C3	2.221(5)	C1-C5	1.430(7)
Cr1-C4	2.238(5)	C1-C7	1.503(7)
Cr1-C5	2.231(5)	C2-C3	1.438(7)
P1-C11	1.840(6)	C2-C8	1.485(7)
P1-C12	1.809(6)	C3-C4	1.416(8)
P1-C13	1.855(6)	C3-C9	1.495(8)
P2-C14	1.831(6)	C4-C5	1.416(8)
P2-C15	1.833(7)	C4-C10	1.511(8)
P2-C16	1.822(6)	C5-C6	1.503(8)
Si1-N2	1.719(5)	C13-C14	1.523(8)

Angles (°)

P2-Cr1-P1	81.45(5)	N2-Si1-C17	108.0(3)
N1-Cr1-P1	87.32(14)	N2-Si1-C18	114.0(3)
N1-Cr1-P2	91.92(16)	N2-Si1-C19	107.1(3)
N1-Cr1-C1	120.5(2)	C17-Si1-C18	109.3(5)
N1-Cr1-C2	94.32(19)	C17-Si1-C19	110.0(5)
N1-Cr1-C3	103.2(2)	C19-Si1-C18	108.3(4)
N1-Cr1-C4	138.0(2)	N2-N1-Cr1	172.1(4)
N1-Cr1-C5	156.6(2)	N1-N2-Si1	132.5(4)
C1-Cr1-P1	97.32(14)	C2-C1-Cr1	71.30(3)
C1-Cr1-P2	147.59(14)	C2-C1-C5	108.1(4)

C1-Cr1-C2	37.73(18)	C2-C1-C7	124.8(5)
C1-Cr1-C3	63.08(19)	C5-C1-Cr1	72.70(3)
C1-Cr1-C4	62.50(19)	C5-C1-C7	126.3(5)
C1-Cr1-C5	37.74(19)	C7-C1-Cr1	129.4(4)
C2-Cr1-P1	125.87(14)	C1-C2-Cr1	71.00(3)
C2-Cr1-P2	152.18(14)	C1-C2-C3	107.9(4)
C2-Cr1-C3	38.01(19)	C1-C2-C8	126.2(5)
C2-Cr1-C4	62.55(19)	C3-C2-Cr1	72.10(3)
C2-Cr1-C5	62.81(19)	C3-C2-C8	125.9(5)
C3-Cr1-P1	160.37(15)	C8-C2-Cr1	123.8(4)
C3-Cr1-P2	114.21(15)	C2-C3-Cr1	69.90(3)
C3-Cr1-C4	37.00(2)	C2-C3-C9	126.3(6)
C3-Cr1-C5	62.30(2)	C4-C3-Cr1	72.20(3)
C4-Cr1-P1	134.68(17)	C4-C3-C2	107.5(4)
C4-Cr1-P2	95.39(15)	C4-C3-C9	126.2(6)
C5-Cr1-P1	102.02(15)	C9-C3-Cr1	125.1(4)
C5-Cr1-P2	110.50(15)	C3-C4-Cr1	70.80(3)
C5-Cr1-C4	36.90(2)	C3-C4-C10	124.5(6)
C11-P1-Cr1	125.0(2)	C5-C4-Cr1	71.20(3)
C11-P1-C13	100.3(3)	C5-C4-C3	108.9(5)
C12-P1-Cr1	115.0(2)	C5-C4-C10	126.2(6)
C12-P1-C11	100.2(3)	C10-C4-Cr1	129.7(4)
C12-P1-C13	101.9(3)	C1-C5-Cr1	69.60(3)
C13-P1-Cr1	111.2(18)	C1-C5-C6	126.0(6)
C14-P2-Cr1	105.6(19)	C4-C5-Cr1	71.80(3)
C14-P2-C15	102.0(3)	C4-C5-C1	107.7(5)
C15-P2-Cr1	121.3(3)	C4-C5-C6	125.9(6)
C16-P2-Cr1	122.7(2)	C6-C5-Cr1	129.9(4)
C16-P2-C14	102.4(3)	C14-C13-P1	109.9(4)
C16-P2-C15	99.70(4)	C13-C14-P2	108.4(4)

22 crystalizes in the monoclinic space group $P2_1/c$. The N1-N2 bond length is 1.257(6) Å, which is slightly larger than the N-N bond distance in **21** and the neutral dinitrogen complex. The Cr1-N1 bond distance of 1.684(4) Å, falls into the range of Cr-N double bond distances.[66,81]

In 2019, Xi et.al. reported a chromium dinitrogen complex (**A**) that reacts with 1 equivalent of $SiMe_3Cl$ at -73°C, and double silylation of the dinitrogen ligand on one of the N atoms happens, as shown in **Scheme 3.4** [78]. In this complex (**B**) the Cr− N distance is 1.680 Å, indicating a double bond character and the N−N distance is 1.372 Å, which is longer compared to **22**, due to the coordination of two $SiMe_3$ groups to the dinitrogen.

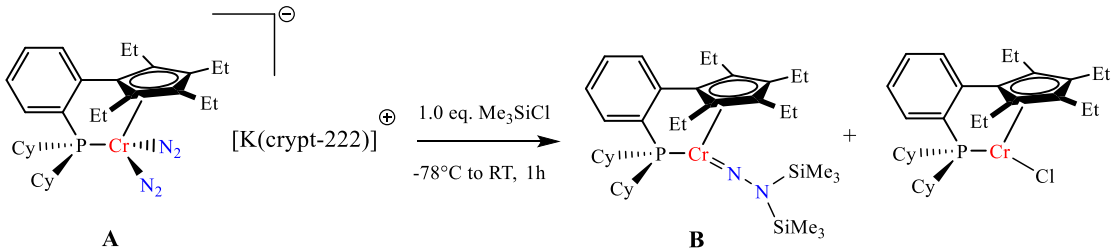

Scheme 3.4 Synthesis of compound **B** from the reaction of **A** with Me_3SiCl reagent. [78]

22 is a 16 electron complex. The proton NMR of **22** shows sharp peaks in the diamagnetic region, consistent with a Cr(II) low spin d^4 ion. Examples of diamagnetic Cr(II) complexes are known.[102] The reaction of this compound with an excess of TMSCl, did not result in any additional functionalization of the dinitrogen, even at high temperature or prolonged period of time.

Crown ethers are common reagents for sequestering of different metal ions and making stable adducts with those ions. A variety of crown ethers, with different cavity sizes, exist that can be selectively used to trap a specific ion based on size. 15-crown-5 reagent is mainly used to trap Na ions. In the reduction reaction of **10**, it was attempted to use 15-crown-5 to separate the sodium ion from the complex by making Na-crown ether adduct.

The reduction of **9** was repeated in THF under nitrogen. 2 equivalents of sodium metal were added to the solution of **9**. This addition resulted in a color change from brown to orange after 2 h. The solution was stirred overnight and then it was filtered. To this orange-red solution, 2 equivalents of 15-crown-5 were added. After 1h of stirring, the solution was filtered, and the solvent was removed under vacuum. The orange powder was washed with pentanes to remove side products. The powder was dissolved in Et_2O and was kept at -30°C for 2days to obtain dark orange crystals of the product. The structure of the product was determined using X-ray crystallography to be a mononuclear chromium complex, i.e. [Cp*(dmpe)Cr(μ-N_2)Na(15-crown-5)] (**23**). The molecular structure of **23** is depicted in **Figure 3.8**, while the corresponding interatomic distances and angles are listed in **Table 3.5**.

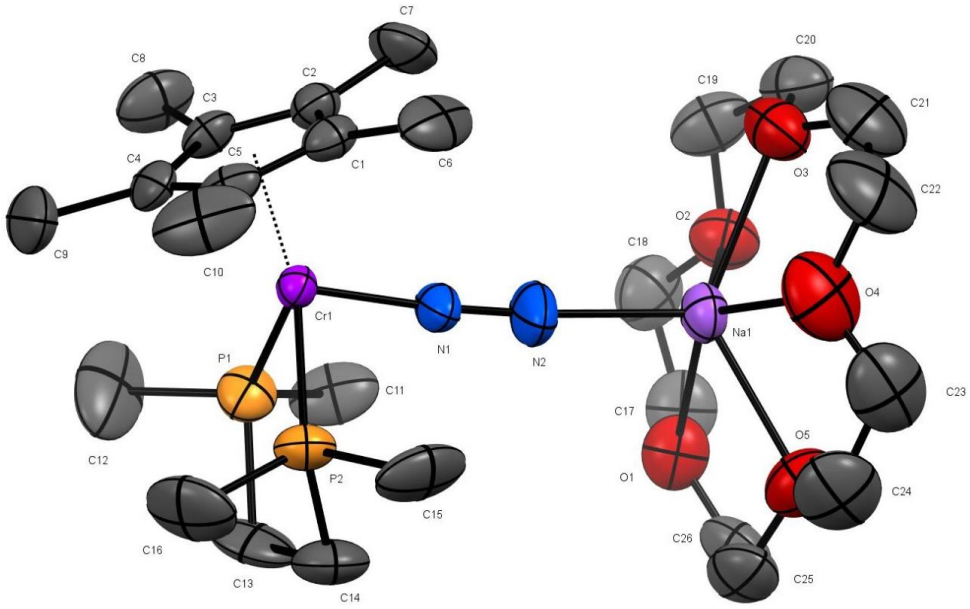

Figure 3.8 Molecular structure of [Cp*(dmpe)Cr(μ-N_2)Na(15-crown-5)] (**23**) represented as 50% probability thermal ellipsoids. Hydrogen atoms have been omitted for clarity.

Table 3.5 Interatomic distances (Å) and angles (º) for [Cp*(dmpe)Cr(μ-N_2)Na(15-crown-5)] (**23**).

Distances (Å)

Cr1-P1	2.206(2)	C2-C3	1.392(11)
Cr1-P2	2.209(2)	C2-C7	1.526(11)
Cr1-N1	1.755(6)	C3-C4	1.438(11)
Cr1-C1	2.185(8)	C3-C8	1.489(11)
Cr1-C2	2.185(8)	C4-C5	1.420(11)
Cr1-C3	2.189(7)	C4-C9	1.511(12)
Cr1-C4	2.186(7)	C5-C10	1.519(11)
Cr1-C5	2.186(7)	C13-C14	1.487(15)
P1-C11	1.834(10)	O1-C17	1.401(12)
P1-C12	1.847(12)	O1-C26	1.365(13)
P1-C13	1.843(11)	O2-C18	1.397(15)
P2-C14	1.865(10)	O2-C19	1.398(12)
P2-C15	1.826(10)	O3-C20	1.400(13)
P2-C16	1.834(11)	O3-C21	1.377(13)
Na1-N2	2.222(8)	O4-C22	1.401(14)
Na1-O1	2.473(9)	O4-C23	1.362(14)
Na1-O2	2.414(9)	O5-C24	1.374(14)
Na1-O3	2.378(9)	O5-C25	1.390(12)
Na1-O4	2.365(10)	C17-C18	1.449(17)
Na1-O5	2.384(10)	C19-C20	1.483(17)
N1-N2	1.173(9)	C21-C22	1.403(18)
C1-C2	1.380(11)	C23-C24	1.438(18)
C1-C5	1.411(11)	C25-C26	1.469(16)
C1-C6	1.519(11)		

Angles (°)

P1-Cr1-P2	82.98(10)	C2-C1-Cr1	71.6(5)
N1-Cr1-P1	90.7(2)	C2-C1-C5	108.5(7)
N1-Cr1-P2	86.7(2)	C2-C1-C6	125.7(9)
N1-Cr1-C1	93.5(3)	C5-C1-Cr1	71.2(5)
N1-Cr1-C2	91.5(3)	C5-C1-C6	125.8(9)
N1-Cr1-C3	121.9(3)	C6-C1-Cr1	122.7(5)
N1-Cr1-C4	153.8(3)	C1-C2-Cr1	71.6(5)
N1-Cr1-C5	126.8(4)	C1-C2-C3	109.7(7)
C1-Cr1-P1	160.5(2)	C1-C2-C7	125.2(8)
C1-Cr1-P2	116.3(2)	C3-C2-Cr1	71.6(4)
C1-Cr1-C2	36.8(3)	C3-C2-C7	125.2(8)
C1-Cr1-C3	62.4(3)	C7-C2-Cr1	124.1(6)
C1-Cr1-C4	63.1(3)	C2-C3-Cr1	71.3(4)
C1-Cr1-C5	37.7(3)	C2-C3-C4	107.3(7)
C2-Cr1-P1	124.1(2)	C2-C3-C8	126.6(9)
C2-Cr1-P2	152.9(2)	C4-C3-Cr1	70.7(4)
C2-Cr1-C3	37.1(3)	C4-C3-C8	125.4(9)
C2-Cr1-C5	62.4(3)	C8-C3-Cr1	130.6(6)
C3-Cr1-P1	99.4(2)	C3-C4-Cr1	70.9(4)
C3-Cr1-P2	151.1(2)	C3-C4-C9	125.3(9)
C4-Cr1-P1	107.8(3)	C5-C4-Cr1	71.1(4)
C4-Cr1-P2	113.3(2)	C5-C4-C3	106.9(7)
C4-Cr1-C2	62.9(3)	C5-C4-C9	127.5(9)
C4-Cr1-C3	38.4(3)	C9-C4-Cr1	127.9(6)
C4-Cr1-C5	37.9(3)	C1-C5-Cr1	71.1(4)
C5-Cr1-P1	142.6(3)	C1-C5-C4	107.6(7)
C5-Cr1-P2	97.5(2)	C1-C5-C10	125.9(10)
C5-Cr1-C3	63.3(3)	C4-C5-Cr1	71.0(4)
C11-P1-Cr1	118.4(4)	C4-C5-C10	126.0(10)
C11-P1-C12	98.4(7)	C10-C5-Cr1	129.8(6)
C11-P1-C13	98.9(5)	C14-C13-P1	109.9(6)

C12-P1-Cr1	124.9(4)	C13-C14-P2	106.8(7)
C13-P1-Cr1	112.8(4)	C17-O1-Na1	114.0(8)
C13-P1-C12	98.90(7)	C26-O1-Na1	112.5(8)
C14-P2-Cr1	109.4(4)	C26-O1-C17	115.4(10)
C15-P2-Cr1	119.0(4)	C18-O2-Na1	109.0(9)
C15-P2-C14	99.50(6)	C18-O2-C19	114.7(11)
C15-P2-C16	99.0(7)	C19-O2-Na1	107.5(8)
C16-P2-Cr1	125.3(4)	C20-O3-Na1	112.8(8)
C16-P2-C14	100.5(6)	C21-O3-Na1	112.4(9)
N2-Na1-O1	98.50(4)	C21-O3-C20	114.2(11)
N2-Na1-O2	116.9(4)	C22-O4-Na1	114.5(10)
N2-Na1-O3	109.5(4)	C23-O4-Na1	113.9(9)
N2-Na1-O4	103.7(5)	C23-O4-C22	116.9(14)
N2-Na1-O5	112.9(4)	C24-O5-Na1	110.8(9)
O2-Na1-O1	66.20(3)	C24-O5-C25	117.1(12)
O3-Na1-O1	134.8(4)	C25-O5-Na1	111.1(9)
O3-Na1-O2	69.60(4)	O1-C17-C18	110.2(11)
O3-Na1-O5	127.4(4)	O2-C18-C17	105.6(13)
O4-Na1-O1	135.8(4)	O2-C19-C20	105.8(11)
O4-Na1-O2	130.6(4)	O3-C20-C19	110.6(11)
O4-Na1-O3	71.20(4)	O3-C21-C22	118.3(13)
O4-Na1-O5	69.90(4)	O4-C22-C21	116.9(13)
O5-Na1-O1	66.40(4)	O4-C23-C24	114.0(14)
O5-Na1-O2	114.1(4)	O5-C24-C23	111.4(13)
N2-N1-Cr1	174.9(7)	O5-C25-C26	103.1(11)
N1-N2-Na1	167.0(10)	O1-C26-C25	110.9(11)

23 crystalizes in the tetragonal space group $P4_12_12$. The structure of this complex is very similar to **21**. The sodium ion occupies the cavity of 15-crown-5 from one side and on the other side coordinates to the dinitrogen ligand. The dinitrogen bond length of 1.173(9) Å is in the range of dinitrogen triple bond distances and is shorter than the N≡N

bond distance in the neutral dinitrogen complex **10**. The IR spectrum taken in the solid state showed two distinct stretches at 1796 and 1879 cm^{-1}, which are in the range of N≡N triple bond stretching frequencies.[80,101,103] The magnetic moment of this 18 electron complex, was found to be 0.4 (1) μ_B when measured at room temperature, which can be caused by the presence of paramagnetic impurities of dinitrogen complex **10** in the sample.

Based on the result from the reduction reactions, it was concluded that addition of electrons to this system is not helping with the activation of the bridging dinitrogen ligand. There are many examples of reaction of dinitrogen complexes with Lewis acids (LA) in the literature.[104] The transition metal center upon complexation of the Lewis acid in terms of d ⇀ π*electron back donation, can be studied.[105–107] Therefore the reaction of **10** toward Lewis acids such as $B(C_6F_5)_3$ and Me_3Si^+ was studied.

2 equivalents of $B(C_6F_5)_3$ were added slowly to a Et_2O solution of **10**. The color of the solution changed from green-brown to maroon by the end of the addition. After about 1h of stirring, the solution was filtered to remove insoluble impurities. The solvent was removed under vacuum and the remaining powder was washed with pentanes. The maroon residue redissolved in a minimum amount of diethyl ether and was cooled to -30°C for overnight to yield maroon crystals. Determination of the structure by X-ray crystallography revealed it to be a dinuclear chromium complex with bridging dinitrogen ligand, i.e., $[(Cp^*(dmpe)Cr)_2(\mu\text{-}N_2)](FB(C_6F_5)_3)$ (**24**). The molecular structure of **24** is depicted in **Figure 3.9** while the corresponding interatomic distances and bond angles are listed in **Table 3.6**.

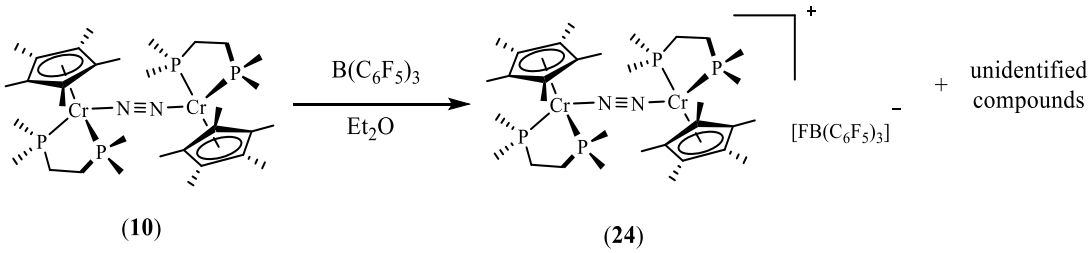

Scheme 3.5 Synthesis of $[(Cp^*(dmpe)Cr)_2(\mu\text{-}N_2)](FB(C_6F_5)_3)]$ (**24**).

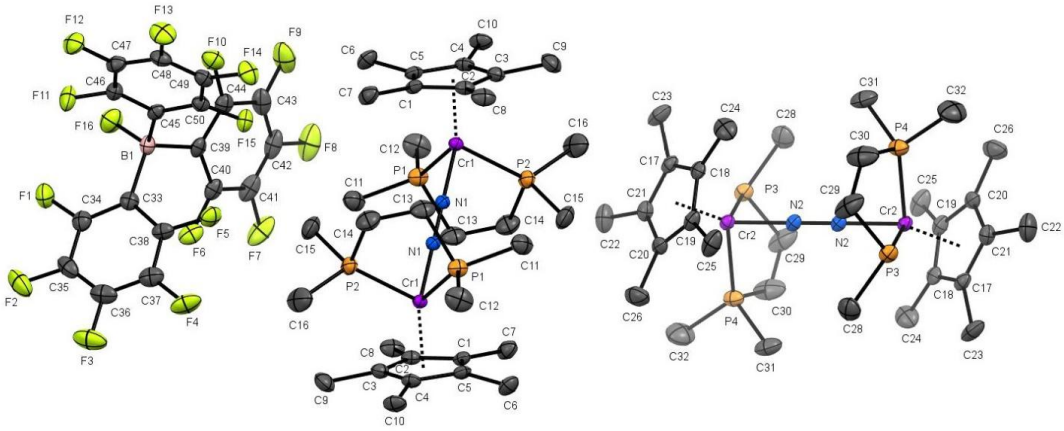

Figure 3.9 Molecular structure of $[(Cp^*(dmpe)Cr)_2(\mu\text{-}N_2)](FB(C_6F_5)_3)$ (**24**) represented as 50% probability thermal ellipsoids. Hydrogen atoms have been omitted for clarity. The asymmetric unit contains two chemically equivalent molecules and one of the counterions is not shown here.

Table 3.6 Interatomic distances (Å) and angles (º) for the N_2-containing cation of $[(Cp^*(dmpe)Cr)_2(\mu\text{-}N_2)](FB(C_6F_5)_3)$ (**24**).

Distances (Å)

Cr1-P1	2.2993(12)	P4-C31	1.806(5)
Cr1-P2	2.3217(11)	P4-C32	1.831(6)
Cr1-N1	1.784(3)	N1-N1	1.220(5)
Cr1-C1	2.248(3)	N2-N2	1.209(5)
Cr1-C2	2.244(3)	C1-C2	1.422(5)
Cr1-C3	2.209(4)	C1-C5	1.411(5)
Cr1-C4	2.196(4)	C1-C7	1.504(5)
Cr1-C5	2.201(3)	C2-C3	1.412(5)
Cr2-P3	2.3074(12)	C2-C8	1.508(5)
Cr2-P4	2.3042(12)	C3-C4	1.437(6)
Cr2-N2	1.797(3)	C3-C9	1.508(6)
Cr2-C17	2.206(3)	C4-C5	1.439(5)
Cr2-C18	2.235(3)	C4-C10	1.479(5)
Cr2-C19	2.239(3)	C5-C6	1.509(5)
Cr2-C20	2.219(3)	C13-C14	1.481(7)
Cr2-C21	2.206(4)	C17-C18	1.413(5)
P1-C11	1.824(5)	C17-C21	1.428(6)
P1-C12	1.827(5)	C17-C23	1.498(5)
P1-C13	1.857(4)	C18-C19	1.423(5)
P2-C14	1.852(5)	C18-C24	1.485(6)
P2-C15	1.820(5)	C19-C20	1.404(6)
P2-C16	1.827(5)	C19-C25	1.501(6)
P3-C27	1.816(5)	C20-C21	1.436(6)
P3-C28	1.807(5)	C20-C26	1.493(6)
P3-C29	1.821(5)	C21-C22	1.500(6)
P4-C30	1.843(5)	C29-C30	1.393(7)

Angles (°)

P1-Cr1-P2	81.79(4)	C29-P3-Cr2	105.80(17)
N1-Cr1-P1	87.55(9)	C30-P4-Cr2	109.17(18)
N1-Cr1-P2	90.26(8)	C31-P4-Cr2	115.74(17)
N1-Cr1-C1	103.57(12)	C31-P4-C30	103.8(3)
N1-Cr1-C2	104.74(13)	C31-P4-C32	101.2(3)
N1-Cr1-C3	134.41(14)	C32-P4-Cr2	124.6(2)
N1-Cr1-C4	166.10(13)	C32-P4-C30	99.5(3)
N1-Cr1-C5	132.01(13)	N1-N1-Cr1	175.2(3)
C1-Cr1-P1	118.81(11)	N2-N2-Cr2	176.9(3)
C1-Cr1-P2	155.15(11)	C2-C1-Cr1	71.41(19)
C2-Cr1-P1	154.34(10)	C2-C1-C7	125.4(3)
C2-Cr1-P2	119.86(10)	C5-C1-Cr1	69.70(19)
C2-Cr1-C1	36.92(14)	C5-C1-C2	107.8(3)
C3-Cr1-P1	137.95(11)	C5-C1-C7	126.6(4)
C3-Cr1-P2	93.44(10)	C7-C1-Cr1	127.7(3)
C3-Cr1-C1	62.12(14)	C1-C2-Cr1	71.7(2)
C3-Cr1-C2	36.97(14)	C1-C2-C8	127.1(3)
C4-Cr1-P1	101.68(11)	C3-C2-Cr1	70.2(2)
C4-Cr1-P2	101.25(10)	C3-C2-C1	108.5(3)
C4-Cr1-C1	62.92(13)	C3-C2-C8	124.3(4)
C4-Cr1-C2	62.78(13)	C8-C2-Cr1	127.6(3)
C4-Cr1-C3	38.08(14)	C2-C3-Cr1	72.9(2)
C4-Cr1-C5	38.21(14)	C2-C3-C4	108.5(3)
C5-Cr1-P1	92.96(10)	C2-C3-C9	124.1(4)
C5-Cr1-P2	137.33(11)	C4-C3-Cr1	70.5(2)
C5-Cr1-C1	36.97(13)	C4-C3-C9	126.5(4)
C5-Cr1-C2	61.99(14)	C9-C3-Cr1	131.0(3)
C5-Cr1-C3	62.90(14)	C3-C4-Cr1	71.5(2)
P4-Cr2-P3	81.56(4)	C3-C4-C5	106.3(3)
N2-Cr2-P3	89.24(9)	C3-C4-C10	126.2(4)
N2-Cr2-P4	90.39(10)	C5-C4-Cr1	71.09(19)

N2-Cr2-C17	130.95(14)	C5-C4-C10	126.6(4)
N2-Cr2-C18	102.40(13)	C10-C4-Cr1	130.6(3)
N2-Cr2-C19	104.10(14)	C1-C5-Cr1	73.33(19)
N2-Cr2-C20	134.21(14)	C1-C5-C4	108.9(3)
N2-Cr2-C21	164.58(14)	C1-C5-C6	124.7(3)
C17-Cr2-P3	93.26(10)	C4-C5-Cr1	70.70(19)
C17-Cr2-P4	138.43(12)	C4-C5-C6	125.4(3)
C17-Cr2-C18	37.11(14)	C6-C5-Cr1	130.8(3)
C17-Cr2-C19	62.18(13)	C14-C13-P1	109.4(3)
C17-Cr2-C20	62.75(14)	C13-C14-P2	111.6(3)
C17-Cr2-C21	37.78(15)	C18-C17-Cr2	72.6(2)
C18-Cr2-P3	120.14(11)	C18-C17-C21	108.3(3)
C18-Cr2-P4	154.44(11)	C18-C17-C23	124.9(4)
C18-Cr2-C19	37.10(14)	C21-C17-Cr2	71.1(2)
C19-Cr2-P3	155.20(10)	C21-C17-C23	125.8(4)
C19-Cr2-P4	118.50(11)	C23-C17-Cr2	130.8(3)
C20-Cr2-P3	136.44(12)	C17-C18-Cr2	70.3(2)
C20-Cr2-P4	93.23(11)	C17-C18-C19	108.0(3)
C20-Cr2-C18	61.99(14)	C17-C18-C24	125.0(4)
C20-Cr2-C19	36.73(15)	C19-C18-Cr2	71.6(2)
C21-Cr2-P3	100.89(11)	C19-C18-C24	126.7(4)
C21-Cr2-P4	102.49(11)	C24-C18-Cr2	128.1(3)
C21-Cr2-C18	62.47(14)	C18-C19-Cr2	71.31(19)
C21-Cr2-C19	62.36(15)	C18-C19-C25	127.2(4)
C21-Cr2-C20	37.87(14)	C20-C19-Cr2	70.9(2)
C11-P1-Cr1	118.26(16)	C20-C19-C18	108.4(3)
C11-P1-C12	102.4(2)	C20-C19-C25	124.1(4)
C11-P1-C13	101.2(2)	C25-C19-Cr2	127.8(3)
C12-P1-Cr1	124.05(18)	C19-C20-Cr2	72.4(2)
C12-P1-C13	102.5(2)	C19-C20-C21	108.2(3)
C13-P1-Cr1	105.07(15)	C19-C20-C26	124.2(4)
C14-P2-Cr1	109.94(16)	C21-C20-Cr2	70.6(2)
C15-P2-Cr1	114.74(17)	C21-C20-C26	126.5(4)

C15-P2-C14	103.3(2)	C26-C20-Cr2	131.9(3)
C15-P2-C16	100.2(3)	C17-C21-Cr2	71.1(2)
C16-P2-Cr1	126.03(18)	C17-C21-C20	107.1(3)
C16-P2-C14	99.6(3)	C17-C21-C22	125.2(4)
C27-P3-Cr2	124.98(17)	C20-C21-Cr2	71.5(2)
C27-P3-C29	103.6(3)	C20-C21-C22	126.7(4)
C28-P3-Cr2	117.42(17)	C22-C21-Cr2	131.6(3)
C28-P3-C27	100.4(3)	C30-C29-P3	115.3(4)
C28-P3-C29	101.7(3)	C29-C30-P4	114.5(3)

The adducts between the dinitrogen complex and the strong Lewis acid i.e., $B(C_6F_5)_3$ was not observed, but instead this reaction resulted in oxidation of the starting dinitrogen complex. There are similar examples in the literature, that instead of N_2-LA adduct the oxidation of dinitrogen complex happens.[108,109] Decomposition of the reduced Lewis acid causes the transfer of one fluoride anion from the decomposed LA to the $B(C_6F_5)_3$ and makes a counterion in the final product. The fluoride abstraction of $B(C_6F_5)_3$ from different reagents to make the $FB(C_6F_5)_3$ ion have been reported previously. [110] In the synthesis of **24,** the fluoride abstraction is happening from the decomposed $B(C_6F_5)_3$, which makes it the first example of this type of reactions. **24** crystalizes in the triclinic space group $P\bar{1}$. The N-N bond distances in this dinuclear dinitrogen complex are 1.220(5) and 1.209(5) Å, which unexpectedly is longer than the N-N bond length in the neutral dinitrogen complex. **24** is a mixed-valent complex with the oxidation state of I and II of the chromium centers. The ^{1}H-NMR spectrum of **24** is consistent with the presence of a paramagnetic chromium complex. The appearance of the peaks is similar to the neutral dinitrogen complex, but the chemical shifts are different as shown in **Figure 3.10**.

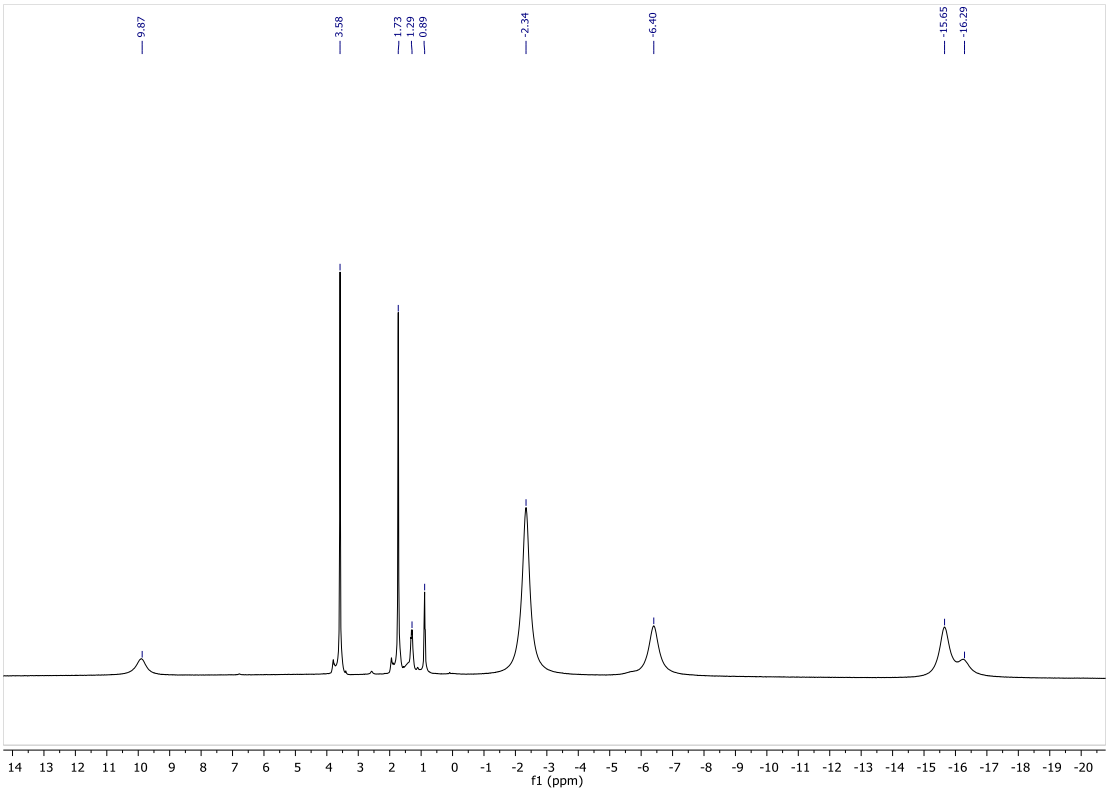

Figure 3.10 ^{1}H-NMR spectrum of [(Cp*(dmpe)Cr)$_2$(μ-N$_2$)](FB(C$_6$F$_5$)$_3$) (**24**) recorded in THF-d$_8$ at 400 MHz. Peaks at 0.9 and 1.3 ppm are related to pentane solvent.

Reactivity of dinitrogen complex **10** with stronger Lewis acid, Me_3Si^+ was also studied. 1 equivalent of Me_3SiCl (TMSCl) and 1 equivalent of Sodium Tetrakis[(3,5-trifluoromethyl)phenyl]borate ($NaBAr^F_4$) were mixed in diethyl ether.[111] After 30 minutes of stirring the solution ($TMSBAr^F_{4)}$ was filtered to remove the NaCl and was added slowly to the Et_2O solution of **10**. The color of the solution changed from green-brown to maroon by the end of the addition. After about 1h of stirring, the solution was filtered to remove the impurities. The solvent was removed under vacuum and the remaining powder was washed with pentanes. The maroon residue redissolved in minimum amount of diethyl ether and was cooled to -30°C overnight to yield maroon crystals. Determination of the structure by X-ray crystallography revealed it to be a dinuclear chromium complex with a bridging dinitrogen ligand i.e., [(Cp*(dmpe)Cr)$_2$(μ-N$_2$)]BAr^F_4 (**25**). The molecular structure of **25** is depicted in **Figure 3.11** while the

corresponding interatomic distances and bond angles are listed in **Table 3.7**. The cation in this structure is the same as **24**. Si_2Me_6 is expected to be a side product in this reaction but there is no experimental evidence for its formation.

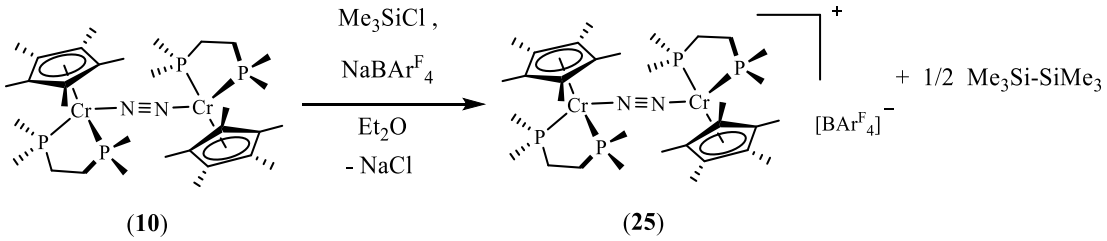

(**10**) (**25**)

Scheme 3.6 Synthesis of $[(Cp^*(dmpe)Cr)_2(\mu\text{-}N_2)]BAr^F{}_4$ (**25**).

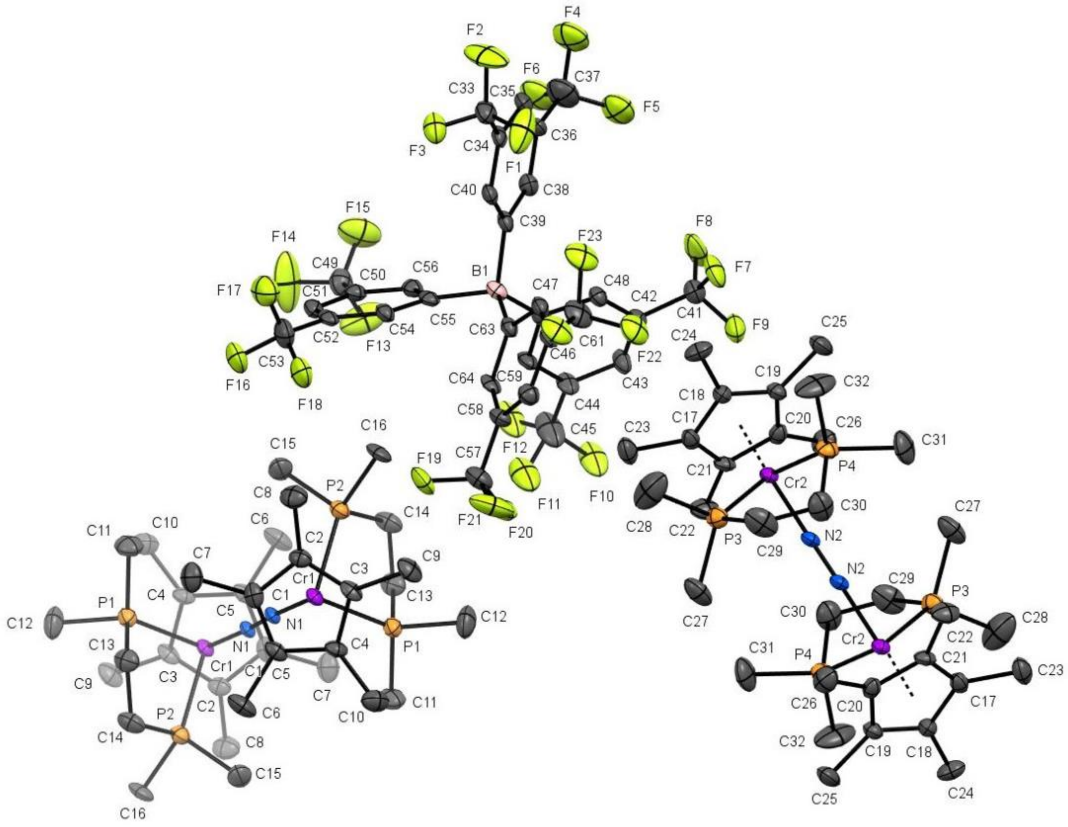

Figure 3.11 Molecular structure of $[(Cp^*(dmpe)Cr)_2(\mu\text{-}N_2)]BAr^F{}_4$ (**25**) represented as 50% probability thermal ellipsoids. Hydrogen atoms have been omitted for clarity. The asymmetric unit contains two molecules and one of the counterions is not shown here.

Table 3.7 Interatomic distances (Å) and angles (º) for the N_2-containing cation of $[(Cp^*(dmpe)Cr)_2(\mu\text{-}N_2)]BAr^F{}_4$ (**25**).

Distances (Å)			
Cr1-P1	2.3166(8)	Cr2-P3	2.3176(8)
Cr1-P2	2.2991(8)	Cr2-P4	2.2935(8)
Cr1-N1	1.788(2)	Cr2-N2	1.785(2)

Cr1-C1	2.251(2)	Cr2-C24	2.189(2)
Cr1-C2	2.237(2)	Cr2-C25	2.223(2)
Cr1-C3	2.202(2)	Cr2-C26	2.243(2)
Cr1-C4	2.191(2)	Cr2-C27	2.228(2)
Cr1-C5	2.223(2)	Cr2-C28	2.186(2)
P1-C11	1.830(3)	P3-C17	1.827(3)
P1-C12	1.822(3)	P3-C18	1.827(3)
P1-C13	1.852(3)	P3-C19	1.859(3)
P2-C14	1.837(3)	P4-C20	1.832(3)
P2-C15	1.823(3)	P4-C21	1.821(3)
P2-C16	1.824(3)	P4-C22	1.814(3)
N1-N1	1.211(4)	N2-N2	1.200(4)
C1-C2	1.417(4)	C19-C20	1.529(4)
C1-C5	1.420(3)	C23-C24	1.501(4)
C1-C6	1.501(4)	C24-C25	1.435(4)
C2-C3	1.433(3)	C24-C28	1.436(3)
C2-C7	1.498(4)	C25-C26	1.416(4)
C3-C4	1.443(3)	C25-C29	1.504(4)
C3-C8	1.497(4)	C26-C27	1.416(4)
C4-C5	1.423(3)	C26-C30	1.507(4)
C4-C9	1.499(3)	C27-C28	1.427(4)
C5-C10	1.503(3)	C27-C31	1.509(3)
C13-C14	1.516(4)	C28-C32	1.500(4)

Angles (°)

P2-Cr1-P1	82.10(3)	P4-Cr2-P3	81.80(3)
N1-Cr1-P1	88.78(7)	N2-Cr2-P3	91.79(7)
N1-Cr1-P2	87.75(7)	N2-Cr2-P4	86.02(7)
N1-Cr1-C1	106.48(9)	N2-Cr2-C24	164.40(10)
N1-Cr1-C2	137.26(9)	N2-Cr2-C25	137.57(10)
N1-Cr1-C3	165.97(9)	N2-Cr2-C26	105.88(9)
N1-Cr1-C4	130.16(9)	N2-Cr2-C27	101.31(9)

N1-Cr1-C5	103.09(9)	N2-Cr2-C28	128.09(10)
C1-Cr1-P1	116.83(7)	C24-Cr2-P3	102.93(7)
C1-Cr1-P2	155.86(7)	C24-Cr2-P4	100.99(7)
C2-Cr1-P1	93.07(7)	C24-Cr2-C25	37.95(9)
C2-Cr1-P2	134.81(7)	C24-Cr2-C26	62.81(9)
C2-Cr1-C1	36.81(9)	C24-Cr2-C27	63.13(9)
C3-Cr1-P1	103.85(7)	C25-Cr2-P3	92.86(7)
C3-Cr1-P2	99.87(7)	C25-Cr2-P4	136.38(7)
C3-Cr1-C1	62.53(9)	C25-Cr2-C26	36.97(9)
C3-Cr1-C2	37.67(9)	C25-Cr2-C27	62.16(9)
C3-Cr1-C5	62.88(9)	C26-Cr2-P3	117.51(7)
C4-Cr1-P1	140.72(7)	C26-Cr2-P4	156.22(7)
C4-Cr1-P2	93.17(7)	C27-Cr2-P3	153.69(7)
C4-Cr1-C1	62.73(9)	C27-Cr2-P4	121.45(7)
C4-Cr1-C2	63.14(9)	C27-Cr2-C26	36.92(9)
C4-Cr1-C3	38.34(9)	C28-Cr2-P3	139.63(7)
C4-Cr1-C5	37.60(9)	C28-Cr2-P4	93.67(7)
C5-Cr1-P1	153.29(7)	C28-Cr2-C24	38.33(9)
C5-Cr1-P2	121.66(7)	C28-Cr2-C25	63.27(9)
C5-Cr1-C1	37.00(9)	C28-Cr2-C26	62.71(9)
C5-Cr1-C2	61.95(9)	C28-Cr2-C27	37.72(9)
C11-P1-Cr1	126.01(10)	C17-P3-Cr2	124.65(9)
C11-P1-C13	99.79(13)	C17-P3-C18	100.44(14)
C12-P1-Cr1	114.10(9)	C17-P3-C19	100.32(13)
C12-P1-C11	100.95(14)	C18-P3-Cr2	114.74(10)
C12-P1-C13	102.89(13)	C18-P3-C19	103.86(13)
C13-P1-Cr1	110.09(9)	C19-P3-Cr2	110.20(9)
C14-P2-Cr1	105.74(9)	C20-P4-Cr2	105.54(9)
C15-P2-Cr1	119.91(10)	C21-P4-Cr2	118.76(10)
C15-P2-C14	101.67(13)	C21-P4-C20	101.71(13)
C15-P2-C16	101.41(15)	C22-P4-Cr2	124.34(11)
C16-P2-Cr1	123.31(10)	C22-P4-C20	102.20(14)
C16-P2-C14	101.39(13)	C22-P4-C21	101.05(14)

N11-N1-Cr1	174.2(2)	N22-N2-Cr2	174.3(3)
C2-C1-Cr1	71.06(14)	C20-C19-P3	110.37(17)
C2-C1-C5	108.0(2)	C19-C20-P4	108.78(17)
C2-C1-C6	124.2(2)	C23-C24-Cr2	129.89(18)
C5-C1-Cr1	70.43(13)	C25-C24-Cr2	72.29(14)
C5-C1-C6	127.5(2)	C25-C24-C23	125.9(2)
C6-C1-Cr1	128.57(17)	C25-C24-C28	107.3(2)
C1-C2-Cr1	72.14(14)	C28-C24-Cr2	70.70(13)
C1-C2-C3	108.4(2)	C28-C24-C23	126.1(2)
C1-C2-C7	124.3(2)	C24-C25-Cr2	69.75(13)
C3-C2-Cr1	69.86(13)	C24-C25-C29	126.5(2)
C3-C2-C7	126.2(2)	C26-C25-Cr2	72.28(14)
C7-C2-Cr1	132.97(17)	C26-C25-C24	108.2(2)
C2-C3-Cr1	72.47(14)	C26-C25-C29	124.2(2)
C2-C3-C4	107.4(2)	C29-C25-Cr2	132.98(18)
C2-C3-C8	125.1(2)	C25-C26-Cr2	70.75(14)
C4-C3-Cr1	70.42(13)	C25-C26-C30	124.2(2)
C4-C3-C8	126.7(2)	C27-C26-Cr2	70.97(14)
C8-C3-Cr1	130.34(17)	C27-C26-C25	108.4(2)
C3-C4-Cr1	71.24(13)	C27-C26-C30	127.1(2)
C3-C4-C9	126.6(2)	C30-C26-Cr2	128.45(17)
C5-C4-Cr1	72.41(14)	C26-C27-Cr2	72.10(14)
C5-C4-C3	107.3(2)	C26-C27-C28	108.3(2)
C5-C4-C9	125.1(2)	C26-C27-C31	127.9(2)
C9-C4-Cr1	130.26(17)	C28-C27-Cr2	69.53(14)
C1-C5-Cr1	72.56(14)	C28-C27-C31	123.6(2)
C1-C5-C4	108.9(2)	C31-C27-Cr2	127.93(17)
C1-C5-C10	125.6(2)	C24-C28-Cr2	70.98(14)
C4-C5-Cr1	69.99(13)	C24-C28-C32	126.0(2)
C4-C5-C10	125.2(2)	C27-C28-Cr2	72.75(14)
C10-C5-Cr1	128.25(17)	C27-C28-C24	107.7(2)
C14-C13-P1	110.83(17)	C27-C28-C32	125.3(2)
C13-C14-P2	108.41(17)	C32-C28-Cr2	130.72(18)

25 crystalizes in the triclinic space group $P\bar{1}$. The structure is similar to the structure of **24**, the only difference between these two is the counterion. Similar to **24**, the N-N bond length (1.211(4) and 1.200(4) Å) shows an increase compared to the neutral dinitrogen compound. **25** is a mixed-valent complex with the oxidation state of I and II in the chromium centers. The complex displayed a curiously low effective magnetic moment, of 2.2 (1) μ_B at 295 K. The IR spectrum taken in the solid state did not show the stretches related to the N_2 ligand due to the presence of two inversion centers in the structure. The ^{1}H NMR spectrum of **25** is consistent with the presence of a paramagnetic chromium complex as shown in **Figure 3.12**.

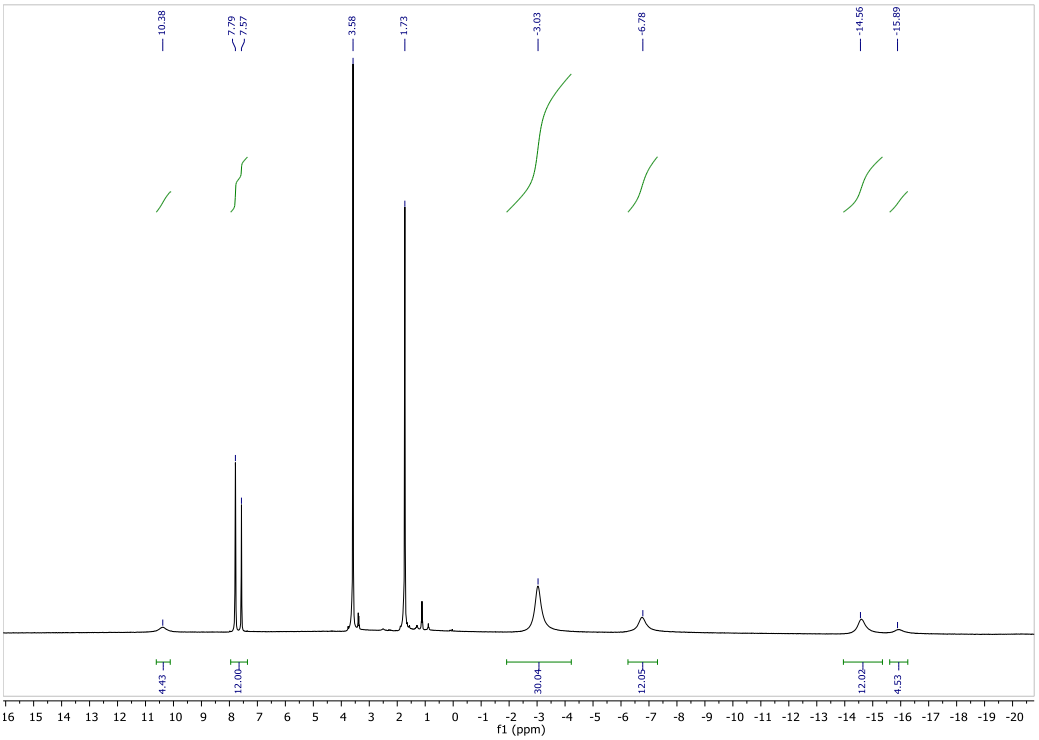

Figure 3.12 ^{1}H-NMR spectrum of $[(Cp^*(dmpe)Cr)_2(\mu\text{-}N_2)]BAr^F{}_4$ (**25**) recorded in THF-d_8 at 400 MHz.

The next action was to test the reactivity of **10** toward proton sources. Brookhart's acid, i.e. $[H(OEt_2)_2]^+[(3,5\text{-}(CF_3)_2C_6H_3)_4B]^-$ ($HBAr^F_4$), was chosen for this matter and was synthesized according to literature procedures.[112,113] Due to the large size of its counter anion, the latter is generally considered a non-coordinating ion. This property of Brookhart's acid makes it favorable to be used in our reaction, since we are dealing with dinitrogen, a weakly coordinated ligand in our system.

1 equivalent of $HBAr^F_4$ was added slowly to a Et_2O solution of **10**. During the addition bubbles started to evolve from the solution (presumably hydrogen gas). The color of the solution changed from green-brown to maroon by the end of the addition. After about 30 minutes of stirring, the solution was filtered to remove any insoluble impurities. The solvent was reduced under vacuum to make a concentrated solution and then was cooled to -30°C for overnight to yield maroon crystals. Determination of the structure by X-ray crystallography (measurement of the unit cell) and proton NMR revealed it to be the dinuclear chromium complex $[(Cp^*(dmpe)Cr)_2(\mu\text{-}N_2)]BAr^F_4$ (**25**).

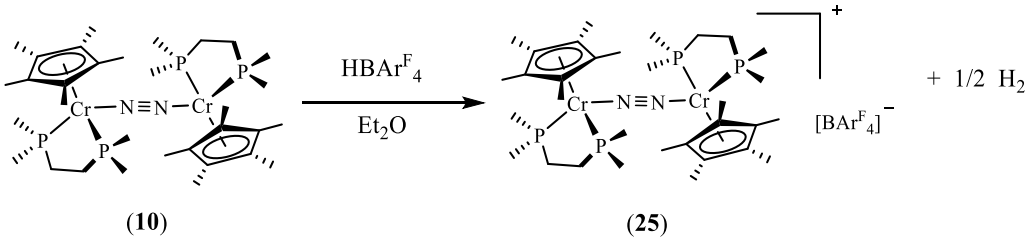

Figure 3.13 Synthesis of $[(Cp^*(dmpe)Cr)_2(\mu\text{-}N_2)]BAr^F_4$ (**25**) by the reaction of **10** with 1 equivalent of Brookhart's acid.

To test if further oxidation of **25** by protons is possible, the reaction of dinitrogen complex **10** and the acid was repeated with 2 equivalents of acid. 2 equivalents of $HBAr^F_4$ were dissolved in diethyl ether and were added dropwise to the Et_2O solution of **10**.

During the addition bubbles started to evolve from the solution. The color of solution changed from green-brown to maroon after adding almost half of the acid solution. By the end of the addition a green precipitate was observed at the bottom of the flask. After about 10 minutes of stirring, the mixture was cooled to -30°C for overnight to yield green crystals. Determination of the structure by X-ray crystallography revealed it to be a dinuclear chromium complex, namely $[(Cp^*(dmpe)Cr)_2(\mu\text{-}N_2)](BAr^F{}_4)_2$ (**26**). The molecular structure of **26** is depicted in **Figure 3.14** while the corresponding interatomic distances and angles are listed in **Table 3.8**.

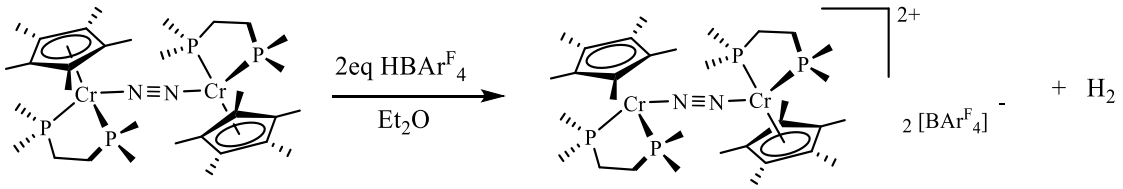

(**10**) (**26**)

Scheme 3.7 Synthesis of $[(Cp^*(dmpe)Cr)_2(\mu\text{-}N_2)](BAr^F{}_4)_2$ (**26**).

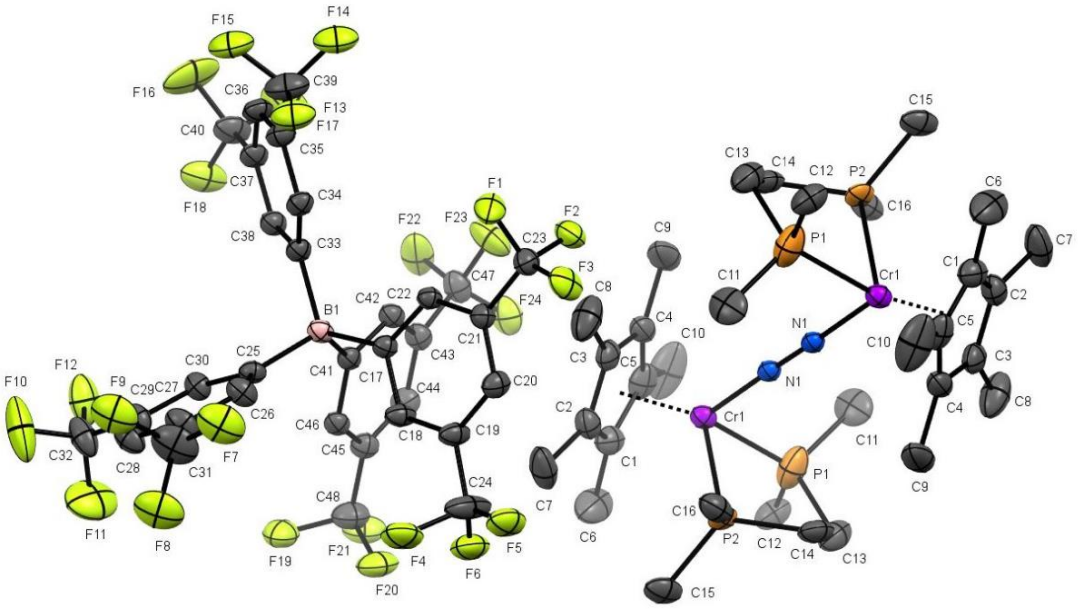

Figure 3.14 Molecular structure of $[(Cp^*(dmpe)Cr)_2(\mu\text{-}N_2)](BAr^F{}_4)_2$ (**26**) represented as 50% probability thermal ellipsoids. Hydrogen atoms and one counterion have been omitted for clarity.

Table 3.8 Interatomic distances (Å) and angles (º) for the N_2-containing cation of $[(Cp^*(dmpe)Cr)_2(\mu\text{-}N_2)](BAr^F{}_4)_2$ (**26**).

Distances (Å)

Cr1-P1	2.398(11)	P2-C16	1.817(14)
Cr1-P2	2.404(8)	N1-N1	1.201(7)
Cr1-N1	1.834(4)	C1-C2	1.415(9)
Cr1-C1	2.258(6)	C1-C5	1.416(9)
Cr1-C2	2.250(6)	C1-C6	1.509(9)
Cr1-C3	2.238(6)	C2-C3	1.410(9)

Cr1-C4	2.225(6)	C2-C7	1.497(8)
Cr1-C5	2.244(6)	C3-C4	1.415(9)
P1-C11	1.812(14)	C3-C8	1.498(9)
P1-C12	1.814(14)	C4-C5	1.409(9)
P1-C13	1.844(14)	C4-C9	1.502(9)
P2-C14	1.839(14)	C5-C10	1.498(9)
P2-C15	1.817(14)	C13-C14	1.537(18)

Angles (°)

P1-Cr1-P2	82.0(5)	C15-P2-C16	92(2)
N1-Cr1-P1	89.2(4)	C16-P2-Cr1	116(2)
N1-Cr1-P2	90.0(4)	C16-P2-C14	101(2)
N1-Cr1-C1	162.2(2)	N1-N1-Cr1	178.3(5)
N1-Cr1-C2	135.1(2)	C2-C1-Cr1	71.4(3)
N1-Cr1-C3	103.63(19)	C2-C1-C5	107.1(5)
N1-Cr1-C4	100.77(19)	C2-C1-C6	126.7(7)
N1-Cr1-C5	129.3(2)	C5-C1-Cr1	71.1(3)
C1-Cr1-P1	101.3(4)	C5-C1-C6	125.9(7)
C1-Cr1-P2	105.5(4)	C6-C1-Cr1	127.7(5)
C2-Cr1-P1	135.7(4)	C1-C2-Cr1	72.0(3)
C2-Cr1-P2	95.4(3)	C1-C2-C7	124.9(7)
C2-Cr1-C1	36.6(2)	C3-C2-Cr1	71.2(3)
C3-Cr1-P1	154.8(4)	C3-C2-C1	108.7(5)
C3-Cr1-P2	119.0(4)	C3-C2-C7	125.9(7)
C3-Cr1-C1	61.4(2)	C7-C2-Cr1	128.8(4)
C3-Cr1-C2	36.6(2)	C2-C3-Cr1	72.1(3)
C3-Cr1-C5	61.2(2)	C2-C3-C4	107.7(5)
C4-Cr1-P1	120.0(4)	C2-C3-C8	122.5(7)
C4-Cr1-P2	155.3(4)	C4-C3-Cr1	71.0(3)
C4-Cr1-C1	61.6(2)	C4-C3-C8	129.4(7)
C4-Cr1-C2	61.3(2)	C8-C3-Cr1	127.6(4)
C4-Cr1-C3	37.0(2)	C3-C4-Cr1	72.0(3)

C4-Cr1-C5	36.8(2)	C3-C4-C9	125.0(7)
C5-Cr1-P1	93.8(4)	C5-C4-Cr1	72.3(3)
C5-Cr1-P2	140.5(4)	C5-C4-C3	107.9(5)
C5-Cr1-C1	36.7(2)	C5-C4-C9	126.4(7)
C5-Cr1-C2	60.9(2)	C9-C4-Cr1	128.7(4)
C11-P1-Cr1	115.6(19)	C1-C5-Cr1	72.2(3)
C11-P1-C12	97(3)	C1-C5-C10	127.6(8)
C11-P1-C13	113(2)	C4-C5-Cr1	70.9(3)
C12-P1-Cr1	121(2)	C4-C5-C1	108.6(5)
C12-P1-C13	100.9(15)	C4-C5-C10	123.3(8)
C13-P1-Cr1	108.4(10)	C10-C5-Cr1	128.6(5)
C14-P2-Cr1	102.2(8)	C14-C13-P1	112.1(14)
C15-P2-Cr1	122.3(14)	C13-C14-P2	109.7(18)
C15-P2-C14	121.5(19)		

26 crystalizes in the triclinic space group $P\bar{1}$. Structural analysis shows that some of the fluorine atoms of the counterion suffer positional disorder over two sets of positions which were successfully modelled. Similar to the monocationic dinitrogen complexes, the dinitrogen N-N distance in **26** (1.201(7) Å) is larger than that of the neutral dinitrogen complex **10** but very close to the N-N bond distance in **25** (1.211(4) and 1.200(4) Å). Using DFT calculations the same result was gained for the bond distances, the cationic dinitrogen complexes **25** and **26** show an increase in the N-N bond distance, compared to the neutral dinitrogen complex **10**, but the reason is unknown (The details of these calculations will be discussed in the chapter 4).

The magnetic moment observed for **26** was 4.6(1) μ_B (298 K). For two high spin Cr(II) complexes that do not communicate electronically, the effective magnetic moment is 6.9 μ_B. We have not performed a variable temperature collection of the complex magnetic moment to determine with certainty if the two metal centers are magnetically coupled.

The reactivity of the dicationic dinitrogen complex at high temperature was studied in different solvents including THF, CH_2Cl_2 and benzene to see if the N-N cleavage might occur.

26 was dissolved in THF and transferred to an ampule. The solution was heated under nitrogen atmosphere at 70°C for 7 days and during this time the color of solution turned blue. After filtration, the solvent was removed, and the remaining residue was washed with pentanes and toluene. An Et_2O extraction was layered with pentanes and then stored at -30°C to get blue crystals of the product. Crystallization of the blue product was done for 4 times with the same method to get a pure product with a yield of 42%. Determination of the structure by X-ray crystallography revealed it to be a monocationic chromium complex, i.e. $[Cp^*(dmpe)CrF]BAr^F{}_4$ (**27**). The molecular structure of **27** is depicted in **Figure 3.15** while the corresponding interatomic distances and angles are listed in **Table 3.9**.

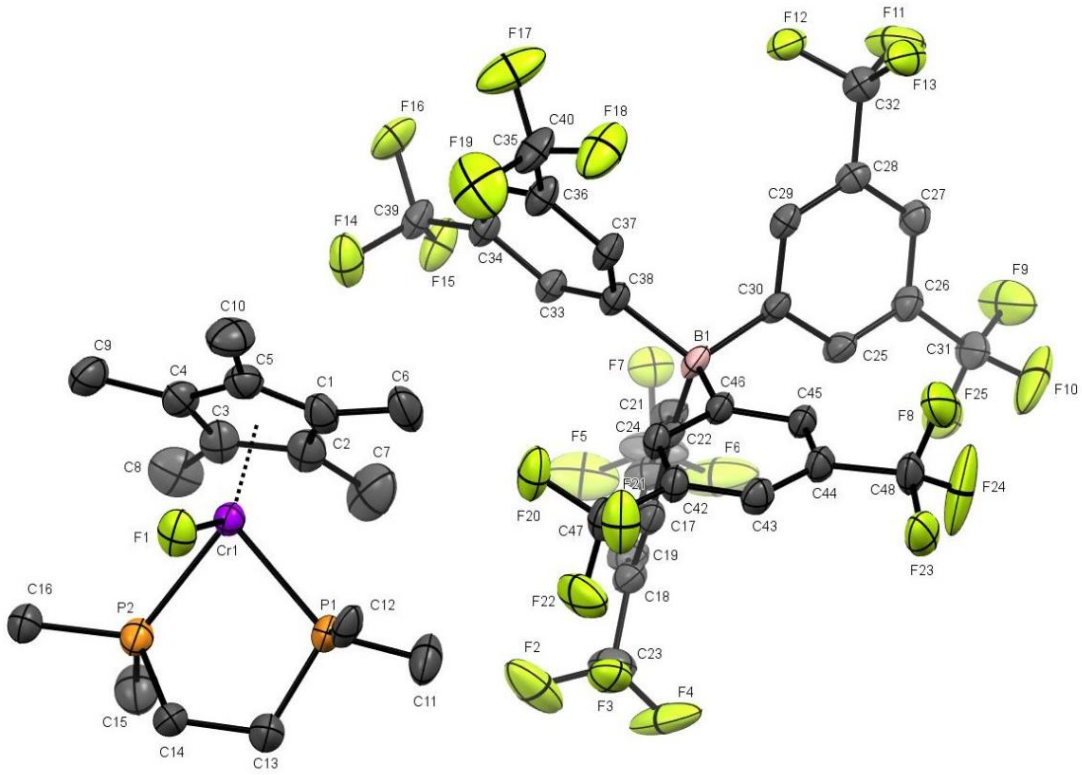

Figure 3.15 Molecular structure of [Cp*(dmpe)CrF]BAr$^{F}_{4}$ (**27**) represented as 50% probability thermal ellipsoids. Hydrogen atoms have been omitted for clarity.

Table 3.9 Interatomic distances (Å) and angles (º) for the cation of [Cp*(dmpe)CrF]BAr$^{F}_{4}$ (**27**).

Distances (Å)			
Cr1-F1	1.888(3)	P2-C16	1.810(11)
Cr1-P1	2.4480(18)	C1-C2	1.42

Cr1-P2	2.4527(19)	C1-C5	1.42
Cr1-C1	2.237(5)	C1-C6	1.5095
Cr1-C2	2.257(5)	C2-C3	1.42
Cr1-C3	2.230(4)	C2-C7	1.5095
Cr1-C4	2.193(4)	C3-C4	1.42
Cr1-C5	2.197(5)	C3-C8	1.5095
P1-C11	1.787(10)	C4-C5	1.42
P1-C12	1.815(10)	C4-C9	1.5095
P1-C13	1.853(11)	C5-C10	1.5095
P2-C14	1.833(9)	C13-C14	1.559(12)
P2-C15	1.800(10)		

Angles (°)

P1-Cr1-P2	82.40(2)	C15-P2-C14	103.6(6)
C1-Cr1-P1	100.0(2)	C15-P2-C16	101.6(8)
C1-Cr1-P2	158.5(19)	C16-P2-Cr1	117.3(9)
C1-Cr1-C2	36.84(7)	C16-P2-C14	105.4(8)
C2-Cr1-P1	100.2(2)	C2-C1-Cr1	72.35(15)
C2-Cr1-P2	121.7(19)	C2-C1-C5	108
C3-Cr1-P1	130.3(2)	C2-C1-C6	126
C3-Cr1-P2	100.12(18)	C5-C1-Cr1	69.81(15)
C3-Cr1-C1	61.90(10)	C5-C1-C6	126
C3-Cr1-C2	36.89(7)	C6-C1-Cr1	123.5(13)
C4-Cr1-P1	161.3(2)	C1-C2-Cr1	70.82(15)
C4-Cr1-P2	111.4(16)	C1-C2-C3	108
C4-Cr1-C1	62.47(11)	C1-C2-C7	126
C4-Cr1-C2	62.15(10)	C3-C2-Cr1	70.52(14)
C4-Cr1-C3	37.44(7)	C3-C2-C7	126
C4-Cr1-C5	37.74(7)	C7-C2-Cr1	124.27(14)
C5-Cr1-P1	130.5(2)	C2-C3-Cr1	72.58(15)
C5-Cr1-P2	147.0(15)	C2-C3-C4	108
C5-Cr1-C1	37.34(8)	C2-C3-C8	126

C5-Cr1-C2	62.09(11)	C4-C3-Cr1	69.86(15)
C5-Cr1-C3	62.52(10)	C4-C3-C8	126
C11-P1-Cr1	128.8(8)	C8-C3-Cr1	123.19(14)
C11-P1-C12	105.2(8)	C3-C4-Cr1	72.70(15)
C11-P1-C13	101.8(7)	C3-C4-C9	126
C12-P1-Cr1	107.1(7)	C5-C4-Cr1	71.30(15)
C12-P1-C13	105.8(10)	C5-C4-C3	108
C13-P1-Cr1	106.2(5)	C5-C4-C9	126
C14-P2-Cr1	102.4(3)	C9-C4-Cr1	121.72(14)
C15-P2-Cr1	124.4(5)	C1-C5-Cr1	72.85(15)
C4-C5-C10	126	C1-C5-C10	126
C10-C5-Cr1	121.89(14)	C4-C5-Cr1	70.96(14)
C14-C13-P1	111.6(9)	C4-C5-C1	108
C13-C14-P2	106.6(8)		

27 crystalizes in the triclinic space group $P\bar{1}$. The replacement of dinitrogen ligand with a fluoride atom, presumably originating in the $BAr^F{}_4$ counterion, can be seen in the structure. This is the first example of a fluoride abstraction reaction from a $BAr^F{}_4$ anion. The fluorine atoms of the counterion suffer positional disorder over two sets of positions. The effective magnetic moment for **27** was found to be 3.8 (1) μ_B when measured at room temperature, consistent with 3 unpaired electrons of a Cr(III) d^3 complex. The ^{1}H NMR spectrum of **27** shows seven broad peaks from 8.4 to −57.0 ppm, which is consistent with the paramagnetic property of this complexes.

To see if the cleavage of the dinitrogen ligand in **26** can be gained, the reactivity of **26** at high temperature was also monitored in CD_2Cl_2 using proton NMR spectroscopy. Crystals of **26** were put in an NMR tube and CD_2Cl_2 was vacuum transferred to the tube at low temperature. The tube was warmed up to room temperature; the color of solution started to change from brown to purple during this time. The first ^{1}H-NMR was recorded about 15 minutes after the start of the reaction. The tube was heated up to 60°C and no decomposition of the product was observed at that temperature.

In a separate reaction, **26** was dissolved in CH_2Cl_2 and was allowed to stir at room temperature. After a few minutes, the same color change was observed. After one day, the solution was filtered, and the solvent was removed under vacuum. The remaining purple powder was washed with pentanes and redissolved in Et_2O. Pure quantities of product, with a yield of 85%, were crystalized by cooling this ethereal solution to -30°C for one day. Determination of the structure by X-ray crystallography revealed it to be a monocationic chromium chloride complex, i.e. $[Cp^*(dmpe)CrCl]BAr^F{}_4$ (**28**). The molecular structure of **28** is depicted in **Figure 3.16** while the corresponding interatomic distances and angles are listed in **Table 3.10**.

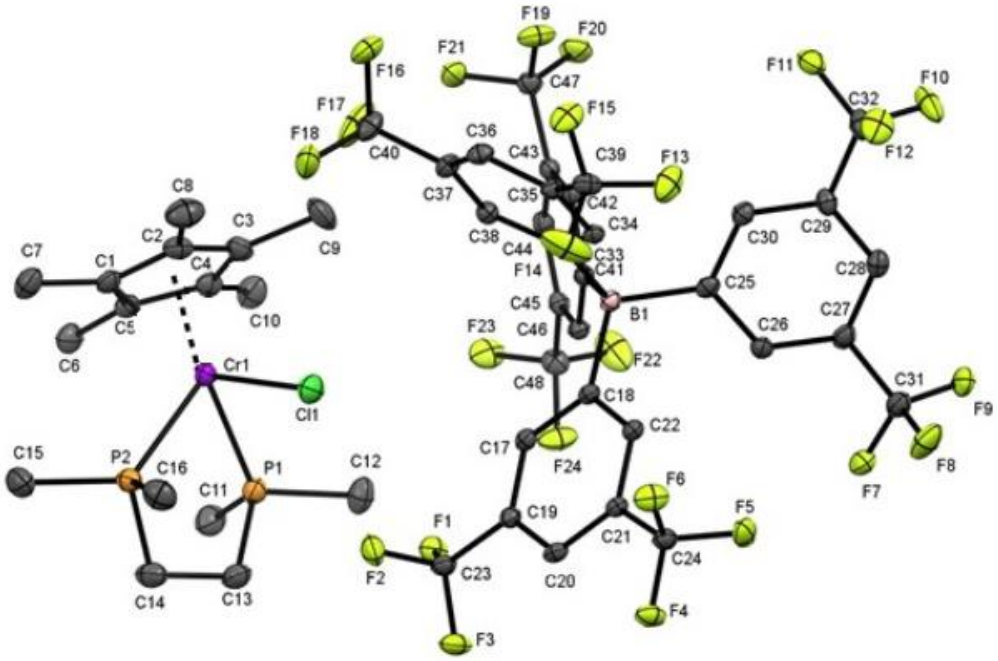

Figure 3.16 Molecular structure of $[Cp^*(dmpe)CrCl]BAr^F{}_4$ (**28**) represented as 50% probability thermal ellipsoids. Hydrogen atoms have been omitted for clarity.

Table 3.10 Interatomic distances (Å) and angles (º) for the cation of [Cp*(dmpe)CrCl]BAr^F_4 (**28**).

Distances (Å)

Cr1-Cl1	2.2704(10)	C1-C2	1.414(5)
Cr1-P1	2.4631(11)	C1-C5	1.422(5)
Cr1-P2	2.4812(10)	C1-C7	1.496(5)
Cr1-C1	2.243(3)	C2-C3	1.426(5)
Cr1-C2	2.231(3)	C2-C8	1.491(5)
Cr1-C3	2.231(3)	C3-C4	1.413(5)
Cr1-C4	2.232(3)	C3-C9	1.497(5)
Cr1-C5	2.230(3)	C4-C5	1.437(5)
P1-C11	1.795(4)	C4-C10	1.497(5)
P1-C12	1.806(4)	C5-C6	1.497(5)
P1-C13	1.841(4)	C13-C14	1.506(5)
P2-C14	1.827(4)	P2-C16	1.809(4)
P2-C15	1.821(4)		

Angles (°)

Cl1-Cr1-P1	89.20(4)	C15-P2-C14	102.62(19)
Cl1-Cr1-P2	91.16(4)	C16-P2-Cr1	114.43(14)
P1-Cr1-P2	82.33(3)	C16-P2-C14	105.6(2)
C1-Cr1-Cl1	130.28(10)	C16-P2-C15	102.1(2)
C1-Cr1-P1	140.38(10)	C2-C1-Cr1	71.10(19)
C1-Cr1-P2	97.82(9)	C2-C1-C5	108.9(3)
C2-Cr1-Cl1	96.40(10)	C2-C1-C7	124.0(3)
C2-Cr1-P1	159.52(10)	C5-C1-Cr1	70.96(18)
C2-Cr1-P2	117.10(10)	C5-C1-C7	126.9(3)
C2-Cr1-C1	36.85(13)	C7-C1-Cr1	128.3(2)
C2-Cr1-C4	62.32(13)	C1-C2-Cr1	72.05(19)

C3-Cr1-Cl1	91.88(9)	C1-C2-C3	107.3(3)
C3-Cr1-P1	123.16(10)	C1-C2-C8	126.3(4)
C3-Cr1-P2	154.37(11)	C3-C2-Cr1	71.4(2)
C3-Cr1-C1	61.49(13)	C3-C2-C8	126.3(4)
C3-Cr1-C2	37.27(14)	C8-C2-Cr1	124.6(3)
C3-Cr1-C4	36.92(13)	C2-C3-Cr1	71.37(19)
C4-Cr1-Cl1	120.67(9)	C2-C3-C9	125.6(4)
C4-Cr1-P1	97.91(10)	C4-C3-Cr1	71.57(19)
C4-Cr1-P2	148.15(9)	C4-C3-C2	108.9(3)
C4-Cr1-C1	61.98(12)	C4-C3-C9	125.5(4)
C5-Cr1-Cl1	153.87(9)	C9-C3-Cr1	125.4(3)
C5-Cr1-P1	106.02(9)	C3-C4-Cr1	71.51(19)
C5-Cr1-P2	111.52(9)	C3-C4-C5	107.5(3)
C5-Cr1-C1	37.07(12)	C3-C4-C10	126.1(3)
C5-Cr1-C2	62.29(13)	C5-C4-Cr1	71.15(18)
C5-Cr1-C3	62.04(12)	C5-C4-C10	126.2(3)
C5-Cr1-C4	37.58(12)	C10-C4-Cr1	126.9(2)
C11-P1-Cr1	122.18(14)	C1-C5-Cr1	71.97(18)
C11-P1-C12	103.1(2)	C1-C5-C4	107.4(3)
C11-P1-C13	105.0(2)	C1-C5-C6	126.9(3)
C12-P1-Cr1	117.13(15)	C4-C5-Cr1	71.27(18)
C12-P1-C13	104.17(18)	C4-C5-C6	125.3(3)
C13-P1-Cr1	103.41(13)	C6-C5-Cr1	127.8(2)
C14-P2-Cr1	106.39(13)	C14-C13-P1	110.5(3)
C15-P2-Cr1	123.96(14)	C13-C14-P2	111.2(3)

28 crystalizes in the triclinic space group $P\bar{1}$. In the crystal structure of **28**, some of the fluorine atoms of the counterion suffer positional disorder over two sets of positions. The effective magnetic moment for **28** was found to be 3.8 (1) μ_B when measured at room temperature, consistent with 3 unpaired electrons of a high spin Cr(III) d^3 complex. The ^{1}H-NMR spectrum of **28** shows broad and shifted peaks, which is consistent with the paramagnetic property of this complexes.

The reactivity of the dicationic dinitrogen complex (**26**) at high temperature in a nonpolar solvent, such as benzene was also studied. **26** was heated in C_6D_6 and monitored by ^{1}H-NMR spectroscopy for 30 days at 70°C. The starting compound is not soluble in benzene and after a couple of days the color of benzene solution started to change. During the 30 days of heating, some oily brown compound precipitated out of the solution. On day 3, a broad peak started to appear at 24.2 ppm. After about 18 days of heating, the appearance and chemical shift of this peak changed to a semi-doublet peak at 20.1 ppm. This peak was never observed in the THF and CH_2Cl_2 reaction.

The same reaction was done in a larger scale in benzene, but unfortunately due to the complexity of the reaction mixture, the separation and crystallization of the products was not possible.

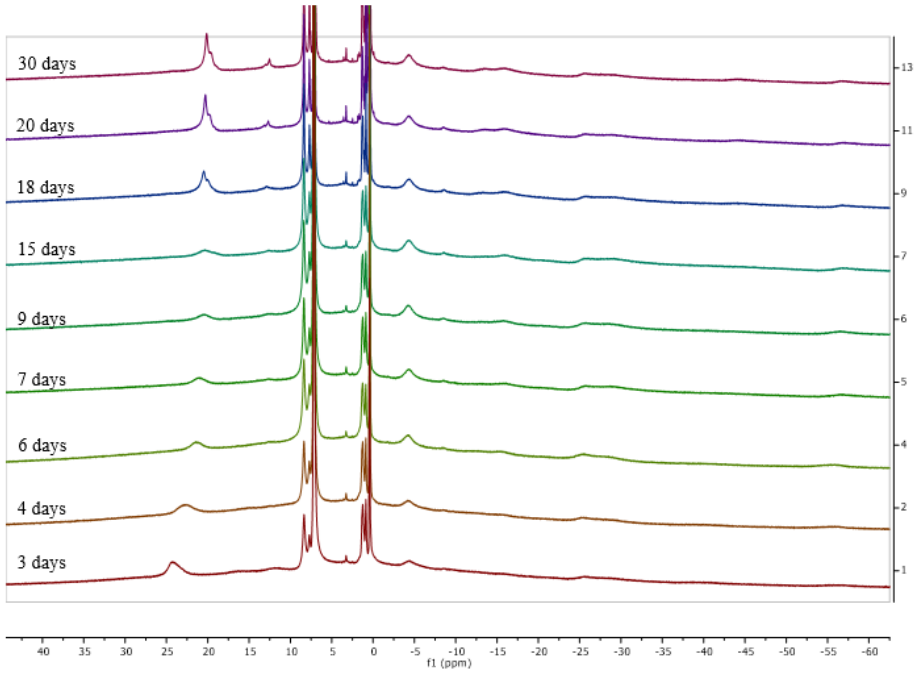

Figure 3.17 ^{1}H-NMR spectra of the reaction of $[(Cp^*(dmpe)Cr)_2(\mu\text{-}N_2)](BAr^F{}_4)_2$ (**26**) at high temperature (70°C) in C_6D_6 for 30 days. The initial spectrum at the beginning of the experiment was not recorded due to the insolubility of the **26** in benzene.

Having the neutral, monocationic, and dicationic dinitrogen complexes in hand, raises the question about the possibility of cleavage of dinitrogen in these complexes. In theory, from the splitting of the dicationic dinitrogen complex, two equivalents of a monocationic nitride complex should be produced. Also, from the splitting of the monocationic dinitrogen complex, one neutral and one cationic nitride complexes can be produced. Finally, cleavage of the N-N bond of neutral **10** might be expected to yield two equivalents of neutral **13**. Therefore, it was decided to synthesize the cationic nitride complex by reacting **13** with an oxidant such as ferricenium (e.g. $FcBAr^F_4$).

$FcBAr^F_4$ was synthesized according to the literature procedures.[114,115] 1 equivalent of $FcBAr^F_4$ in benzene was added slowly to the benzene solution of neutral nitride complex **13**. By the end of the addition the color of solution changed to brown-purple and precipitation of the product appeared in the flask. After 10 minutes of stirring the ferrocene was removed as a yellow solution, by filtration. The remaining residue was washed with pentanes and was then dissolved in minimal diethyl ether. The solution was filtered again and was then kept at -30°C overnight to yield brown-purple crystals. Determination of the structure by X-ray crystallography revealed it to be a mononuclear chromium nitride complex, i.e. $[(Cp^*(dmpe)CrN]BAr^F_4$ (**29**). The molecular structure of **29** is depicted in **Figure 3.18** while the corresponding interatomic distances and angles are listed in **Table 3.11**.

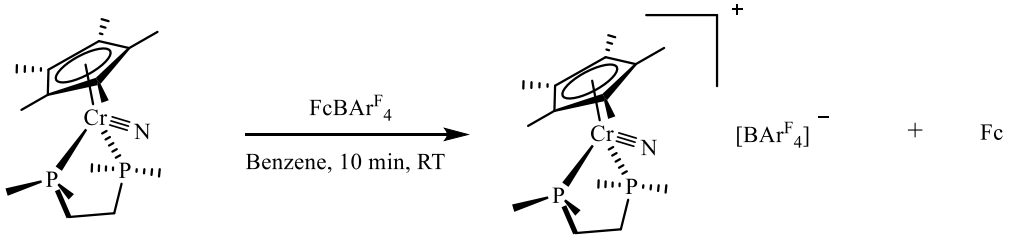

Scheme 3.8 Synthesis of $[(Cp^*(dmpe)CrN]BAr^F_4$ (**29**)

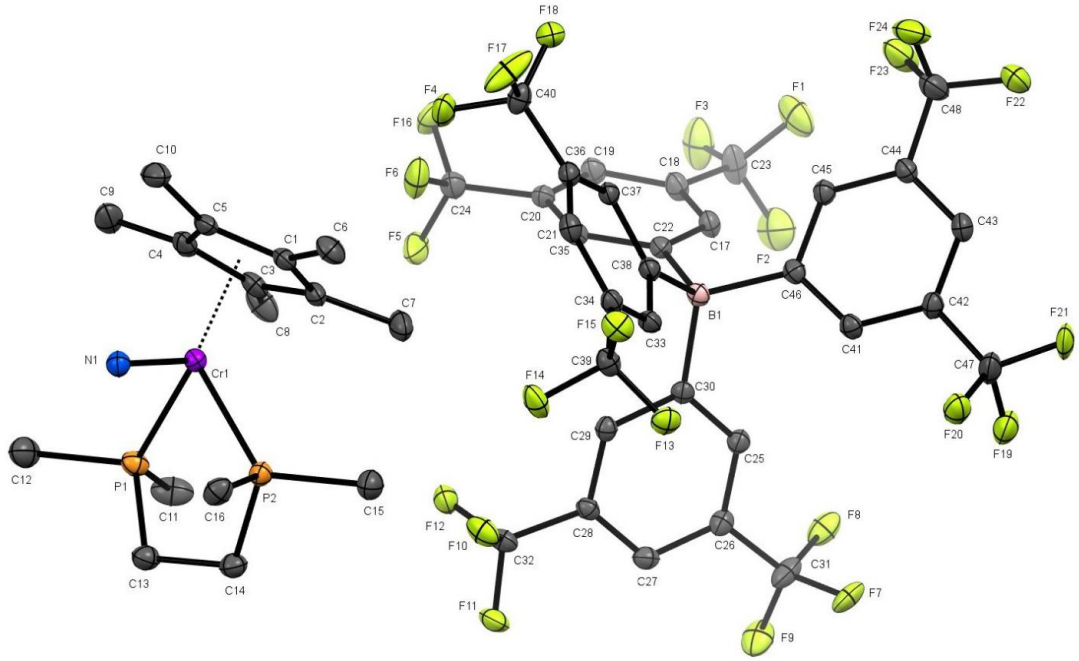

Figure 3.18 Molecular structure of [(Cp*(dmpe)CrN]BAr$^{F}_{4}$ (**29**) represented as 50% probability thermal ellipsoids. Hydrogen atoms and the counterion have been omitted for clarity.

Table 3.11 Interatomic distances (Å) and angles (º) for the cation of [(Cp*(dmpe)CrN]BAr$^{F}_{4}$ (**29**).

Distances (Å)

Cr1-P1	2.3872(13)	P2-C16	1.810(5)
Cr1-P2	2.4080(13)	C1-C2	1.437(6)
Cr1-N1	1.581(4)	C1-C5	1.420(6)
Cr1-C1	2.237(4)	C1-C6	1.495(6)

Cr1-C2	2.365(4)	C2-C3	1.403(6)
Cr1-C3	2.354(4)	C2-C7	1.500(6)
Cr1-C4	2.230(5)	C3-C4	1.444(7)
Cr1-C5	2.213(4)	C3-C8	1.496(7)
P1-C11	1.809(6)	C4-C5	1.422(7)
P1-C12	1.822(6)	C4-C9	1.497(7)
P1-C13	1.826(5)	C5-C10	1.494(7)
P2-C14	1.832(5)	C13-C14	1.531(7)
P2-C15	1.817(5)		

Angles (°)

P1-Cr1-P2	84.63(4)	C15-P2-C14	104.4(2)
N1-Cr1-P1	89.74(14)	C16-P2-Cr1	111.84(17)
N1-Cr1-P2	92.33(14)	C16-P2-C14	105.2(2)
N1-Cr1-C1	115.26(18)	C16-P2-C15	102.0(2)
N1-Cr1-C2	151.11(18)	C2-C1-Cr1	76.7(2)
N1-Cr1-C3	143.17(19)	C2-C1-C6	126.5(4)
N1-Cr1-C4	106.94(19)	C5-C1-Cr1	70.5(2)
N1-Cr1-C5	93.06(18)	C5-C1-C2	108.3(4)
C1-Cr1-P1	153.88(12)	C5-C1-C6	124.8(4)
C1-Cr1-P2	100.89(12)	C6-C1-Cr1	124.4(3)
C1-Cr1-C2	36.24(16)	C1-C2-Cr1	67.0(2)
C1-Cr1-C3	59.89(16)	C1-C2-C7	126.2(4)
C2-Cr1-P1	117.99(12)	C3-C2-Cr1	72.3(2)
C2-Cr1-P2	97.92(12)	C3-C2-C1	107.8(4)
C3-Cr1-P1	95.81(11)	C3-C2-C7	125.7(4)
C3-Cr1-P2	124.40(13)	C7-C2-Cr1	131.4(3)
C3-Cr1-C2	34.59(16)	C2-C3-Cr1	73.1(2)
C4-Cr1-P1	105.22(13)	C2-C3-C4	108.4(4)
C4-Cr1-P2	158.14(12)	C2-C3-C8	127.0(5)
C4-Cr1-C1	61.87(17)	C4-C3-Cr1	67.0(2)

C4-Cr1-C2	60.23(16)	C4-C3-C8	124.2(5)
C4-Cr1-C3	36.58(17)	C8-C3-Cr1	131.3(3)
C5-Cr1-P1	141.07(13)	C3-C4-Cr1	76.4(3)
C5-Cr1-P2	133.93(13)	C3-C4-C9	125.4(5)
C5-Cr1-C1	37.20(16)	C5-C4-Cr1	70.7(3)
C5-Cr1-C2	60.64(15)	C5-C4-C3	107.5(4)
C5-Cr1-C3	60.72(16)	C5-C4-C9	126.7(5)
C5-Cr1-C4	37.34(18)	C9-C4-Cr1	123.7(3)
C11-P1-Cr1	124.2(2)	C1-C5-Cr1	72.3(2)
C11-P1-C12	103.4(3)	C1-C5-C4	107.8(4)
C11-P1-C13	104.2(3)	C1-C5-C10	126.1(4)
C12-P1-Cr1	114.51(19)	C4-C5-Cr1	72.0(3)
C12-P1-C13	104.6(3)	C4-C5-C10	126.1(5)
C13-P1-Cr1	104.00(16)	C10-C5-Cr1	123.2(3)
C14-P2-Cr1	105.84(16)	C14-C13-P1	110.4(3)
C15-P2-Cr1	125.81(18)	C13-C14-P2	110.2(3)

29 crystalizes in the triclinic space group $P\bar{1}$. The geometry around the six coordinated chromium metal in **29** is pseudo-octahedral and very similar to the neutral nitride complex (**13**). The formal oxidation state of the Cr is +V in this terminal nitride compound and it displayed an effective magnetic moment of 1.6 (1) μ_B at room temperature, consistent with the assignment of the metal center as a d^1 Cr(V) ion. The Cr-N bond distance in **29** is 1.581(4) Å, which is very close to the neutral nitride complex **13** (i.e. 1.588(3) Å). Based on a CSD search on over 100 chromium complexes with terminal nitride ligands, it was found that there is a relation between the bond distance and the coordination number, which was discussed in the last chapter. In **Figure 3.19** the relation between the oxidation state and bond distance in terminal chromium nitride complexes is shown.

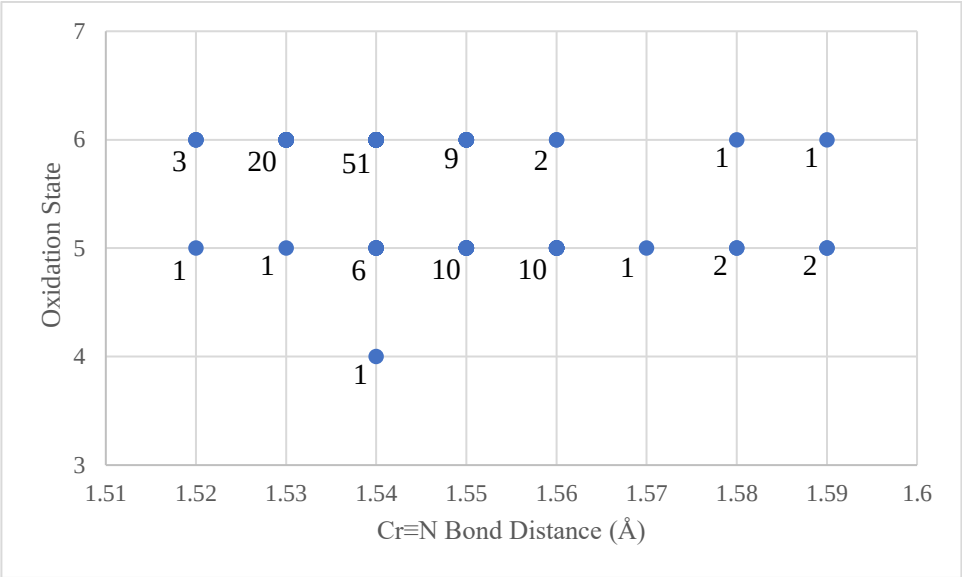

Figure 3.19 CSD search on over 100 Cr-N bond distances in terminal chromium nitride complexes. The relation between the bond distance and the oxidation state is shown in this figure. The cationic chromium complex **29** is not shown in the graph. Each point represents a number i.e., 3 terminal nitride complexes with the Cr-N bond distance of 1.52 Å are shown in this graph.

29 has a low solubility and the proton NMR of **29** in benzene-d_6 at room temperature shows five broad peaks from +3.6 to 11.8 ppm, which is consistent with the presence of a paramagnetic chromium complex, as shown in **Figure 3.20**.

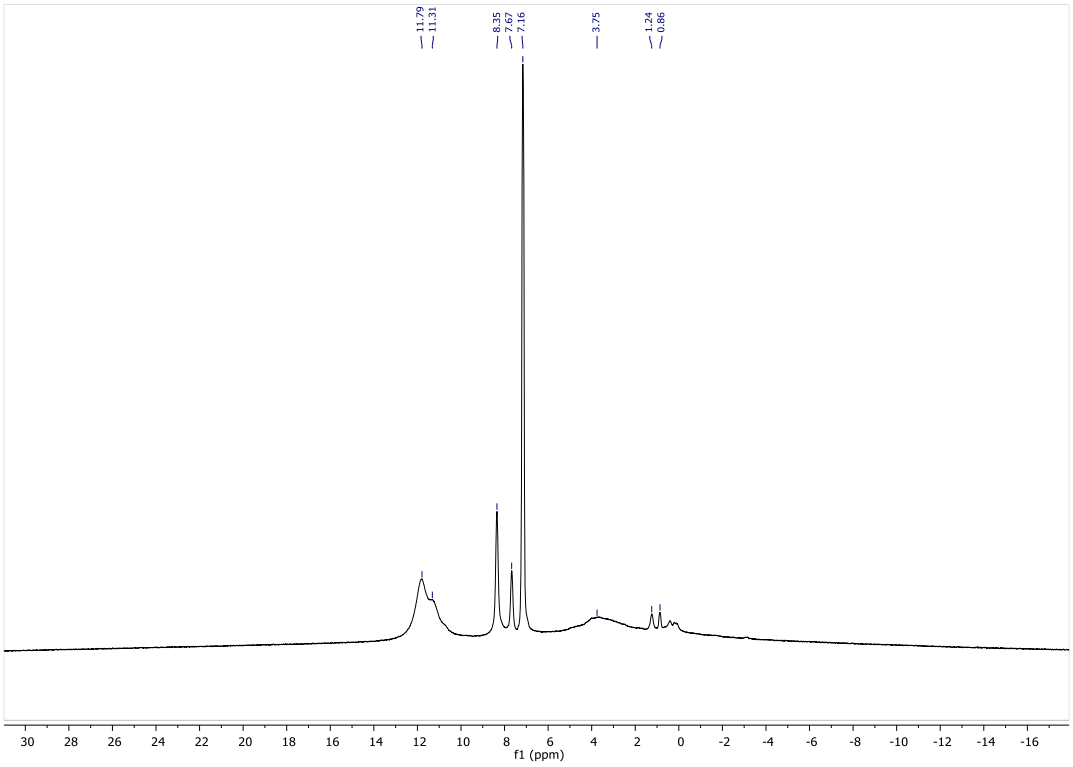

Figure 3.20 ^{1}H- spectrum of [(Cp*(dmpe)CrN]BAr$^{F}_{4}$ (**29**) recorded in C_6D_6 at 400 MHz. Pentanes was used to wash the crystals and peaks at 0.9 and 1.2 ppm are related to the pentanes impurities.

29 is stable in the solid state at low temperature, but when dissolved in benzene, Et_2O or THF and kept at room temperature it starts to react. **29** displays a brown-purple color in these solvents but after about 1 day the color of solution changes to blue and an oily brown compound precipitates out of the solution.

To gain more information about the reactivity of the cationic nitride complex at elevated temperatures, the reactions of **29** in THF-d_8 and benzene-d_6 were done in an NMR tube. The reaction in benzene was done at 70°C for 8 days. The peaks at 16.3 ppm

show a small shift as being heated, shown in **Figure 3.21**. After about 3 days, the peaks are almost stable at 15.8 ppm.

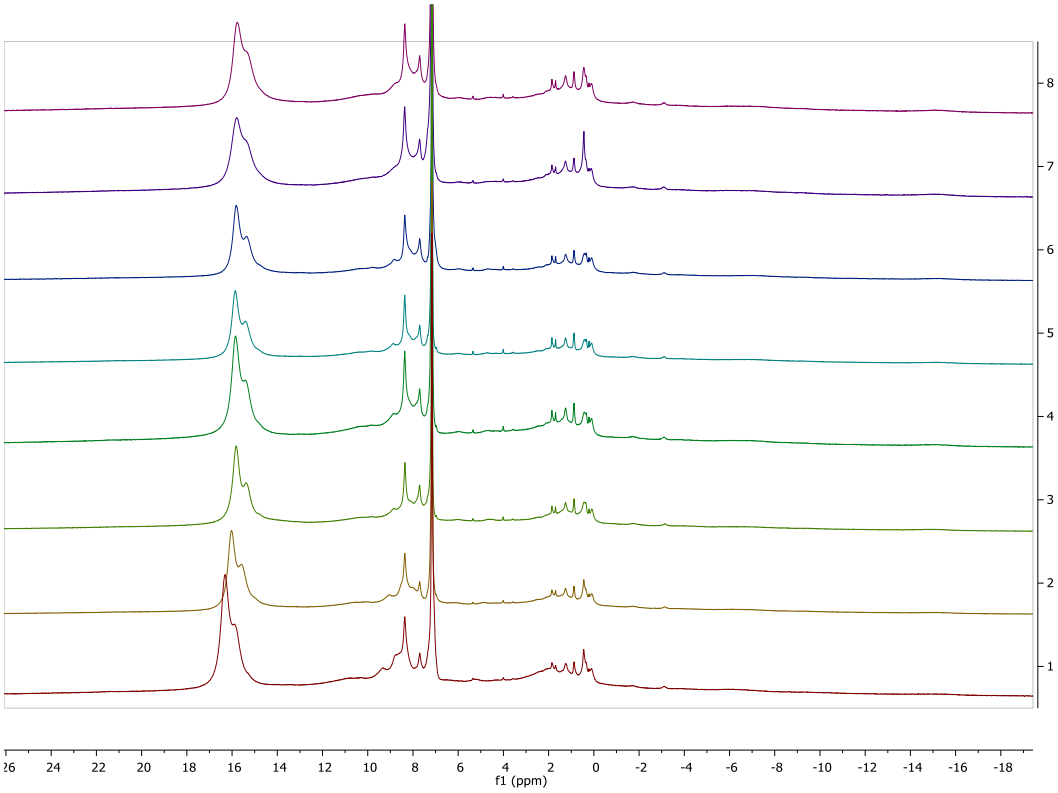

Figure 3.21 ^{1}H-NMR spectra of [(Cp*(dmpe)CrN]BAr$^{F}_{4}$ (**29**) recorded in C_6D_6 at 400 MHz were monitored for 8 days at 70°C. The numbers on the right side of the spectra indicate the number of days from the beginning of the experiment.

29 was also monitored in an NMR reaction at 50°C in THF-d_8. The color of the solution changed from brown-purple to blue after a couple of hours of heating. The reaction was monitored for 5 days and the changes in the proton NMR of the compound can be seen in **Figure 3.22**. After 5 days, the temperature was increased to 70°C for 2 days but no changes were observed in the proton NMR.

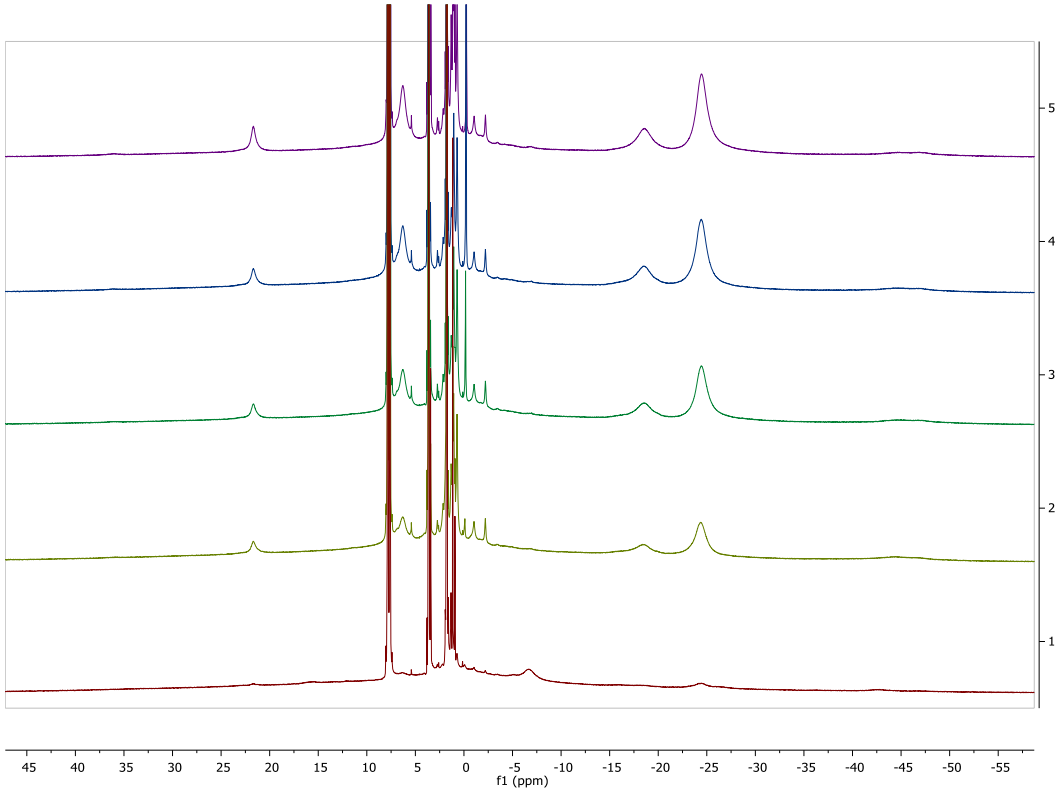

Figure 3.22 ^{1}H-NMR spectra of [(Cp*(dmpe)CrN]BAr$^{F}_{4}$ (**29**) recorded in THF-d_8 at 400 MHz. The first spectrum is of the starting compound and spectra 2 to 5 represents day 1 to 4 of reaction at 50°C.

To be able to characterize the compound, the reaction in THF was done on a larger scale. A THF solution of **29** was added to an ampule in a glove box under nitrogen atmosphere. The ampule was sealed and brought out of the box. After heating at 50°C, (under N_2 gas) for about 2h the color of solution changed to blue. The solution was heated for one day and after that the flask was brought into the box. After filtration, the solvent was removed under vacuum. The remaining blue compound was washed with pentanes and was redissolved in a minimal amount of Et_2O. The ethereal solution was layered with pentanes and was kept at -30°C. After one day an oily precipitation was observed at the bottom of the vial and the solution above the oil was transferred to another vial. The

process of cooling and removing the oil was repeated for 5 times and finally some blue crystals appeared around the vial. Determination of the structure by X-ray crystallography revealed it to be a mononuclear chromium complex, i.e. [Cp*Cr($NPMe_2CH_2CH_2PMe_2$)] BAr^F_4 (**30**). The molecular structure of **30** is depicted in **Figure 3.23**, while the corresponding interatomic distances and angles are listed in **Table 3.12**.

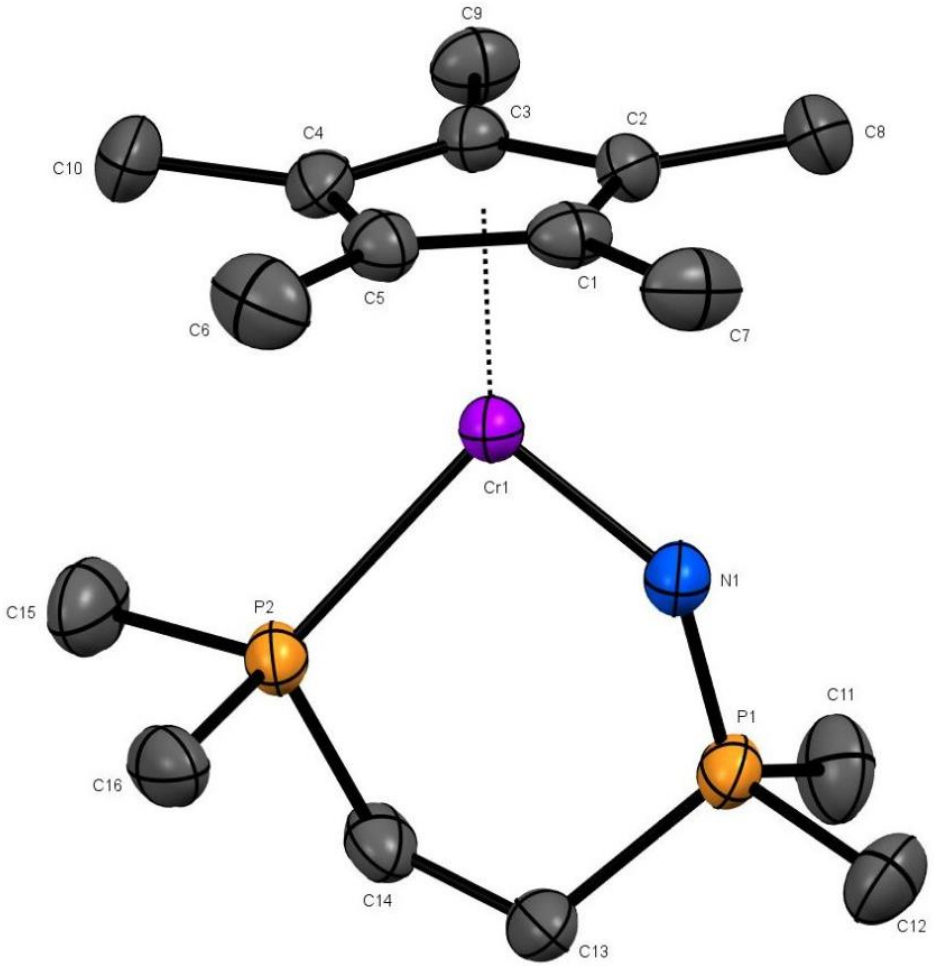

Figure 3.23 Molecular structure of [Cp*Cr($NPMe_2CH_2CH_2PMe_2$)] BAr^F_4 (**30**) represented as 50% probability thermal ellipsoids. Hydrogen atoms and the counterion have been omitted for clarity.

Table 3.12 Interatomic distances (Å) and angles (º) for the cation of [Cp*Cr($NPMe_2CH_2CH_2PMe_2$)] BAr^F_4 (**30**).

Distances (Å)

Cr1-P2	2.4300(16)	P2-C16	1.794(6)
Cr1-N1	1.796(4)	C1-C2	1.418(8)
Cr1-C1	2.210(5)	C1-C5	1.414(8)
Cr1-C2	2.223(5)	C1-C7	1.507(8)
Cr1-C3	2.232(5)	C2-C3	1.433(7)
Cr1-C4	2.252(5)	C2-C8	1.502(7)
Cr1-C5	2.224(5)	C3-C4	1.427(7)
P1-N1	1.564(5)	C3-C9	1.494(7)
P1-C11	1.782(6)	C4-C5	1.417(8)
P1-C12	1.782(6)	C4-C10	1.496(8)
P1-C13	1.816(6)	C5-C6	1.502(8)
P2-C14	1.816(6)	C13-C14	1.519(8)
P2-C15	1.798(6)		

Angles (°)

N1-Cr1-P2	92.26(15)	P1-N1-Cr1	143.6(3)
N1-Cr1-C1	107.1(2)	C2-C1-Cr1	71.80(3)
N1-Cr1-C2	102.1(2)	C2-C1-C7	124.8(5)
N1-Cr1-C3	128.7(2)	C5-C1-Cr1	72.00(3)
N1-Cr1-C4	164.0(2)	C5-C1-C2	108.3(5)
N1-Cr1-C5	139.4(2)	C5-C1-C7	126.9(6)
C1-Cr1-P2	144.6(16)	C7-C1-Cr1	121.0(4)
C1-Cr1-C2	37.30(2)	C1-C2-Cr1	70.90(3)
C1-Cr1-C3	62.47(19)	C1-C2-C3	107.8(5)
C1-Cr1-C4	61.90(2)	C1-C2-C8	126.7(5)

C1-Cr1-C5	37.20(2)	C3-C2-Cr1	71.60(3)
C2-Cr1-P2	163.5(14)	C3-C2-C8	125.5(5)
C2-Cr1-C3	37.52(18)	C8-C2-Cr1	122.7(4)
C2-Cr1-C4	62.06(19)	C2-C3-Cr1	70.90(3)
C2-Cr1-C5	62.10(2)	C2-C3-C9	125.4(5)
C3-Cr1-P2	126.2(14)	C4-C3-Cr1	72.20(3)
C3-Cr1-C4	37.10(19)	C4-C3-C2	107.5(5)
C4-Cr1-P2	103.2(14)	C4-C3-C9	127.0(5)
C5-Cr1-P2	111.3(15)	C9-C3-Cr1	123.9(4)
C5-Cr1-C3	62.1(2)	C3-C4-Cr1	70.70(3)
C5-Cr1-C4	36.90(2)	C3-C4-C10	126.0(6)
N1-P1-C11	111.5(3)	C5-C4-Cr1	70.50(3)
N1-P1-C12	113.4(3)	C5-C4-C3	107.9(5)
N1-P1-C13	114.2(2)	C5-C4-C10	125.9(6)
C11-P1-C13	106.4(3)	C10-C4-Cr1	127.7(4)
C12-P1-C11	105.3(3)	C1-C5-Cr1	70.9(3)
C12-P1-C13	105.4(3)	C1-C5-C4	108.4(5)
C14-P2-Cr1	112.1(19)	C1-C5-C6	126.5(6)
C15-P2-Cr1	120.9(3)	C4-C5-Cr1	72.60(3)
C15-P2-C14	102.0(3)	C4-C5-C6	125.0(6)
C16-P2-Cr1	114.7(2)	C6-C5-Cr1	124.9(4)
C16-P2-C14	103.6(3)	C14-C13-P1	113.1(4)
C16-P2-C15	101.5(4)	C13-C14-P2	114.9(4)

30 crystalizes in the triclinic space group $P\bar{1}$. The insertion of nitride into the phosphorus atom of the dmpe ligand can be seen in this molecule. Curiously, there is an empty coordination site on the Cr1 in **30**. The Cr1-N1 bond length is 1.796(4) Å which is in the range of Cr-N single bond distances.[66] Using DFT calculations, at the UB3LYP level of density functional theory and the basis set of 6-31G(d), the optimized structure of **30** was found to be in agreement with the crystal structure of this complex (**Table 3.13**). The formal oxidation state of +III can be assigned for this complex, assuming the phosphiniminato is a negatively charged ligand.

Table 3.13 Calculated and experimental bond distances (Å) and angles (°) for [Cp*Cr($NPMe_2CH_2CH_2PMe_2$)] BAr^F_4 (**30**).

	Experimental	**Calculation**
Cr-N	1.796(4)	1.80569
N-P	1.564(5)	1.59052
Cr-P	2.4300(16)	2.48764
Cr-N-P	143.6(3)	144.66824

The same reaction was repeated, but this time different solvents were used for the crystallization. The blue product was redissolved in THF and was layered with pentanes. After a few days blue crystals of the product appeared on the side of the vial and some oily product was collected on the bottom of the vial. Determination of the structure by X-ray crystallography revealed it to be a mononuclear chromium complex similar to **30**, but with a THF molecule coordinated to the Cr center, i.e. [Cp*Cr($NPMe_2CH_2CH_2PMe_2$)THF] BAr^F_4 (**31**). The molecular structure of **31** is depicted in **Figure 3.24** while the corresponding interatomic distances and angles are listed in **Table 3.14**.

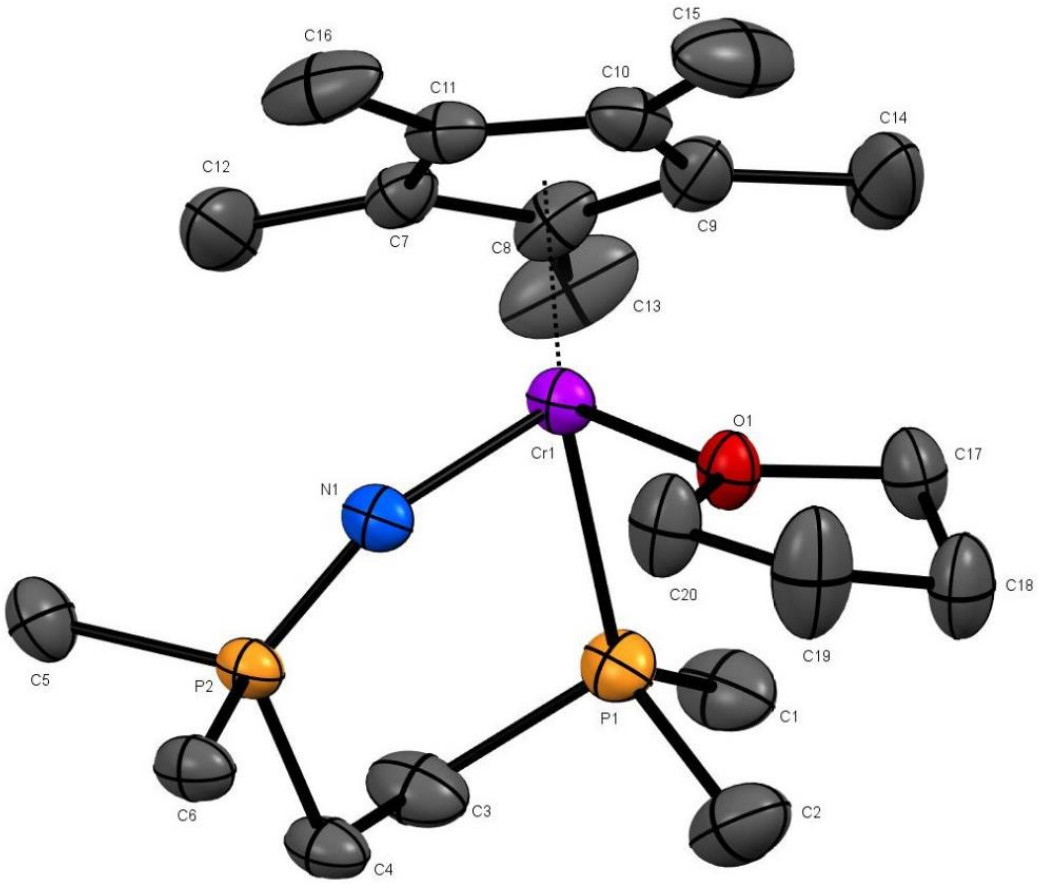

Figure 3.24 Molecular structure of [Cp*Cr($NPMe_2CH_2CH_2PMe_2$)THF] BAr^F_4 (**31**) represented as 50% probability thermal ellipsoids. Hydrogen atoms and the counterion have been omitted for clarity.

Table 3.14 Interatomic distances (Å) and angles (º) for the cation of [Cp*Cr($NPMe_2CH_2CH_2PMe_2$)THF] BAr^F_4 (**31**).

Distances (Å)

Cr1-P1	2.4400(13)	O1-C17	1.442(6)
Cr1-N1	1.879(4)	O1-C20	1.466(6)
Cr1-O1	2.111(3)	C17-C18	1.507(8)
Cr1-C7	2.293(3)	C18-C19	1.480(9)
Cr1-C8	2.296(3)	C19-C20	1.427(8)
Cr1-C9	2.277(3)	C7-C8	1.42
Cr1-C10	2.264(3)	C7-C11	1.42
Cr1-C11	2.274(3)	C7-C12	1.5095
P1-C1	1.792(6)	C8-C9	1.42
P1-C2	1.856(7)	C8-C13	1.5095
P1-C3	1.857(6)	C9-C10	1.42
P2-N1	1.537(4)	C9-C14	1.5095
P2-C4	1.818(5)	C10-C11	1.42
P2-C5	1.806(5)	C10-C15	1.5095
P2-C6	1.815(5)	C11-C16	1.5095
C3-C4	1.498(7)		

Angles (°)

N1-Cr1-P1	87.56(12)	P2-N1-Cr1	144.4(2)
N1-Cr1-O1	90.79(16)	C4-C3-P1	113.6(4)
N1-Cr1-C7	97.78(14)	C3-C4-P2	112.8(4)
N1-Cr1-C8	129.07(15)	C17-O1-Cr1	128.5(3)
N1-Cr1-C9	156.01(14)	C17-O1-C20	108.9(4)
N1-Cr1-C10	126.17(14)	C20-O1-Cr1	122.6(3)
N1-Cr1-C11	96.11(14)	O1-C17-C18	104.9(4)

O1-Cr1-P1	93.28(12)	C19-C18-C17	104.4(5)
O1-Cr1-C7	149.48(13)	C20-C19-C18	107.8(5)
O1-Cr1-C8	139.21(13)	C19-C20-O1	107.4(4)
O1-Cr1-C9	103.64(12)	C8-C7-Cr1	72.05(8)
O1-Cr1-C10	90.83(13)	C8-C7-C11	108
O1-Cr1-C11	113.92(13)	C8-C7-C12	126
C7-Cr1-P1	116.21(8)	C11-C7-Cr1	71.13(9)
C7-Cr1-C8	36.1	C11-C7-C12	126
C8-Cr1-P1	96.35(7)	C12-C7-Cr1	122.49(8)
C9-Cr1-P1	110.23(9)	C7-C8-Cr1	71.90(8)
C9-Cr1-C7	60.36(6)	C7-C8-C9	108
C9-Cr1-C8	36.2	C7-C8-C13	126
C10-Cr1-P1	145.97(9)	C9-C8-Cr1	71.20(9)
C10-Cr1-C7	60.55(6)	C9-C8-C13	126
C10-Cr1-C8	60.52(6)	C13-C8-Cr1	122.58(8)
C10-Cr1-C9	36.4	C8-C9-Cr1	72.61(9)
C10-Cr1-C11	36.5	C8-C9-C14	126
C11-Cr1-P1	152.43(8)	C10-C9-Cr1	71.26(9)
C11-Cr1-C7	36.2	C10-C9-C8	108
C11-Cr1-C8	60.37(6)	C10-C9-C14	126
C11-Cr1-C9	60.65(6)	C14-C9-Cr1	121.84(8)
C1-P1-Cr1	128.4(3)	C9-C10-Cr1	72.30(9)
C1-P1-C2	99.9(4)	C9-C10-C15	126
C1-P1-C3	100.7(3)	C11-C10-Cr1	72.15(8)
C2-P1-Cr1	111.8(2)	C11-C10-C9	108
C2-P1-C3	100.4(3)	C11-C10-C15	126
C3-P1-Cr1	111.8(2)	C15-C10-Cr1	121.29(8)
N1-P2-C4	114.7(2)	C7-C11-Cr1	72.64(8)
N1-P2-C5	117.1(2)	C7-C11-C16	126
N1-P2-C6	113.2(2)	C10-C11-Cr1	71.37(9)
C5-P2-C4	103.6(3)	C10-C11-C7	108
C5-P2-C6	102.9(3)	C10-C11-C16	126
C6-P2-C4	103.7(2)	C16-C11-Cr1	121.70(8)

31 crystalizes in the monoclinic space group $P2_1/n$. Similar to the previous structure, the nitride has been inserted into the P atom of dmpe. The Cr1-N1 bond length is 1.879(4) Å which is in the range of Cr-N single bonds.[66] There is one THF molecule coordinated to the chromium center because the crystallization has been done in the THF solvent. Similar to **30**, the formal oxidation state of +III can be assigned for **31**. The effective magnetic moment of these two compounds (**30** and **31**) was found to be 2.7 (1) μ_B when measured at room temperature, which is lower than the expected value of 3.8 μ_B for a Cr(III) d^3 metal center. This difference in the calculated and measured magnetic moment, can be the result of presence of impurities in the sample.

The ^{1}H-NMR of **29** in C_6D_6 at room temperature was monitored for 16 days to follow the changes that happen in the solution of **29**. The appearance of peaks is similar to the original proton NMR of **29** (**Figure 3.20**) but the chemical shift of the peak at 11.7 ppm shows a strange shift to the downfield and after that to the upfield during 16 days, as shown in **Figure 3.25**.

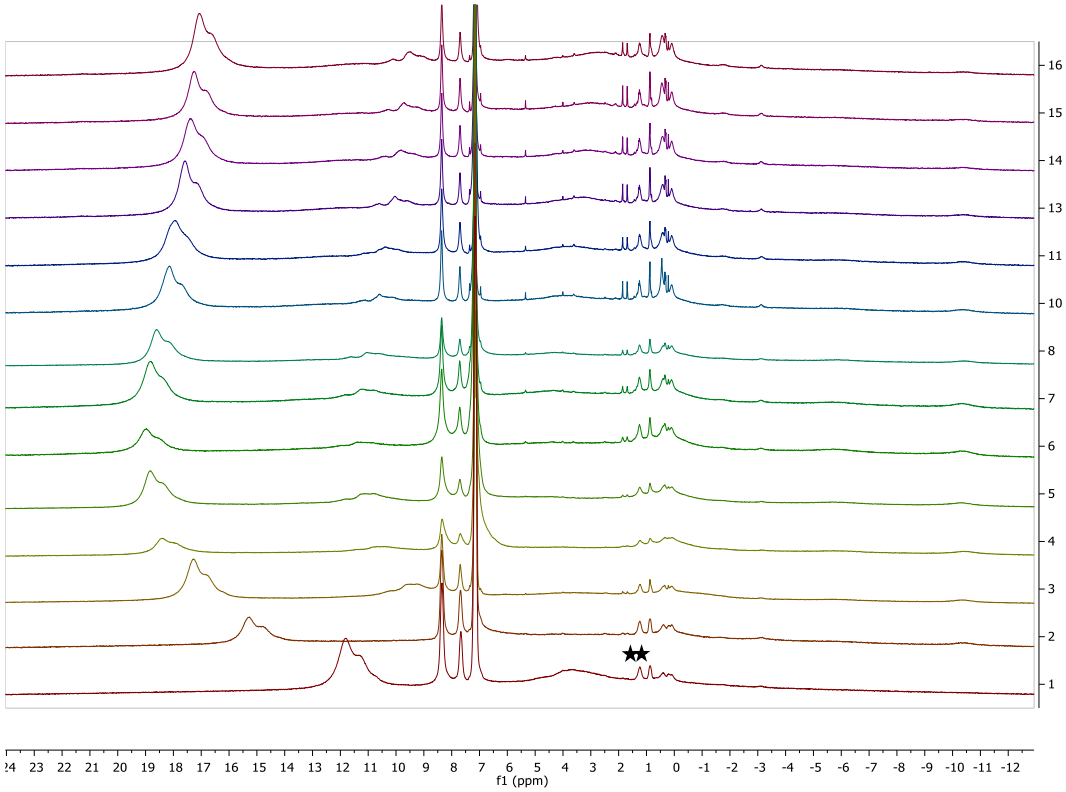

Figure 3.25 ^{1}H- spectrum of [(Cp*(dmpe)CrN]BAr$^{F}_{4}$ (**29**) recorded in C_6D_6 at 400 MHz was monitored for 16 days, at room temperature. The numbers on the right side of the spectra indicate the number of days from the beginning of the experiment. Black stars show the pentanes impurity peaks at 0.9 and 1.2 ppm.

To investigate the changes that happen with the cationic nitride complex in benzene, a separate large scale reaction was done. **29** was dissolved in benzene and after 2 days at room temperature, the solution turned from brown-purple to blue and some oily compound precipitated out. The solution above the oily precipitate was filtered and was kept in a vial at room temperature. After several days, a couple of crystals appeared on the sides of the vial. Determination of the structure by X-ray crystallography revealed it to be a chromium complex, i.e. [Cp*Cr(HNPMe$_2$CH$_2$CH$_2$PMe$_2$)F] BAr$^{F}_{4}$ (**32**). The

molecular structure of **32** is depicted in **Figure 3.26** while the corresponding interatomic distances and angles are listed in **Table 3.15**.

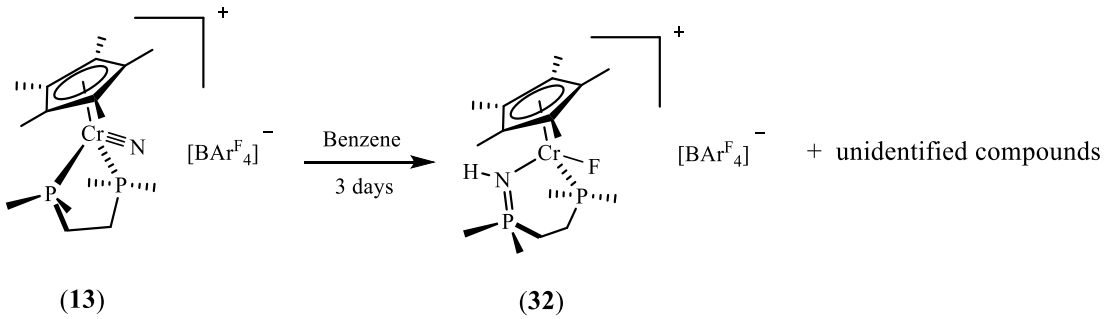

(**13**) (**32**)

Scheme 3.9 Synthesis of [Cp*Cr(HNPMe$_2$CH$_2$CH$_2$PMe$_2$)F] BAr$^F_4$ (**32**).

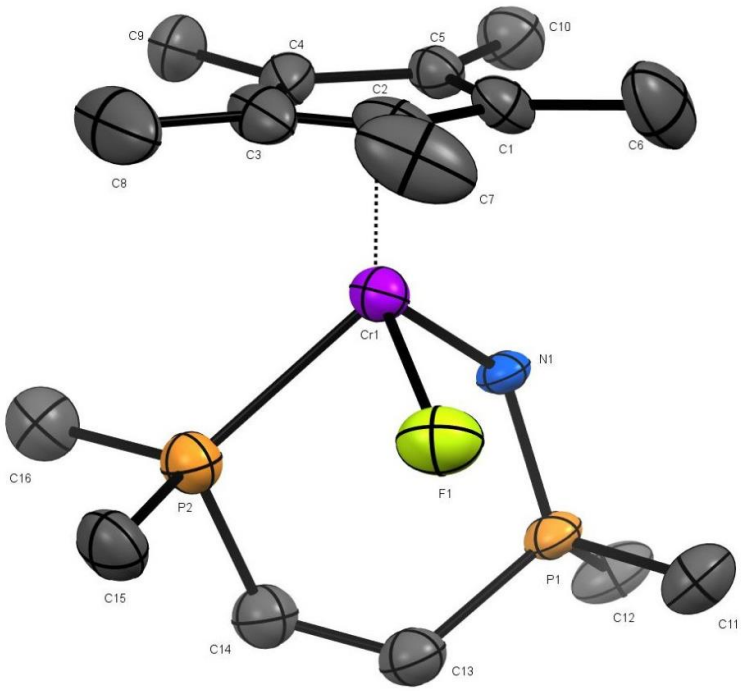

Figure 3.26 Molecular structure of [Cp*Cr(HNPMe$_2$CH$_2$CH$_2$PMe$_2$)F] BAr$^F_4$ (**32**) represented as 50% probability thermal ellipsoids. Hydrogen atoms and the counterion have been omitted for clarity.

Table 3.15 Interatomic distances (Å) and angles (º) for the cation of [Cp*Cr(HNPMe$_2$CH$_2$CH$_2$PMe$_2$)F] BAr$^F_4$ (**32**).

Distances (Å)

Cr1-C1	2.209(7)	C3-C4	1.428(12)
Cr1-C2	2.233(8)	C3-C8	1.508(12)
Cr1-C3	2.219(8)	C4-C5	1.420(10)
Cr1-C4	2.236(8)	C4-C9	1.495(12)
Cr1-C5	2.241(6)	C5-C10	1.489(10)
Cr1-P2	2.435(4)	P1-N1	1.609(6)
Cr1-F1	1.903(6)	P1-C11	1.785(10)
Cr1-N1	2.036(6)	P1-C12	1.765(9)
C1-C2	1.422(11)	P1-C13	1.841(10)
C1-C5	1.417(10)	P2-C14	1.848(10)
C1-C6	1.483(12)	P2-C15	1.800(9)
C2-C3	1.405(13)	P2-C16	1.781(10)
C2-C7	1.500(13)	C13-C14	1.490(14)

Angles (°)

C1-Cr1-C2	37.3(3)	C3-C2-Cr1	71.1(4)
C1-Cr1-C3	62.2(3)	C3-C2-C1	108.0(7)
C1-Cr1-C4	62.2(3)	C3-C2-C7	125.6(10)
C1-Cr1-C5	37.1(3)	C7-C2-Cr1	123.4(7)
C1-Cr1-P2	165.2(2)	C2-C3-Cr1	72.1(5)
C2-Cr1-C4	61.9(3)	C2-C3-C4	108.5(7)
C2-Cr1-C5	61.8(3)	C2-C3-C8	126.0(10)
C2-Cr1-P2	131.5(3)	C4-C3-Cr1	71.9(4)
C3-Cr1-C2	36.8(4)	C4-C3-C8	125.4(11)
C3-Cr1-C4	37.4(3)	C8-C3-Cr1	125.1(6)
C3-Cr1-C5	61.9(3)	C3-C4-Cr1	70.7(5)

C3-Cr1-P2	103.2(2)	C3-C4-C9	127.0(8)
C4-Cr1-C5	37.0(3)	C5-C4-Cr1	71.7(4)
C4-Cr1-P2	105.0(2)	C5-C4-C3	107.4(7)
C5-Cr1-P2	135.7(2)	C5-C4-C9	125.5(8)
F1-Cr1-C1	104.7(3)	C9-C4-Cr1	125.5(6)
F1-Cr1-C2	92.9(4)	C1-C5-Cr1	70.2(4)
F1-Cr1-C3	115.9(4)	C1-C5-C4	108.1(7)
F1-Cr1-C4	152.8(4)	C1-C5-C10	126.0(7)
F1-Cr1-C5	140.8(3)	C4-C5-Cr1	71.3(4)
F1-Cr1-P2	83.5(3)	C4-C5-C10	125.9(7)
F1-Cr1-N1	91.6(3)	C10-C5-Cr1	123.3(5)
N1-Cr1-C1	101.1(3)	N1-P1-C11	112.1(6)
N1-Cr1-C2	137.7(3)	N1-P1-C12	111.9(5)
N1-Cr1-C3	150.1(3)	N1-P1-C13	110.4(4)
N1-Cr1-C4	113.7(3)	C11-P1-C13	102.5(6)
N1-Cr1-C5	89.6(3)	C12-P1-C11	105.8(6)
N1-Cr1-P2	90.8(2)	C12-P1-C13	113.7(6)
C2-C1-Cr1	72.2(4)	C14-P2-Cr1	110.4(4)
C2-C1-C6	126.1(8)	C15-P2-Cr1	113.3(5)
C5-C1-Cr1	72.7(4)	C15-P2-C14	102.8(6)
C5-C1-C2	108.0(7)	C16-P2-Cr1	124.7(5)
C5-C1-C6	125.8(8)	C16-P2-C14	99.2(6)
C6-C1-Cr1	124.3(7)	C16-P2-C15	103.6(6)
C1-C2-Cr1	70.4(4)	P1-N1-Cr1	125.8(4)
C1-C2-C7	126.4(10)	C14-C13-P1	115.1(8)

In **32** the insertion of nitride into the chromium-phosphorus bond of the dmpe ligand, and coordination of one fluoride atom, makes a pseudo-octahedral geometry around the Cr1 center. The molecule shows that some of the fluorine atoms of the counterion suffer positional disorder over two sets of positions due to the low quality of the crystal, but the analysis of the structure shows that **32** crystallizes in the monoclinic space group $P2_1/c$. The Cr1-N1 bond length is 2.036(6) Å, which is in the range of Cr-N

single bond distances.[66,78] Further characterization of this compound was not possible due to the lack of pure material. This crystal was the only solid product that was separated from this reaction. Despite several attempts, from dissolving **29** in benzene only oily products precipitated out of the solution. In the IR spectrum of the blue product, a peak at 3388 cm^{-1} was observed which can be assigned to the stretching frequency of the N-H group of a phosphiniminato unit, as shown in **Figure 3.27**.

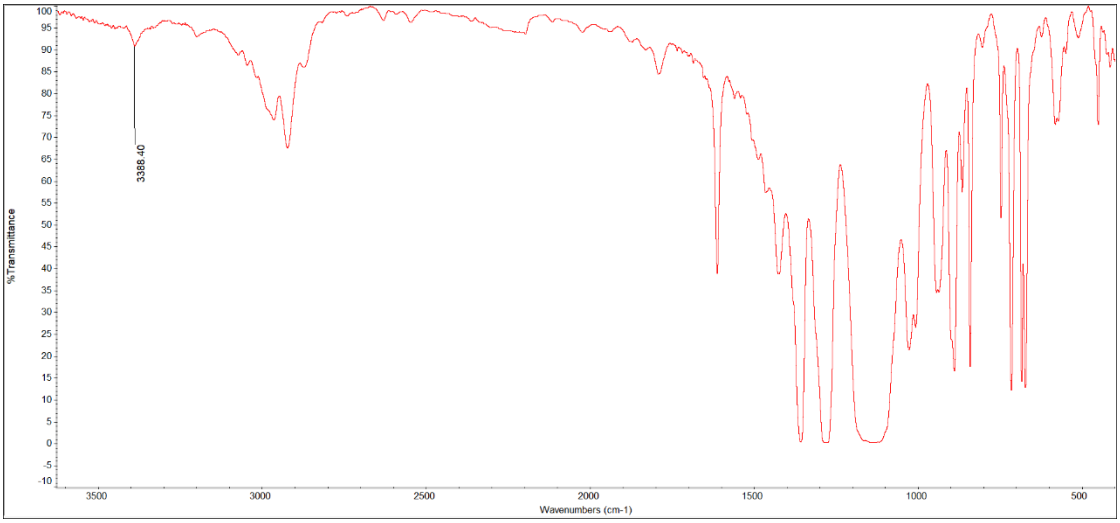

Figure 3.27 IR spectrum of the blue product resulted from dissolving **29** in benzene.

The LIFDI-MS analysis was done on the blue solution resulted from dissolving **29** in benzene. A peak with the mass of 371.37 which is the mass of **32**, was observed in the spectrum as shown in **Figure 3.28**. A hydrogen atom transfer happens on the nitrogen site of **32** to make the mass of 371.37, but it is not clear if it is happening before the fluoride transfer or after that. Using DFT calculations (at the UB3LYP level of density functional theory and the basis set of 6-31G(d)) the optimized structure of **32** was found to be in agreement with the crystal structure of this complex. With the existence of a hydrogen on the N atom of phosphiniminato ligand, the formal oxidation state of +III can

be assigned to this chromium complex. The calculated and experimental data for selected bond distances and angles of **32**, are shown in **Table 3.16**.

Table 3.16 Calculated and experimental data for selected bond distances and angles of **32**.

	Experimental	Calculation
Cr-N	2.036(6)	2.04338
N-P	1.609(6)	1.63054
Cr-P	2.435(4)	2.49028
Cr-F	1.903(6)	1.85722
Cr-N-P	125.8(4)	124.84773

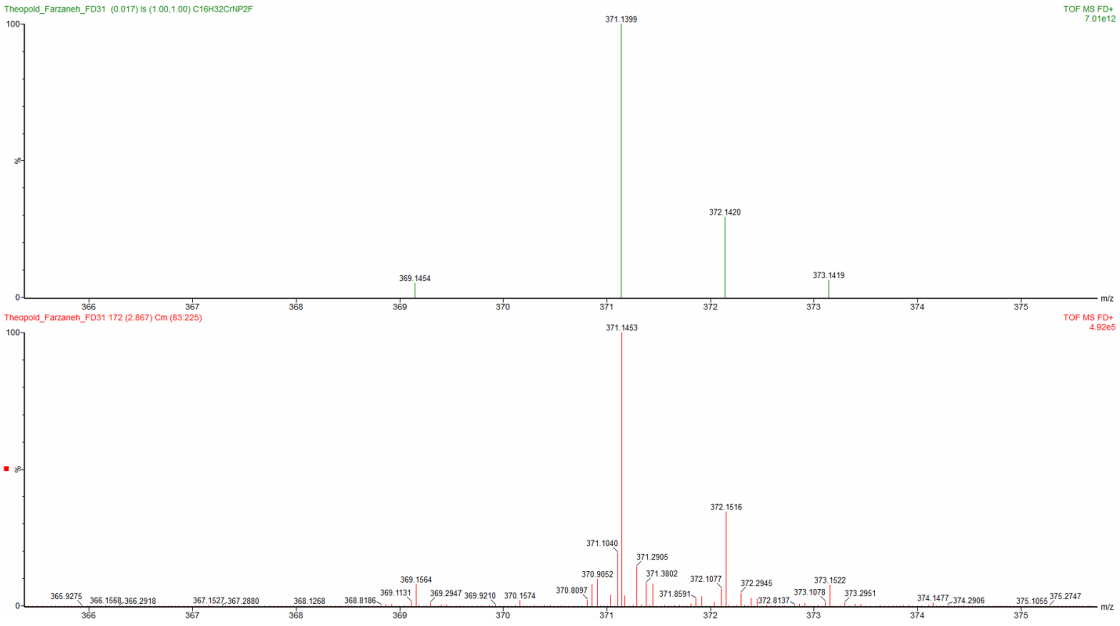

Figure 3.28 LIFDI-MS spectrum of the product of the decomposition of **29** in solution (bottom), predicted isotope pattern for a complex with a formula corresponding to **32** ($C_{16}H_{32}NFP_2Cr$ top).

There is another interesting peak in the LIFDI spectrum of this complex, with mass of 164, which is corresponding to the $N[PMe_2CH_2]_2$ fragment, which might be created during the LIFDI analysis.[32]

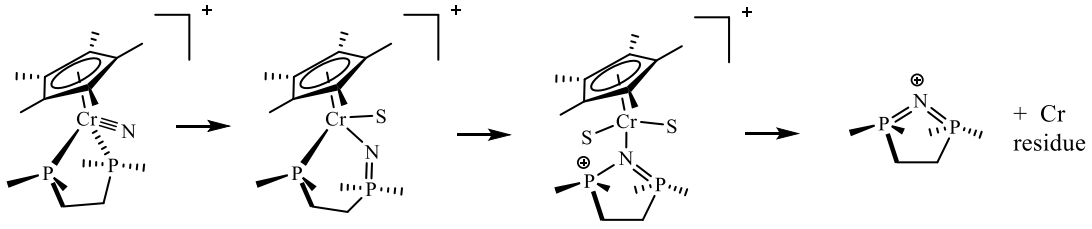

Scheme 3.10 Proposed mechanism for the production of $N[PMe_2CH_2]_2$ fragment.

Based on these results we can conclude that the cationic nitride complex is not stable in most solvents, even at room temperature. It decomposes to a blue compound which we know is the result of insertion of nitride to the P atom of the dmpe ligand. The Cr-N, N-P and Cr-C(Cp*) distances of **30**, **31** and **32** are listed in **Table 3.17**. For all three compounds the Cr-N bond distance falls in the range of single bond distances. [60,66] The N-P bond distance in **30** and **31** are very close and slightly longer than the N-P distance in **32**, but they all are in the range of typical N-P double bond distances.[116] The Cr-N distance in **32** is longer compared to the Cr-N bond distance in **30** and **31** due to the existence of a H atom on the nitrogen site of the coordinated ligand.

Table 3.17 Selected angle and bond lengths (Å) for **30**, **31**, and **32**.

	30	**31**	**32**
Cr-N-P	143.6(3)	144.4(2)	125.8(4)
Cr-N	1.796	1.879	2.036
N-P	1.564	1.537	1.609
Cr-P	2.43	2.44	2.435
Cr-F	-	-	1.903
Cr-O	-	2.111	-
Cr-C1	2.21	2.293	2.209
Cr-C2	2.223	2.296	2.233
Cr-C3	2.232	2.277	2.219
Cr-C4	2.252	2.264	2.236
Cr-C5	2.224	2.274	2.241
Avg Cr-C	2.2282	2.2808	2.2276

3.3 Conclusion

The neutral chromium nitride (**13**) and dinitrogen (**10**) complexes were studied in a variety of reactions, with the goal of finding a method to interconvert them. Both neutral dinitrogen and nitride complexes decompose upon heating. The dinitrogen complex decomposes to a mixture of unidentified complexes and the nitride to a dinuclear chromium complex with a bridging phosphiniminato ligand, i.e. [$Cp^*_2Cr_2(\mu,\mu$-$\{NP(CH_3)_2\}_2C_2H_4)$] (**19**). Reduction of the **10** produces new dinitrogen complexes, i.e. **20**, **21** and **23** with N≡N bond length shorter than the original neutral dinitrogen complex. From the oxidation of **10** and **13**, cationic dinitrogen and nitride complexes were synthesized, i.e. $[(Cp^*(dmpe)Cr)_2(\mu\text{-}N_2)]BAr^F{}_4$ (**25**), $[(Cp^*(dmpe)Cr)_2(\mu\text{-}N_2)](BAr^F{}_4)_2$ (**26**), and $[Cp^*(dmpe)CrN]BAr^F{}_4$ (**29**). The cationic nitride complex **29** is not stable in

most solvents, even at room temperature. It decomposes to a blue compound which we know is the result of insertion of nitride to the P atom of the dmpe ligand.

3.4 Experimental

General considerations

All reactions were done under a nitrogen atmosphere using standard Schlenk, vacuum line, and glove box techniques. Pentane, toluene, and diethyl ether were dried by passing through activated alumina columns followed by a nitrogen purge to remove dissolved oxygen. Tetrahydrofuran (THF) was dried under nitrogen gas by distillation over Na and benzophenone ketyl solution. C_6D_6 and THF-d_8 were dried over sodium and stored over Na/K alloy under vacuum. Organic chemicals were bought from Fischer, Aldrich, or Acros and all inorganic chemicals were purchased from Strem. Carbon monoxide gas was purchased from Matheson. Brookhart's acid, i.e. $[H(OEt_2)_2]^+[(3,5\text{-}(CF_3)_2C_6H_3)_4B]^-$ ($HBAr^F_4$), was synthesized according to literature procedures.[112,113] $FcBAr^F_4$ was synthesized according to the literature procedures.[114,115] NMR spectra were taken on a Bruker AVIII-400 spectrometer and were referenced to the residual protons of the solvent (C_6D_6, 7.16 ppm; THF-d_8, 3.58, 1.73 ppm). FT-IR spectra were recorded on a Nicolet Magna-IR 560 spectrometer with a resolution of 4 cm^{-1}. Magnetic susceptibilities (χm) were obtained in the solid state at room temperature using a Johnson Matthey magnetic susceptibility balance and corrected for diamagnetism using Pascal constants to give effective magnetic moments (μ_{eff}).[117] Mass spectra (LIFDI-MS) were obtained in the University of Delaware Mass Spectrometry Laboratory. X-ray crystallographic studies were conducted at the University of Delaware X-ray crystallographic facility. Elemental analyses were obtained from Robertson Microlit, Ledgewood, NJ 07852. The photochemical reactor was a Rayonet Model RPR100, equipped with 16 14W monochromatic 254nm low-pressure mercury vapor lamps.

3.4.1 Preparation of [Cp*$_2$Cr$_2$(μ,μ-{NP(CH$_3$)$_2$}$_2$C$_2$H$_4$)] (19): [Cp*(dmpe)Cr≡N] (**13**) (0.100 g, 0.285 mmol) was dissolved in 10 ml THF and transferred to an ampule under N_2 atmosphere in a glove box. The flask was then evacuated and brought out of the glove box and was heated at 85 °C with stirring for 24 hours. During this time the color of solution changed from purple to green. The flask was transferred to the box, the solvent was removed, and the residue was washed with cold pentanes. The green [Cp*$_2$Cr$_2$(μ,μ-{NP(CH$_3$)$_2$}$_2$C$_2$H$_4$)] extracted with diethyl ether, filtered and cooled to -30 °C to afford green crystals of desired product. (0.031 g, 40 % yield).

3.4.2 Alternative preparation of [Cp*$_2$Cr$_2$(μ,μ-{NP(CH$_3$)$_2$}$_2$C$_2$H$_4$)] (19): [Cp*dmpeCr≡N] (0.100 g, 0.285 mmol) was dissolved in 10 ml THF and transferred to a quartz ampule under N_2 atmosphere in a glove box. The flask was then evacuated and brought out of the glove box and was stirred for 24 hours while being irradiated with 254 nm UV light, during this time the color changed gradually from purple to green. The same procedure can be applied in glass ampule under 250 nm light. The workup of this compound is as described above with a higher yield of 95%. ^{1}H-NMR (400 MHz, C_6D_6): 1.1 (br, 6H), 4.8 (br, 15H), 5.4 (br, 2H) ppm; IR(KBr): 2970 (s), 2907 (m), 2853 (s), 1413 (w), 1372 (s), 1293 (s), 1280 (s), 1157 (s), 1111 (m), 1063 (w), 1026 (w), 918 (s), 853 (s), 834 (s), 782 (s), 733 (s), 698 (s), 638 (w), 619 (w), 546 (w), 492 (w), 440 (s) cm^{-1}; m.p. 170-175 °C; μ_{eff} (293 K) = 2.0 (1) μ_B; LIFDI-MS spectrum : m/z 552.1962 [M$^+$]. Calcd.: m/z 552.1946 [M$^+$]; UV-Vis (Et_2O): λ_{max} (ε): 278 (14788), 352 (3382), 379 (3733), 415 (2308), 511 (928), 656 (1240) nm (cm^{-1} M^{-1}). Anal. Calcd. For $C_{26}H_{46}P_2N_7Cr_2$: C, 56.51; H, 8.39; N, 5.07; Found C, 55.43; H, 7.94; N, 4.72.

3.4.3 Preparation of Na$_2$[Cp*dmpeCr(N$_2$)]$_4$ (20): 2 equivalents of Na metal chunks (0.025 g, 1.073 mmol) were added to the THF solution of [Cp*(dmpe)CrCl] (**9**) (0.200 g, 0.536 mmol) and the mixture was allowed to stir overnight to ensure the complete reduction of [Cp*(dmpe)CrCl] (**9**). The solution turned from brown to red-orange and a

white precipitate formed. The white solid was removed *via* filtration. The THF solvent was then removed under vacuum to yield an orange residue. The solid was extracted with pentanes and filtered to remove insoluble side products. The solid was recrystallized by cooling a saturated pentanes solution to -30 °C overnight to yield red orange crystals (0.085 g, 49 % yield). ^{1}H-NMR (400 MHz, C_6D_6) -28.4 (br, 2H), -15.2 (br, 6H), 11.0 (br, 6H), 18.6 (br, 2H), 21.8 (br, 15H) ppm. IR(KBr): 2960 (s), 2899 (s), 2850 (s), 1957 (s), 1888 (w), 1706 (m), 1677 (s), 1423 (s), 1374 (s), 1292 (m), 1276 (s), 1262 (m), 1170 (w), 1057 (m), 1026 (s), 922 (w), 889 (m), 684 (m), 627 (s), 592 (m), 514 (m), 496 (s) cm^{-1}; m.p. 210-215 °C; μ_{eff} (293K) = 1.6 (1) μ_B; LIFDI-MS spectrum : m/z 337.1305 [[Cp*Cr(dmpe)]$^+$]. Calcd.: m/z 337.1306 [[Cp*Cr(dmpe)]$^+$].

3.4.4 Preparation of [Cp*(dmpe)Cr(μ-N_2)Na(TMEDA)$_2$] (21): 2 equivalents of Na metal chunks (0.012 g, 0.536 mmol) was added to the THF solution of [Cp*(dmpe)CrCl] (**9**) (0.100 g, 0.268 mmol) and the mixture was allowed to stir overnight. During this time, the solution turned from brown to red-orange and a white precipitate formed. The white solid was removed *via* filtration. TMEDA (0.062 g, 0.536 mmol) was then added to the solution dropwise. The solution was allowed to stir for an additional hour. The solvent was removed under vacuum to yield an orange residue. The solid was extracted with pentanes and filtered to remove the side products. The solution was cooled to -30 °C overnight to yield red orange crystals of [Cp*(dmpe)Cr(μ-N_2)Na(TMEDA)$_2$] (**21**) (0.098 g, 59 % yield). ^{1}H-NMR (400 MHz, C_6D_6): 1.17 (br, 8H), 1.48 (br, 6H), 2.06 (s, 24H), 2.11 (br, 2H), 2.18 (s, 8H), 2.34 (br, 15H) ppm; IR(KBr): 2956 (m), 2882 (m), 2831 (m), 2786 (m),1942 (s) (tentatively assigned as the N_2 stretch of **21**),1879 (w),1771 (w), 1466 (w), 1416 (s), 1363 (m), 1296 (s), 1279 (m), 1255 (s), 1179 (s), 1157 (s), 1134 (s), 1101 (s), 1081 (s), 1038 (s), 1028 (s), 917 (m), 831 (s), 815 (s), 788 (s), 755 (w), 712 (s), 681(m), 655 (s), 641 (s), 620 (s), 604 (s), 571 (s), 565 (s), 546 (s), 524 (w), 459 (w) cm^{-1}; m.p. 65-72 °C; μ_{eff} (293K) = 0.8 (1) μ_B; LIFDI-MS Spectrum : m/z 337.1303 [[Cp*Cr(dmpe)]$^+$]. Calcd.: m/z 337.1306 [[Cp*Cr(dmpe)]$^+$]; UV-Vis (λ_{max} (Et_2O), ε): 278, 16165; 335, 8418; 561, 6839 (nm, cm^{-1} M^{-1}).

3.4.5 Preparation of [Cp*(dmpe)Cr(NNSiMe$_3$)] (22): 2 equivalents of TMSCl (0.026 g, 0.236 mmol) were added to a THF solution of [Cp*(dmpe)Cr(μ-N_2)Na(TMEDA)$_2$] (**21**) (0.147 g, 0.236 mmol). After the addition, the color of solution changed from orange to brown. The mixture was allowed to stir for an additional hour. After filtration, the solvent was removed under vacuum to yield a brown residue. The solid was extracted with pentanes and recrystallized by cooling a saturated pentanes solution to -30 °C overnight to yield brown crystals of [Cp*(dmpe)Cr(NNSiMe$_3$)] (**22**) (0.076 g, 73 % yield). ^{1}H-NMR (400 MHz, C_6D_6) 0.25 (s, 9H), 0.93 (d, $^2J_{PH}$ = 4.0 Hz, 6H), 1.31 (d, $^2J_{PH}$ = 8.0 Hz, 6H), 1.36 (m, 2H), 1.71 (m, 2H), 1.84 (s, 15H) ppm; IR(KBr): 2961 (m), 2895 (m), 2856 (m), 2717 (s), 2365 (m), 2332 (m), 2154 (m), 2044 (m), 1961 (m), 1889 (w), 1720 (s), 1645 (s), 1587 (w), 1556 (w), 1482 (s), 1451 (s), 1416 (m), 1376 (m), 1287 (s), 1274 (s), 1242 (s), 1127 (m), 1073 (s), 1022 (s), 929 (m), 886 (m), 863 (m), 828 (m), 746 (s), 715 (s), 689(s), 639 (m), 623 (s), 590 (s), 482 (s), 451 (s) cm^{-1}; m.p. 112-116 °C; LIFDI-MS Spectrum : m/z 337.1306 [[Cp*Cr(dmpe)]$^+$]. Calcd.: m/z 337.1306 [[Cp*Cr(dmpe)]$^+$]; UV-Vis (Et_2O): λ_{max} (ε): 270 (8812), 300 (7128), 872 (709) nm (cm^{-1} M^{-1}).

3.4.6 Preparation of [Cp*(dmpe)Cr(μ-N_2)Na(15-crown-5)] (23): 2 equivalents of Na metal chunks (0.012 g, 0.536 mmol) were added to a THF solution of [Cp*(dmpe)CrCl] (**9**) (0.100 g, 0.268 mmol) and the mixture was allowed to stir overnight. During this time, the solution turned from brown to red-orange and a white precipitate formed. The white solid was removed *via* filtration. 15-crown-5 (0.118 g, 0.536 mmol) was then added to the solution dropwise. The solution was allowed to stir for an additional hour. The solvent was removed under vacuum to yield an orange residue. The solid was washed with pentanes to remove the side products. The solid was recrystallized by cooling a saturated Et_2O solution to -30 °C overnight to yield red orange crystals (0.205 g, 63 % yield). ^{1}H-NMR (400 MHz, C_6D_6): 1.2 (m, 2H), 1.7 (br, 6H), 2.4 (br, 6H), 2.6 (s, 2H), 3.0 (s, 15H) ppm; IR(KBr): 2956 (m), 2882 (m), 2831 (m), 2786 (m),1942 (s) (tentatively assigned as

the N_2 stretch of **23**),1879 (w),1771 (w), 1466 (w), 1416 (s), 1363 (m), 1296 (s), 1279 (m), 1255 (s), 1179 (s), 1157 (s), 1134 (s), 1101 (s), 1081 (s), 1038 (s), 1028 (s), 917 (m), 831 (s), 815 (s), 788 (s), 755 (w), 712 (s), 681(m), 655 (s), 641 (s), 620 (s), 604 (s), 571 (s), 565 (s), 546 (s), 524 (w), 459 (w) cm-^{1}; m.p. 94-100 °C; μ_{eff} (293K) = 0.4 (1) $\mu_{B;}$ LIFDI-MS Spectrum : m/z 337.1310 [[Cp*Cr(dmpe)]$^{+}$]. Calcd.: m/z 337.1306 [[Cp*Cr(dmpe)]$^{+}$]; UV-Vis (Et_2O): λ_{max} (ε) 278 (16165), 335 (8418), 561 (6839), nm (cm^{-1} M^{-1}).

3.4.7 Preparation of [(Cp*(dmpe)Cr)$_2$(μ-N$_2$)](FB(C$_6$F$_5$)$_3$) (24): 2 equivalents of $B(C_6F_5)_3$ (0.292 g, 0.570 mmol) were added to a stirred diethyl ether solution of $[Cp^*(dmpe)Cr]_2(\mu\text{-}N_2)$ (**10**) (0.200 g, 0.285 mmol) piecewise. The solution turned from green-brown to maroon by the end of addition. The solution was allowed to stir for an additional hour. The solution was filtered, and the solvent was removed under vacuum to yield a maroon solid. The solid was washed with pentanes. The maroon solid was recrystallized by cooling a saturated diethyl ether solution to -30 °C overnight to yield dark maroon crystals (0.176 g, 50 % yield). ^{1}H-NMR (400 MHz, THF-d_8) -16.2 (br, 2H), -15.7 (br, 6H), -6.4 (br, 6H), -2.3 (br, 15H), 9.9 (br, 2H) ppm.

3.4.8 Preparation of [(Cp*(dmpe)Cr)$_2$(μ-N$_2$)]BAr$^{F}_4$ (25): 1 equivalent of $HBAr^{F}_4$ (0.288 g, 0.285mmol) was dissolved in Et_2O and was added to a stirred diethyl ether solution of $[Cp^*(dmpe)Cr]_2(\mu\text{-}N_2)$ (**10**) (0.200 g, 0.285 mmol) dropwise. During the addition bubbles (presumably hydrogen) evolved from the solution. The solution turned from green-brown to maroon by the end of addition. The solution was allowed to stir for 30 minutes. The solvent was then removed under vacuum to yield a maroon solid. The solid was washed with pentanes. The maroon solid was recrystallized by cooling a saturated diethyl ether solution to -30 °C overnight to yield dark maroon crystals (0.321 g, 72 % yield). ^{1}H-NMR (400 MHz, THF-d_8): -15.9 (br, 4H), -14.6 (br, 12H), -6.8 (br, 12H), -3.0 (br, 30H), 7.6 (s, 4H), 7.8 s, 8H), 10.4 (br, 4H) ppm; IR(KBr): 2972 (w), 2918 (w), 2856 (w), 1610 (s), 1425 (w), 1358 (s), 1279 (s), 1129 (w), 1027 (w), 934 (s), 886

(m), 868 (w), 839 (s), 805 (w), 744 (s), 715 (s), 684 (s), 669 (s), 621 (s), 529 (w), 453 (s) cm^{-1}; m.p. 135-140 °C; μ_{eff} (293 K) = 2.2 (1) μ_B; LIFDI-MS Spectrum : m/z 337.1357 [[Cp*Cr(dmpe)]$^+$]. Calcd.: m/z 337.1306 [[Cp*Cr(dmpe)]$^+$]; UV-Vis (Et_2O): λ_{max} (ε) 243 (22071), 344 (26947), 366 (28187), 481 (9556), 547 (7639), 785 (2500) nm (cm^{-1} M^{-1}). Anal. Calcd For $C_{64}H_{74}P_4N_2F_{24}BCr_2$: C, 49.09; H, 4.76; N, 1.79; Found C, 49.01; H,4.80; N, 1.24.

3.4.9 Preparation of [(Cp*(dmpe)Cr)$_2$(μ-N$_2$)](BAr$^F_4$)$_2$ (26): 2 equivalents of $HBAr^F_4$ (0.577 g, 0.570 mmol) were dissolved in 15 ml Et_2O and were added to a stirred diethyl ether solution of [Cp*(dmpe)Cr]$_2$(μ-N_2) (**10**) (0.200 g, 0.285 mmol) dropwise. During the addition gas bubbles (presumably hydrogen) evolved from the solution. After the addition of almost half of the acid the color changed from green- brown to maroon and after that a green solid started to precipitate out of the solution. The solution was allowed to stir for 10 minutes after the completion of addition. The green solid was collected *via* filtration. The solid was washed with 10 ml of pentanes and diethyl ether.

3.4.10 Alternative preparation of [(Cp*(dmpe)Cr)$_2$(μ-N$_2$)](BAr$^F_4$)$_2$ (26): $NaBAr^F_4$ (0.253 g, 0.285 mmol) was dissolved in 10 ml Et_2O and was added to a stirred diethyl ether solution of [Cp*(dmpe)CrCl] (0.106 g, 0.285 mmol) under a nitrogen atmosphere dropwise. The solution turned from brown to maroon. The solution was allowed to stir for another 30 minutes. The solution then was filtered, and the solvent was reduced under vacuum to make a concentrated solution. The solution was cooled down to -30 °C overnight, affording the desired green product (0.242 g, 70 % yield). ^{1}H-NMR (400 MHz, THF-d_8): -15.9 (br, 2H), -14.7 (br, 6H), -6.7 (br, 6H), -2.9 (br, 15H), 7.6 (s, 4H), 7.8 (s, 8H), 10.3 (br, 2H) ppm; IR(KBr): 2968 (w), 2923 (w), 2860 (w), 1614 (s), 1425 (s), 1358 (s), 1278 (s), 1127 (w), 1022 (w), 1002 (s), 951 (s), 934 (s), 891 (m), 840 (s), 807 (w), 748 (s), 715 (s), 684 (s), 672 (s), 580 (w), 533 (w), 453 (s) cm^{-1}; m.p. 145-150 °C; μ_{eff} (293 K) = 4.6 (1) μ_B. LIFDI-MS Spectrum : m/z 337.1307 [[Cp*Cr(dmpe)]$^+$]. Calcd.: m/z

337.1306 [[Cp*Cr(dmpe)]$^+$]; Anal. Calcd For $C_{96}H_{86}P_4N_2F_{48}B_2Cr_2$: C, 47.47; H, 3.57; N, 1.15; Found C, 47.49; H, 4.52; N, 0.75.

3.4.11 Preparation of [Cp*(dmpe)CrF]BAr$^F_4$ (27): 26 was dissolved (0.150 g, 0.062 mmol) in 10 ml THF and transferred to an ampule. The solution was heated to 70°C for 7 days and during this time the color of solution turned blue. After filtration, the solvent was removed, and the remaining residue was washed with pentanes and toluene. The extracts with Et_2O were combined and layered with pentanes and then stored at -30°C to get blue crystals of the product (0.060 g, 40% yield).). ^{1}H-NMR (400 MHz, C_6D_6): -57.0 (br), -25.7 (br), -15.9 (br), -8.5 (br), -4.2 (br), 7.7 (br), 8.4 (br) ppm; IR(KBr): 2987 (m), 2920 (w), 2870 (w), 1791 (s), 1613 (s), 1429 (m), 1359 (s), 1283 (w), 1136 (w), 942 (m), 899 (m), 893 (m), 874 (s), 841 (s), 802 (s), 745 (m), 686 (s), 671 (s), 653 (s), 579 (s), 553 (m), 542 (s), 475 (s), 446 (s), 430 (s) cm^{-1}; m.p. 105-112 °C; μ_{eff} (293 K) = 3.8 (1) μ_B. LIFDI-MS Spectrum : m/z 356.1290 [[Cp*(dmpe)CrF]$^+$]. Calcd.: m/z 356.1290 [[Cp*(dmpe)CrF]$^+$]; UV-Vis (Et_2O): λ_{max} (ε) 258 (10106), 344 (26947), 280 (7600), 405 (126), 518 (911), 589 (727) nm (cm^{-1} M^{-1}). Anal. Calcd For $C_{48}H_{43}P_2F_{25}BCr$: C, 47.27; H, 3.55; Found C, 47.09; H, 3.33.

3.4.12 Preparation of [Cp*(dmpe)CrCl]BAr$^F_4$ (28): 26 (0.150 g, 0.062 mmol) was dissolved in 10 ml CH_2Cl_2 and was allowed to stir at room temperature. After one day of stirring, the solution was filtered, and the solvent was removed under vacuum. The remaining purple powder was washed with pentanes and redissolved in Et_2O. The solid was recrystallized by cooling a saturated diethyl ether solution to -30 °C overnight to yield purple crystals (0.130 g, 85 % yield).). ^{1}H-NMR (400 MHz, THF-*d*$_8$): -54.8 (br), -34.5 (br), -26.9 (br), -22.9 (br), -12.5 (br), 7.6 (s), 7.8 (s) ppm; IR(KBr): 2978 (m), 2913 (m), 1613 (s), 1490 (m), 1425 (s), 1357 (s), 1283 (w), 1120 (w), 1028 (s), 997 (m), 948 (s), 938 (s), 9001 (s), 888 (s), 839 (s), 745 (s), 719 (s), 686 (s), 669 (s), 581 (m), 450 (s) cm^{-1}; m.p. 115-119 °C; μ_{eff} (293 K) = 3.8 (1) μ_B. LIFDI-MS Spectrum : m/z 372.0978 [[Cp*(dmpe)CrCl]$^+$]. Calcd.: m/z 372.0995 [[Cp*(dmpe)CrCl]$^+$]; UV-Vis (Et_2O): λ_{max} (ε)

271 (17489), 593 (1698) nm (cm^{-1} M^{-1}). Anal. Calcd For $C_{48}H_{43}P_2F_{24}BCrCl$: C, 46.64; H, 3.51 Found C, 45.44; H, 3.25.

3.4.13 Preparation of [(Cp*(dmpe)CrN]BAr^F_4 (29): $FcBAr^F_4$ (0.299 g, 0.285 mmol) was added to a stirred benzene solution of [Cp*dmpeCr≡N] (**13**) (0.100 g, 0.285 mmol) slowly. The solution turned from purple to brown-purple by the end of addition and some precipitation appeared in the flask. The solution was allowed to stir for another 10 minutes. The solution then was filtered to remove the ferrocene solution from the solid. The remining solid was washed with pentanes to remove the residual ferrocene. The solid was redissolved in minimal Et_2O, layered with pentanes and stored at -30°C for overnight to yield brown-purple crystals of [(Cp*(dmpe)CrN]BAr^F_4 (**29**) (0.294 g, 85 % yield). ^{1}H-NMR (400 MHz, C_6D_6): 3.67 (br), 7.7 (br), 8.4 (br), 10.7 (br), 11.2 (br), 11.8 (br) ppm; IR(KBr): 2975 (m), 2917 (m), 2872 (m), 1796 (s), 1610 (s), 1421 (m), 1358 (s), 1278 (s), 1122 (w), 1026 (w), 1000 (s), 975 (s), 948 (s), 936 (s), 918 (s), 901 (s), 889 (s), 840 (s), 745 (s), 713 (s), 683 (s), 671 (s), 651 (m), 619 (s), 580 (m), 449 (s), 403 (s) cm^{-1}; m.p. 195-200 °C; μ_{eff} (293 K) = 1.6 (1) μ_B; LIFDI-MS spectrum : m/z 351.1343 [[Cp*(dmpe)CrN]$^+$]. Calcd.: m/z 351.1337 [[Cp*(dmpe)CrN]$^+$]; UV-Vis (Benzene): λ_{max} (ε) 248 (11111), 270 (7383), 280 (6425), 303 (4030) nm (cm^{-1} M^{-1}). Anal. Calcd For $C_{48}H_{43}P_2NF_{24}BCr$: C, 47.47; H, 3.57; N, 1.15; Found C, 46.97; H, 3.44; N, 1.28.

3.4.14 Preparation of [Cp*Cr(NPMe$_2$CH$_2$CH$_2$PMe$_2$)]BAr^F_4 (30): [(Cp*(dmpe)CrN]BAr^F_4 (**29**) (0.100 g, 0.082 mmol) was dissolved in 5ml THF and transferred to an ampule under nitrogen atmosphere. The solution was heated at 50°C for 24 h. During this time, the color of solution changed from brown-purple to blue. After filtration, the solvent was removed under vacuum. The remaining blue compound was washed with pentanes and was redissolved in minimal amounts of Et_2O. The ethereal solution was layered with pentanes and was kept at -30°C. After one day the solution was transferred to a new vial to remove the oily precipitation. This process was repeated 5 times to get blue crystals of [Cp*Cr(NPMe$_2$CH$_2$CH$_2$PMe$_2$)] BAr^F_4 (**30**) (0.030 g, 30 %

yield). ^{1}H-NMR (400 MHz, THF-d_8): -24.5 (br), -18.6 (br), 6.3 (br) ppm; IR(KBr): 2989 (m), 2917 (m), 1789 (s), 1611 (s), 1425 (s), 1355 (s), 1283 (w), 1138 (w), 1026 (s), 1009 (s), 931 (m), 890 (m), 864 (s), 839 (s), 802 (s), 788 (s), 745 (s), 719 (s), 684 (s), 569 (m), 549 (s), 510 (m), 448 (m), 418 (m) cm^{-1}; m.p. 207-215 °C; μ_{eff} (293 K) = 2.7 (1) μ_B; LIFDI-MS spectrum : m/z 351.1360 [[Cp*(dmpe)CrN]$^{+}$]. Calcd.: m/z 351.1337 [[Cp*(dmpe)CrN]$^{+}$]; Anal. Calcd For $C_{48}H_{43}P_2NF_{24}BCr$: C, 47.47; H, 3.57; N, 1.15; Found C, 46.89; H, 3.47; N, 1.29.

3.4.15 Preparation of [Cp*Cr(NPMe$_2$CH$_2$CH$_2$PMe$_2$)THF] BAr$^{F}_4$ (31) : The same procedure as 31 for the synthesis. The crystallization is done by layering the THF solution with pentanes at low temperature to get the crystals of [Cp*Cr(NP)] BAr$^{F}_4$ (**31**) (0.037 g, 35% yield). ^{1}H-NMR (400 MHz, THF-d_8): -36.4 (br), -24.5 (br), -18.5 (br), -15.8 (br), 7.6(s), 7.8 (s), 56.4 (br), 103.6(br) ppm; IR(KBr): 2983 (m), 2872 (m), 1610 (s), 1425 (s), 1355 (s), 1277 (w), 1125 (w), 1027 (s), 1005 (s), 941 (m), 887 (m), 864 (s), 840 (s), 804 (s), 745 (s), 715 (s), 683 (s), 671 (s), 568 (m), 510 (m), 448 (m) cm^{-1}; m.p. 185-190 °C; μ_{eff} (293 K) = 2.7 (1) μ_B; LIFDI-MS spectrum : m/z 351.1373 [[Cp*(dmpe)CrN]$^{+}$]. Calcd.: m/z 351.1337 [[Cp*(dmpe)CrN]$^{+}$].

Chapter 4

DFT CALCULATIONS

4.1 Introduction

In order to gain more information about the interconversion between the dinitrogen and nitride isomers, Density Functional Theory (DFT) was used to calculate the relative free energies of dinitrogen and nitride complexes to identify the thermodynamic product of the interconversion reaction.

All the calculations were performed for chromium complexes with two different ligands i.e., Cp and Cp*. The Cp* ligand is a much stronger σ-donor compared to Cp, therefore by comparing the activation energy of the interconversion reaction for these two ligands, we will be able to gain more information about the effect of the coordination environment around the chromium complex on the interconversion reaction. Also, Cp is smaller than Cp* and therefore easier to calculate.

Gaussian 09 [118] was used to fully optimize all the structures at the B3LYP level of density functional theory with two different basis sets of 6-31G(d) and TZVP.

4.2 Results and Discussion

The calculations for optimization of $[Cp^*(dmpe)Cr]_2(\mu\text{-}N_2)$ (**10**), $[Cp^*(dmpe)Cr{\equiv}N]$ (**13**), $[(Cp^*(dmpe)Cr)_2(\mu\text{-}N_2)]BAr^F{}_4$ (**25**), $[(Cp^*(dmpe)Cr)_2(\mu\text{-}N_2)](BAr^F{}_4)_2$ (**26**), and $[Cp^*(dmpe)Cr{\equiv}N]BAr^F{}_4$ (**29**) were done at the UB3LYP level with the basis sets of TZVP and 6-31G(d). The same calculations were done for their

isomers with Cp ligand, i.e., **10′**, **13′**, **25′**, **26′**, and **29′**, as shown in **Table 4.1**. The multiplicity of **13** and **13′** was considered to be 1 and 2 respectively. For the cationic nitride complexes **29** and **29′**, the formal oxidation state of chromium metal is +V, therefore the multiplicity of 2 was used for the calculations. To find the multiplicities of the rest of molecules, calculations were performed on Cp isomers, to reduce the computational cost and the results were applied to the Cp* isomers.

The formal oxidation state of chromium center in dinitrogen complexes **10** and **10′** is +I, and multiplicities of 1, 3, 5, 7, 9, or 11 are possible for these molecules. For complex **10′**, the calculations were performed for all possible multiplicities and the calculations for the structures with multiplicities of 1, 3, 5, 7 and 11 converged. Among all these multiplicities, only the multiplicities of 1 and 3 showed the correct structure of the dinitrogen complex. The structure with the multiplicity of 1 has a slightly higher (about 9 kcal) E_0 (the total electronic energy) compared to the same structure with multiplicity of 3. On the other hand, since we know complex **10** is paramagnetic, the multiplicity of 1 can be ruled out for this complex. The magnetic moment of **10** was found to be 2.0 (1) μ_B at room temperature.

The same method was used to find the multiplicity of mono and dicationic dinitrogen complexes. For **25**/**25′** the multiplicities of 2 and 4 converged successfully. The multiplicity of 4 was used for the rest of calculations since the E_0 was lower for structures with multiplicity of 4. For the same reason, the multiplicity of 5 was considered for **26**/**26′.**

Table 4.1 Calculated bond distance (Å) and angle (°) for **10**, **13**, **25**, **26**, and **29** and their Cp version. E_0 (Hartree) = the total electronic energy. ^{4}**25** (4= multiplicity) did not converged with TZVP basis set.

Bond distance (Å) and angle (°)		^{3}10	^{1}13	^{4}25	^{5}26	^{2}29
TZVP	E_0	-4821.330175	-2410.6436722	-	-4820.9650545	-2410.4656741
	Cr-N	1.8687	1.5648	-	1.8727	1.5568
	N-N	1.1861	-	-	1.18274000	-
	Av. Cr-P	2.3553	2.3517	-	2.4993625	2.4500
	Av. Cr-N-N	177.2476	-	-	179.0247	-
6-31G(d)	E_0	-4820.600635	-2410.2833181	-4820.47702	-4820.2522682	-2410.1136518
	Cr-N	1.8526	1.5553	1.860505	1.8545	1.5440
	N-N	1.1992	-	1.1924	1.1960	-
	Av. Cr-P	2.3365	2.3360	2.4122	2.4882	2.4397
	Av. Cr-N-N	176.7334	-	177.5753	179.0034	-
Bond distance (Å) and angle (°)		^{3}10'	^{1}13'	^{4}25'	^{5}26'	^{2}29'
TZVP	E_0	-4428.060545	-2214.0029212	-4427.91899	-4427.6680343	-2213.8126983
	Cr-N	1.8369	1.5592	1.8369	1.698025	1.5506
	N-N	1.1778	-	1.16748	1.1749	-
	Av. Cr-P	2.3333	2.3374	2.3333	2.4684	2.4304
	Av. Cr-N-N	178.8606	-	178.8659	175.023375	-
6-31G(d)	E_0	-4427.454170	-2213.7040593	-4427.32183	-4427.0795279	-2213.5227502
	Cr-N	1.8201	1.5506	1.8325	1.8233	1.5385
	N-N	1.1901	-	1.18165	1.1874	-
	Av. Cr-P	2.3155	2.3216	2.3907	2.4582	2.4209
	Av. Cr-N-N	178.6976	-	176.7153	174.4106	-

The DFT calculations accurately reproduced the solid-state geometries of **10**, **13**, **25**, **26**, and **29**. The computed structural details are in reasonable agreement (difference is less than 0.02 Å for the distances and 3.3 ° for the angles) with the experimental parameters. Error in some cases might be due to comparison of the geometrical parameters calculated in gas phase with those obtained experimentally in solid state.

By comparing the bond distances and angles of the optimized structures of **10**, **13**, **25**, **26**, and **29** with the experimental results from X-ray crystallographic, it was concluded that the outcomes from the calculations with the basis set of 6-31G(d) are closer to the experimental structural data compared to TZVP. Also, the structures from basis set of 6-31G(d) have lower E_0.

The DFT calculations on dinitrogen (**10**) and nitride (**13**) complexes showed that the dinitrogen complex is the thermodynamic product of the interconversion process. In other words, the combination of two nitrides to make a dinitrogen complex is the thermodynamically favorable reaction. The energy (E_0) difference between **10** and two nitrides (**13***2) was calculated to be 21.3 kcal.

To suggest a structure for the transition state, calculations were done with the basis set of 6-31G(d). A zigzag dimeric structure was proposed as the transition state in the conversion of two nitrides to the dinitrogen complex **10**, as shown in **Scheme 4.1**. This type of transition state has been reported before based on DFT calculations.[28,29,52,119] The calculated structure of the transition states for both Cp and Cp* systems are very similar as shown in **Figure 4.1**. The Cr-N bond distances in **TS** and **TS′** are in the range of Cr-N double bond distances and N-N bond in the range of single bond distances.[66,81]

It should be mentioned that the optimization calculations for the **TS** and **TS′** were done for both multiplicities of 1 and 3. The imaginary frequency of the optimized

structure, was more negative for the multiplicity of 1 compared to the multiplicity of 3. Also, the transition state with multiplicity of 1 has lower E_0 (21.8 kcal for Cp* and 23.5 kcal for Cp systems, ΔE_0=1.7 kcal) compared to the transition state structure with multiplicity of 3, as shown in **Table 4.2**. Based on these results, the optimized structures of transition state with multiplicity of 1 were used for future calculations.

Table 4.2 TS and TS′ comparison. E_0 is in Hartree.

	TS	***TS'***
Imaginary frequency M=1	-757.81	-741.8
Imaginary frequency M=3	-	-81.09
E_0 for M=1	-4820.506941110	-4427.356657130
E_0 for M=3	-4820.472095	-4427.319102
ΔE_0	0.034845640	0.037554840
ΔE_0(kcal)	21.86595271	23.56600009

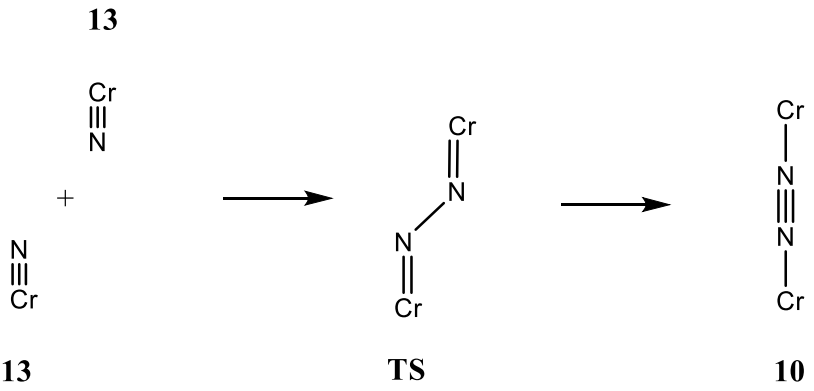

Scheme 4.1 Proposed mechanism for the coupling of two nitrides to make a dinitrogen complex.

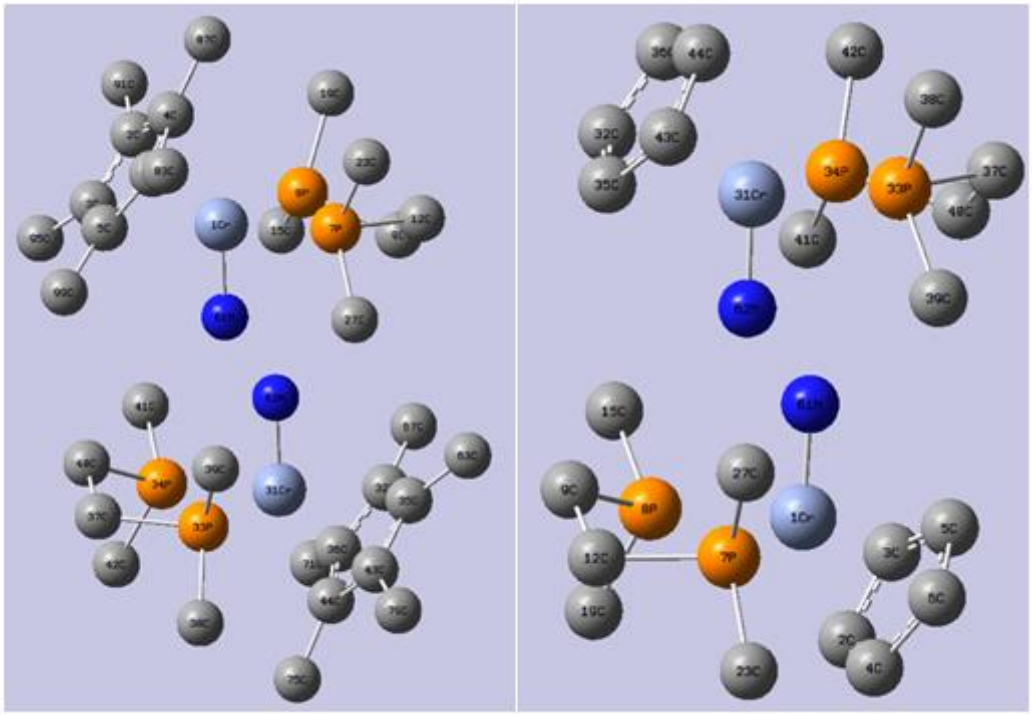

Figure 4.1 Calculated structures of TS (a) and TS′ (b).

Table 4.3 Selected bond distance (Å) and angles(°) for TS and TS′ (Multiplicity of 1).

Bond distance (Å) and angle (°)	TS	TS'
N-N	1.76206	1.71075
Av. Cr-N	1.67359	1.62733
Av. Cr-N-N	151.12184	143.354

The free energy of activation for the N-N coupling step that forms the dinitrogen complex, in the Cp* ligand platform, was calculated to be 56.4 kcal/mol, as shown in **Figure 4.2**. This amount of energy is considerable and is in agreement with the experimental results since the conversion of nitride complex to the dinitrogen was not observed even at high temperatures (Chapter 3, pages 141-148) . Instead, the insertion of N atom into the P atom of dmpe ligand happened upon heating **13** to produce the dinuclear chromium complex, i.e. [$Cp^*_2Cr_2(\mu,\mu\text{-}\{NP(CH_3)_2\}_2C_2H_4)$] (**19**). This might be the result of lower activation energy for the conversion of **13** to **19** compared to the conversion of two nitrides (2***13)** to **10**.

For the Cp platform, the free energy of activation was found to be 47.0 kcal/mol, which is lower than the Cp* platform. One reason can be the steric hindrance for the Cp* compared to the Cp ligand platform. The methyl groups on the Cp* ring can prevent the two nitride complexes to decrease their distance and couple easily.

Table 4.4 Calculated thermochemistry values from Gaussian for the reaction of two nitrides to make dinitrogen complex at 298.15 K. Al the values are in Hartree.

6-31g(d)	^{3}10	^{3}10'	^{1}13	^{1}13'	^{1}TS	^{1}TS'
E_0	-4820.6006348	-4427.4541700	-2410.2833181	-2213.7040593	-4820.50694111	-4427.3566
E_{ZPE}	0.88308300	0.60138500	0.43918700	0.30013000	0.88143800	0.60108100
E_{tot}	0.93895705	0.64173103	0.46723314	0.31947271	0.93710050	0.64031113
H_{corr}	0.93990100	0.64267400	0.46817800	0.32041700	0.93804500	0.64125400
G_{corr}	0.79869800	0.52683000	0.38362000	0.25430200	0.79736100	0.53206200
E_0+E_{ZPE}	-4819.71755183	-4426.85278505	-2409.84413118	-2213.4039293	-4819.62550311	-4426.75557
E_0+E_{tot}	-4819.66167778	-4426.81243902	-2409.81608504	-2213.3845866	-4819.56984061	-4426.71634
E_0+H_{corr}	-4819.66073383	-4426.81149605	-2409.81514018	-2213.3836423	-4819.56889611	-4426.71540
E_0+G_{corr}	-4819.801937	-4426.92734	-2409.899698	-2213.449757	-4819.70958	-4426.82459

E_{ZPE} = zero-point energy of the molecule.
E_{tot} = total internal energy (Et + Er + Ev + Ee).
G_{corr} = correction to the Gibbs free energy due to internal energy.
H_{corr} = correction to the enthalpy due to internal energy.

Table 4.5 Computed activation parameters and reaction thermodynamics (free energies and enthalpies in kcal/mol) for the reaction of two nitrides to make the dinitrogen complex.

	ΔG	ΔH	$\Delta G^{‡}$	$\Delta H^{‡}$
13*2	-1.59	-19.11	56.36	38.52
13'*2	-17.46	-27.74	47.01	32.56

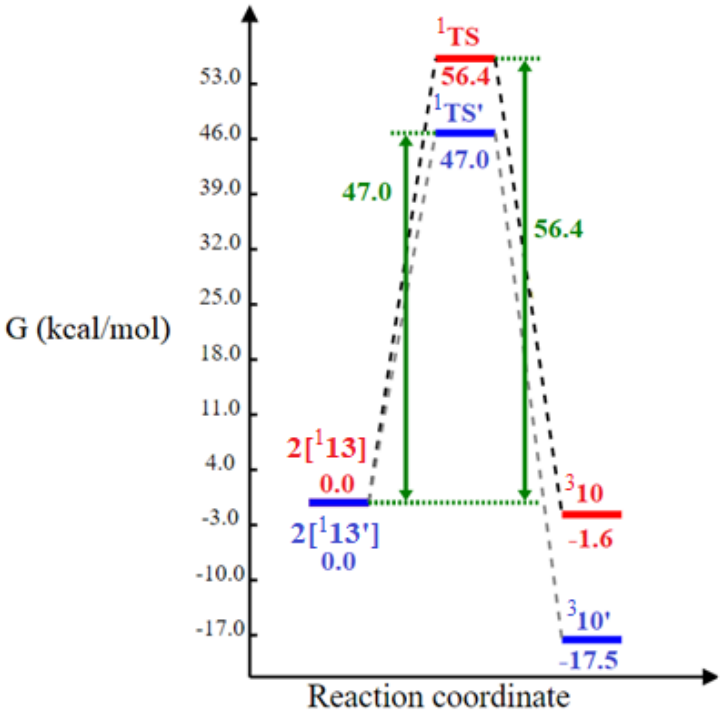

Figure 4.2 Activation enthalpy profiles for the conversion of nitride complexes to the dinitrogen complex.

The Intrinsic Reaction Coordinates (IRC) calculations using B3LYP functional and the basis set 6-31G(d) was done and the results supported the proposed structure for the transition state of the reaction. In the IRC method, the transition state is connected to the reactant and product by a fast descend path. IRC also can be defined as the minimum energy reaction pathway (MERP) between the transition state of a reaction and its reactants and products. The initial geometry given in the calculation is the transition state structure (with the highest energy in the path) and the reaction can be followed for the forward (to the product) or reverse (to the reactants) path. For the forward reaction, the

reaction coordinate is positive and for the reverse it is negative. The IRC path of the TS is shown in **Figure 4.3**. The optimized structures from the forward and reverse path, matched with the original optimized structures of **13** and **10** and the energy difference (E_0) between the optimized structures and the structures from IRC calculations, is less than 0.5 ev (Comparing **10** from IRC path with **10** from optimization and etc. The energy difference between the reactant and the product i.e., E_{010}-E_{013}, cannot be compared with the energy difference that we get from the optimized structures). The only thing that we get from these graphs is to find out if the reaction is going in a correct direction, in other words, is combining two nitrides can make the dinitrogen complex or not. The same calculation was performed for Cp platform as shown in **Figure 4.4**.

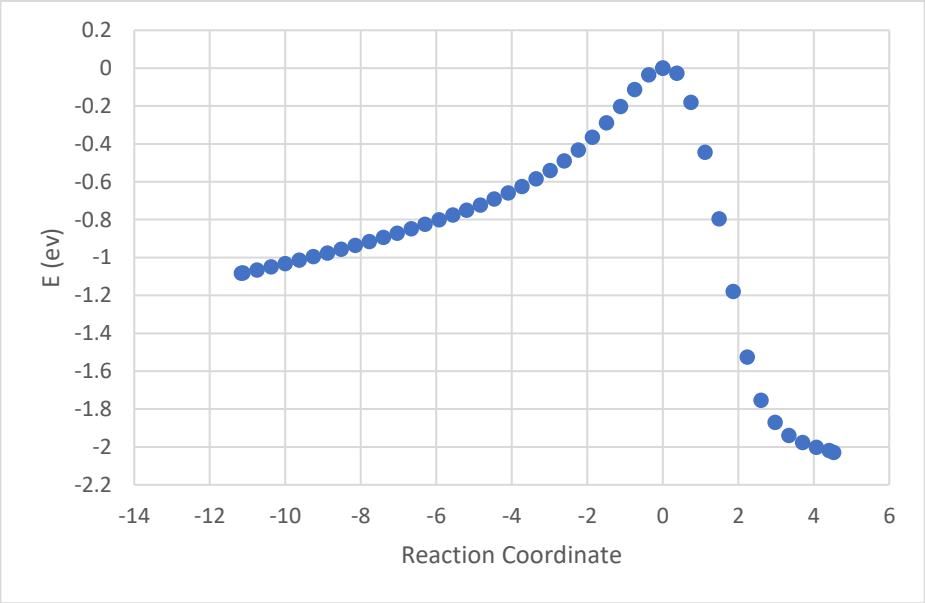

Figure 4.3 IRC path for the reaction of two **13** molecules to make **10**.

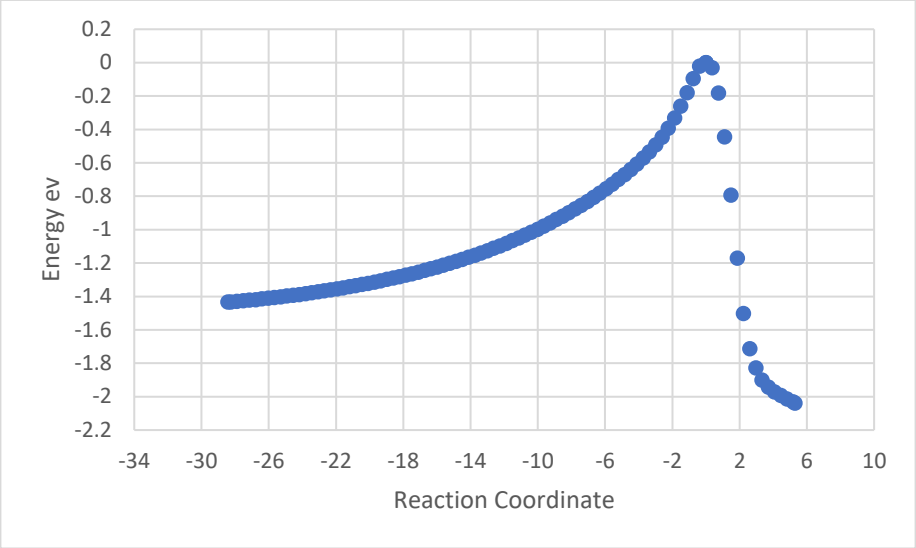

Figure 4.4 IRC path for the reaction of two **13′** molecules to make **10′**.

Natural Bond Orbital (NBO) calculations[120] were done for **10**, **10′**, **13**, **13′**, **TS** and **TS′**. In **Table 4.6**, the atomic charges of the atoms from the Natural Population Analysis (NPA) are shown. The N atom in **13** is more negative compared to the **13′**, which can lead to a higher free energy of activation due to the higher repulsion between the two nitrogen atoms during the coupling reaction. P atom possesses the largest positive charge in all molecules and in the nitride structures, the N atoms possess the largest negative charge.

Table 4.6 NPA charges on selected atoms of Nitride, Transition state and the Dinitrogen complexes. There is an inversion center in dinitrogen and TS complexes, therefore only half of the molecule is shown in the table.

Atom(s)	13'	13	TS'	TS	10'	10
Cr	0.08014	0.15861	0.16520	0.28838	0.20718	0.35100
N	-0.30568	-0.33784	-0.33002	-0.37959	-0.24575	-0.29781
P1	1.09116	1.06966	1.07303	1.04429	1.04061	1.00620
P2	1.08141	1.05883	1.08484	1.06030	1.04949	1.01961

Qualitative representations of the highest occupied and lowest unoccupied molecular orbitals for complexes **10**, **13**, **TS**, **10′**, **13′** and **TS′** are presented in **Figure 4.5** and the energies (E_0) of the relevant frontier orbitals are also shown in **Figure 4.6**. The highest occupied MO of **13**, **TS** and **10** is mainly *d* orbitals of chromium metal with small contribution of *p* orbitals of dmpe ligand in **13**, *s* orbitals of N^{2-} ligand in TS and *p* orbitals of N_2 ligand in **10**. In **13** The LUMO is localized on the s and p orbitals of Cr atom with significant contribution of the *s* orbitals of the dmpe ligand. The LUMO in TS is mainly made of *d* and *p* orbitals of Cr atom and N ligand respectively, and in the dinitrogen complex it is mainly the *p* and *d* orbitals of Cr metal. The value of the energy separation between the HOMO and LUMO of **TS** is smaller than that of **10** and **13**.

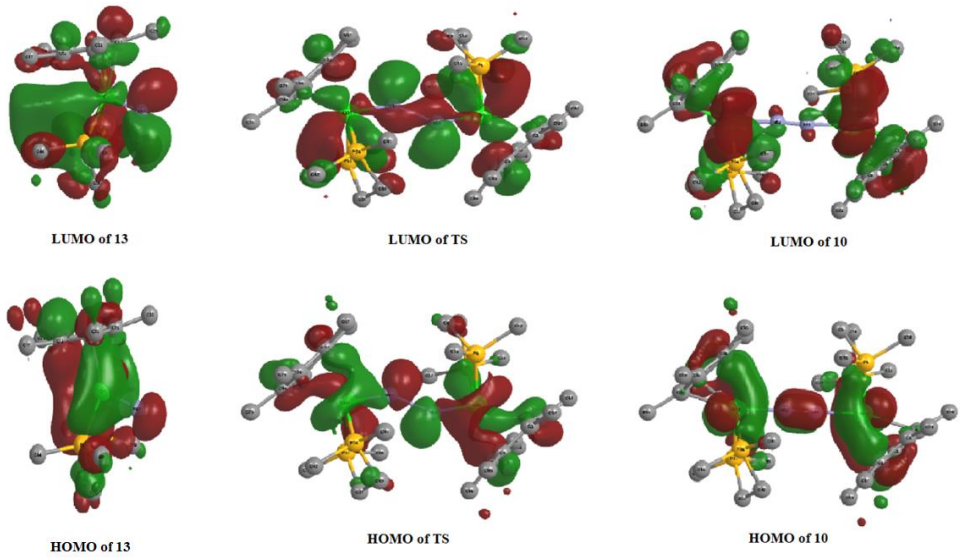

Figure 4.5 Qualitative frontier molecular orbitals for **13**, **TS** and **10**.

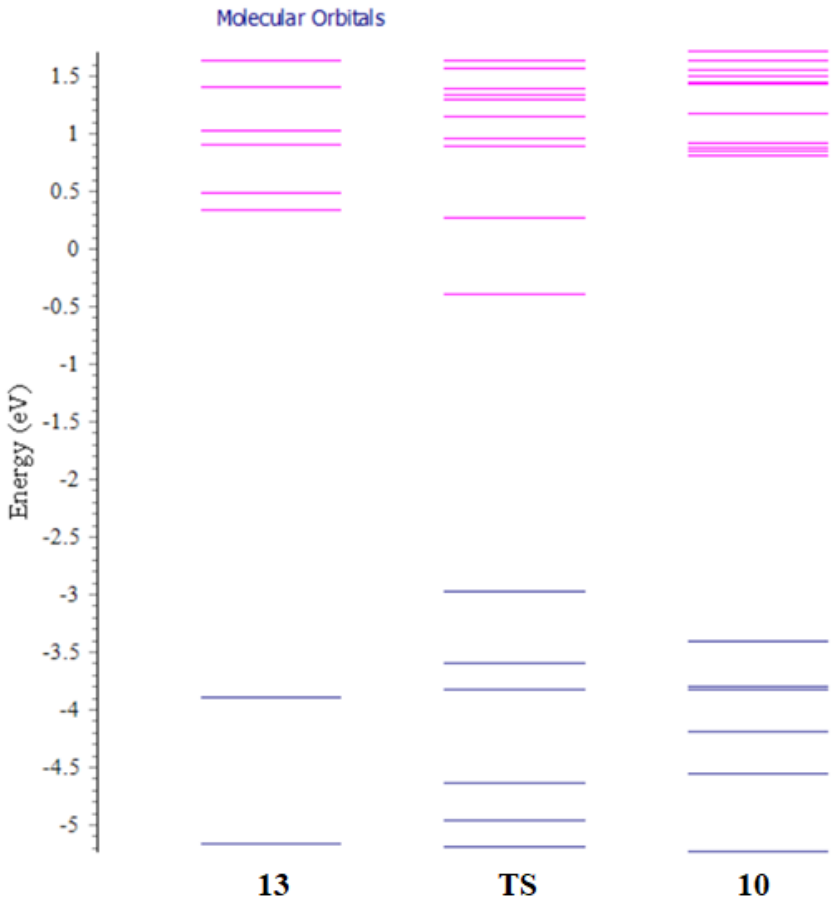

Figure 4.6 The energies (E_0)of the relevant frontier orbitals of **13**, **TS** and **10**.

4.3 Conclusion

The optimized structures of $[Cp^*(dmpe)Cr]_2(\mu\text{-}N_2)$ (**10**), $[Cp^*(dmpe)Cr{\equiv}N]$ (**13**), $[(Cp^*(dmpe)Cr)_2(\mu\text{-}N_2)]BAr^F{}_4$ (**25**), $[(Cp^*(dmpe)Cr)_2(\mu\text{-}N_2)](BAr^F{}_4)_2$ (**26**), and $[Cp^*(dmpe)Cr{\equiv}N]BAr^F{}_4$ (**29**) were calculated. The same calculation was performed on the Cp analges of these complexes. The optimized structures are in agreement with the crystallographic structural data. The dinitrogen complex was determined to be the thermodynamic product in the interconversion reaction. The structure of the transition state was calculated to be a zigzag structure of Cr-N-N-Cr fragments. The free energy of activation for both Cp* and Cp ligand platform was calculated to be 56.4 and 47.0 kcal/mol, respectively. The higher free activation energy for the Cp* ligand can be related to the steric hindrance around the nitride complex and the higher negative charge on the nitride ligand in Cp* platform. These results are in agreement with the experimental findings, since the coupling of the nitride complexes to make the dinitrogen complex was not observed experimentally even at high temperatures.

REFERENCES

(1) Rosca, V.; Duca, M.; DeGroot, M. T.; Koper, M. T. M. Nitrogen Cycle Electrocatalysis. *Chem. Rev.* **2009**, *109* (6), 2209–2244. https://doi.org/10.1021/cr8003696.

(2) Schendzielorz, F.; Finger, M.; Abbenseth, J.; Würtele, C.; Krewald, V.; Schneider, S. Metal-Ligand Cooperative Synthesis of Benzonitrile by Electrochemical Reduction and Photolytic Splitting of Dinitrogen. *Angew. Chemie - Int. Ed.* **2019**, *58* (3), 830–834. https://doi.org/10.1002/anie.201812125.

(3) Shima, T.; Luo, G.; Hu, S.; Luo, Y.; Hou, Z. Experimental and Computational Studies of Dinitrogen Activation and Hydrogenation at a Tetranuclear Titanium Imide/Hydride Framework. *J. Am. Chem. Soc.* **2019**, *141* (6), 2713–2720. https://doi.org/10.1021/jacs.8b13341.

(4) Field, L. D.; Li, H. L.; Dalgarno, S. J.; McIntosh, R. D. Ammonia and Hydrazine from Coordinated Dinitrogen by Complexes of Iron(0). *Eur. J. Inorg. Chem.* **2019**, *2019* (14), 2006–2011. https://doi.org/10.1002/ejic.201900058.

(5) Adli, N. M.; Zhang, H.; Mukherjee, S.; Wu, G. Review—Ammonia Oxidation Electrocatalysis for Hydrogen Generation and Fuel Cells. *J. Electrochem. Soc.* **2018**, *165* (15), J3130–J3147. https://doi.org/10.1149/2.0191815jes.

(6) Ren, X.; Zhao, J.; Wei, Q.; Ma, Y.; Guo, H.; Liu, Q.; Wang, Y.; Cui, G.; Asiri, A. M.; Li, B.; Tang, B.; Sun, X. High-Performance N2 -to-NH3 Conversion Electrocatalyzed by Mo2C Nanorod. *ACS Cent. Sci.* **2019**, *5* (1), 116–121. https://doi.org/10.1021/acscentsci.8b00734.

(7) Bhattacharya, P.; Heiden, Z. M.; Chambers, G. M.; Johnson, S. I.; Bullock, R. M.; Mock, M. T. Catalytic Ammonia Oxidation to Dinitrogen by Hydrogen Atom Abstraction. *Angew. Chemie - Int. Ed.* **2019**, *58* (34), 11618–11624. https://doi.org/10.1002/anie.201903221.

(8) Little, D. J.; Smith, M. R.; Hamann, T. W. Electrolysis of Liquid Ammonia for Hydrogen Generation. *Energy Environ. Sci.* **2015**, *8* (9), 2775–2781.

https://doi.org/10.1039/c5ee01840d.

(9) Little, D. J.; Edwards, D. O.; Smith, M. R.; Hamann, T. W. As Precious as Platinum: Iron Nitride for Electrocatalytic Oxidation of Liquid Ammonia. *ACS Appl. Mater. Interfaces* **2017**, *9* (19), 16488–16494. https://doi.org/10.1021/acsami.7b02639.

(10) David, W. I. F.; Makepeace, J. W.; Callear, S. K.; Hunter, H. M. A.; Taylor, J. D.; Wood, T. J.; Jones, M. O.; Facility, I.; Oxford, H.; Ox, D. Hydrogen Production from Ammonia Using Sodium Amide. **2014**. https://doi.org/10.1021/ja5042836.

(11) Chen, J. S. Nitrogen Fixation. In *Handbook on Clostridia*; 2005; pp 261–276. https://doi.org/10.1201/9780429445651-41.

(12) Doyle, L. R.; Wooles, A. J.; Liddle, S. T. Bimetallic Cooperative Cleavage of Dinitrogen to Nitride and Tandem Frustrated Lewis Pair Hydrogenation to Ammonia. *Angew. Chemie - Int. Ed.* **2019**, *58* (20), 6674–6677. https://doi.org/10.1002/anie.201902195.

(13) Pool, J. A.; Lobkovsky, E.; Chirik, P. J. Hydrogenation and Cleavage of Dinitrogen to Ammonia with a Zirconium Complex. *Nature* **2004**, *427* (6974), 527–530. https://doi.org/10.1038/nature02274.

(14) Bhutto, S. M.; Holland, P. L. Dinitrogen Activation and Functionalization Using β-Diketiminate Iron Complexes. *Eur. J. Inorg. Chem.* **2019**, *2019* (14), 1861–1869. https://doi.org/10.1002/ejic.201900133.

(15) Habibzadeh, F.; Miller, S. L.; Hamann, T. W.; Smith, M. R. Homogeneous Electrocatalytic Oxidation of Ammonia to N 2 under Mild Conditions. *Proc. Natl. Acad. Sci. U. S. A.* **2019**, *116* (8), 2849–2853. https://doi.org/10.1073/pnas.1813368116.

(16) Chakraborty, J.; Mandal, U.; Ghiviriga, I.; Abboud, K. A.; Veige, A. S. Ammonia Synthesis through Hydrolysis of a Trianionic Pincer Ligand-Supported Molybdenum–Nitride Complex. *Chem. - A Eur. J.* **2019**, *25* (62), 14059–14063. https://doi.org/10.1002/chem.201903740.

(17) Ahmed, A.; Radenahmad, N.; Cheok, Q.; Shams, S.; Kim, J. H.; Azad, A. K. Ammonia-Fed Fuel Cells : A Comprehensive Review. **2016**, *60*, 822–835. https://doi.org/10.1016/j.rser.2016.01.120.

(18) Rees, N. V; Compton, R. G. Carbon-Free Energy: A Review of Ammonia- and Hydrazine-Based Electrochemical Fuel Cells. *Energy and Environmental Science*. 2011, pp 1255–1260. https://doi.org/10.1039/c0ee00809e.

(19) Environ, E.; Sch, F. Environmental Science Ammonia as a Possible Element in an Energy Infrastructure : Catalysts for Ammonia Decomposition. **2012**, 6278–6289. https://doi.org/10.1039/c2ee02865d.

(20) Itabashi, T.; Mori, I.; Arashiba, K.; Eizawa, A.; Nakajima, K.; Nishibayashi, Y. Effect of Substituents on Molybdenum Triiodide Complexes Bearing PNP-Type Pincer Ligands toward Catalytic Nitrogen Fixation. *Dalt. Trans.* **2019**, *48* (10), 3182–3186. https://doi.org/10.1039/c8dt04975k.

(21) Weyrich, T.; Krahmer, J.; Engesser, T. A.; Näther, C.; Tuczek, F. Molybdenum Dinitrogen Complex Supported by a Cyclohexane-Based Triphosphine Ligand and Dmpm. *Dalt. Trans.* **2019**, *48* (18), 6019–6025. https://doi.org/10.1039/c8dt04738c.

(22) Van Der Ham, C. J. M.; Koper, M. T. M.; Hetterscheid, D. G. H. Challenges in Reduction of Dinitrogen by Proton and Electron Transfer. *Chemical Society Reviews*. 2014, pp 5183–5191. https://doi.org/10.1039/c4cs00085d.

(23) Vyas, N.; Pandey, B.; Ojha, A.; Grover, A. Revisiting Mechanistic Studies on Dinitrogen Reduction to Ammonia by an Iron Dinitrogen Complex as Nitrogenase Mimic. *Int. J. Quantum Chem.* **2019**, *119* (24), 1–12. https://doi.org/10.1002/qua.26025.

(24) MacLeod, K. C.; Holland, P. L. Recent Developments in the Homogeneous Reduction of Dinitrogen by Molybdenum and Iron. *Nat. Chem.* **2013**, *5* (7), 559–565. https://doi.org/10.1038/nchem.1620.

(25) Katayama, A.; Ohta, T.; Wasada-Tsutsui, Y.; Inomata, T.; Ozawa, T.; Ogura, T.; Masuda, H. A Dinitrogen Molybdenum Complex Induces Dinitrogen Cleavage

by One-Electron Oxidation. *Angew. Chemie Int. Ed.* **2019**, *58* (33), 1–7. https://doi.org/10.1002/anie.201905299.

(26) Mo, Z.; Shima, T.; Hou, Z. Synthesis and Diverse Transformations of a Dinitrogen Dititanium Hydride Complex Bearing Rigid Acridane-Based PNP-Pincer Ligands. *Angew. Chem. Int. Ed. Engl.* **2020**, 2–12. https://doi.org/10.1002/anie.201916171.

(27) Laplaza, C. E.; Cummins, C. C. Dinitrogen Cleavage by a Three-Coordinate Molybdenum (III) Complex Author (s): Catalina E . Laplaza and Christopher C . Cummins Published by : American Association for the Advancement of Science Stable URL : Http://Www.Jstor.Org/Stable/2887967 JSTOR I. *Science (80-.).* **1995**, *268* (5212), 861–863.

(28) NIGEL J. BROOKES, DAVID C. GRAHAM, GEMMA CHRISTIAN, ROBERT STRANGER, B. F. Y.; Brookes, N. J.; Graham, D. C.; Christian, G.; Stranger, R.; Yates, B. F. The Influence of Peripheral Ligand Bulk on Nitrogen Activation by Three-Coordinate Molybdenum Complexes—A Theoretical Study Using the ONIOM Method. *J. Comput. Chem.* **2009**, *28* (1), 73–86. https://doi.org/10.1002/jcc.

(29) Laplaza, C. E.; Johnson, M. J. A.; Peters, J. C.; Odom, A. L.; Kim, E.; Cummins, C. C.; George, G. N.; Pickering, I. J.; V, S. U.; Box, P. O. Dinitrogen Cleavage by Three-Coordinate Molybdenum (III) Complexes : Mechanistic and Structural Data 1. **1996**, *7863* (Iii), 8623–8638. https://doi.org/10.1021/ja960574x.

(30) Solari, E.; Silva, C. Da; Iacono, B.; Hesschenbrouck, J.; Rizzoli, C.; Scopelliti, R.; Floriani, C. Photochemical Activation of the N???N Bond in a Dimolybdenum-Dinitrogen Complex: Formation of a Molybdenum Nitride. *Angew. Chemie - Int. Ed.* **2001**, *40* (20), 3907–3909. https://doi.org/10.1002/1521-3773(20011015)40:20<3907::AID-ANIE3907>3.0.CO;2-#.

(31) Fryzuk, M. D.; Kozak, C. M.; Bowdridge, M. R.; Patrick, B. O.; Rettig, S. J. Nitride Formation by Thermolysis of a Kinetically Stable Niobium Dinitrogen

Complex. *J. Am. Chem. Soc.* **2002**, *124* (28), 8389–8397. https://doi.org/10.1021/ja025997f.

(32) Betley, T. A.; Peters, J. C. A Tetrahedrally Coordinated L3Fe-Nx Platform That Accommodates Terminal Nitride (FeIV≡N) and Dinitrogen (Fe I-N2-FeI) Ligands. *J. Am. Chem. Soc.* **2004**, *126* (20), 6252–6254. https://doi.org/10.1021/ja048713v.

(33) Hirotsu, M.; Fontaine, P. P.; Epshteyn, A.; Zavalij, P. Y.; Sita, L. R. Dinitrogen Activation at Ambient Temperatures: New Modes of H2 and PhSiH3 Additions for an "End-on-Bridged" [Ta(IV)] 2(μ-H1:H1-N2) Complex and for the Bis(μ-Nitrido) [Ta(V)(μ-N)]2 Product Derived from Facile N≡N Bond Cleavage. *J. Am. Chem. Soc.* **2007**, *129* (30), 9284–9285. https://doi.org/10.1021/ja072248v.

(34) Fontaine, P. P.; Yonke, B. L.; Zavalij, P. Y.; Sita, L. R. Dinitrogen Complexation and Extent of NtN Activation within the Group 6 "End-On-Bridged" Dinuclear Complexes, {(H5-C5Me5)M[N(i-Pr)C(Me)N(i-Pr)]}2(μ-H1:H1-N2)(M = Mo and W). **2010**, *20* (June), 159–161.

(35) Keane, A. J.; Yonke, B. L.; Hirotsu, M.; Zavalij, P. Y.; Sita, L. R. Fine-Tuning the Energy Barrier for Metal-Mediated Dinitrogen N???N Bond Cleavage. *J. Am. Chem. Soc.* **2014**, *136* (28), 9906–9909. https://doi.org/10.1021/ja505309j.

(36) Keane, A. J.; Farrell, W. S.; Yonke, B. L.; Zavalij, P. Y.; Sita, L. R. Metal-Mediated Production of Isocyanates, R $_3$ EN□C□O from Dinitrogen, Carbon Dioxide, and R $_3$ ECl. *Angew. Chemie Int. Ed.* **2015**, *54* (35), 10220–10224. https://doi.org/10.1002/anie.201502293.

(37) Tran, B. L.; Pinter, B.; Nichols, A. J.; Konopka, F. T.; Thompson, R.; Chen, C. H.; Krzystek, J.; Ozarowski, A.; Telser, J.; Baik, M. H.; Meyer, K.; Mindiola, D. J. A Planar Three-Coordinate Vanadium(II) Complex and the Study of Terminal Vanadium Nitrides from N2: A Kinetic or Thermodynamic Impediment to N-N Bond Cleavage? *J. Am. Chem. Soc.* **2012**, *134* (31), 13035–13045. https://doi.org/10.1021/ja303360v.

(38) Miyazaki, T.; Tanaka, H.; Tanabe, Y.; Yuki, M.; Nakajima, K.; Yoshizawa, K.;

Nishibayashi, Y. Cleavage and Formation of Molecular Dinitrogen in a Single System Assisted by Molybdenum Complexes Bearing Ferrocenyldiphosphine. *Angew. Chemie - Int. Ed.* **2014**, *53* (43), 11488–11492. https://doi.org/10.1002/anie.201405673.

(39) Silantyev, G. A.; Förster, M.; Schluschaß, B.; Abbenseth, J.; Würtele, C.; Volkmann, C.; Holthausen, M. C.; Schneider, S.; Fçrster, M.; Schluschaß, B.; Abbenseth, J.; Christian, W.; Volkmann, C.; Holthausen, M. C.; Schneider, S. Dinitrogen Splitting Coupled to Protonation. *Angew. Chemie - Int. Ed.* **2017**, *56* (21), 5872–5876. https://doi.org/10.1002/anie.201701504.

(40) Jia, H. P.; Quadrelli, E. A. Mechanistic Aspects of Dinitrogen Cleavage and Hydrogenation to Produce Ammonia in Catalysis and Organometallic Chemistry: Relevance of Metal Hydride Bonds and Dihydrogen. *Chem. Soc. Rev.* **2014**, *43* (2), 547–564. https://doi.org/10.1039/c3cs60206k.

(41) Fryzuk, M. D.; Johnson, S. A.; Canada, V. T. Z. The Continuing Story of Dinitrogen Activation. *Coord. Chem. Rev.* **2000**, *200–202*, 379–409. https://doi.org/10.1016/S0010-8545(00)00264-2.

(42) Liu, C. G.; Liu, S.; Zheng, T. Computational Study of Metal-Dinitrogen Keggin-Type Polyoxometalate Complexes [PW<inf>11</Inf>O<inf>39</Inf>M^{II}N<inf>2</Inf>)]$^{5-}$ (M = Ru, Os, Re, Ir): Bonding Nature and Dinitrogen Splitting. *Inorg. Chem.* **2015**, *54* (16), 7929–7935. https://doi.org/10.1021/acs.inorgchem.5b01002.

(43) Shaver, M. P.; Fryzuk, M. D. Activation of Molecular Nitrogen: Coordination, Cleavage and Functionalization of N2 Mediated by Metal Complexes. *Advanced Synthesis and Catalysis*. 2003, pp 1061–1076. https://doi.org/10.1002/adsc.200303081.

(44) Lu, E.; Atkinson, B. E.; Wooles, A. J.; Boronski, J. T.; Doyle, L. R.; Tuna, F.; Cryer, J. D.; Cobb, P. J.; Vitorica-Yrezabal, I. J.; Whitehead, G. F. S.; Kaltsoyannis, N.; Liddle, S. T. Back-Bonding between an Electron-Poor, High-Oxidation-State Metal and Poor π-Acceptor Ligand in a Uranium(v)–Dinitrogen

Complex. *Nat. Chem.* **2019**, *11* (9), 806–811. https://doi.org/10.1038/s41557-019-0306-x.

(45) Lv, Z. J.; Huang, Z.; Zhang, W. X.; Xi, Z. Scandium-Promoted Direct Conversion of Dinitrogen into Hydrazine Derivatives via N-C Bond Formation. *J. Am. Chem. Soc.* **2019**, *141* (22), 8773–8777. https://doi.org/10.1021/jacs.9b04293.

(46) Shanahan, J. P.; Szymczak, N. K. Hydrogen Bonding to a Dinitrogen Complex at Room Temperature: Impacts on N2 Activation. *J. Am. Chem. Soc.* **2019**, *141* (21), 8550–8556. https://doi.org/10.1021/jacs.9b02288.

(47) Nesbit, M. A.; Oyala, P. H.; Peters, J. C. Characterization of the Earliest Intermediate of Fe-N2 Protonation: CW and Pulse EPR Detection of an Fe-NNH Species and Its Evolution to Fe-NNH2. *J. Am. Chem. Soc.* **2019**, *141* (20), 8116–8127. https://doi.org/10.1021/jacs.8b12082.

(48) Tanabe, Y.; Nishibayashi, Y. Recent Advances in Nitrogen Fixation upon Vanadium Complexes. *Coord. Chem. Rev.* **2019**, *381*, 135–150. https://doi.org/10.1016/j.ccr.2018.11.005.

(49) Dmitry V. Yandulov and Richard R. Schrock. Catalytic Reduction of Dinitrogen to Ammonia at a Single Molybdenum Center Dmitry. **2003**, *301* (July), 76–79.

(50) Chalkley, M. J.; Del Castillo, T. J.; Matson, B. D.; Roddy, J. P.; Peters, J. C. Catalytic N2-to-NH3 Conversion by Fe at Lower Driving Force: A Proposed Role for Metallocene-Mediated PCET. *ACS Cent. Sci.* **2017**, *3* (3), 217–223. https://doi.org/10.1021/acscentsci.7b00014.

(51) Kuriyama, S.; Arashiba, K.; Tanaka, H.; Matsuo, Y.; Nakajima, K.; Yoshizawa, K.; Nishibayashi, Y. Direct Transformation of Molecular Dinitrogen into Ammonia Catalyzed by Cobalt Dinitrogen Complexes Bearing Anionic PNP Pincer Ligands. *Angew. Chemie - Int. Ed.* **2016**, *55* (46), 14291–14295. https://doi.org/10.1002/anie.201606090.

(52) Katayama, A.; Ohta, T.; Wasada-Tsutsui, Y.; Inomata, T.; Ozawa, T.; Ogura, T.; Masuda, H. Dinitrogen-Molybdenum Complex Induces Dinitrogen Cleavage by

One-Electron Oxidation. *Angew. Chemie - Int. Ed.* **2019**, *58* (33), 11279–11284. https://doi.org/10.1002/anie.201905299.

(53) Liao, Q.; Saffon-Merceron, N.; Mézailles, N. N2 Reduction into Silylamine at Tridentate Phosphine/Mo Center: Catalysis and Mechanistic Study. *ACS Catal.* **2015**, *5* (11), 6902–6906. https://doi.org/10.1021/acscatal.5b01626.

(54) Kuriyama, S.; Arashiba, K.; Nakajima, K.; Tanaka, H.; Yoshizawa, K.; Nishibayashi, Y. Nitrogen Fixation Catalyzed by Ferrocene-Substituted Dinitrogen-Bridged Dimolybdenum-Dinitrogen Complexes: Unique Behavior of Ferrocene Moiety as Redox Active Site. *Chem. Sci.* **2015**, *6* (7), 3940–3951. https://doi.org/10.1039/c5sc00545k.

(55) Kuriyama, S.; Arashiba, K.; Nakajima, K.; Tanaka, H.; Kamaru, N.; Yoshizawa, K.; Nishibayashi, Y. Catalytic Formation of Ammonia from Molecular Dinitrogen by Use of Dinitrogen-Bridged Dimolybdenum-Dinitrogen Complexes Bearing Pnp-Pincer Ligands: Remarkable Effect of Substituent at Pnp-Pincer Ligand. *J. Am. Chem. Soc.* **2014**, *136* (27), 9719–9731. https://doi.org/10.1021/ja5044243.

(56) Arashiba, K.; Kinoshita, E.; Kuriyama, S.; Eizawa, A.; Nakajima, K.; Tanaka, H.; Yoshizawa, K.; Nishibayashi, Y. Catalytic Reduction of Dinitrogen to Ammonia by Use of Molybdenum-Nitride Complexes Bearing a Tridentate Triphosphine as Catalysts. *J. Am. Chem. Soc.* **2015**, *137* (17), 5666–5669. https://doi.org/10.1021/jacs.5b02579.

(57) Arashiba, K.; Miyake, Y.; Nishibayashi, Y. A Molybdenum Complex Bearing PNP-Type Pincer Ligands Leads to the Catalytic Reduction of Dinitrogen into Ammonia. *Nat. Chem.* **2011**, *3* (2), 120–125. https://doi.org/10.1038/nchem.906.

(58) Eizawa, A.; Arashiba, K.; Tanaka, H.; Kuriyama, S.; Matsuo, Y.; Nakajima, K.; Yoshizawa, K.; Nishibayashi, Y. Remarkable Catalytic Activity of Dinitrogen-Bridged Dimolybdenum Complexes Bearing NHC-Based PCP-Pincer Ligands toward Nitrogen Fixation. *Nat. Commun.* **2017**, *8*, 1–12. https://doi.org/10.1038/ncomms14874.

(59) Nishibayashi, Y.; Takemoto, S.; Iwai, S.; Hidai, M. Formation of Ammonia in the Reactions of a Tungsten Dinitrogen with Ruthenium Dihydrogen Complexes under Mild Reaction Conditions. *Inorg. Chem.* **2000**, *39* (26), 5946–5957. https://doi.org/10.1021/ic000799f.

(60) SYNTHESIS, CATALYSIS, AND REACTIVITY OF LOW-VALENT CHROMIUM COMPLEXES SUPPORTED BY A B -DIKETIMINATE LIGAND, University of Delaware, 2009.

(61) Yu-Ting Hung. SYNTHESIS AND REACTIVITY STUDIES OF CHROMIUM COMPLEXES SUPPORTED BY B–DIKETIMINATE LIGANDS, University of Delaware, 2017.

(62) Cummins, D. C. SYNTHESIS AND REACTIVITY OF DINITROGEN, OXO, AND NITRIDO COMPLEXES OF FIRST ROW TRANSITION METALS SUPPORTED BY HYRDOTRIS(PYRAZOLYL)BORATE LIGANDS, University of Delaware, 2017.

(63) Tanabe, Y.; Nishibayashi, Y. Catalytic Dinitrogen Fixation to Form Ammonia at Ambient Reaction Conditions Using Transition Metal-Dinitrogen Complexes. *Chem. Rec.* **2016**, 1549–1577. https://doi.org/10.1002/tcr.201600025.

(64) Heintz, R. A.; Ostrander, R. L.; Rheingold, A. L.; Theopold, K. H. [(H5-C5R5)CrR]n: A New Class of Paramagnetic Alkyls and Hydrides of Divalent Chromium. *J. Am. Chem. Soc.* **1994**, *116* (25), 11387–11396. https://doi.org/10.1021/ja00104a019.

(65) Köhler, F. H.; Metz, B.; Strauss, W. (Arene)Cyclopentadienylchromium Chemistry. Synthesis, EPR, NMR, and Cyclic Voltammetry of Neutral Compounds and Their Monocations. *Inorg. Chem.* **1995**, *34* (17), 4402–4413. https://doi.org/10.1021/ic00121a019.

(66) Odom, A. L.; Cummins, C. C. A Chromium(VI) Nitrido-Silylmethyl Complex and a Chromium(V) μ-Nitrido Dimer: Synthetic and Structural Details. *Organometallics* **1996**, *15* (3), 898–900. https://doi.org/10.1021/om950842k.

(67) Mindiola, D. J.; Cummins, C. C. Deprotonated 2,3:5,6-Dibenzo-7-Aza

Bicyclo[2.2.1]Hepta-2,5-Diene as a Nitrido Nitrogen Source by Anthracene Elimination: Synthesis of an Iodide(Nitride)Chromium(VI) Complex. *Angew. Chemie - Int. Ed.* **1998**, *37* (7), 945–947. https://doi.org/10.1002/(SICI)1521-3773(19980420)37:7<945::AID-ANIE945>3.0.CO;2-X.

(68) Carpino, L. A.; Padykula, R. E.; Barr, D. E.; Hall, F. H.; Krause, J. G.; Dufresne, R. F.; Thoman, C. J. Synthesis, Characterization, and Thermolysis of 7-Amino-7-Azabenzonorbornadienes. *J. Org. Chem.* **1988**, *53* (11), 2565–2572. https://doi.org/10.1021/jo00246a031.

(69) Stoian, S. A.; Vela, J.; Smith, J. M.; Sadique, A. R.; Holland, P. L.; Münck, E.; Bominaar, E. L. Mössbauer and Computational Study of an N2-Bridged Diiron Diketiminate Complex: Parallel Alignment of the Iron Spins by Direct Antiferromagnetic Exchange with Activated Dinitrogen. *J. Am. Chem. Soc.* **2006**, *128* (31), 10181–10192. https://doi.org/10.1021/ja062051n.

(70) Janiak, C.; Silvestre, J.; Theopold, K. H. Metal-Metal Bonding in Paramagnetic Chromium(III) Complexes – An MO-Theoretical Case Study. *Chem. Ber.* **1993**, *126* (3), 631–643. https://doi.org/10.1002/cber.19931260313.

(71) Richeson, D. S.; Mitchell, J. F.; Theopold, K. H. Synthesis and Reaction Chemistry Od a New Class of Paramagnetic Chromium(III) Alkyls. *Organometallics* **1989**, No. 7, 2570–2577.

(72) Gore-Randall, E.; Irwin, M.; Denning, M. S.; Goicoechea, J. M. Synthesis and Characterization of Alkali-Metal Salts of 2,2′-and 2,4′-Bipyridyl Radicals and Dianions. *Inorg. Chem.* **2009**, *48* (17), 8304–8316. https://doi.org/10.1021/ic9009459.

(73) Wang, M.; Weyhermüller, T.; Bill, E.; Ye, S.; Wieghardt, K. Structural and Spectroscopic Characterization of Rhenium Complexes Containing Neutral, Monoanionic, and Dianionic Ligands of 2,2′-Bipyridines and 2,2′:6,2-Terpyridines: An Experimental and Density Functional Theory (DFT)-Computational Study. *Inorg. Chem.* **2016**, *55* (10), 5019–5036. https://doi.org/10.1021/acs.inorgchem.6b00609.

(74) Wang, M.; Weyhermüller, T.; England, J.; Wieghardt, K. Molecular and Electronic Structures of Six-Coordinate “Low- Valent” [M(Mebpy)3]0 (M = Ti, V, Cr, Mo) and [M(Tpy)2]0 (M = Ti, V, Cr), and Seven-Coordinate [MoF(Mebpy)3](PF6) and [MX(Tpy) 2](PF6) (M = Mo, X = Cl and M = W, X = F). *Inorg. Chem.* **2013**, *52* (21), 12763–12776. https://doi.org/10.1021/ic402037e.

(75) Connor, G. P.; Holland, P. L. Coordination Chemistry Insights into the Role of Alkali Metal Promoters in Dinitrogen Reduction. *Catal. Today* **2017**, *286*, 21–40. https://doi.org/10.1016/j.cattod.2016.08.014.

(76) Del Bene, J. E.; Frisch, M. J.; Raghavachari, K.; Pople, J. A.; Schleyer, P. V. R. A Molecular Orbital Study of Some Lithium Ion Complexes. *J. Phys. Chem.* **1983**, *87* (1), 73–78. https://doi.org/10.1021/j100224a018.

(77) Hung, Y. T.; Yap, G. P. A.; Theopold, K. H. Unexpected Reactions of Chromium Hydrides with a Diazoalkane. *Polyhedron* **2019**, *157*, 381–388. https://doi.org/10.1016/j.poly.2018.10.030.

(78) Yin, J.; Li, J.; Wang, G. X.; Yin, Z. B.; Zhang, W. X.; Xi, Z. Dinitrogen Functionalization Affording Chromium Hydrazido Complex. *J. Am. Chem. Soc.* **2019**, *141* (10), 4241–4247. https://doi.org/10.1021/jacs.9b00822.

(79) Thomas, B. J.; Noh, S. K.; Schulte, G. K.; Sendlinger, S. C.; Theopold, K. H. Paramagnetic Alkylchromium Compounds as Homogeneous Catalysts for the Polymerization of Ethylene. *J. Am. Chem. Soc.* **1991**, *113* (8), 893–902.

(80) Klopsch, I.; Yuzik-Klimova, E. Y.; Schneider, S. Functionalization of N2 by Mid to Late Transition Metals via N–N Bond Cleavage. In *Topics in Organometallic Chemistry*; 2017; Vol. 60, pp 71–112. https://doi.org/10.1007/3418_2016_12.

(81) Wu, P. SYNTHESIS, CHARACTERIZATION AND REACTIVITY OF IMIDO CHROMIUM(VI) COMPLEXES. *Director* **2018**, *15* (29), 7577–7588.

(82) Klopsch, I.; Finger, M.; Würtele, C.; Milde, B.; Werz, D. B.; Schneider, S.; Wu, C.; Milde, B.; Werz, D. B.; Schneider, S.; Würtele, C.; Milde, B.; Werz, D. B.; Schneider, S. Dinitrogen Splitting and Functionalization in the Coordination Sphere of Rhenium. *J. Am. Chem. Soc.* **2014**, *136* (19), 6881–6883.

https://doi.org/10.1021/ja502759d.

(83) Bucinsky, L.; Breza, M.; Lee, W. T.; Hickey, A. K.; Dickie, D. A.; Nieto, I.; Degayner, J. A.; Harris, T. D.; Meyer, K.; Krzystek, J.; Ozarowski, A.; Nehrkorn, J.; Schnegg, A.; Holldack, K.; Herber, R. H.; Telser, J.; Smith, J. M. Spectroscopic and Computational Studies of Spin States of Iron(IV) Nitrido and Imido Complexes. *Inorg. Chem.* **2017**, *56* (8), 4751–4768. https://doi.org/10.1021/acs.inorgchem.7b00512.

(84) Curtis, E. R.; Hannigan, M. D.; Vitek, A. K.; Zimmerman, P. M. Quantum Chemical Investigation of Dimerization in the Schlenk Equilibrium of Thiophene Grignard Reagents. *J. Phys. Chem. A* **2020**, *124* (8), 1480–1488. https://doi.org/10.1021/acs.jpca.9b09985.

(85) Shen, L.; Zhao, Y.; Dai, D.; Yang, Y. W.; Wu, B.; Yang, X. J. Stabilization of Grignard Reagents by a Pillar[5]Arene Host-Schlenk Equilibria and Grignard Reactions. *Chem. Commun.* **2020**, *56* (9), 1381–1384. https://doi.org/10.1039/c9cc08728a.

(86) Peltzer, R. M.; Eisenstein, O.; Nova, A.; Cascella, M. How Solvent Dynamics Controls the Schlenk Equilibrium of Grignard Reagents: A Computational Study of CH3MgCl in Tetrahydrofuran. *J. Phys. Chem. B* **2017**, *121* (16), 4226–4237. https://doi.org/10.1021/acs.jpcb.7b02716.

(87) Yang, L.; Powell, D. R.; Houser, R. P. Structural Variation in Copper(i) Complexes with Pyridylmethylamide Ligands: Structural Analysis with a New Four-Coordinate Geometry Index, T4. *J. Chem. Soc. Dalt. Trans.* **2007**, No. 9, 955–964. https://doi.org/10.1039/b617136b.

(88) Barluzzi, L.; Chatelain, L.; Fadaei-Tirani, F.; Zivkovic, I.; Mazzanti, M. Facile N-Functionalization and Strong Magnetic Communication in a Diuranium(v) Bis-Nitride Complex. *Chem. Sci.* **2019**, *10* (12), 3543–3555. https://doi.org/10.1039/c8sc05721d.

(89) Wang, D.; Loose, F.; Chirik, P. J.; Knowles, R. R. N-H Bond Formation in a Manganese(V) Nitride Yields Ammonia by Light-Driven Proton-Coupled

Electron Transfer. *J. Am. Chem. Soc.* **2019**, *141* (12), 4795–4799. https://doi.org/10.1021/jacs.8b12957.

(90) Scheibel, M. G.; Abbenseth, J.; Kinauer, M.; Heinemann, F. W.; Würtele, C.; De Bruin, B.; Schneider, S. Homolytic N-H Activation of Ammonia: Hydrogen Transfer of Parent Iridium Ammine, Amide, Imide, and Nitride Species. *Inorg. Chem.* **2015**, *54* (19), 9290–9302. https://doi.org/10.1021/acs.inorgchem.5b00829.

(91) Askevold, B.; Nieto, J. T.; Tussupbayev, S.; Diefenbach, M.; Herdtweck, E.; Holthausen, M. C.; Schneider, S. Ammonia Formation by Metal-Ligand Cooperative Hydrogenolysis of a Nitrido Ligand. *Nat. Chem.* **2011**, *3* (7), 532–537. https://doi.org/10.1038/nchem.1051.

(92) Tran, B. L.; Pink, M.; Gao, X.; Park, H.; Mindiola, D. J. Low-Coordinate and Neutral Nitrido Complexes of Vanadium. *J. Am. Chem. Soc.* **2010**, *132* (5), 1458–1459. https://doi.org/10.1021/ja908303k.

(93) Silvia, J. S.; Cummins, C. C. Two-Electron Reduction of a Vanadium(V) Nitride by CO to Release Cyanate and Open a Coordination Site. *J. Am. Chem. Soc.* **2009**, *131* (2), 446–447. https://doi.org/10.1021/ja807767w.

(94) A. T. McPhail, G. R. Knox, C. G. R. and G. A. S. Metal-Carbonyl and Metal-Nitrosyl Complexes. Part X.l Photochemical Generation of Organometallic Nitrenes and the Crystal Structure of a - Carbonylat Ion Product, Lsocyanatocar Bony1 -n-Cyclopentad Ienyl Bis(t Ri Pheny1phosphine)Molybdenum. *J. Chem. Soc.* **1971**, No. 0, 705–712.

(95) Ananias, S. R.; Mauro, A. E.; Zutin, K.; Picchi, C. M. C.; Santos, R. H. A. Mono- and Dinuclear Palladium(II) Compounds Containing Nitrogen Ligands. Crystal and Molecular Structure of [Pd(N,C-Dmba)(NCO)(2,3-Lut)] and [Pd(H 2CCOMe)Cl(2,2′-Bipy)]. *Transit. Met. Chem.* **2004**, *29* (3), 284–290. https://doi.org/10.1023/B:TMCH.0000020370.34647.b9.

(96) Mandal, L.; Mandal, S.; Mohanta, S. Syntheses, Crystal Structures, Magnetochemistry and Catechol Oxidase Activity of a Tetracopper(II)

Compound and a New Type of Dicopper(II)-Based 1D Coordination Polymer. *New J. Chem.* **2017**, *41* (11), 4689–4701. https://doi.org/10.1039/c7nj00286f.

(97) Singh, D.; Buratto, W. R.; Torres, J. F.; Murray, L. J. Activation of Dinitrogen by Polynuclear Metal Complexes. *Chem. Rev.* **2020**, *120* (12), 5517–5581. https://doi.org/10.1021/acs.chemrev.0c00042.

(98) Gidt, W.; Smytschkow, I.; Sun, Y.; Langer, J.; Böttcher, T.; Kratzert, D.; Klingele, J.; Oelkers, B.; Sitzmann, H. Paramagnetic Chromium(II) Complexes and Chromium(IV) Nitrides with Bulky Alkylcyclopentadienyl Ligands. *Eur. J. Inorg. Chem.* **2018**, *2018* (40), 4472–4480. https://doi.org/10.1002/ejic.201800901.

(99) Monillas, W. H.; Young, J. F.; Yap, G. P. A. A.; Theopold, K. H. A Well-Defined Model System for the Chromium-Catalyzed Selective Oligomerization of Ethylene. *Dalt. Trans.* **2013**, *42* (25), 9198–9210. https://doi.org/10.1039/C3DT00109A.

(100) Monillas, W. H.; Yap, G. P. A.; Theopold, K. H. Reactivity of a Low-Valent Chromium Dinitrogen Complex. *Inorganica Chim. Acta* **2011**, *369* (1), 103–119. https://doi.org/10.1016/j.ica.2010.11.024.

(101) Chatt, J.; Dilworth, J. R.; Richards, R. L. Recent Advances in the Chemistry of Nitrogen Fixation. *Chem. Rev.* **1978**, *78* (6), 589–625. https://doi.org/10.1021/cr60316a001.

(102) Jandciu, E. W. Amide-Stabilized, Diamagnetic Chromium(II) Nitrosyl Complexes. *Organometallics* **1999**, *18* (10), 1994–2004. https://doi.org/10.1021/om980954m.

(103) Lang, J.; Mohrbach, J.; Dillinger, S.; Hewer, J. M.; Niedner-Schatteburg, G. Vibrational Blue Shift of Coordinated N2 in [Fe3O(OAc)6(N2)n]+: "Non-Classical" Dinitrogen Complexes. *Chem. Commun.* **2017**, *53* (2), 420–423. https://doi.org/10.1039/c6cc07481b.

(104) Simonneau, A.; Etienne, M. Enhanced Activation of Coordinated Dinitrogen with P-Block Lewis Acids. *Chem. - A Eur. J.* **2018**, *24* (48), 12458–12463.

(105) Geri, J. B.; Shanahan, J. P.; Szymczak, N. K. Testing the Push − Pull Hypothesis: Lewis Acid Augmented N 2 Activation at Iron. **2017**, *2* (0), 2–6. https://doi.org/10.1021/jacs.7b01982.

(106) Chatt, J.; Crabtree, R. H.; Richards, R. L. Dinitrogen- and Carbonyl-Complexes as Bases towards Trimethylaluminium. *J. Chem. Soc. Chem. Commun.* **1972**, *0* (9), 534. https://doi.org/10.1039/C39720000534.

(107) Chatt, B. J.; Jeffery, E. A.; Richards, R. L.; Fixation, N. The Basic Strengths of Some Dinitrogen Complexes of Molybdenum(o), Tungsten(o), Rhenium(!), And Osmium(I1). **1973**.

(108) Chatt, J.; Dilworth, J. R.; Leigh, G. J.; Richards, R. L. Polynuclear Dinitrogen Complexes. *J. Chem. Soc. D Chem. Commun.* **1970**, No. 15, 955–956. https://doi.org/10.1039/C29700000955.

(109) Chatt, J.; Dilworth, J. R.; Gunz, H. P.; Leigh, G. J.; Sanders, J. R. The Interaction of Dinitrogen Complexes of Rhenium and Osmium with Metal Salts. *J. Chem. Soc. D Chem. Commun.* **1970**, No. 2, 90–91. https://doi.org/10.1039/C29700000090.

(110) Caputo, C. B.; Stephan, D. W. Activation of Alkyl C-F Bonds by B(C 6F 5) 3: Stoichiometric and Catalytic Transformations. *Organometallics* **2012**, *31* (1), 27–30. https://doi.org/10.1021/om200885c.

(111) Piascik, A. D.; Hill, P. J.; Crawford, A. D.; Doyle, L. R.; Green, J. C.; Ashley, A. E. Cationic Silyldiazenido Complexes of the Fe(Diphosphine)2(N2) Platform: Structural and Electronic Models for an Elusive First Intermediate in N2 Fixation. *Chem. Commun.* **2017**, *53* (54), 7657–7660. https://doi.org/10.1039/c7cc04188h.

(112) Brookhart, M.; Grant, B.; Volpe, A. F. [(3,5-(CF3)2C6H3)4B]- [H(OEt2)2]+: A Convenient Reagent for Generation and Stabilization of Cationic, Highly Electrophilic Organometallic Complexes. *Organometallics* **1992**, *11* (11), 3920–3922. https://doi.org/10.1021/om00059a071.

(113) Yakelis, N. A.; Bergman, R. G. Safe Preparation and Purification of Sodium

Tetrakis[(3,5-Trifluoromethyl)Phenyl]Borate (NaBArF 24): Reliable and Sensitive Analysis of Water in Solutions of Fluorinated Tetraarylborates. *Organometallics* **2005**, *24* (14), 3579–3581. https://doi.org/10.1021/om0501428.

(114) Le Bras, J.; Jiao, H.; Meyer, W. E.; Hampel, F.; Gladysz, J. A. Synthesis, Crystal Structure, and Reactions of the 17-Valence-Electron Rhenium Methyl Complex [(H5-C5Me5)Re(NO)(P(4-C6H 4CH3)3)(CH3)]•+ B(3,5-C6H3(CF3)2)-4: *J. Organomet. Chem.* **2000**, *616* (1–2), 54–66. https://doi.org/10.1016/S0022-328X(00)00531-3.

(115) Chávez, I.; Alvarez-Carena, A.; Molins, E.; Roig, A.; Maniukiewicz, W.; Arancibia, A.; Arancibia, V.; Brand, H.; Manuel Manríquez, J. Selective Oxidants for Organometallic Compounds Containing a Stabilising Anion of Highly Reactive Cations: (3,5(CF3)2C6H3)4B -)Cp2Fe+ and (3,5(CF3)2C6H3)4B -)Cp*2Fe+. *J. Organomet. Chem.* **2000**, *601* (1), 126–132. https://doi.org/10.1016/S0022-328X(00)00044-9.

(116) Yi, X. Y.; Lam, T. C. H.; Sau, Y. K.; Zhang, Q. F.; Williams, I. D.; Leung, W. H. Electrophilic Ruthenium(VI) Nitrido Complex Containing Kläui's Oxygen Tripodal Ligand. *Inorg. Chem.* **2007**, *46* (17), 7193–7198. https://doi.org/10.1021/ic7007683.

(117) Bain, G. A.; Berry, J. F. Diamagnetic Corrections and Pascal's Constants. *J. Chem. Educ.* **2008**, *85* (4), 532–536. https://doi.org/10.1021/ed085p532.

(118) M. J. Frisch, G. W. Trucks, H. B. Schlegel, G. E. Scuseria, M. A. Robb, J. R. Cheeseman, G. Scalmani, V. Barone, G. A. Petersson, H. Nakatsuji, X. Li, M. Caricato, A. Marenich, J. Bloino, B. G. Janesko, R. Gomperts, B. Mennucci, H. P. Hratchian, J. V. Ort, and D. J. F. Gaussian 09, Revision A.02. **2016**.

(119) Liu, C.; Liu, S.; Zheng, T. Computational Study of Metal − Dinitrogen Keggin-Type Polyoxometalate Complexes [PW 11 O 39 M II N 2)] 5 − (M = Ru , Os , Re , Ir): Bonding Nature and Dinitrogen Splitting. **2015**. https://doi.org/10.1021/acs.inorgchem.5b01002.

(120) E. D. Glendening, A. E. Reed, J. E. Carpenter, and F. W. NBO Version 3.1.

APPENDIX A

CRYSTALLOGRAPHIC INFORMATION OF COMPLEXES

Table A.1 Crystal data and structure refinement for [Cp*$_4$Cr$_4$N$_3$Cl] (1)

Identification code	kla1082
Empirical formula	$C_{64}H_{74}BCr_2F_{24}N_2P_4$
Formula weight	1565.94
Temperature/K	100.03
Crystal system	triclinic
Space group	P-1
a/Å	13.2445(13)
b/Å	15.1502(15)
c/Å	19.799(2)
α/°	108.916(2)
β/°	102.218(2)
γ/°	99.465(2)
Volume/Å^3	3554.5(6)
Z	2
ρ_{calc}g/cm^3	1.463
μ/mm^{-1}	0.499
F(000)	1602.0
Crystal size/mm^3	0.236 × 0.119 × 0.107
Radiation	MoKα (λ = 0.71073)
2Θ range for data collection/°	3.252 to 56.732
Index ranges	$-17 \leq h \leq 17$, $-20 \leq k \leq 20$, $-26 \leq l \leq 26$
Reflections collected	117083
Independent reflections	17781 [R_{int} = 0.0832, R_{sigma} = 0.0594]
Data/restraints/parameters	17781/616/1013
Goodness-of-fit on F^2	1.025
Final R indexes [I>=2σ (I)]	R_1 = 0.0507, wR_2 = 0.1146
Final R indexes [all data]	R_1 = 0.0783, wR_2 = 0.1286
Largest diff. peak/hole / e Å^{-3}	0.92/-0.59

Table A.2 Crystal data and structure refinement for [Cp*Cr(μ-Cl)(μ-dbabh)CrCp*] (2).

Identification code	kla0939
Empirical formula	$C_{22}H_{27}ClCrN_2$
Formula weight	406.90
Temperature/K	200(2)
Crystal system	monoclinic
Space group	$P2_1/n$
a/Å	7.9294(7)
b/Å	13.7686(12)
c/Å	18.3470(16)
α/°	90
β/°	96.5440(10)
γ/°	90
Volume/Å^3	1990.0(3)
Z	4
ρ_{calc}g/cm^3	1.358
μ/mm^{-1}	0.717
F(000)	856.0
Crystal size/mm^3	0.801 × 0.680 × 0.557
Radiation	MoKα (λ = 0.71073)
2Θ range for data collection/°	3.708 to 55.414
Index ranges	? ≤ h ≤ ?, ? ≤ k ≤ ?, ? ≤ l ≤ ?
Reflections collected	4626
Independent reflections	4626 [R_{int} = ?, R_{sigma} = 0.0092]
Data/restraints/parameters	4626/0/242
Goodness-of-fit on F^2	1.111
Final R indexes [I>=2σ (I)]	R_1 = 0.0337, wR_2 = 0.0862
Final R indexes [all data]	R_1 = 0.0375, wR_2 = 0.0901
Largest diff. peak/hole / e Å^{-3}	0.44/-0.48

Table A.3 Crystal data and structure refinement for $[Cp^*Cr(N_3)_3Li(THF)]_n$ (3).

Identification code	kla0931
Empirical formula	$C_{14}H_{23}CrN_9OLi$
Formula weight	392.35
Temperature/K	200(2)
Crystal system	triclinic
Space group	$P\bar{1}$
a/Å	8.2520(9)
b/Å	8.6136(10)
c/Å	13.7053(15)
α/°	90.2890(18)
β/°	99.2758(17)
γ/°	95.8995(18)
Volume/Å^3	956.10(18)
Z	2
ρ_{calc}g/cm^3	1.363
μ/mm^{-1}	0.621
F(000)	410.0
Crystal size/mm^3	0.284 × 0.253 × 0.079
Radiation	MoKα (λ = 0.71073)
2Θ range for data collection/°	4.756 to 55.392
Index ranges	$-10 \leq h \leq 10$, $-11 \leq k \leq 11$, $-17 \leq l \leq 17$
Reflections collected	18668
Independent reflections	4465 [R_{int} = 0.0370, R_{sigma} = 0.0355]
Data/restraints/parameters	4465/0/240
Goodness-of-fit on F^2	1.027
Final R indexes [I>=2σ (I)]	R_1 = 0.0475, wR_2 = 0.1263
Final R indexes [all data]	R_1 = 0.0625, wR_2 = 0.1375
Largest diff. peak/hole / e Å^{-3}	0.51/-0.46

Table A.4 Crystal data and structure refinement for [Cp*ClCr(μ-N_3)]$_2$ (4).

Identification code	kla0959
Empirical formula	$C_{20}H_{30}N_6Cl_2Cr_2$
Formula weight	529.40
Temperature/K	200(2)
Crystal system	monoclinic
Space group	$P2_1/c$
a/Å	18.506(4)
b/Å	8.576(2)
c/Å	17.361(4)
α/°	90
β/°	116.904(4)
γ/°	90
Volume/Å^3	2457.3(10)
Z	4
ρ_{calc}g/cm^3	1.431
μ/mm^{-1}	1.120
F(000)	1096.0
Crystal size/mm^3	0.189 × 0.184 × 0.162
Radiation	MoKα (λ = 0.71073)
2Θ range for data collection/°	4.694 to 55.884
Index ranges	$-24 \leq h \leq 22$, $-11 \leq k \leq 11$, $-22 \leq l \leq 22$
Reflections collected	25467
Independent reflections	5770 [R_{int} = 0.0679, R_{sigma} = 0.0620]
Data/restraints/parameters	5770/31/291
Goodness-of-fit on F^2	1.094
Final R indexes [I>=2σ (I)]	R_1 = 0.0737, wR_2 = 0.2216
Final R indexes [all data]	R_1 = 0.0855, wR_2 = 0.2269
Largest diff. peak/hole / e Å^{-3}	0.69/-0.59

Table A.5 Crystal data and structure refinement for $[Cp^*ClCr]_4(\mu\text{-}N)_2(\mu\text{-}N_3)_2$ (5).

Identification code	kla0971
Empirical formula	$C_{20}H_{30}Cl_2Cr_2N_4$
Formula weight	501.38
Temperature/K	200.01
Crystal system	orthorhombic
Space group	Pbcn
a/Å	24.981(7)
b/Å	11.603(3)
c/Å	17.611(5)
α/°	90
β/°	90
γ/°	90
Volume/Å^3	5105(3)
Z	8
ρ_{calc}g/cm^3	1.305
μ/mm^{-1}	1.072
F(000)	2080.0
Crystal size/mm^3	0.391 × 0.237 × 0.184
Radiation	MoKα (λ = 0.71073)
2Θ range for data collection/°	3.26 to 55.578
Index ranges	$-32 \leq h \leq 29$, $-15 \leq k \leq 15$, $-23 \leq l \leq 22$
Reflections collected	47363
Independent reflections	5994 [R_{int} = 0.0288, R_{sigma} = 0.0175]
Data/restraints/parameters	5994/0/263
Goodness-of-fit on F^2	1.151
Final R indexes [I>=2σ (I)]	R_1 = 0.0611, wR_2 = 0.2225
Final R indexes [all data]	R_1 = 0.0702, wR_2 = 0.2357
Largest diff. peak/hole / e Å^{-3}	2.42/-0.45

Table A.6 Crystal data and structure refinement for [Cp*ClCr(N^N)] (6).

Identification code	kla0939
Empirical formula	$C_{22}H_{27}ClCrN_2$
Formula weight	406.90
Temperature/K	200(2)
Crystal system	monoclinic
Space group	$P2_1/n$
a/Å	7.9294(7)
b/Å	13.7686(12)
c/Å	18.3470(16)
α/°	90
β/°	96.5440(10)
γ/°	90
Volume/Å^3	1990.0(3)
Z	4
ρ_{calc}g/cm^3	1.358
μ/mm^{-1}	0.717
F(000)	856.0
Crystal size/mm^3	0.801 × 0.680 × 0.557
Radiation	MoKα (λ = 0.71073)
2Θ range for data collection/°	3.708 to 55.414
Index ranges	? ≤ h ≤ ?, ? ≤ k ≤ ?, ? ≤ l ≤ ?
Reflections collected	4626
Independent reflections	4626 [R_{int} = ?, R_{sigma} = 0.0092]
Data/restraints/parameters	4626/0/242
Goodness-of-fit on F^2	1.111
Final R indexes [I>=2σ (I)]	R_1 = 0.0337, wR_2 = 0.0862
Final R indexes [all data]	R_1 = 0.0375, wR_2 = 0.0901
Largest diff. peak/hole / e Å^{-3}	0.44/-0.48

Table A.7 Crystal data and structure refinement for [Cp*Cr(N^N)] (7).

Identification code	kla0973
Empirical formula	$C_{22}H_{27}CrN_2$
Formula weight	371.45
Temperature/K	293(2)
Crystal system	triclinic
Space group	$P\bar{1}$
a/Å	9.7446(8)
b/Å	10.5289(8)
c/Å	10.7486(9)
α/°	113.0160(10)
β/°	107.3200(10)
γ/°	93.8310(10)
Volume/Å^3	947.69(13)
Z	2
ρ_{calc}g/cm^3	1.302
μ/mm^{-1}	0.610
F(000)	394.0
Crystal size/mm^3	0.685 × 0.329 × 0.178
Radiation	MoKα (λ = 0.71073)
2Θ range for data collection/°	4.298 to 55.492
Index ranges	$-12 \leq h \leq 12$, $-13 \leq k \leq 13$, $-14 \leq l \leq 14$
Reflections collected	18466
Independent reflections	4445 [R_{int} = 0.0165, R_{sigma} = 0.0122]
Data/restraints/parameters	4445/0/233
Goodness-of-fit on F^2	1.070
Final R indexes [I>=2σ (I)]	R_1 = 0.0299, wR_2 = 0.0839
Final R indexes [all data]	R_1 = 0.0319, wR_2 = 0.0858
Largest diff. peak/hole / e Å^{-3}	0.37/-0.23

Table A.8 Crystal data and structure refinement for $[Cp^*Cr(\mu\text{-}N_2)PMe_3]_4Na$ (8).

Identification code	kla0994
Empirical formula	$C_{60}Cr_4H_{112}N_8Na_{0.21}O_2P_4$
Formula weight	1314.28
Temperature/K	200.0
Crystal system	orthorhombic
Space group	I222
a/Å	10.386(2)
b/Å	18.477(4)
c/Å	19.255(4)
α/°	90
β/°	90
γ/°	90
Volume/Å^3	3695.1(13)
Z	2
ρ_{calc}g/cm^3	1.181
μ/mm^{-1}	5.928
F(000)	1405.0
Crystal size/mm^3	0.336 × 0.168 × 0.142
Radiation	CuKα (λ = 1.54184)
2Θ range for data collection/°	9.676 to 134.988
Index ranges	$-12 \le h \le 12$, $-22 \le k \le 22$, $-23 \le l \le 23$
Reflections collected	23684
Independent reflections	3283 [R_{int} = 0.1067, R_{sigma} = 0.0729]
Data/restraints/parameters	3283/9/167
Goodness-of-fit on F^2	1.098
Final R indexes [I>=2σ (I)]	R_1 = 0.0469, wR_2 = 0.1238
Final R indexes [all data]	R_1 = 0.0577, wR_2 = 0.1305
Largest diff. peak/hole / e Å^{-3}	0.39/-0.35
Flack parameter	0.058(13)

Table A.9 Crystal data and structure refinement for [Cp*(dmpe)CrCl] (9).

Identification code	kla0990
Empirical formula	$C_{16}H_{31}ClCrP_2$
Formula weight	372.80
Temperature/K	200(2)
Crystal system	orthorhombic
Space group	Pbca
a/Å	13.949(3)
b/Å	15.832(5)
c/Å	17.230(7)
α/°	90
β/°	90
γ/°	90
Volume/Å^3	3805(2)
Z	8
ρ_{calc}g/cm^3	1.302
μ/mm^{-1}	7.729
F(000)	1584.0
Crystal size/mm^3	0.254 × 0.214 × 0.128
Radiation	CuKα (λ = 1.54184)
2Θ range for data collection/°	9.888 to 152.17
Index ranges	$-17 \leq h \leq 16$, $-19 \leq k \leq 19$, $-21 \leq l \leq 21$
Reflections collected	61237
Independent reflections	3959 [R_{int} = 0.1139, R_{sigma} = 0.0518]
Data/restraints/parameters	3959/42/236
Goodness-of-fit on F^2	1.021
Final R indexes [I>=2σ (I)]	R_1 = 0.0635, wR_2 = 0.1552
Final R indexes [all data]	R_1 = 0.0874, wR_2 = 0.1780
Largest diff. peak/hole / e Å^{-3}	0.80/-0.61

Table A.10 Crystal data and structure refinement for $[Cp^*(dmpe)Cr]_2(\mu\text{-}N_2)$ (10).

Identification code	kla0965
Empirical formula	$C_{16}H_{31}CrNP_2$
Formula weight	351.36
Temperature/K	199.99
Crystal system	monoclinic
Space group	$P2_1/c$
a/Å	9.1615(15)
b/Å	22.829(4)
c/Å	9.8611(16)
α/°	90
β/°	116.292(2)
γ/°	90
Volume/Å^3	1849.1(5)
Z	4
ρ_{calc}g/cm^3	1.262
μ/mm^{-1}	0.784
F(000)	752.0
Crystal size/mm^3	0.479 × 0.457 × 0.225
Radiation	MoKα (λ = 0.71073)
2Θ range for data collection/°	3.568 to 55.458
Index ranges	$-11 \leq h \leq 11$, $-29 \leq k \leq 29$, $-12 \leq l \leq 12$
Reflections collected	27474
Independent reflections	4285 [R_{int} = 0.0177, R_{sigma} = 0.0112]
Data/restraints/parameters	4285/0/190
Goodness-of-fit on F^2	1.104
Final R indexes [I>=2σ (I)]	R_1 = 0.0489, wR_2 = 0.1370
Final R indexes [all data]	R_1 = 0.0517, wR_2 = 0.1393
Largest diff. peak/hole / e Å^{-3}	1.07/-0.66

Table A.11 Crystal data and structure refinement for [Cp*dmpeCr(μ-N)CrCp*Cl] (11).

Identification code	kla0972
Empirical formula	$C_{13}H_{23}CrN_{0.5}PCl_{0.5}$
Formula weight	287.01
Temperature/K	200(2)
Crystal system	orthorhombic
Space group	$P2_12_12_1$
a/Å	8.6637(16)
b/Å	16.498(6)
c/Å	20.443(4)
α/°	90
β/°	90
γ/°	90
Volume/Å^3	2922.1(13)
Z	8
ρ_{calc}g/cm^3	1.305
μ/mm^{-1}	8.096
F(000)	1216.0
Crystal size/mm^3	0.180 × 0.122 × 0.106
Radiation	CuKα (λ = 1.54184)
2Θ range for data collection/°	6.884 to 151.354
Index ranges	$-10 \leq h \leq 10$, $-20 \leq k \leq 20$, $-25 \leq l \leq 23$
Reflections collected	20659
Independent reflections	5837 [R_{int} = 0.0483, R_{sigma} = 0.0637]
Data/restraints/parameters	5837/0/289
Goodness-of-fit on F^2	1.206
Final R indexes [I>=2σ (I)]	R_1 = 0.0746, wR_2 = 0.2031
Final R indexes [all data]	R_1 = 0.0813, wR_2 = 0.2107
Largest diff. peak/hole / e Å^{-3}	0.53/-0.90
Flack parameter	0.068(6)

Table A.12 Crystal data and structure refinement for [Cp*dmpeCr(μ-N)Cr(N$_3$)$_2$Cp*] (12).

Identification code	kla0988
Empirical formula	$C_{208}H_{368}Cr_{16}N_{56}P_{16}$
Formula weight	4981.08
Temperature/K	200(2)
Crystal system	orthorhombic
Space group	Pbca
a/Å	18.570(4)
b/Å	17.648(4)
c/Å	19.426(4)
α/°	90.00(3)
β/°	90.13(3)
γ/°	90.00(3)
Volume/Å^3	6366(2)
Z	1
ρ_{calc}g/cm^3	1.299
μ/mm^{-1}	6.778
F(000)	2632.0
Crystal size/mm^3	0.211 × 0.153 × 0.134
Radiation	CuKα (λ = 1.54184)
2Θ range for data collection/°	8.27 to 150.676
Index ranges	$-22 \leq h \leq 21$, $-19 \leq k \leq 22$, $-24 \leq l \leq 24$
Reflections collected	79051
Independent reflections	6517 [R_{int} = 0.2283, R_{sigma} = 0.1649]
Data/restraints/parameters	6517/0/348
Goodness-of-fit on F^2	1.034
Final R indexes [I>=2σ (I)]	R_1 = 0.1064, wR_2 = 0.2508
Final R indexes [all data]	R_1 = 0.1868, wR_2 = 0.3283
Largest diff. peak/hole / e Å^{-3}	0.54/-1.16

Table A.13 Crystal data and structure refinement for [Cp*(dmpe)Cr≡N] (13).

Identification code	kla0979
Empirical formula	$C_{32}H_{62}Cr_2N_2P_4$
Formula weight	702.71
Temperature/K	200.01
Crystal system	monoclinic
Space group	$P2_1/n$
a/Å	8.6727(4)
b/Å	13.5764(6)
c/Å	16.1856(7)
α/°	90
β/°	92.497(2)
γ/°	90
Volume/Å^3	1903.95(15)
Z	2
ρ_{calc}g/cm^3	1.226
μ/mm^{-1}	6.448
F(000)	752.0
Crystal size/mm^3	0.268 × 0.197 × 0.126
Radiation	CuKα (λ = 1.54178)
2Θ range for data collection/°	8.504 to 151.358
Index ranges	$-9 \leq h \leq 10$, $-14 \leq k \leq 16$, $-19 \leq l \leq 20$
Reflections collected	27112
Independent reflections	3867 [R_{int} = 0.0884, R_{sigma} = 0.0662]
Data/restraints/parameters	3867/0/190
Goodness-of-fit on F^2	1.195
Final R indexes [I>=2σ (I)]	R_1 = 0.0609, wR_2 = 0.1803
Final R indexes [all data]	R_1 = 0.0781, wR_2 = 0.1973
Largest diff. peak/hole / e Å^{-3}	0.56/-0.71

Table A.14 Crystal data and structure refinement for [Cp*(dmpe)Cr=NMe]OTf (14).

Identification code	kla0993
Empirical formula	$C_{18}H_{34}NO_3F_3P_2SCr$
Formula weight	515.46
Temperature/K	200
Crystal system	orthorhombic
Space group	Pnma
a/Å	16.546(2)
b/Å	11.9538(12)
c/Å	12.3421(12)
α/°	90
β/°	90
γ/°	90
Volume/Å^3	2441.1(5)
Z	4
ρ_{calc}g/cm^3	1.403
μ/mm^{-1}	6.268
F(000)	1080.0
Crystal size/mm^3	0.424 × 0.288 × 0.244
Radiation	CuKα (λ = 1.54184)
2Θ range for data collection/°	8.938 to 151.244
Index ranges	$-20 \leq h \leq 18$, $-14 \leq k \leq 14$, $-15 \leq l \leq 15$
Reflections collected	38547
Independent reflections	2646 [R_{int} = 0.0467, R_{sigma} = 0.0234]
Data/restraints/parameters	2646/79/190
Goodness-of-fit on F^2	1.169
Final R indexes [I>=2σ (I)]	R_1 = 0.0437, wR_2 = 0.1259
Final R indexes [all data]	R_1 = 0.0451, wR_2 = 0.1284
Largest diff. peak/hole / e Å^{-3}	0.59/-0.50

Table A.15 Crystal data and structure refinement for [Cp*(dmpe)CrN]$_2$(μ-MgCl$_2$) (15).

Identification code	kla0991
Empirical formula	$C_{40}H_{78}Cl_2Cr_2MgN_2O_2P_4$
Formula weight	942.13
Temperature/K	200(2)
Crystal system	monoclinic
Space group	C2/c
a/Å	13.200(7)
b/Å	15.003(10)
c/Å	25.66(2)
α/°	90
β/°	99.74(3)
γ/°	90
Volume/Å^3	5008(6)
Z	4
ρ_{calc}g/cm^3	1.249
μ/mm^{-1}	6.135
F(000)	2008.0
Crystal size/mm^3	0.484 × 0.287 × 0.198
Radiation	CuKα (λ = 1.54184)
2Θ range for data collection/°	6.99 to 151.352
Index ranges	$-16 \leq h \leq 15$, $-18 \leq k \leq 18$, $-32 \leq l \leq 32$
Reflections collected	35190
Independent reflections	5045 [R_{int} = 0.0492, R_{sigma} = 0.0345]
Data/restraints/parameters	5045/101/276
Goodness-of-fit on F^2	1.084
Final R indexes [I>=2σ (I)]	R_1 = 0.0575, wR_2 = 0.1589
Final R indexes [all data]	R_1 = 0.0627, wR_2 = 0.1644
Largest diff. peak/hole / e Å^{-3}	0.64/-0.81

Table A.16 Crystal data and structure refinement for [Cp*Cr(μ-{NPMe$_2$C$_2$H$_4$PMe$_2$N}Cr(NCO)Cp*] (16).

Identification code	kla1046
Empirical formula	$C_{27}H_{46}Cr_2N_3OP_2$
Formula weight	594.61
Temperature/K	200.01
Crystal system	monoclinic
Space group	$P2_1/c$
a/Å	17.9443(5)
b/Å	10.3219(3)
c/Å	16.6118(5)
α/°	90
β/°	100.191(2)
γ/°	90
Volume/Å^3	3028.28(15)
Z	4
ρ_{calc}g/cm^3	1.304
μ/mm^{-1}	7.085
F(000)	1260.0
Crystal size/mm^3	0.125 × 0.124 × 0.067
Radiation	CuKα (λ = 1.54184)
2Θ range for data collection/°	5.004 to 149.632
Index ranges	$-22 \leq h \leq 22$, $-12 \leq k \leq 11$, $-18 \leq l \leq 20$
Reflections collected	44647
Independent reflections	6090 [R_{int} = 0.0774, R_{sigma} = 0.0602]
Data/restraints/parameters	6090/0/331
Goodness-of-fit on F^2	1.121
Final R indexes [I>=2σ (I)]	R_1 = 0.0619, wR_2 = 0.1638
Final R indexes [all data]	R_1 = 0.0863, wR_2 = 0.1875
Largest diff. peak/hole / e Å^{-3}	0.66/-0.88

Table A.17 Crystal data and structure refinement for $[Cp^*(CO)_2(OCN)Cr]_2(\mu$-dmpe) (17).

Identification code	kla1045
Empirical formula	$C_{40}H_{62}Cr_2N_2O_8P_2$
Formula weight	864.85
Temperature/K	200(2)
Crystal system	triclinic
Space group	$P\bar{1}$
a/Å	8.7702(4)
b/Å	9.5064(4)
c/Å	13.8919(5)
α/°	95.087(2)
β/°	100.547(2)
γ/°	102.791(2)
Volume/Å^3	1100.26(8)
Z	1
ρ_{calc}g/cm^3	1.305
μ/mm^{-1}	5.160
F(000)	458.0
Crystal size/mm^3	0.235 × 0.158 × 0.08
Radiation	CuKα (λ = 1.54178)
2Θ range for data collection/°	6.532 to 134.942
Index ranges	$-10 \leq h \leq 10$, $-11 \leq k \leq 11$, $-16 \leq l \leq 16$
Reflections collected	21897
Independent reflections	3824 [R_{int} = 0.0751, R_{sigma} = 0.0541]
Data/restraints/parameters	3824/0/251
Goodness-of-fit on F^2	1.096
Final R indexes [I>=2σ (I)]	R_1 = 0.0582, wR_2 = 0.1589
Final R indexes [all data]	R_1 = 0.0841, wR_2 = 0.1804
Largest diff. peak/hole / e Å^{-3}	0.76/-0.54

Table A.18 Crystal data and structure refinement for [Cp*(OCN)$_2$Cr(μ-N)CrdmpeCp*] (18).

Identification code	kla1055
Empirical formula	$C_{32}Cr_2H_{54}N_3O_3P_2$
Formula weight	694.72
Temperature/K	200.0
Crystal system	monoclinic
Space group	$P2_1/c$
a/Å	11.8781(3)
b/Å	30.2749(8)
c/Å	10.2260(2)
α/°	90
β/°	102.382(2)
γ/°	90
Volume/Å^3	3591.82(15)
Z	4
ρ_{calc}g/cm^3	1.285
μ/mm^{-1}	6.092
F(000)	1476.0
Crystal size/mm^3	0.172 × 0.17 × 0.101
Radiation	CuKα (λ = 1.54178)
2Θ range for data collection/°	7.62 to 129.994
Index ranges	$-13 \leq h \leq 13$, $-34 \leq k \leq 34$, $-11 \leq l \leq 12$
Reflections collected	34012
Independent reflections	5993 [R_{int} = 0.0999, R_{sigma} = 0.1087]
Data/restraints/parameters	5993/0/348
Goodness-of-fit on F^2	1.052
Final R indexes [I>=2σ (I)]	R_1 = 0.0561, wR_2 = 0.1349
Final R indexes [all data]	R_1 = 0.0950, wR_2 = 0.1639
Largest diff. peak/hole / e Å^{-3}	0.49/-0.44

Table A.19 Crystal data and structure refinement for [Cp*$_2$Cr$_2$(μ,μ-{NP(CH$_3$)$_2$}$_2$C$_2$H$_4$)] (19).

Identification code	kla0998
Empirical formula	$C_{26}H_{46}Cr_2N_2P_2$
Formula weight	552.59
Temperature/K	200.01
Crystal system	orthorhombic
Space group	Pbca
a/Å	16.2067(11)
b/Å	15.5371(11)
c/Å	23.1090(16)
α/°	90
β/°	90
γ/°	90
Volume/Å^3	5819.0(7)
Z	8
ρ_{calc}g/cm^3	1.262
μ/mm^{-1}	0.873
F(000)	2352.0
Crystal size/mm^3	0.538 × 0.255 × 0.228
Radiation	MoKα (λ = 0.71073)
2Θ range for data collection/°	3.524 to 55.026
Index ranges	$-21 \leq h \leq 21$, $-20 \leq k \leq 20$, $-30 \leq l \leq 30$
Reflections collected	85416
Independent reflections	6687 [R_{int} = 0.0304, R_{sigma} = 0.0136]
Data/restraints/parameters	6687/0/303
Goodness-of-fit on F^2	1.066
Final R indexes [I>=2σ (I)]	R_1 = 0.0399, wR_2 = 0.1051
Final R indexes [all data]	R_1 = 0.0480, wR_2 = 0.1126
Largest diff. peak/hole / e Å^{-3}	0.91/-0.38

Table A.20 Crystal data and structure refinement for $Na_2[Cp^*dmpeCrN_2]_4$ (20).

Identification code	kla0976
Empirical formula	$C_{32}H_{62}Cr_2N_4NaP_4$
Formula weight	753.72
Temperature/K	200.0
Crystal system	triclinic
Space group	$P\bar{1}$
a/Å	9.8858(12)
b/Å	12.993(2)
c/Å	16.024(3)
α/°	91.236(8)
β/°	106.329(9)
γ/°	97.081(7)
Volume/Å^3	1956.6(6)
Z	2
ρ_{calc}g/cm^3	1.279
μ/mm^{-1}	6.426
F(000)	802.0
Crystal size/mm^3	0.661 × 0.15 × 0.146
Radiation	CuKα (λ = 1.54184)
2Θ range for data collection/°	5.758 to 151.466
Index ranges	$-12 \leq h \leq 12$, $-16 \leq k \leq 16$, $-20 \leq l \leq 20$
Reflections collected	51620
Independent reflections	7770 [R_{int} = 0.0764, R_{sigma} = 0.0514]
Data/restraints/parameters	7770/0/406
Goodness-of-fit on F^2	1.206
Final R indexes [I>=2σ (I)]	R_1 = 0.0696, wR_2 = 0.2039
Final R indexes [all data]	R_1 = 0.0818, wR_2 = 0.2240
Largest diff. peak/hole / e Å^{-3}	0.63/-0.99

Table A.21 Crystal data and structure refinement for [Cp*(dmpe)Cr(μ-N_2)Na(TMEDA)$_2$] (21).

Identification code	kla0982
Empirical formula	$C_{28}H_{63}CrN_6NaP_2$
Formula weight	620.77
Temperature/K	200.0
Crystal system	monoclinic
Space group	$P2_1/c$
a/Å	17.4993(9)
b/Å	12.6961(7)
c/Å	17.5248(9)
α/°	90
β/°	105.956(3)
γ/°	90
Volume/Å^3	3743.5(3)
Z	4
ρ_{calc}g/cm^3	1.101
μ/mm^{-1}	3.611
F(000)	1352.0
Crystal size/mm^3	0.289 × 0.266 × 0.17
Radiation	CuKα (λ = 1.54178)
2Θ range for data collection/°	5.252 to 150.978
Index ranges	$-21 \leq h \leq 21$, $-15 \leq k \leq 15$, $-21 \leq l \leq 19$
Reflections collected	117729
Independent reflections	7474 [R_{int} = 0.1097, R_{sigma} = 0.0666]
Data/restraints/parameters	7474/0/360
Goodness-of-fit on F^2	1.117
Final R indexes [I>=2σ (I)]	R_1 = 0.0686, wR_2 = 0.1963
Final R indexes [all data]	R_1 = 0.0837, wR_2 = 0.2106
Largest diff. peak/hole / e Å^{-3}	0.75/-0.67

Table A.22 Crystal data and structure refinement for [Cp*(dmpe)Cr(μ-N_2)$SiMe_3$] (22).

Identification code	kla1003
Empirical formula	$C_{19}H_{40}CrN_2P_2Si$
Formula weight	438.56
Temperature/K	200.0
Crystal system	monoclinic
Space group	$P2_1/c$
a/Å	9.5108(11)
b/Å	27.819(2)
c/Å	9.8135(12)
α/°	90
β/°	107.651(6)
γ/°	90
Volume/$Å^3$	2474.2(5)
Z	4
$\rho_{calc}g/cm^3$	1.177
μ/mm^{-1}	5.514
F(000)	944.0
Crystal size/mm^3	0.419 × 0.317 × 0.119
Radiation	CuKα (λ = 1.54184)
2Θ range for data collection/°	6.354 to 154.924
Index ranges	$-10 \leq h \leq 11$, $-35 \leq k \leq 34$, $-12 \leq l \leq 12$
Reflections collected	29576
Independent reflections	4986 [R_{int} = 0.0541, R_{sigma} = 0.0395]
Data/restraints/parameters	4986/0/238
Goodness-of-fit on F^2	1.090
Final R indexes [I>=2σ (I)]	R_1 = 0.0957, wR_2 = 0.2459
Final R indexes [all data]	R_1 = 0.1085, wR_2 = 0.2588
Largest diff. peak/hole / e $Å^{-3}$	0.62/-1.04

Table A.23 Crystal data and structure refinement for [Cp*(dmpe)Cr(μ-N_2)Na(15-crown-5)] (23).

Identification code	kla1040
Empirical formula	$C_{26}H_{51}CrN_2NaO_5P_2$
Formula weight	608.61
Temperature/K	200.0
Crystal system	tetragonal
Space group	$P4_12_12$
a/Å	14.1225(2)
b/Å	14.1225(2)
c/Å	33.4227(7)
α/°	90
β/°	90
γ/°	90
Volume/$Å^3$	6666.0(2)
Z	8
$\rho_{calc}g/cm^3$	1.213
μ/mm^{-1}	4.133
F(000)	2608.0
Crystal size/mm^3	0.369 × 0.219 × 0.146
Radiation	CuKα (λ = 1.54178)
2Θ range for data collection/°	6.794 to 127.336
Index ranges	$-15 \leq h \leq 15$, $-16 \leq k \leq 16$, $-38 \leq l \leq 38$
Reflections collected	83653
Independent reflections	5461 [R_{int} = 0.0995, R_{sigma} = 0.0454]
Data/restraints/parameters	5461/720/390
Goodness-of-fit on F^2	1.088
Final R indexes [I>=2σ (I)]	R_1 = 0.0612, wR_2 = 0.1197
Final R indexes [all data]	R_1 = 0.0896, wR_2 = 0.1397
Largest diff. peak/hole / e $Å^{-3}$	0.57/-0.30
Flack parameter	0.090(14)

Table A.24 Crystal data and structure refinement for [(Cp*(dmpe)Cr)$_2$(μ-N$_2$)](FB(C$_6$F$_5$)$_3$) (24).

Identification code	kla0996
Empirical formula	$C_{50}H_{62}BCr_2F_{16}N_2P_4$
Formula weight	1233.70
Temperature/K	199.99
Crystal system	triclinic
Space group	$P\bar{1}$
a/Å	13.070(3)
b/Å	13.470(3)
c/Å	17.438(3)
α/°	84.971(8)
β/°	80.214(11)
γ/°	66.068(13)
Volume/Å^3	2764.5(11)
Z	2
ρ_{calc}g/cm^3	1.482
μ/mm^{-1}	5.137
F(000)	1266.0
Crystal size/mm^3	0.269 × 0.251 × 0.179
Radiation	CuKα (λ = 1.54184)
2Θ range for data collection/°	5.144 to 151.286
Index ranges	$-16 \leq h \leq 16$, $-16 \leq k \leq 16$, $-21 \leq l \leq 19$
Reflections collected	73942
Independent reflections	10943 [R_{int} = 0.1196, R_{sigma} = 0.0748]
Data/restraints/parameters	10943/0/695
Goodness-of-fit on F^2	1.134
Final R indexes [I>=2σ (I)]	R_1 = 0.0767, wR_2 = 0.2126
Final R indexes [all data]	R_1 = 0.0974, wR_2 = 0.2343
Largest diff. peak/hole / e Å^{-3}	1.01/-1.16

Table A.25 Crystal data and structure refinement for $[(Cp^*(dmpe)Cr)_2(\mu\text{-}N_2)]BAr^F{}_4$ (25).

Identification code	kla0997
Empirical formula	$C_{64}H_{74}BCr_2F_{24}N_2P_4$
Formula weight	1565.94
Temperature/K	200(2)
Crystal system	triclinic
Space group	$P\bar{1}$
a/Å	13.3198(2)
b/Å	15.2823(3)
c/Å	19.9876(3)
α/°	109.0290(10)
β/°	102.2070(11)
γ/°	99.6078(10)
Volume/Å^3	3634.79(11)
Z	2
ρ_{calc}g/cm^3	1.431
μ/mm^{-1}	4.196
F(000)	1602.0
Crystal size/mm^3	0.293 × 0.17 × 0.143
Radiation	CuKα (λ = 1.54178)
2Θ range for data collection/°	4.88 to 109.688
Index ranges	$-13 \leq h \leq 13$, $-15 \leq k \leq 15$, $-21 \leq l \leq 20$
Reflections collected	39784
Independent reflections	8157 [R_{int} = 0.1009, R_{sigma} = 0.1014]
Data/restraints/parameters	8157/477/1004
Goodness-of-fit on F^2	1.051
Final R indexes [I>=2σ (I)]	R_1 = 0.0723, wR_2 = 0.1726
Final R indexes [all data]	R_1 = 0.1039, wR_2 = 0.1934
Largest diff. peak/hole / e Å^{-3}	0.70/-0.52

Table A.26 Crystal data and structure refinement for [(Cp*(dmpe)Cr)$_2$(μ-N$_2$)](BAr$^F{}_4$)$_2$ (26).

Identification code	kla1011
Empirical formula	$C_{96}H_{86}B_2Cr_2F_{48}N_2P_4$
Formula weight	2429.16
Temperature/K	200(2)
Crystal system	triclinic
Space group	$P\bar{1}$
a/Å	13.3515(4)
b/Å	13.7555(5)
c/Å	15.1944(5)
α/°	104.9310(17)
β/°	97.4458(16)
γ/°	93.895(2)
Volume/Å^3	2658.60(15)
Z	1
ρ_{calc}g/cm^3	1.517
μ/mm^{-1}	3.428
F(000)	1226.0
Crystal size/mm^3	0.436 × 0.311 × 0.088
Radiation	CuKα (λ = 1.54178)
2Θ range for data collection/°	6.092 to 134.99
Index ranges	$-15 \leq h \leq 15$, $-16 \leq k \leq 16$, $-18 \leq l \leq 18$
Reflections collected	40568
Independent reflections	9248 [R_{int} = 0.0734, R_{sigma} = 0.0609]
Data/restraints/parameters	9248/448/892
Goodness-of-fit on F^2	1.088
Final R indexes [I>=2σ (I)]	R_1 = 0.0865, wR_2 = 0.2331
Final R indexes [all data]	R_1 = 0.1124, wR_2 = 0.2654
Largest diff. peak/hole / e Å^{-3}	0.88/-0.78

Table A.27 Crystal data and structure refinement for [Cp*(dmpe)CrF]BAr$^{F}_{4}$ (27).

Identification code	kla1062
Empirical formula	$BC_{48}CrF_{25}H_{45}OP_2$
Formula weight	1237.59
Temperature/K	100
Crystal system	triclinic
Space group	$P\bar{1}$
a/Å	12.1087(7)
b/Å	13.1135(6)
c/Å	17.4738(10)
α/°	95.757(4)
β/°	94.943(4)
γ/°	97.597(4)
Volume/Å^3	2722.5(3)
Z	2
ρ_{calc}g/cm^3	1.510
μ/mm^{-1}	3.394
F(000)	1250.0
Crystal size/mm^3	0.202 × 0.166 × 0.076
Radiation	CuKα (λ = 1.54178)
2Θ range for data collection/°	7.402 to 118.104
Index ranges	$-13 \leq h \leq 13$, $-14 \leq k \leq 14$, $-19 \leq l \leq 19$
Reflections collected	56982
Independent reflections	7625 [R_{int} = 0.0841, R_{sigma} = 0.0712]
Data/restraints/parameters	7625/1900/912
Goodness-of-fit on F^2	1.056
Final R indexes [I>=2σ (I)]	R_1 = 0.0676, wR_2 = 0.1738
Final R indexes [all data]	R_1 = 0.0915, wR_2 = 0.1944
Largest diff. peak/hole / e Å^{-3}	0.59/-0.40

Table A.28 Crystal data and structure refinement for [Cp*(dmpe)CrCl]BAr$^{F}_{4}$ (28).

Identification code	kla1064
Empirical formula	$C_{48}H_{43}BClCrF_{24}P_2$
Formula weight	1236.02
Temperature/K	100(2)
Crystal system	triclinic
Space group	$P\bar{1}$
a/Å	12.9422(5)
b/Å	13.4986(5)
c/Å	15.3934(5)
α/°	88.336(2)
β/°	75.194(2)
γ/°	87.535(2)
Volume/Å^3	2597.10(16)
Z	2
ρ_{calc}g/cm^3	1.581
μ/mm^{-1}	3.977
F(000)	1246.0
Crystal size/mm^3	0.216 × 0.087 × 0.064
Radiation	CuKα (λ = 1.54178)
2Θ range for data collection/°	5.94 to 130.728
Index ranges	$-15 \leq h \leq 15$, $-15 \leq k \leq 15$, $-18 \leq l \leq 18$
Reflections collected	57639
Independent reflections	8605 [R_{int} = 0.0507, R_{sigma} = 0.0330]
Data/restraints/parameters	8605/0/703
Goodness-of-fit on F^2	1.187
Final R indexes [I>=2σ (I)]	R_1 = 0.0496, wR_2 = 0.1376
Final R indexes [all data]	R_1 = 0.0594, wR_2 = 0.1463
Largest diff. peak/hole / e Å^{-3}	0.92/-0.75

Table A.29 Crystal data and structure refinement for [(Cp*(dmpe)CrN]BAr$^{F}_{4}$ (29).

Identification code	kla1043
Empirical formula	$C_{48}H_{43}BCrF_{24}NP_2$
Formula weight	1214.58
Temperature/K	100(2)
Crystal system	triclinic
Space group	$P\bar{1}$
a/Å	12.8251(4)
b/Å	13.4583(5)
c/Å	16.3694(6)
α/°	74.297(2)
β/°	74.090(2)
γ/°	87.135(2)
Volume/Å^3	2614.89(16)
Z	2
ρ_{calc}g/cm^3	1.543
μ/mm^{-1}	3.485
F(000)	1226.0
Crystal size/mm^3	0.408 × 0.235 × 0.102
Radiation	CuKα (λ = 1.54178)
2Θ range for data collection/°	5.826 to 142.764
Index ranges	$-15 \leq h \leq 15$, $-16 \leq k \leq 16$, $-20 \leq l \leq 20$
Reflections collected	61473
Independent reflections	9726 [R_{int} = 0.0551, R_{sigma} = 0.0353]
Data/restraints/parameters	9726/1266/815
Goodness-of-fit on F^2	1.118
Final R indexes [I>=2σ (I)]	R_1 = 0.0802, wR_2 = 0.2048
Final R indexes [all data]	R_1 = 0.0929, wR_2 = 0.2201
Largest diff. peak/hole / e Å^{-3}	1.62/-1.40

Table A.30 Crystal data and structure refinement for [Cp*Cr(NPMe$_2$CH$_2$CH$_2$PMe$_2$)] BAr$^F_4$ (30).

Identification code	kla1048
Empirical formula	$C_{48}H_{43}BCrF_{24}NP_2$
Formula weight	1214.58
Temperature/K	200(2)
Crystal system	triclinic
Space group	$P\bar{1}$
a/Å	12.2628(4)
b/Å	13.0546(4)
c/Å	17.6860(6)
α/°	73.864(2)
β/°	81.998(2)
γ/°	83.740(2)
Volume/Å^3	2685.88(15)
Z	2
ρ_{calc}g/cm^3	1.502
μ/mm^{-1}	3.393
F(000)	1226.0
Crystal size/mm^3	0.2 × 0.1 × 0.07
Radiation	CuKα (λ = 1.54178)
2Θ range for data collection/°	5.236 to 118.136
Index ranges	$-13 \leq h \leq 13$, $-14 \leq k \leq 14$, $-19 \leq l \leq 19$
Reflections collected	56735
Independent reflections	7529 [R_{int} = 0.0666, R_{sigma} = 0.0393]
Data/restraints/parameters	7529/1026/815
Goodness-of-fit on F^2	1.069
Final R indexes [I>=2σ (I)]	R_1 = 0.0674, wR_2 = 0.1697
Final R indexes [all data]	R_1 = 0.0900, wR_2 = 0.1873
Largest diff. peak/hole / e Å^{-3}	0.73/-0.47

Table A.31 Crystal data and structure refinement for [Cp*Cr(NPMe$_2$CH$_2$CH$_2$PMe$_2$)THF] BAr$^F{}_4$ (31).

Identification code	kla1073
Empirical formula	$BC_{57.5}CrF_{24}H_{62.5}NO_2P_2$
Formula weight	1380.33
Temperature/K	120.01
Crystal system	monoclinic
Space group	$P2_1/n$
a/Å	12.3992(5)
b/Å	24.0246(9)
c/Å	21.2547(8)
α/°	90
β/°	90.273(3)
γ/°	90
Volume/Å^3	6331.4(4)
Z	4
ρ_{calc}g/cm^3	1.448
μ/mm^{-1}	2.972
F(000)	2822.0
Crystal size/mm^3	0.444 × 0.293 × 0.072
Radiation	CuKα (λ = 1.54178)
2Θ range for data collection/°	8.024 to 151.182
Index ranges	$-15 \leq h \leq 14$, $-30 \leq k \leq 30$, $-26 \leq l \leq 26$
Reflections collected	104957
Independent reflections	12848 [R_{int} = 0.0868, R_{sigma} = 0.0800]
Data/restraints/parameters	12848/2578/1130
Goodness-of-fit on F^2	1.057
Final R indexes [I>=2σ (I)]	R_1 = 0.0664, wR_2 = 0.1800
Final R indexes [all data]	R_1 = 0.0885, wR_2 = 0.1994
Largest diff. peak/hole / e Å^{-3}	0.88/-0.47

Table A.32 Crystal data and structure refinement for [Cp*Cr(NPMe$_2$CH$_2$CH$_2$PMe$_2$)F] BAr$^F{}_4$ (32).

Identification code	kla1063
Empirical formula	$C_{51}H_{46}BCrF_{25}NP_2$
Formula weight	1272.64
Temperature/K	200(2)
Crystal system	monoclinic
Space group	$P2_1/c$
a/Å	12.7123(4)
b/Å	18.6521(6)
c/Å	24.2959(8)
α/°	90
β/°	97.051(2)
γ/°	90
Volume/Å^3	5717.3(3)
Z	4
ρ_{calc}g/cm^3	1.479
μ/mm^{-1}	3.242
F(000)	2572.0
Crystal size/mm^3	0.519 × 0.495 × 0.184
Radiation	CuKα (λ = 1.54178)
2Θ range for data collection/°	5.99 to 149.696
Index ranges	$-15 \leq h \leq 13$, $-23 \leq k \leq 23$, $-30 \leq l \leq 29$
Reflections collected	95131
Independent reflections	11395 [R_{int} = 0.1425, R_{sigma} = 0.0751]
Data/restraints/parameters	11395/1636/907
Goodness-of-fit on F^2	1.064
Final R indexes [I>=2σ (I)]	R_1 = 0.1201, wR_2 = 0.2904
Final R indexes [all data]	R_1 = 0.1676, wR_2 = 0.3319
Largest diff. peak/hole / e Å^{-3}	0.95/-0.74

APPENDIX B

MISCELLANEOUS CRYSTAL STRUCTURES

In this appendix the data for some crystal structure are provided. These compounds were characterized using X-ray crystallography technique.

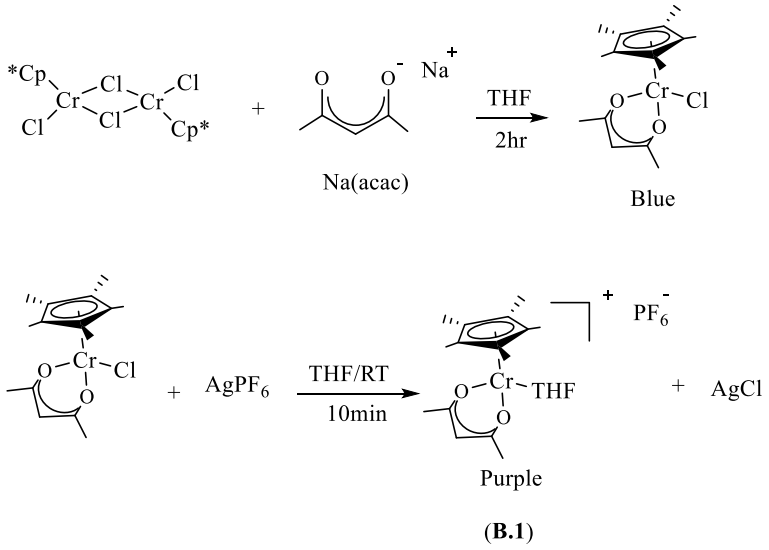

Scheme B.1 Synthesis of $[Cp^*Cr(acac)THF]PF_6$ (**B.1**).

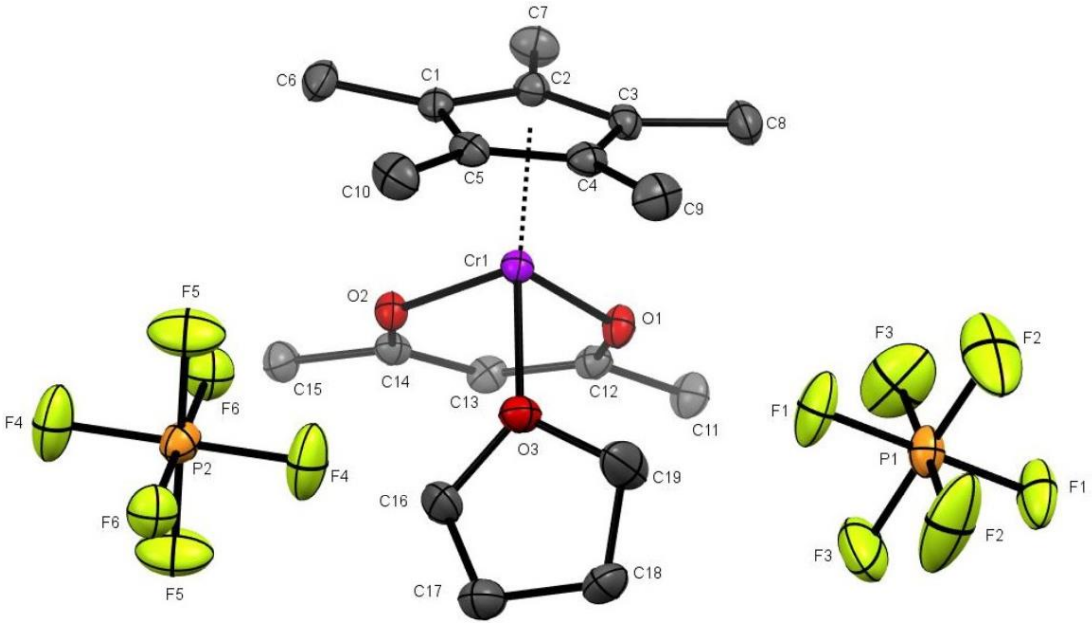

Figure B.1 Molecular structure of the [Cp*Cr(acac)THF]PF_6 (**B.1**) represented as 50% probability thermal ellipsoids. Hydrogen atoms have been omitted for clarity.

Table B.1 Interatomic distances (Å) and angles (º) for [Cp*Cr(acac)THF]PF_6 (**B.1**).

Distances (Å)

Cr1-O1	1.9500(16)	O2-C4	1.280(3)
Cr1-O2	1.9539(16)	O3-C19	1.453(4)
Cr1-O3	2.0508(17)	O3-C16	1.456(3)
Cr1-C6	2.182(2)	C1-C2	1.501(3)
Cr1-C10	2.212(2)	C2-C3	1.392(3)
Cr1-C7	2.218(2)	C3-C4	1.390(3)
Cr1-C8	2.232(2)	C4-C5	1.498(3)
Cr1-C9	2.241(2)	C6-C10	1.427(3)
P1-F1	1.576(2)	C6-C7	1.432(3)
P1-F1	1.576(2)	C6-C11	1.503(3)
P1-F3	1.5810(19)	C7-C8	1.404(3)

P1-F3	1.5810(19)	C7-C12	1.503(3)
P1-F2	1.5989(18)	C8-C9	1.432(3)
P1-F2	1.5989(18)	C8-C13	1.508(4)
P2-F4	1.549(2)	C9-C10	1.416(3)
P2-F4	1.549(2)	C9-C14	1.495(4)
P2-F6	1.574(2)	C10-C15	1.500(3)
P2-F6	1.574(2)	C16-C17	1.474(4)
P2-F5	1.5850(18)	C17-C18	1.495(4)
P2-F5	1.5850(18)	C18-C19	1.463(4)
O1-C2	1.277(3)		

Angles (°)

O1-Cr1-O2	90.93(7)	F62-P2-F5	90.70(14)
O1-Cr1-O3	92.74(7)	F4-P2-F52	90.70(14)
O2-Cr1-O3	90.86(8)	F42-P2-F52	89.43(13)
O1-Cr1-C6	103.58(8)	F6-P2-F52	90.70(14)
O2-Cr1-C6	100.15(8)	F62-P2-F52	89.17(12)
O3-Cr1-C6	160.04(8)	F5-P2-F52	179.82(18)
O1-Cr1-C10	141.04(8)	C2-O1-Cr1	127.16(15)
O2-Cr1-C10	91.47(8)	C4-O2-Cr1	126.90(15)
O3-Cr1-C10	126.09(8)	C19-O3-C16	107.8(2)
C6-Cr1-C10	37.91(9)	C19-O3-Cr1	120.89(18)
O1-Cr1-C7	89.66(8)	C16-O3-Cr1	122.92(16)
O2-Cr1-C7	136.32(9)	O1-C2-C3	124.6(2)
O3-Cr1-C7	132.73(8)	O1-C2-C1	115.2(2)
C6-Cr1-C7	37.96(9)	C3-C2-C1	120.2(2)
C10-Cr1-C7	62.83(9)	C4-C3-C2	125.0(2)
O1-Cr1-C8	112.03(8)	O2-C4-C3	124.7(2)
O2-Cr1-C8	153.42(8)	O2-C4-C5	115.2(2)
O3-Cr1-C8	100.81(8)	C3-C4-C5	120.1(2)
C6-Cr1-C8	62.59(9)	C10-C6-C7	107.7(2)
C10-Cr1-C8	62.34(9)	C10-C6-C11	125.9(2)

C7-Cr1-C8	36.77(9)	C7-C6-C11	126.3(2)
O1-Cr1-C9	149.07(8)	C10-C6-Cr1	72.15(13)
O2-Cr1-C9	117.89(8)	C7-C6-Cr1	72.39(13)
O3-Cr1-C9	97.48(8)	C11-C6-Cr1	121.22(17)
C6-Cr1-C9	62.67(9)	C8-C7-C6	108.0(2)
C10-Cr1-C9	37.07(9)	C8-C7-C12	126.2(2)
C7-Cr1-C9	62.16(9)	C6-C7-C12	125.9(2)
C8-Cr1-C9	37.35(9)	C8-C7-Cr1	72.14(13)
F1-P1-F1	180.00(16)	C6-C7-Cr1	69.66(13)
F1-P1-F3	90.29(15)	C12-C7-Cr1	122.21(17)
F1-P1-F3	89.71(15)	C7-C8-C9	108.5(2)
F1-P1-F3	89.71(15)	C7-C8-C13	126.5(2)
F1-P1-F3	90.29(15)	C9-C8-C13	124.9(2)
F3-P1-F3	180	C7-C8-Cr1	71.09(13)
F1-P1-F2	90.42(11)	C9-C8-Cr1	71.66(13)
F1-P1-F2	89.58(11)	C13-C8-Cr1	125.58(18)
F3-P1-F2	90.23(11)	C10-C9-C8	107.7(2)
F3-P1-F2	89.77(11)	C10-C9-C14	126.7(2)
F1-P1-F2	89.58(11)	C8-C9-C14	125.5(2)
F1-P1-F2	90.42(11)	C10-C9-Cr1	70.34(13)
F3-P1-F2	89.77(11)	C8-C9-Cr1	70.99(13)
F3-P1-F2	90.23(11)	C14-C9-Cr1	127.13(18)
F2-P1-F2	180.00(14)	C9-C10-C6	108.0(2)
F4-P2-F4	89.7(3)	C9-C10-C15	125.3(2)
F4-P2-F6	178.04(18)	C6-C10-C15	126.7(2)
F4-P2-F6	91.7(2)	C9-C10-Cr1	72.59(13)
F4-P2-F6	91.7(2)	C6-C10-Cr1	69.94(13)
F4-P2-F6	178.04(18)	C15-C10-Cr1	121.89(17)
F6-P2-F6	87.0(3)	O3-C16-C17	105.5(2)
F4-P2-F5	89.43(13)	C16-C17-C18	105.0(3)
F4-P2-F5	90.70(14)	C19-C18-C17	106.1(3)
F6-P2-F5	89.17(13)	O3-C19-C18	107.8(3)

Table B.1.a Crystal data and structure refinement for $[Cp^*Cr(acac)THF]PF_6$ (B.1).

Identification code	kla0938
Empirical formula	$C_{19}H_{30}CrF_6O_3P$
Formula weight	503.40
Temperature/K	200(2)
Crystal system	monoclinic
Space group	C2/c
a/Å	13.4861(6)
b/Å	11.5494(5)
c/Å	29.0801(13)
α/°	90
β/°	90.4920(10)
γ/°	90
Volume/Å^3	4529.2(3)
Z	8
ρ_{calc}g/cm^3	1.476
μ/mm^{-1}	0.642
F(000)	2088.0
Crystal size/mm^3	0.432 × 0.183 × 0.136
Radiation	MoKα (λ = 0.71073)
2Θ range for data collection/°	2.802 to 55.224
Index ranges	$-17 \leq h \leq 17$, $-14 \leq k \leq 15$, $-37 \leq l \leq 37$
Reflections collected	34108
Independent reflections	5247 [R_{int} = 0.0447, R_{sigma} = 0.0317]
Data/restraints/parameters	5247/0/280
Goodness-of-fit on F^2	1.020
Final R indexes [I>=2σ (I)]	R_1 = 0.0467, wR_2 = 0.1200
Final R indexes [all data]	R_1 = 0.0604, wR_2 = 0.1292
Largest diff. peak/hole / e Å^{-3}	0.70/-0.41

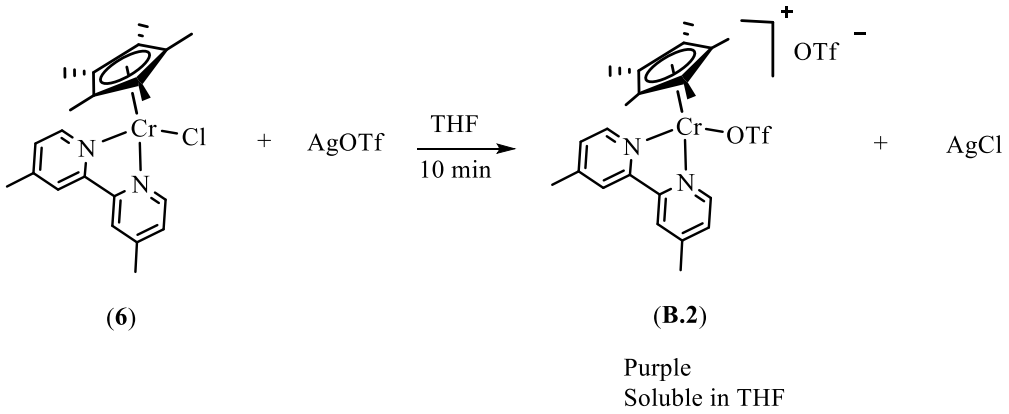

Scheme B.2 Synthesis of [Cp*Cr(N^N)OTf]OTf (**B.2**).

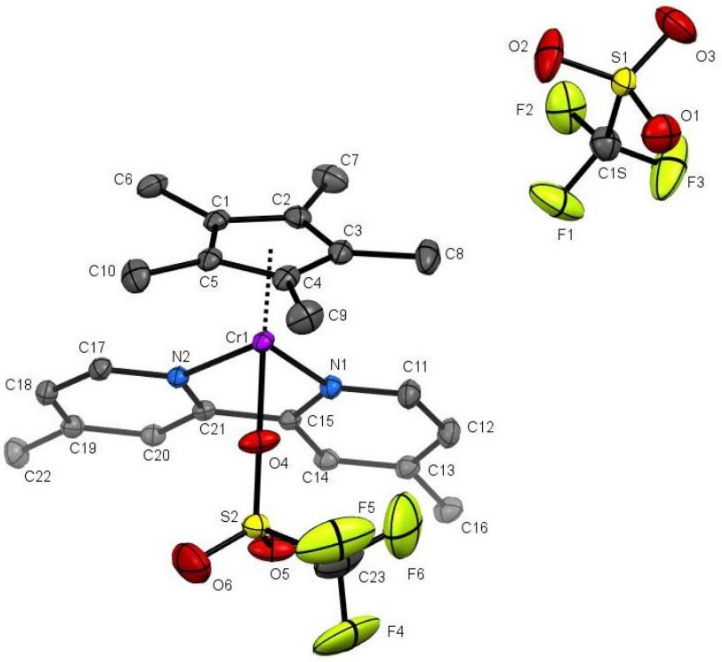

Figure B.2 Molecular structure of the [Cp*Cr(N^N)OTf]OTf (**B.2**) represented as 50% probability thermal ellipsoids. Hydrogen atoms have been omitted for clarity.

Table B.2 Interatomic distances (Å) and angles (º) for [Cp*Cr(N^N)OTf]OTf (**B.2**).

Distances (Å)

Cr1-O4	2.017(2)	C3-C4	1.412(5)
Cr1-N2	2.054(2)	C3-C8	1.496(4)
Cr1-N1	2.075(2)	C4-C5	1.425(4)
Cr1-C2	2.214(3)	C4-C9	1.497(5)
Cr1-C5	2.217(3)	C5-C10	1.500(4)
Cr1-C4	2.225(3)	C11-C12	1.377(4)
Cr1-C1	2.225(3)	C12-C13	1.391(4)
Cr1-C3	2.231(3)	C13-C14	1.395(4)
S2-O5	1.408(3)	C13-C16	1.500(4)
S2-O6	1.416(4)	C14-C15	1.382(3)
S2-O4	1.461(2)	C15-C21	1.484(3)
S2-C23	1.802(6)	C17-C18	1.383(4)
C23-F5	1.280(8)	C18-C19	1.387(4)
C23-F4	1.310(7)	C19-C20	1.394(4)
C23-F6	1.345(10)	C19-C22	1.507(4)
N1-C11	1.346(3)	C20-C21	1.381(4)
N1-C15	1.354(3)	S1-O2	1.407(3)
N2-C17	1.347(3)	S1-O3	1.418(3)
N2-C21	1.353(3)	S1-O1	1.440(3)
C1-C5	1.426(4)	S1-C1S	1.793(4)
C1-C2	1.424(4)	C1S-F3	1.297(5)
C1-C6	1.500(4)	C1S-F1	1.324(5)
C2-C3	1.445(4)	C1S-F2	1.333(5)
C2-C7	1.497(5)		

Angles (°)

O4-Cr1-N2	93.85(10)	C1-C2-C7	125.0(3)

O4-Cr1-N1	95.45(10)	C3-C2-C7	127.4(3)
N2-Cr1-N1	79.10(9)	C1-C2-Cr1	71.72(16)
O4-Cr1-C2	149.24(11)	C3-C2-Cr1	71.66(16)
N2-Cr1-C2	115.32(10)	C7-C2-Cr1	125.2(2)
N1-Cr1-C2	99.31(10)	C4-C3-C2	107.9(3)
O4-Cr1-C5	100.26(10)	C4-C3-C8	125.2(3)
N2-Cr1-C5	108.10(9)	C2-C3-C8	126.9(3)
N1-Cr1-C5	162.12(10)	C4-C3-Cr1	71.32(16)
C2-Cr1-C5	62.81(11)	C2-C3-Cr1	70.40(15)
O4-Cr1-C4	88.06(10)	C8-C3-Cr1	126.3(2)
N2-Cr1-C4	144.72(10)	C3-C4-C5	108.6(3)
N1-Cr1-C4	135.84(10)	C3-C4-C9	126.3(3)
C2-Cr1-C4	62.68(12)	C5-C4-C9	125.1(3)
C5-Cr1-C4	37.42(10)	C3-C4-Cr1	71.74(16)
O4-Cr1-C1	136.96(11)	C5-C4-Cr1	70.99(15)
N2-Cr1-C1	94.26(9)	C9-C4-Cr1	124.1(2)
N1-Cr1-C1	127.59(10)	C4-C5-C1	107.9(3)
C2-Cr1-C1	37.43(11)	C4-C5-C10	124.5(3)
C5-Cr1-C1	37.45(11)	C1-C5-C10	127.5(3)
C4-Cr1-C1	62.39(10)	C4-C5-Cr1	71.59(15)
O4-Cr1-C3	112.17(11)	C1-C5-Cr1	71.57(15)
N2-Cr1-C3	153.18(11)	C10-C5-Cr1	123.8(2)
N1-Cr1-C3	103.70(10)	N1-C11-C12	122.8(3)
C2-Cr1-C3	37.94(11)	C11-C12-C13	120.0(3)
C5-Cr1-C3	62.38(10)	C14-C13-C12	117.0(2)
C4-Cr1-C3	36.94(12)	C14-C13-C16	121.1(3)
C1-Cr1-C3	62.54(10)	C12-C13-C16	121.9(3)
O5-S2-O6	116.6(3)	C15-C14-C13	120.4(2)
O5-S2-O4	114.34(15)	N1-C15-C14	121.8(2)
O6-S2-O4	113.8(2)	N1-C15-C21	114.9(2)
O5-S2-C23	104.7(3)	C14-C15-C21	123.2(2)
O6-S2-C23	103.6(4)	N2-C17-C18	122.4(2)
O4-S2-C23	101.5(2)	C17-C18-C19	119.7(3)

S2-O4-Cr1	138.77(15)	C18-C19-C20	117.8(2)
F5-C23-F4	109.8(6)	C18-C19-C22	121.7(3)
F5-C23-F6	107.9(7)	C20-C19-C22	120.5(3)
F4-C23-F6	108.7(7)	C21-C20-C19	120.0(2)
F5-C23-S2	112.7(5)	N2-C21-C20	121.9(2)
F4-C23-S2	110.5(5)	N2-C21-C15	115.0(2)
F6-C23-S2	107.0(5)	C20-C21-C15	123.1(2)
C11-N1-C15	118.0(2)	O2-S1-O3	117.2(3)
C11-N1-Cr1	126.74(19)	O2-S1-O1	114.9(3)
C15-N1-Cr1	114.95(17)	O3-S1-O1	112.2(3)
C17-N2-C21	118.3(2)	O2-S1-C1S	104.4(2)
C17-N2-Cr1	125.93(18)	O3-S1-C1S	103.1(2)
C21-N2-Cr1	115.75(16)	O1-S1-C1S	102.8(2)
C5-C1-C2	108.2(2)	F3-C1S-F1	113.5(5)
C5-C1-C6	127.3(3)	F3-C1S-F2	104.2(4)
C2-C1-C6	124.5(3)	F1-C1S-F2	100.8(3)
C5-C1-Cr1	70.98(15)	F3-C1S-S1	112.9(3)
C2-C1-Cr1	70.85(15)	F1-C1S-S1	111.7(3)
C6-C1-Cr1	125.66(19)	F2-C1S-S1	112.8(3)
C1-C2-C3	107.5(3)		

Table B.2.a Crystal data and structure refinement for [Cp*Cr(N^N)OTf]OTf (B.2).

Identification code	kla0949
Empirical formula	$C_{24}H_{27}N_2O_6F_6S_2Cr$
Formula weight	669.59
Temperature/K	200(2)
Crystal system	triclinic
Space group	P-1
a/Å	8.7637(7)
b/Å	12.6145(9)
c/Å	13.5537(10)
α/°	95.9740(10)
β/°	94.4670(10)
γ/°	104.9810(10)
Volume/Å^3	1430.98(19)
Z	2
ρ_{calc}g/cm^3	1.554
μ/mm^{-1}	0.626
F(000)	686.0
Crystal size/mm^3	0.892 × 0.721 × 0.565
Radiation	MoKα (λ = 0.71073)
2Θ range for data collection/°	3.04 to 55.392
Index ranges	$-11 \leq h \leq 11$, $-16 \leq k \leq 16$, $-17 \leq l \leq 17$
Reflections collected	38028
Independent reflections	6669 [R_{int} = 0.0406, R_{sigma} = 0.0256]
Data/restraints/parameters	6669/72/377
Goodness-of-fit on F^2	1.000
Final R indexes [I>=2σ (I)]	R_1 = 0.0609, wR_2 = 0.1672
Final R indexes [all data]	R_1 = 0.0713, wR_2 = 0.1833
Largest diff. peak/hole / e Å^{-3}	1.00/-0.77

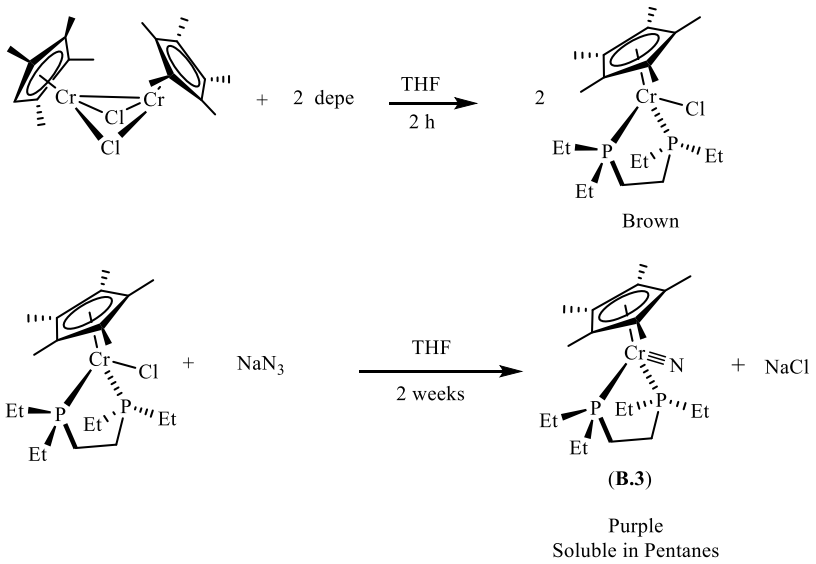

Scheme B.3 Synthesis of [Cp*Cr(depe)N] (**B.3**).

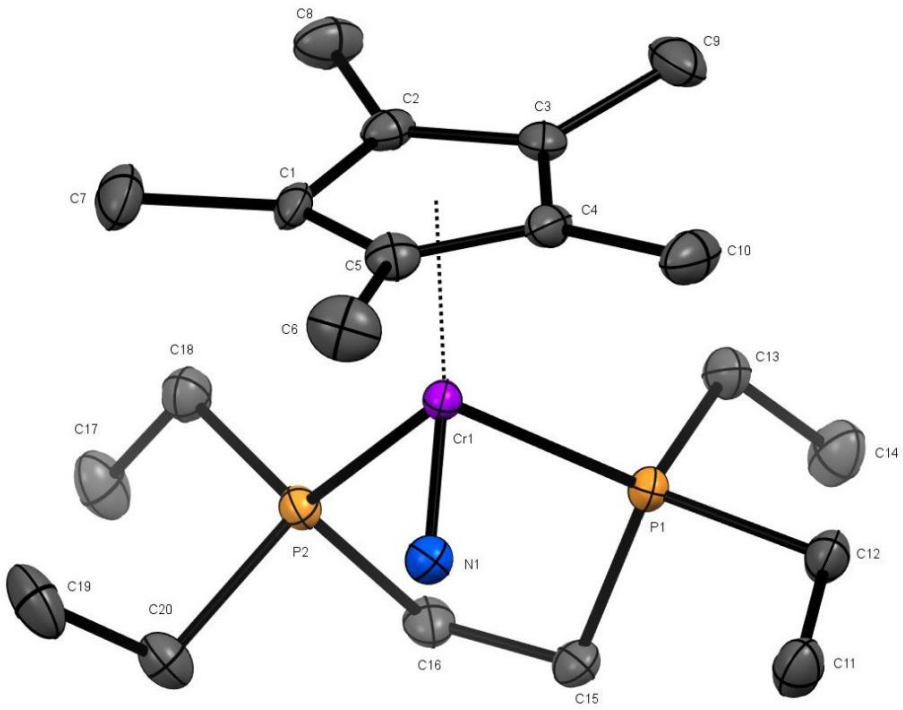

Figure B.3 Molecular structure of the [Cp*Cr(depe)N] (**B.3**) represented as 50% probability thermal ellipsoids. Hydrogen atoms and a pentane molecule have been omitted for clarity.

Table B.3 Interatomic distances (Å) and angles (º) for [Cp*Cr(depe)N] (**B.3**).

Distances (Å)

Cr1-P1	2.2959(9)	C1-C5	1.420(5)
Cr1-P2	2.3160(10)	C1-C7	1.503(5)
Cr1-N1	1.587(3)	C2-C3	1.397(5)
Cr1-C1	2.224(3)	C2-C8	1.504(5)
Cr1-C2	2.394(3)	C3-C4	1.432(5)
Cr1-C3	2.395(3)	C3-C9	1.501(5)
Cr1-C4	2.221(3)	C4-C5	1.422(5)
Cr1-C5	2.180(3)	C4-C10	1.502(5)
P1-C12	1.845(4)	C5-C6	1.497(5)
P1-C13	1.842(4)	C11-C12	1.514(5)
P1-C15	1.837(4)	C13-C14	1.516(5)
P2-C16	1.860(4)	C15-C16	1.523(5)
P2-C18	1.840(4)	C17-C18	1.522(5)
P2-C20	1.839(4)	C19-C20	1.519(6)
C1-C2	1.437(5)		

Angles (°)

P1-Cr1-P2	82.70(3)	C20-P2-C16	100.13(18)
P1-Cr1-C2	114.43(9)	C20-P2-C18	104.04(18)
P1-Cr1-C3	93.59(9)	C2-C1-Cr1	78.48(19)
P2-Cr1-C2	101.40(8)	C2-C1-C7	125.1(4)
P2-Cr1-C3	127.15(9)	C5-C1-Cr1	69.53(18)
N1-Cr1-P1	91.78(11)	C5-C1-C2	107.5(3)
N1-Cr1-P2	88.79(11)	C5-C1-C7	125.8(4)
N1-Cr1-C1	117.16(15)	C7-C1-Cr1	129.0(3)
N1-Cr1-C2	152.72(14)	C1-C2-Cr1	65.50(17)
N1-Cr1-C3	144.05(14)	C1-C2-C8	125.4(3)

N1-Cr1-C4	108.52(14)	C3-C2-Cr1	73.08(19)
N1-Cr1-C5	94.90(14)	C3-C2-C1	108.0(3)
C1-Cr1-P1	150.29(10)	C3-C2-C8	126.5(4)
C1-Cr1-P2	103.27(9)	C8-C2-Cr1	130.3(2)
C1-Cr1-C2	36.01(13)	C2-C3-Cr1	73.02(19)
C1-Cr1-C3	59.35(12)	C2-C3-C4	108.9(3)
C2-Cr1-C3	33.90(12)	C2-C3-C9	125.5(4)
C4-Cr1-P1	103.80(10)	C4-C3-Cr1	65.41(18)
C4-Cr1-P2	161.05(9)	C4-C3-C9	125.3(3)
C4-Cr1-C1	62.40(13)	C9-C3-Cr1	133.1(2)
C4-Cr1-C2	59.66(12)	C3-C4-Cr1	78.7(2)
C4-Cr1-C3	35.89(13)	C3-C4-C10	126.6(4)
C5-Cr1-P1	140.66(10)	C5-C4-Cr1	69.60(19)
C5-Cr1-P2	136.07(10)	C5-C4-C3	107.1(3)
C5-Cr1-C1	37.61(13)	C5-C4-C10	125.7(4)
C5-Cr1-C2	60.28(12)	C10-C4-Cr1	123.4(2)
C5-Cr1-C3	60.02(13)	C1-C5-Cr1	72.85(19)
C5-Cr1-C4	37.68(14)	C1-C5-C4	108.2(3)
C12-P1-Cr1	120.76(13)	C1-C5-C6	126.6(4)
C13-P1-Cr1	120.68(12)	C4-C5-Cr1	72.7(2)
C13-P1-C12	101.65(17)	C4-C5-C6	125.2(3)
C15-P1-Cr1	105.24(11)	C6-C5-Cr1	120.9(3)
C15-P1-C12	103.31(18)	C11-C12-P1	113.6(3)
C15-P1-C13	102.61(18)	C14-C13-P1	117.6(3)
C16-P2-Cr1	110.20(12)	C16-C15-P1	108.7(2)
C18-P2-Cr1	124.12(13)	C15-C16-P2	108.8(2)
C18-P2-C16	101.66(18)	C17-C18-P2	116.7(3)
C20-P2-Cr1	113.56(13)	C19-C20-P2	113.6(3)

Table B.3.a Crystal data and structure refinement for [Cp*Cr(depe)N] (B.3).

Identification code	kla0989
Empirical formula	$C_{20}H_{38}CrNP_2$
Formula weight	406.45
Temperature/K	200(2)
Crystal system	monoclinic
Space group	$P2_1/n$
a/Å	8.6700(8)
b/Å	14.2590(12)
c/Å	18.0665(16)
α/°	90
β/°	90.088(3)
γ/°	90
Volume/Å^3	2233.5(3)
Z	4
ρ_{calc}g/cm^3	1.209
μ/mm^{-1}	5.562
F(000)	876.0
Crystal size/mm^3	0.456 × 0.444 × 0.246
Radiation	CuKα (λ = 1.54178)
2Θ range for data collection/°	7.898 to 151.314
Index ranges	$-10 \leq h \leq 10$, $-17 \leq k \leq 17$, $0 \leq l \leq 22$
Reflections collected	4565
Independent reflections	4565 [R_{int} = 0.0470, R_{sigma} = 0.0301]
Data/restraints/parameters	4565/0/226
Goodness-of-fit on F^2	1.110
Final R indexes [I>=2σ (I)]	R_1 = 0.0468, wR_2 = 0.1291
Final R indexes [all data]	R_1 = 0.0479, wR_2 = 0.1300
Largest diff. peak/hole / e Å^{-3}	0.42/-0.42

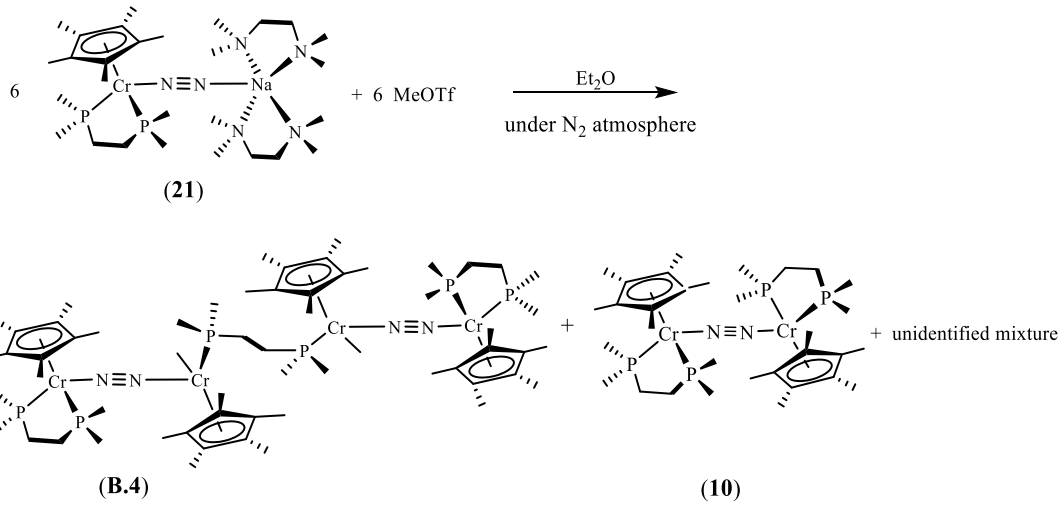

Scheme B.4 Synthesis of $([Cp^*(dmpe)Cr](\mu\text{-}N_2)[Cp^*CrMe])_2(\mu\text{-dmpe})$ (**B.4**).

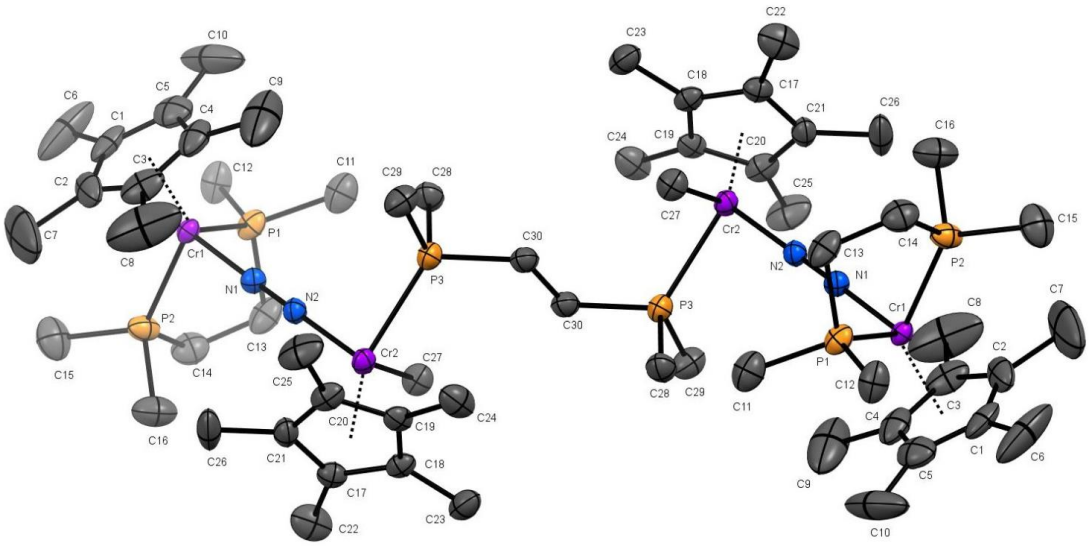

Figure B.4 Molecular structure of the $([Cp^*(dmpe)Cr](\mu\text{-}N_2)[Cp^*CrMe])_2(\mu\text{-dmpe})$ (**B.4**) represented as 50% probability thermal ellipsoids. Hydrogen atoms and a pentane molecule have been omitted for clarity.

Table B.4 Interatomic distances (Å) and angles (º) for $[[Cp^*(dmpe)Cr]_2(\mu\text{-}N_2)]_2(\mu\text{-}dmpe)$ (**B.4**).

Distances (Å)

Cr1-P1	2.270(7)	P3-C30	1.841(9)
Cr1-P2	2.288(7)	N1-N2	1.203(9)
Cr1-N1	1.767(7)	C13-C14	1.57(2)
Cr1-C1	2.262(6)	C17-C18	1.412(12)
Cr1-C2	2.216(6)	C17-C21	1.419(13)
Cr1-C3	2.208(6)	C17-C22	1.505(13)
Cr1-C4	2.250(6)	C18-C19	1.401(12)
Cr1-C5	2.282(6)	C18-C23	1.499(13)
Cr2-P3	2.385(4)	C19-C20	1.414(13)
Cr2-N2	1.836(7)	C19-C24	1.490(12)
Cr2-C17	2.257(9)	C20-C21	1.449(14)
Cr2-C18	2.242(8)	C20-C25	1.478(14)
Cr2-C19	2.269(8)	C21-C26	1.465(13)
Cr2-C20	2.282(9)	C30-C30	1.502(18)
Cr2-C21	2.267(9)	C1-C2	1.42
Cr2-C27	2.118(10)	C1-C5	1.42
P1-C11	1.807(13)	C1-C6	1.5095
P1-C12	1.810(13)	C2-C3	1.42
P1-C13	1.845(14)	C2-C7	1.5095
P2-C14	1.851(14)	C3-C4	1.42
P2-C15	1.807(13)	C3-C8	1.5095
P2-C16	1.813(13)	C4-C5	1.42
P3-C28	1.810(10)	C4-C9	1.5095
P3-C29	1.794(11)	C5-C10	1.5095

Angles (°)

P1-Cr1-P2	81.2(3)	C29-P3-Cr2	116.9(4)

P1-Cr1-C5	93.6(4)	C29-P3-C28	103.1(5)
N1-Cr1-P1	93.7(6)	C29-P3-C30	99.0(5)
N1-Cr1-P2	92.9(4)	C30-P3-Cr2	121.0(3)
N1-Cr1-C1	154.7(3)	N2-N1-Cr1	172.5(6)
N1-Cr1-C2	126.7(3)	N1-N2-Cr2	172.1(6)
N1-Cr1-C3	94.5(3)	C14-C13-P1	105.2(12)
N1-Cr1-C4	94.7(3)	C13-C14-P2	107.3(12)
N1-Cr1-C5	126.0(3)	C18-C17-Cr2	71.1(5)
C1-Cr1-P1	104.1(5)	C18-C17-C21	107.7(8)
C1-Cr1-P2	107.4(4)	C18-C17-C22	126.0(9)
C1-Cr1-C5	36.42(10)	C21-C17-Cr2	72.1(5)
C2-Cr1-P1	139.4(6)	C21-C17-C22	126.3(9)
C2-Cr1-P2	98.5(4)	C22-C17-Cr2	123.0(6)
C2-Cr1-C1	36.96(9)	C17-C18-Cr2	72.3(5)
C2-Cr1-C4	61.92(15)	C17-C18-C23	125.1(9)
C2-Cr1-C5	61.41(14)	C19-C18-Cr2	73.0(5)
C3-Cr1-P1	153.6(4)	C19-C18-C17	108.9(8)
C3-Cr1-P2	123.3(4)	C19-C18-C23	125.6(9)
C3-Cr1-C1	61.85(14)	C23-C18-Cr2	125.8(6)
C3-Cr1-C2	37.44(11)	C18-C19-Cr2	70.8(4)
C3-Cr1-C4	37.13(10)	C18-C19-C20	108.9(8)
C3-Cr1-C5	61.52(14)	C18-C19-C24	126.7(9)
C4-Cr1-P1	117.1(4)	C20-C19-Cr2	72.4(5)
C4-Cr1-P2	159.5(3)	C20-C19-C24	124.0(10)
C4-Cr1-C1	61.23(14)	C24-C19-Cr2	128.9(6)
C4-Cr1-C5	36.51(9)	C19-C20-Cr2	71.4(5)
C5-Cr1-P2	141.1(4)	C19-C20-C21	106.8(8)
N2-Cr2-P3	91.0(2)	C19-C20-C25	126.4(10)
N2-Cr2-C17	111.5(3)	C21-C20-Cr2	70.9(5)
N2-Cr2-C18	148.0(3)	C21-C20-C25	126.6(10)
N2-Cr2-C19	147.6(3)	C25-C20-Cr2	127.3(7)
N2-Cr2-C20	111.4(3)	C17-C21-Cr2	71.4(5)
N2-Cr2-C21	93.7(3)	C17-C21-C20	107.7(8)

N2-Cr2-C27	91.4(4)	C17-C21-C26	126.3(10)
C17-Cr2-P3	156.4(2)	C20-C21-Cr2	72.0(5)
C17-Cr2-C19	60.8(3)	C20-C21-C26	125.7(10)
C17-Cr2-C20	61.4(3)	C26-C21-Cr2	126.1(7)
C17-Cr2-C21	36.6(3)	C301-C30-P3	113.1(8)
C18-Cr2-P3	120.8(2)	C2-C1-Cr1	69.8(2)
C18-Cr2-C17	36.6(3)	C2-C1-C5	108
C18-Cr2-C19	36.2(3)	C2-C1-C6	126
C18-Cr2-C20	60.8(3)	C5-C1-Cr1	72.6(2)
C18-Cr2-C21	60.9(3)	C5-C1-C6	126
C19-Cr2-P3	96.5(2)	C6-C1-Cr1	123.29(18)
C19-Cr2-C20	36.2(3)	C1-C2-Cr1	73.3(2)
C20-Cr2-P3	104.7(3)	C1-C2-C3	108
C21-Cr2-P3	139.6(3)	C1-C2-C7	126
C21-Cr2-C19	60.9(3)	C3-C2-Cr1	71.0(2)
C21-Cr2-C20	37.1(4)	C3-C2-C7	126
C27-Cr2-P3	91.6(3)	C7-C2-Cr1	121.46(19)
C27-Cr2-C17	94.8(4)	C2-C3-Cr1	71.6(2)
C27-Cr2-C18	90.6(4)	C2-C3-C8	126
C27-Cr2-C19	119.7(4)	C4-C3-Cr1	73.0(2)
C27-Cr2-C20	151.3(4)	C4-C3-C2	108
C27-Cr2-C21	128.4(4)	C4-C3-C8	126
C11-P1-Cr1	120.5(12)	C8-C3-Cr1	121.16(18)
C11-P1-C12	101.8(14)	C3-C4-Cr1	69.9(2)
C11-P1-C13	100.3(12)	C3-C4-C5	108
C12-P1-Cr1	121.5(17)	C3-C4-C9	126
C12-P1-C13	101(2)	C5-C4-Cr1	72.99(19)
C13-P1-Cr1	107.9(8)	C5-C4-C9	126
C14-P2-Cr1	112.6(7)	C9-C4-Cr1	122.81(18)
C15-P2-Cr1	125.2(11)	C1-C5-Cr1	71.00(19)
C15-P2-C14	99.9(11)	C1-C5-C10	126
C15-P2-C16	99.2(13)	C4-C5-Cr1	70.5(2)
C16-P2-Cr1	115.9(9)	C4-C5-C1	108

C16-P2-C14	100.2(11)	C4-C5-C10	126
C28-P3-Cr2	112.7(4)	C10-C5-Cr1	124.12(19)
C28-P3-C30	101.5(4)		

Table B.4.a Crystal data and structure refinement for [[Cp*(dmpe)Cr]$_2$(μ-N$_2$)]$_2$(μ-dmpe) (B.4).

Identification code	kla1023
Empirical formula	$C_{64}Cr_4H_{124}N_4OP_6$
Formula weight	1359.48
Temperature/K	200(2)
Crystal system	triclinic
Space group	P-1
a/Å	8.655(11)
b/Å	12.003(13)
c/Å	19.21(3)
α/°	90.37(8)
β/°	99.71(8)
γ/°	104.16(6)
Volume/Å^3	1905(5)
Z	1
ρ_{calc}g/cm^3	1.185
μ/mm^{-1}	6.054
F(000)	730.0
Crystal size/mm^3	0.305 × 0.282 × 0.08
Radiation	CuKα (λ = 1.54184)
2Θ range for data collection/°	4.674 to 129.996
Index ranges	$-10 \leq h \leq 10$, $-14 \leq k \leq 14$, $-22 \leq l \leq 22$
Reflections collected	24167
Independent reflections	6230 [R_{int} = 0.1119, R_{sigma} = 0.0917]
Data/restraints/parameters	6230/461/404
Goodness-of-fit on F^2	1.071
Final R indexes [I>=2σ (I)]	R_1 = 0.1023, wR_2 = 0.2621
Final R indexes [all data]	R_1 = 0.1318, wR_2 = 0.2903
Largest diff. peak/hole / e Å^{-3}	1.31/-0.89

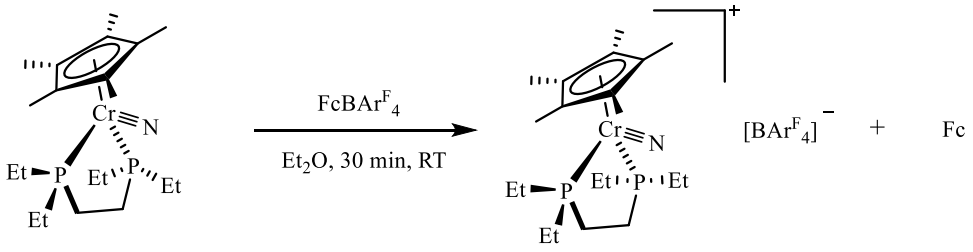

Scheme B.5 Synthesis of [Cp*Cr(depe)N]BAr$^F_4$ (**B.5**).

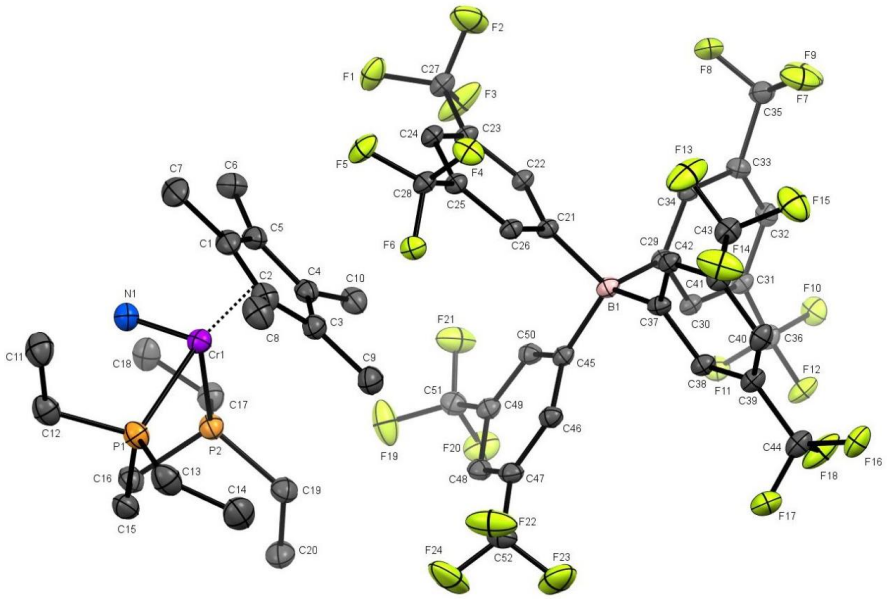

Figure B.5 Molecular structure of the [Cp*Cr(depe)N]BAr$^F_4$ (**B.5**) represented as 50% probability thermal ellipsoids. Hydrogen atoms and a pentane molecule have been omitted for clarity.

Table B.5 Interatomic distances (Å) and angles (º) for the cation of $[[Cp^*(dmpe)Cr]_2(\mu\text{-}N_2)]_2(\mu\text{-dmpe})$ (**B.5**).

Distances (Å)

Cr1-P2	2.3786(12)	C23-C24	1.391(5)
Cr1-P1	2.4333(13)	C23-C22	1.392(5)
Cr1-N1	1.585(4)	C29-C34	1.398(5)
Cr1-C4	2.277(4)	C29-C30	1.394(5)
Cr1-C3	2.354(4)	C29-B1	1.627(5)
Cr1-C5	2.236(4)	C31-C36	1.481(5)
Cr1-C1	2.231(4)	C31-C32	1.389(5)
Cr1-C2	2.298(4)	C31-C30	1.395(5)
P2-C16	1.829(4)	C26-C25	1.387(5)
P2-C17	1.826(5)	C34-C33	1.390(5)
P2-C19	1.833(5)	C41-C40	1.385(5)
P1-C12	1.816(5)	C41-C43	1.491(5)
P1-C15	1.840(5)	C41-C42	1.393(5)
P1-C13	1.817(5)	C28-C25	1.485(5)
F16-C44	1.339(5)	C33-C32	1.389(5)
F1-C27	1.336(5)	C33-C35	1.500(5)
F20-C51	1.329(5)	C39-C40	1.382(5)
F9-C35	1.324(5)	C39-C44	1.501(5)
F17-C44	1.328(5)	C39-C38	1.386(5)
F21-C51	1.317(5)	C48-C47	1.385(6)
F18-C44	1.343(5)	C48-C49	1.391(5)
F7-C35	1.342(5)	C47-C52	1.492(6)
F3-C27	1.298(5)	C47-C46	1.385(5)
F15-C43	1.345(5)	C4-C3	1.424(6)
F14-C43	1.328(5)	C4-C5	1.420(6)
F19-C51	1.348(5)	C4-C10	1.501(5)

F2-C27	1.351(5)	C3-C2	1.419(6)
F13-C43	1.315(5)	C3-C9	1.500(6)
F8-C35	1.306(5)	C51-C49	1.481(5)
F22-C52	1.313(5)	C5-C1	1.428(6)
F23-C52	1.325(5)	C5-C6	1.490(7)
F24-C52	1.321(5)	C1-C2	1.423(7)
F6-C28	1.352(4)	C1-C7	1.505(6)
F12-C36	1.358(4)	C2-C8	1.501(6)
F11-C36	1.349(4)	C16-C15	1.525(6)
F10-C36	1.333(4)	C12-C11	1.528(7)
F5-C28	1.337(4)	C17-C18	1.512(7)
F4-C28	1.346(4)	C19-C20	1.524(6)
C21-C26	1.391(5)	C25-C24	1.394(5)
C21-C22	1.408(5)	C50-C49	1.393(5)
C21-B1	1.637(5)	C37-C42	1.403(5)
C45-C50	1.401(5)	C37-C38	1.401(5)
C45-C46	1.405(5)	C37-B1	1.629(5)
C45-B1	1.638(5)	C13-C14	1.518(8)
C23-C27	1.492(5)		

Angles (°)

P2-Cr1-P1	83.45(4)	F2-C27-C23	111.2(3)
N1-Cr1-P2	89.88(14)	F15-C43-C41	112.8(4)
N1-Cr1-P1	88.09(14)	F14-C43-F15	103.2(3)
N1-Cr1-C4	126.14(18)	F14-C43-C41	112.2(4)
N1-Cr1-C3	156.39(17)	F13-C43-F15	104.1(4)
N1-Cr1-C5	96.30(18)	F13-C43-F14	108.9(4)
N1-Cr1-C1	99.18(18)	F13-C43-C41	114.8(3)
N1-Cr1-C2	131.70(18)	C3-C4-Cr1	75.1(2)
C4-Cr1-P2	94.13(10)	C3-C4-C10	124.9(4)
C4-Cr1-P1	145.74(12)	C5-C4-Cr1	70.1(2)
C4-Cr1-C3	35.76(15)	C5-C4-C3	108.9(4)

C4-Cr1-C2	60.10(15)	C5-C4-C10	125.4(4)
C3-Cr1-P2	104.42(11)	C10-C4-Cr1	128.7(3)
C3-Cr1-P1	111.81(11)	F16-C44-F18	105.5(3)
C5-Cr1-P2	118.13(11)	F16-C44-C39	112.9(3)
C5-Cr1-P1	157.87(12)	F17-C44-F16	106.0(3)
C5-Cr1-C4	36.67(14)	F17-C44-F18	107.8(4)
C5-Cr1-C3	60.48(15)	F17-C44-C39	112.5(3)
C5-Cr1-C2	61.21(16)	F18-C44-C39	111.8(3)
C1-Cr1-P2	154.29(12)	C4-C3-Cr1	69.1(2)
C1-Cr1-P1	120.61(12)	C4-C3-C9	124.6(4)
C1-Cr1-C4	61.12(14)	C2-C3-Cr1	70.1(2)
C1-Cr1-C3	60.26(15)	C2-C3-C4	107.4(4)
C1-Cr1-C5	37.29(16)	C2-C3-C9	127.7(4)
C1-Cr1-C2	36.59(17)	C9-C3-Cr1	130.7(3)
C2-Cr1-P2	138.17(12)	F20-C51-F19	104.1(3)
C2-Cr1-P1	99.96(12)	F20-C51-C49	113.0(4)
C2-Cr1-C3	35.49(15)	F21-C51-F20	106.1(4)
C16-P2-Cr1	102.38(15)	F21-C51-F19	107.0(4)
C16-P2-C19	105.4(2)	F21-C51-C49	114.1(3)
C17-P2-Cr1	118.28(16)	F19-C51-C49	111.7(3)
C17-P2-C16	105.6(2)	F9-C35-F7	105.0(3)
C17-P2-C19	105.5(2)	F9-C35-C33	113.4(3)
C19-P2-Cr1	118.27(14)	F7-C35-C33	111.7(3)
C12-P1-Cr1	111.74(17)	F8-C35-F9	107.8(4)
C12-P1-C15	103.3(2)	F8-C35-F7	106.3(4)
C12-P1-C13	104.2(2)	F8-C35-C33	112.2(3)
C15-P1-Cr1	106.03(15)	C4-C5-Cr1	73.2(2)
C13-P1-Cr1	125.04(17)	C4-C5-C1	107.2(4)
C13-P1-C15	104.4(2)	C4-C5-C6	127.0(4)
C26-C21-C22	115.6(3)	C1-C5-Cr1	71.2(2)
C26-C21-B1	122.0(3)	C1-C5-C6	125.8(4)
C22-C21-B1	122.0(3)	C6-C5-Cr1	121.8(3)
C50-C45-C46	115.1(3)	C5-C1-Cr1	71.5(2)

C50-C45-B1	119.8(3)	C5-C1-C7	124.2(4)
C46-C45-B1	125.0(3)	C2-C1-Cr1	74.3(2)
C24-C23-C27	119.1(3)	C2-C1-C5	108.1(4)
C24-C23-C22	120.7(3)	C2-C1-C7	127.4(4)
C22-C23-C27	120.2(3)	C7-C1-Cr1	124.0(3)
C34-C29-B1	122.7(3)	F22-C52-F23	105.9(4)
C30-C29-C34	115.2(3)	F22-C52-F24	106.6(4)
C30-C29-B1	121.8(3)	F22-C52-C47	113.9(3)
C32-C31-C36	121.9(3)	F23-C52-C47	112.2(4)
C32-C31-C30	120.5(3)	F24-C52-F23	104.2(4)
C30-C31-C36	117.5(3)	F24-C52-C47	113.3(4)
C25-C26-C21	123.1(3)	C3-C2-Cr1	74.4(2)
C33-C34-C29	122.7(3)	C3-C2-C1	108.3(4)
C40-C41-C43	118.5(3)	C3-C2-C8	127.2(4)
C40-C41-C42	120.8(3)	C1-C2-Cr1	69.1(2)
C42-C41-C43	120.7(3)	C1-C2-C8	123.9(4)
F6-C28-C25	112.7(3)	C8-C2-Cr1	128.7(3)
F5-C28-F6	106.2(3)	C15-C16-P2	109.9(3)
F5-C28-F4	107.2(3)	C11-C12-P1	114.3(3)
F5-C28-C25	114.1(3)	C18-C17-P2	114.3(3)
F4-C28-F6	104.9(3)	C20-C19-P2	116.6(3)
F4-C28-C25	111.2(3)	C26-C25-C28	119.6(3)
F12-C36-C31	111.5(3)	C26-C25-C24	120.4(3)
F11-C36-F12	105.2(3)	C24-C25-C28	119.9(3)
F11-C36-C31	112.6(3)	C23-C24-C25	118.1(3)
F10-C36-F12	106.5(3)	C49-C50-C45	123.1(4)
F10-C36-F11	107.0(3)	C23-C22-C21	122.1(3)
F10-C36-C31	113.6(3)	C29-C30-C31	122.9(3)
C34-C33-C35	118.5(3)	C47-C46-C45	122.4(4)
C32-C33-C34	120.9(3)	C42-C37-B1	125.4(3)
C32-C33-C35	120.6(3)	C38-C37-C42	115.0(3)
C40-C39-C44	119.9(3)	C38-C37-B1	119.1(3)
C40-C39-C38	121.2(4)	C48-C49-C51	119.1(3)

C38-C39-C44	118.9(3)	C48-C49-C50	119.9(4)
C47-C48-C49	118.4(3)	C50-C49-C51	120.9(4)
C33-C32-C31	117.7(3)	C41-C42-C37	122.5(3)
C48-C47-C52	119.8(4)	C39-C38-C37	122.6(3)
C48-C47-C46	121.0(4)	C16-C15-P1	112.1(3)
C46-C47-C52	119.2(4)	C14-C13-P1	115.2(4)
C39-C40-C41	117.9(3)	C21-B1-C45	104.1(3)
F1-C27-F2	103.1(3)	C29-B1-C21	112.0(3)
F1-C27-C23	112.2(3)	C29-B1-C45	111.1(3)
F3-C27-F1	108.4(3)	C29-B1-C37	103.7(3)
F3-C27-F2	106.5(4)	C37-B1-C21	113.4(3)
F3-C27-C23	114.6(3)	C37-B1-C45	112.8(3)

Table B.5.a Crystal data and structure refinement for [[Cp*(dmpe)Cr]$_2$(μ-N$_2$)]$_2$(μ-dmpe) (B.5).

Identification code	kla1051
Empirical formula	$C_{52}H_{51}BCrF_{24}NP_2$
Formula weight	1270.68
Temperature/K	100.03
Crystal system	triclinic
Space group	P-1
a/Å	12.1430(4)
b/Å	12.7622(4)
c/Å	18.3123(6)
α/°	89.948(2)
β/°	87.258(2)
γ/°	80.584(2)
Volume/Å^3	2796.37(16)
Z	2
ρ_{calc}g/cm^3	1.509
μ/mm^{-1}	3.285
F(000)	1290.0
Crystal size/mm^3	0.202 × 0.11 × 0.073
Radiation	CuKα (λ = 1.54178)
2Θ range for data collection/°	4.832 to 149.576
Index ranges	$-14 \leq h \leq 15$, $-15 \leq k \leq 15$, $-22 \leq l \leq 22$
Reflections collected	72978
Independent reflections	10969 [R_{int} = 0.0714, R_{sigma} = 0.0494]
Data/restraints/parameters	10969/0/739
Goodness-of-fit on F^2	1.155
Final R indexes [I>=2σ (I)]	R_1 = 0.0717, wR_2 = 0.2062
Final R indexes [all data]	R_1 = 0.0926, wR_2 = 0.2258
Largest diff. peak/hole / e Å^{-3}	0.99/-1.06